Characterization of cAMP nanodomains surrounding the human Glucagon-like peptide 1 receptor using FRET-based reporters

Charakterisierung der Rezeptor-assoziierten cAMP Nanodomänen des humanen Glucagon-like peptide 1 Rezeptors mittels FRET-basierter Sensoren

Doctoral thesis for a doctoral degree
at the Graduate School of Life Sciences,
Julius-Maximilians-Universität Würzburg,
Section Biomedicine
Submitted by

Selma Anton
from Haifa, Israel

Berlin, 2019

Characterization of cAMP nanodomains surrounding the human Glucagon-like peptide 1 receptor using FRET-based reporters

Charakterisierung der Rezeptor-assoziierten cAMP Nanodomänen des humanen Glucagon-like peptide 1 Rezeptors mittels FRET-basierter Sensoren

Doctoral thesis for a doctoral degree
at the Graduate School of Life Sciences,
Julius-Maximilians-Universität Würzburg,
Section Biomedicine
Submitted by

Selma Anton
from Haifa, Israel

Berlin, 2019

Submitted on: ……..

Office stamp

Members of the *Promotionskomitee*:

Chairperson:	Prof. Dr. Manfred Gessler
Primary Supervisor:	Prof. Dr. Martin J. Lohse
Supervisor (Second):	Prof. Dr. Manuela Zaccolo
Supervisor (Third):	Prof. Dr. Peter Gmeiner
Supervisor (Fourth):	Prof. Dr. Katrin Heinze

Date of Public Defence: ……

Date of Receipt of Certificates: …….

Affidavit

I hereby confirm that my thesis entitled **Characterization of cAMP nanodomains surrounding the human Glucagon-like peptide 1 receptor using FRET-based reporters**
is the result of my own work. I did not receive any help or support from commercial consultants. All sources and / or materials applied are listed and specified in the thesis.

Furthermore, I confirm that this thesis has not yet been submitted as part of another examination process neither in identical nor in similar form.

Place, Date Signature

Eidesstattliche Erklärung

Hiermit erkläre ich an Eides statt, die Dissertation „**Charakterisierung der Rezeptor-assoziierten cAMP Nanodomänen des humanen Glucagon-like peptide 1 Rezeptors mittels FRET-basierter Sensoren“** eigenständig, d.h. insbesondere selbständig und ohne Hilfe eines kommerziellen Promotionsberaters, angefertigt und keine anderen als die von mir angegebenen Quellen und Hilfsmittel verwendet zu haben.

Ich erkläre außerdem, dass die Dissertation weder in gleicher noch in ähnlicher Form bereits in einem anderen Prüfungsverfahren vorgelegen hat.

Ort, Datum Unterschrift

Characterization of cAMP nanodomains surrounding the human Glucagon-like peptide 1 receptor using FRET-based reporters

Doctoral thesis by
Selma Anton

Abstract

Cyclic adenosine monophosphate (cAMP), the ubiquitous second messenger produced upon stimulation of GPCRs which couple to the stimulatory G_S protein, orchestrates an array of physiological processes including cardiac function, neuronal plasticity, immune responses, cellular proliferation and apoptosis. By interacting with various effector proteins, among others protein kinase A (PKA) and exchange proteins directly activated by cAMP (Epac), it triggers signaling cascades for the cellular response. Although the functional outcomes of G_SPCR-activation are very diverse depending on the extracellular stimulus, they are all mediated exclusively by this single second messenger. Thus, the question arises how specificity in such responses may be attained. A hypothesis to explain signaling specificity is that cellular signaling architecture, and thus precise operation of cAMP in space and time would appear to be essential to achieve signaling specificity. Compartments with elevated cAMP levels would allow specific signal relay from receptors to effectors within a micro- or nanometer range, setting the molecular basis for signaling specificity. Although the paradigm of signaling compartmentation gains continuous recognition and is thoroughly being investigated, the molecular composition of such compartments and how they are maintained remains to be elucidated. In addition, such compartments would require very restricted diffusion of cAMP, but all direct measurements have indicated that it can diffuse in cells almost freely.

In this work, we present the identification and characterize of a cAMP signaling compartment at a G_SPCR. We created a Förster resonance energy transfer (FRET)-based receptor-sensor conjugate, allowing us to study cAMP dynamics in direct vicinity of the human glucagone-like peptide 1 receptor (hGLP1R). Additional targeting of analogous sensors to the plasma membrane and the cytosol enables assessment of cAMP dynamics in different subcellular regions. We compare both basal and stimulated cAMP levels and study cAMP crosstalk of different receptors. With the design of novel receptor nanorulers up to 60nm in length, which allow mapping cAMP levels in nanometer distance from the hGLP1R, we identify a cAMP nanodomain surrounding it. Further, we show that phosphodiesterases (PDEs), the only enzymes known to degrade cAMP, are decisive in constraining cAMP diffusion into the cytosol thereby maintaining a cAMP gradient. Following the discovery of this nanodomain, we sought to investigate whether downstream effectors such as PKA are present and active within the domain, additionally studying the role of A-kinase anchoring proteins (AKAPs) in targeting PKA to the receptor compartment. We demonstrate that GLP1-produced cAMP signals translate into local nanodomain-restricted PKA phosphorylation and determine that AKAP-tethering is essential for nanodomain PKA.

Taken together, our results provide evidence for the existence of a dynamic, receptor associated cAMP nanodomain and give prospect for which key proteins are likely to be involved in its formation. These conditions would allow cAMP to exert its function in a spatially and temporally restricted manner, setting the basis for a cell to achieve signaling specificity. Understanding the molecular mechanism of cAMP signaling would allow modulation and thus regulation of GPCR signaling, taking advantage of it for pharmacological treatment.

List of figures
List of tables

List of Figures

List of Tables

1 Introduction

1.1 G protein coupled receptors

The ability of individuals to communicate, respond and adapt to the ever-changing environment is the basis for being and staying alive. In order to maintain this ability, the whole organism down to the smallest compartments of its cells needs to perceive external information and translate it into a suitable response. Biological processes are initiated and eventually result in the necessary adaptation to these external environmental influences.

The phospholipid bilayer of cellular membranes constitutes the interface between intra- and extracellular space, forming a barrier for direct interaction. Receptors of various kinds, present within the membrane, are the key to transfer an extracellular signal inside and with this enable the communication between neighboring cells. Approaching signals are processed intracellularly and lead to a specific biological response, which helps the cell maintain its function within its tissue.
Among the various receptor types such as ligand-gated ion channels, enzyme-linked receptors the G protein-coupled receptors (GPCRs) constitute one of the largest families of integral membrane proteins. With over 800 genes responsible for the expression of GPCRs, they are present in almost every human tissue including the cardiovascular system, central nervous system, respiratory system, immune system and digestive system. They take part in the regulation of diverse physiological functions as cell proliferation, differentiation and migration. Malfunction and malregulation of this receptor class is accountable for a plethora of human diseases such as diabetes, coronary heart syndrome, Alzheimer' disease and neurological disorders of various sorts. Therefore, modern medicine is investing a lot of effort in the investigation of GPCRs as drug targets to restore a physiological function. Already almost 30% of marketed drugs act at GPCRs with the tendency rising [1].
Over 800 members of these transmembrane receptors are expressed throughout the human body. About 400 of these are olfactory GPCRs, which can be mainly found in the sensory neurons of the olfactory system, where they facilitate the perception of odors and pheromones. The latter non-olfactory GPCRs have a diverse set of ligands to activate them ranging from ions, over small molecular chemical entities like hormones and peptides to proteins [2]. However, there is still a subset of 140 GPCRs with yet unidentified endogenous ligands, hence these orphan receptors could not yet be linked to a physiological function or pathophysiological process.

1.2 Architecture of GPCRs

All known GPCRs share the common architecture of seven membrane-spanning domains (TM1-7) connected with each other through three extracellular loops (ECL 1-3) and three intracellular loops (ICL 1-3). A disulphide bridge between ECL2 and TM3, and a cytoplasmatic α-helix (Hx8) parallel to the plasma membrane are further common properties. The extracellular N-terminal region (N-terminus) can vary in length among different GPCRs and constitutes a characteristic feature within specific GPCR families (see section about GPCR classification). GPCRs end after Hx8 at their intracellular C-terminal tail (C-terminus), which plays a role in receptor trafficking and is further involved in the interplay with signaling partners. The structure of the intracellular part is highly conserved among different GPCRs, whereas there is only a low degree of sequence conservation at the extracellular domains.

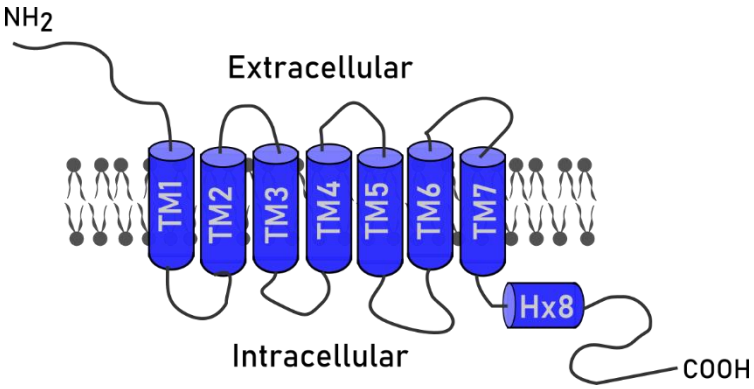

Figure 1.1 Two-dimensional scheme of a GPCR
GPCRs are embedded in the lipid bilayer of cellular membranes and constitute of an extracellular amino-terminus, seven transmembrane spanning helices (TM1-7), an intracellular helix 8 and a carboxy terminus. TM1-7 are connected via three extracellular (ECL1-3) and three intracellular (ICL1-3) loops.

The binding-site crevice is formed through the unique folding of the seven TM domains. This water-filled crevice, which is responsible for recognition and selective binding of the receptor's ligands, extends from the extracellular surface of the receptor into the membrane core. This orthosteric pocket is a dynamic cleft, which allows the engagement of diverse chemical molecules. Interactions such as salt-bridges, hydrogen bonds, dipole-dipole interactions between the ligand and the receptor lead to the conformational change necessary for the activation of the receptor. The interaction might additionally involve the extracellular N-terminus or extracellular membrane connecting loops [3].

1.3 GPCR activation

The essential task of GPCRs lies in receiving an extracellular stimulus, conferring it to the intracellular site and with this initiating a signaling cascade, which results in a distinct physiological outcome. The first step in GPCR-mediated signal transduction is the binding of a ligand, present in the extracellular fluid, to its binding site within the GPCR, thereby initiating the activation process. Recent structural studies of GPCRs deliver information about the different conformations a receptor can adopt. To this date, solved crystal structures largely fall into two classes: active or active-like states and inactive states. The active state shows a conformation in which the receptor is capable to interact with the G protein or other effectors, while the inactive state represents a conformation with an occluded G protein-binding surface [4].

Ligand binding to the extracellular-facing binding pocket facilitates the interaction with key amino acids of the receptor domains. The interactions of the ligand with the receptor trigger a global reorganization of the receptor structure, which is required for G protein binding. Ligand binding by itself, however, is insufficient to fully stabilize the active conformation of the entire receptor. Certain GPCRs exhibit unique mechanisms of interaction with their cognate ligands. The "light-receptor" rhodopsin for instance is special, since the inactive ligand is covalently bound to TM7 inside of the binding pocket. Retinal, one of the vitamin A compounds derived from carotenoids, is the photoactive moiety of rhodopsin, which captures light and converts the photons into chemical signals. Vision starts with the absorption of photons, which trigger the isomerization of the inactive 11-cis retinal to the all-trans state. Rhodopsin undergoes conformational changes resulting in the active-state metarhodopsin II [5].

Comparison of intracellular changes between active and inactive receptors reveals a high degree of structural conservation among all GPCRs, which suggests a common activation mechanism. Crystal structures of GPCRs provide valuable insights into movements of individual transmembrane helices. To this day, 62 unique receptors have been resolved in about 250 crystal structures [6] (annex Table 7.1). One limitation of crystal structures is that they reflect only a snapshot of a state the receptor is in and do not provide information about possible intermediate states the receptor undergoes in the course of activation. However, it is possible to compare the structures of the same receptor bound to different ligands or stabilized under different experimental conditions and subsequently conclude which structural rearrangements occur during the activation process [7]. The active state (agonist bound) and inactive state (antagonist bound) crystal structures of four different receptors (beta 1 adrenergic receptor β_2-AR, muscarinic acetylcholine receptor 2 mAChR2, μ-opioid receptor MOR, adenosine A_{2A} receptor) provide insight into the general activation mechanism of GPCRs [7-9]. Without exception, activation of GPCRs involves a rotation and outward movement of TM6 (typically between 8 and 17 Å), TM5 and 7 additionally rotate away from the receptor, all together breaking the so called ionic lock [10]. A highly conserved DRY/ERY motif is found at the intracellular end of TM3. Through intra- and interhelical interactions with TM6, it serves to constrain the receptor in an inactive state- the feature termed as ionic lock [4, 11]. The rearrangement of the helices affects the position of the connecting loops, all together leading to the opening of a cavity on the intracellular site to accommodate the G protein.

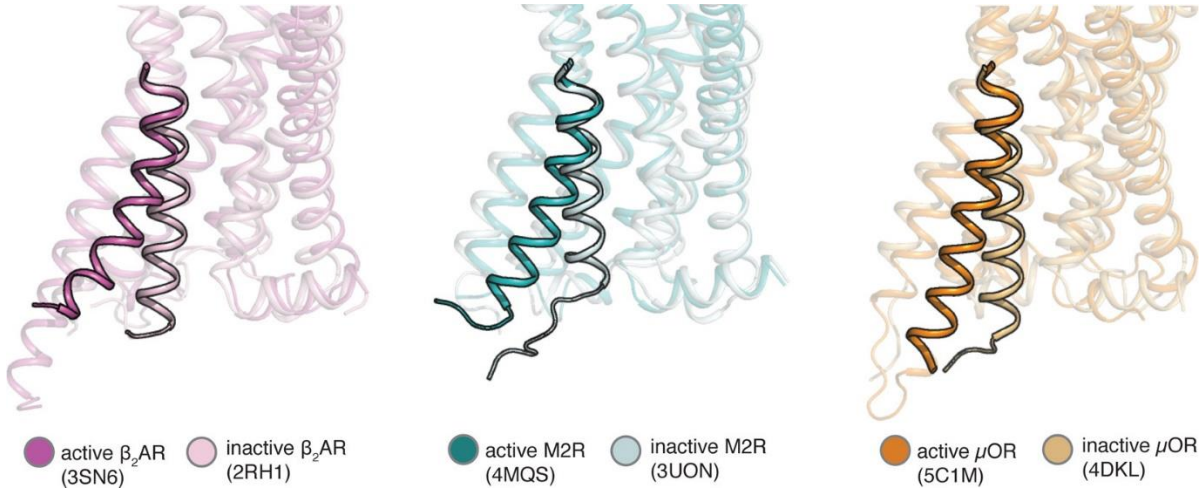

Figure 1.2 Conformational changes in GPCRs upon activation
Crystal structures of three class A GPCRs depicted in the inactive and active conformation reveal a similar pronounced outward movement of TM6 (highlighted) involved in the activation process. β_2AR- β_2-adrenergic receptor, M2R- muscarinic acetylcholine receptor, μOR- μ-opioid receptor (image taken from [12] with permission from the American Chemical Society (ACS); further permission related to the material excerpted should be directed to the ACS https://pubs.acs.org/doi/full/10.1021/acs.chemrev.6b00177#showFigures)

Opposed to former views which described GPCRs as simple bimodal switches, transitioning from the inactive directly to the active state, there is a growing body of evidence showing that the receptors exist in different conformations with energetics that can be influenced by ligands, cytosolic proteins, pH, ions and possibly transmembrane voltage gradients [13]. Application of biophysical methods to study protein structure and dynamics such as crystallography, NMR spectroscopy, fluorescence- and EPR spectroscopy have helped to exemplify that receptors can adopt multiple, functionally distinct conformations [12, 14].

The kinetics behind receptor activation are another important aspect of GPCR signaling being thoroughly studied by the scientific community. Rhodopsin is the prime example to understand the mechanism and kinetics of receptor activation. It has been studied extensively due to its easy accessibility and synchronous activation by a pulse of light. Various biophysical techniques made it easy to optically analyze rhodopsin activation. A time constant of 1.9 milliseconds (ms) has been measured for the movement of TM6 throughout the activation process of rhodopsin [15]. However, conformational rearrangements in other class A GPCRs occur in the range of 30-50 ms [16], and even longer time frames were reported for some class B receptors [17, 18]. This discrepancy compared to rhodopsin can either be attributed to rhodopsin's exemplary function as a sensor for fast light stimuli, or be due to technical limitations in the speed of ligand delivery when studying non-rhodopsin GPCRs. While rhodopsin activation is triggered by a short light pulse, cells expressing other GPCRs need to be superfused with ligand-containing media, where the diffusion speed limits its availability directly at the binding pocket. New approaches such as ligand caging, photoswitching or tethering of ligands to GPCRs are emerging in order to overcome such technical obstacles and be able to study pure activation kinetics.

1.4 GPCR classification

There are two common systems used to classify GPCRs into different groups. The more commonly used system is based on the amino-acid sequence and functional similarities and divides all GPCRs from vertebrates and invertebrates into 7 groups A-F [19, 20] (See Table 1.1).

Class	Attribution
A	Rhodopsin-like family
B	Secretin receptor family
C	Metabotropic glutamate family, GABA receptors, calcium-sensing receptors, taste receptors
D	Fungal mating pheromone receptors
E	Cyclic AMP receptors
F	Frizzled/smoothened receptors

Table 1.1 Classification of GPCRs based on sequence homology and functionality

The second, less common classification system set up by Fredriksson *et* al. [21], is based on the phylogenetic study of the entire mammalian GPCR-encoding genome. Referred to as the GRAFS classification, the members within each group share a common evolutionary origin (See Table 1.2). In the further course of this work, the classification system based on homology and functionality will be employed.

Class	Attribution
G	Glutamate family
R	Rhodopsin family
A	Adhesion family
F	Frizzled/Taste2 family
S	Secretin family

Table 1.2 Classification of GPCRs based on phylogenetic studies

The following paragraphs will describe class-specific features of the different GPCR families.

1.4.1 Class A GPCRs

This is by far the largest group with over 700 individual proteins, including rhodopsin, the adrenergic receptors and the olfactory subgroup. Although the olfactory receptors constitute most of the group, there are almost 200 non-olfactory GPCRs with their 80 known ligands which have already been functionally characterized [22]. Rhodopsin, after which the group has been named, is the most extensively studied GPCR since its discovery. Its amino-acid sequence was disclosed in the 1980ies, and its crystal structure was the first to be solved [23]. Ever since, various groups embarked on structural studies of different GPCRs, giving us insight into activation mechanisms and deepening our understanding of this class of proteins. The first high-resolution crystal structures soon followed [24, 25], and new structures of active, inactive, G protein- or Nanobody (Nb)-bound GPCRs are being disclosed ever since.

1.4.2 Class B GPCRs

Class B, also known as the secretin family, comprises 15 members, encoded by 15 genes. Their ligands are polypeptide hormones. Structurally, class B GPCRs consist of a large N-terminal domain, which seems to be essential for ligand recognition and binding [26]. In contrast to class A GPCRs, which bind their ligand within the transmembrane region [27], a two-step binding mechanism is proposed for class B GPCRs. The ligand is recognized by the long extracellular N-terminus together with the extracellular loops and additionally interacts with residues deep in the helical bundle [28].

1.4.3 Class C GPCRs

This class, referred to as the glutamate receptor family, is encoded by 22 genes of the human genome and contains receptors for the two main neurotransmitters glutamate and γ-aminobutyric acid (GABA), as well as for Ca^{2+}. Similar to the secretin family, class C GPCRs possess a large extracellular domain, which is responsible for ligand recognition. These receptors have a unique activation mode by which they occur as constitutive homo- or heterodimers (i.e. a complex of two identical or different GPCRs) [29].

1.4.4 Class F GPCRs

Also termed Frizzled/Taste2, this family consists of 10 Frizzled proteins (FZD1-10) and smoothened (SMO). The FZDs are activated by 19 unique type of ligands, the secreted lipoglycoprotein growth factors of the WNT family, whereas SMO is indirectly activated by the Hedgehog proteins (HH). FZD receptors are able to signal via the transcription regulator β-catenin (canonical FZD/WNT signaling), in addition to a β-catenin independent, G protein-dependent pathway [30, 31].

1.4.5 Adhesion GPCRs

This family comprises 33 members in humans, which are phylogenetically linked to the secretin like family. A large extracellular N-terminus is not unique to this class but is present in all members. Special in this family is a GPCR proteolysis site (GPS) in close proximity of the membrane, within the highly conserved GPCR autoproteolysis-inducing (GAIN) domain. This domain facilitates an autocatalytic process resulting in the extracellular N-terminal fragment being noncovalently associated with the 7TM/cytoplasmatic C-terminal fragment. The family owes its name to its function as it facilitates cell adhesion, orientation and migration [32].
Despite being widely expressed and remarkable phenotypes are associated with receptor dysfunction, adhesion GPCRs remained "functional orphans" for a long time. Yet, over the past years, several interacting partners have been described. This leads to the notion that these receptors mainly interact with cellular and matricellular ligands, in contrast to other GPCR classes that interact with small molecules or peptides as ligands [33].

1.5 GPCR signaling

Major conformational rearrangements occur within the 7TM helices of a GPCR when its ligand binds, and it transitions from an inactive to an active state. This rearrangement also translates to the cytoplasmatic site, opening up a space for the engagement of interaction partners such as G proteins, G protein-coupled receptor kinases (GRKs) and β-arrestins which can all couple to the receptor and translate the extracellular stimulus to a distinct cellular signal [22].

1.5.1 G protein mediated GPCR signaling

The heterotrimeric guanine nucleotide-binding proteins (G proteins) act as a switch which connect the cell surface receptors to a variety of effectors and by this regulate the processing of information [34, 35]. 35 human genes encode the heterotrimeric G protein which consists of an α-, β- and a γ-subunit. The separate α-subunit is responsible for GTP and GDP binding and for GTP hydrolysis, whereas the β- and γ-subunits are tightly associated and exert different functions. G proteins are referred to by their α-subunit. According to their specific effector proteins, four major Gα families are recognized: $G\alpha_S$, $G\alpha_{i/o}$, $G\alpha_{q/11}$, $G\alpha_{12/13}$ (See Table 1.3) [22, 36].

Gα class	Effector proteins	Signaling effect
G_S	Adenylyl cyclases (ACs)	Activation of ACs; increase of intracellular cAMP production
$G_{i/o}$	Adenylyl cyclases, G protein-coupled inwardly rectifying potassium (GIRK) channels	Inhibition of ACs; decrease of intracellular cAMP production. Opening of GIRK channels.
$G_{q/11}$	Phospholipase Cβ	Activation of PLCβ, production of DAG and IP_3, release of Ca^{2+} from intracellular stores
$G_{12/13}$	Rho guanine-nucleotide exchange factors (GEFs)	Regulation of intracellular kinase activity

Table 1.3 Gα protein classification, effector proteins and intracellular effects

Both $G\alpha_S$ and $G\alpha_i$ regulate membrane embedded ACs. While $G\alpha_S$ activates, $G\alpha_i$ inhibits the AC to convert ATP into the second messenger cyclic adenosine monophosphate (cAMP) [37]. The result is either an increase or a decrease of intracellular cAMP production. The $G\alpha_{q/11}$-family activates the β-isoforms of phospholipase C (PLC-β1-4), which cleave phosphatidylinositol-4,5-bisphosphate (PIP_2) into inositol trisphosphate (IP_3) and membrane-bound diacylglycerol (DAG). IP_3 opens a calcium-channel in the membrane of the endoplasmatic reticulum, and DAG activates protein kinase C (PKC) [38].
$G\alpha_{12/13}$ is known to regulate the GTPase RhoA which controls a variety of processes such as cell shape, morphology and proliferation [39].
The counterpart Gβγ is also capable of activating downstream effectors. Acting as one functional entity, it regulates ACs, PLCβ, inwardly rectifying potassium channels (GIRKs) as well as voltage-gated Ca^{2+}-channels and mitogen activated protein (MAP)-kinases [40].

G-Proteins function in a GTPase cycle (Figure 1.3). In the inactive, GDP-bound state the Gα-subunit is tightly bound to the βγ-subunit. Upon agonist binding to a GPCR, the G protein is recruited and activated. GPCRs act as guanine nucleotide exchange factors (GEFs) whereby they open an exit pathway and promote the release of GDP from Gα. GTP engages the nucleotide binding site which leads to the dissociation of Gβγ. Both GTP-bound Gα and Gβγ can initiate a signal by interacting with downstream effector proteins. The guanine-nucleotide binding site within the Gα subunit is encompassed by two domains: a Ras-like GTPase domain and an α-helical domain. Termination of the Gα-subunit signaling occurs due to the intrinsic GTPase activity of Gα, which hydrolyzes the bound GTP to GDP. Gβγ-signaling is terminated by the re-association with Gα-GDP. Regulators of G protein signaling (RGS) proteins can dramatically enhance the rate of GTP hydrolysis, since they serve as GTPase accelerating proteins (GAPs) for Gα. This whole process represents one G-protein cycle [41-43].

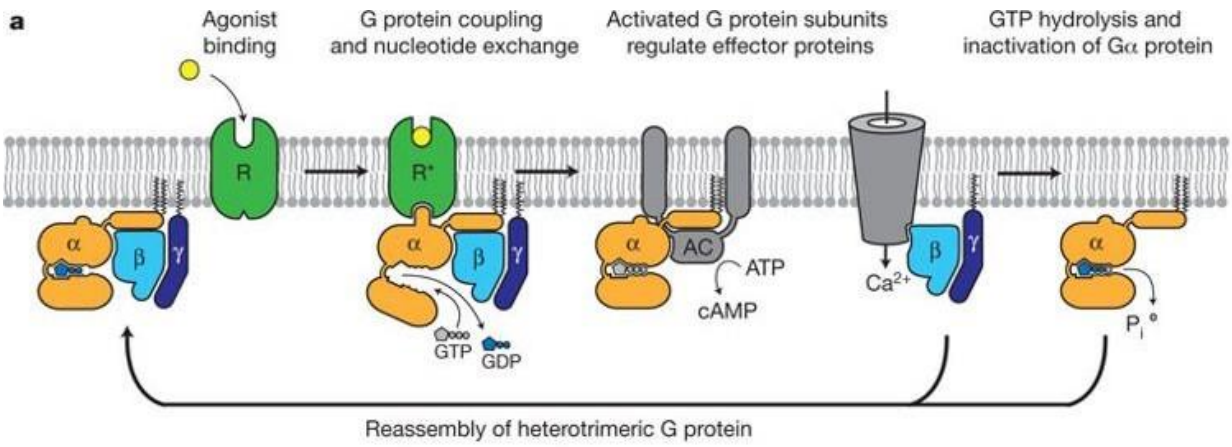

Figure 1.3 G protein-cycle for a GPCR-G protein complex
Agonist binding leads to the recruitment of the heterotrimeric G protein. GDP is released from the α-subunit upon formation of receptor-G protein complex. GTP binding results in dissociation of the α- and βγ-subunits from the receptor, upon which they can regulate their respective effector proteins (G_S protein activates ACs through the α-subunit and Ca^{2+}-channels through the βγ-subunits). The G_S heterotrimer reassembles following hydrolysis of GTP to GDP within the α-subunit (extracted and modified from [8] with permission from Springer Nature; license number: 4564730845716).

It is assumed that an active GPCR can bind only one heterotrimeric G protein at a time. However, the agonist-mediated signal can be amplified through rapid dissociation of the activated bound G protein to make space for subsequent coupling of GDP-bound G proteins to the active receptor, starting a new cycle. This demonstrates that after occupation of a small fraction of receptors with agonist, this fraction of activated receptors is able to interact with a much greater number of G proteins [44].

The dynamics of GPCR-G protein interaction and the role GPCR agonists play is a matter of strong discussion, with controversial models being postulated to describe the underlying mechanisms. The classical model postulated by Tolkovsky and Levitzki [45] implies that GPCRs, the G protein and ACs are freely mobile molecules which can interact randomly by “collision coupling”. Hein *et* al. [44], which support the collision coupling model, find that ligand-free GPCRs and their cognate G proteins localize in distinct spots on the plasma membrane but are not pre-coupled. Ligand binding to the receptors and their activation can trigger the association of GPCRs and G proteins. They draw evidence from the fact that the interaction kinetics between both partners depend on the amount of Gα in the cell. If receptors and G proteins were pre-coupled, the kinetics should be independent of G protein levels.

The contradicting model of pre-coupled GPCRs with G proteins postulates the existence of preassembled complexes between receptors and G proteins in the absence of agonist stimulation, which undergo a conformational rearrangement upon ligand binding and receptor activation [46].
Both models agree that receptor ligand binding is crucial for G protein-activation and triggering the intracellular signaling cascade.

Sungkaworn *et* al. have studied the interaction between G proteins and GPCRs by simultaneously recording the single molecule trajectories of fluorescently tagged G proteins and GPCRs.

Their findings complement both models, as they describe both short- (lifetime 1-2s) and long-lived (lifetime > 4s) complexes in so called hot-spots where both receptors and G proteins are concentrated, however with no agonist being present. They hypothesize that this complex organization increases the speed and efficiency of receptor-G protein-coupling since it can occur in a restricted area [47].

Recently emerged cryo-EM and crystal structures of receptors in complex with their cognate G proteins, such as the β_2-AR [8], adenosine A_{2A}-receptor [7] both class A GPCRs, as well as 2 representatives of class B GPCRs- the human glucagon-like peptide 1 (hGLP1R) [48] and the calitonin gene-related peptide receptor [49] have helped to understand which conformational changes occur when the G proteins binds to the GPCR and which residues interact to facilitate signaling. The active state of the receptor is stabilized by extensive interactions with $G\alpha_S$. The C-terminal α-5 helix of $G\alpha_S$ is one of the best studied regions in G proteins. The interface of interaction is formed by ICL2 and 3, TM3, TM5 and TM6 of the receptor and the α5-helix of $G\alpha_S$. There are no direct interactions with Gβγ. The receptor-mediated conformational changes within the α5-helix transmitted to the nucleotide binding site promote GDP dissociation. This highlights a conserved interaction mechanism among class A and B GPCRs [50].

Although it is known that different receptors can couple to the same Gα protein it is not entirely clear how coupling selectivity is achieved. The analysis of the Gα-bound crystal structure of the β_2-AR and the A_{2A}R resulted in the identification of 25 GCN positions (common Gα numbering) within Gα which contact the receptor. In contrast, there are subtype specific Gα-residues, which surround the conserved residues at the receptor-G protein, interface. The conserved positions would indicate that the binding orientation of the receptor with Gα is similar among different receptor-Gα complexes, while the subtype specific residues could constitute a "selectivity barcode" that ensure selective binding of the receptor to a certain Gα protein. This way, a unique combination of residues around a conserved interface is presented by each of the 16 different Gα paralogs, which determines the selectivity. Additionally, helix 5 of different Gα subtypes might rotate differently at the receptor-G protein interface. Additional residues may be exposed which could contribute to the selectivity barcode. In other words, the same selectivity barcode presented by Gα is read differently by receptors belonging to different subtypes [51].

1.5.2 Arrestin-mediated signaling & internalization

Cellular signaling is a complex process to coordinate which has necessitated the evolution of scaffold proteins whose role is to control the activity of cellular processes driven by receptors, enzymes or channels. GPCRs are able to signal in a G protein independent manner, interacting with a second family of effector proteins that act at the same time as scaffolding proteins- the arrestins [52]. Robert Lefkowitz and Brian Kobilka were awarded with the Noble Prize in Chemistry for their work on GPCRs and the two main families of proteins which regulate them- namely GRKs and β-arrestins. Four members of the arrestin family exist: visual arrestin (arrestin1) [53] and cone arrestin (arrestin4) [54] expressed almost exclusively in the retina, and two non-visual arrestins, β-arrestin1 (arrestin2) and β-arrestin2 (arrestin3). They all belong to a superfamily of structurally and functionally related scaffolding proteins. β-Arrestins are able to interact and modulate the function of several hundreds of activated heptahelical receptors. Depending on the cell type, arrestins are distributed in the cytosol, are bound to the cytoskeleton, localize at endosomes or inside the nucleus. They are integral to the control of cell metabolism, division, motility and crosstalk where they provide highly specific signal integration.

Common to all arrestins is their structural organization into two β-strand sandwich structures, termed the N- and C-domains. These form two baskets connected by a short hinge domain. This gives

rise to the central crest, composed of the finger loop, the middle loop and the C-loop all being key receptor binding motifs [55-57]. The interface of the N- and C-domains is stabilized by hydrophobic interactions and a network of hydrogen bonds which includes the polar core, a network of buried charged residues [58].

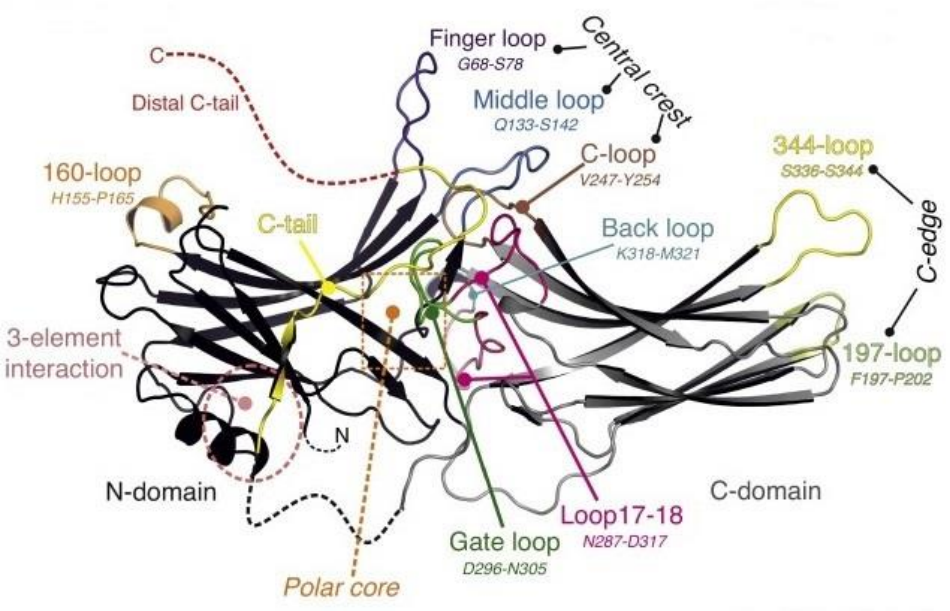

Figure 1.4 General structure of arrestins
The N-domain is depicted in black, the C-domain in grey. Loops are indicated in different colours, the residue numbers refer to bovine arrestin-1. The parts which are not resolved in the crystal structure are shown as dashed lines. The structure model is based on the crystal structure published by Hirsch *et* al. [58] (image taken from Scheerer and Sommer [57] with permission according to the creative commons license http://dx.doi.org/10.1016/j.sbi.2017.05.001)

For arrestins to interact with activated GPCRs, the receptors need to be phosphorylated first. G protein-coupled receptor kinases (GRKs) promote this phosphorylation on serine or threonine residues within the C-terminus or ICL3, creating high-affinity arrestin binding sites [59]. There are seven known GRK isoforms, each capable of imprinting a unique phosphorylation pattern onto the receptor, which in turn enhances β-arrestin affinity to the GPCR and favours a certain arrangement [60, 61]. β-arrestin-binding stabilizes a high agonist affinity state of the receptor, similar to the complex existing between agonist, receptor and heterotrimeric G protein in the absence of GTP [62, 63].

Characteristic conformational changes within the arrestin structure commence upon recruitment to the receptor and interaction with phosphates as a critical first step. Key features of the arrestin activation include breaking of the polar core, accompanied by a movement of the gate loop. The following 21˚ rotation of the N- and C-domain relative to one another opens up a crevice at the base of the finger loop. These structural modifications increase the flexibility of the finger-loop motif, key region for receptor interaction, resulting in the engagement with the cytoplasmatic phosphorylated receptor interface [57, 64, 65].

Receptor-arrestin interaction is often discussed as a two-step interaction process, upon which two different GPCR-arrestin complexes can be formed. This is of high interest, since these complexes are associated with a differential signaling outcome. An initial low-affinity pre-complex is formed when the phosphorylated receptor C-terminus repels the arrestin C-tail to gain access to basic residues in the N-domain resulting in the “tail”-complex. This displacement induces conformational changes and afore mentioned domain movements within arrestin, which expose the polar core and allow the second binding step to form a high affinity complex, also termed as the “core”-complex [66, 67]. Various lines of evidence suggest that the core complex blocks G protein recruitment and is therefore crucial for mediating receptor desensitization within a timeframe of seconds to minutes [68-71]. On the other hand, the more loose tail-interaction leads to receptor internalization but not desensitization [68]. Receptor desensitization i.e. the reduced responsiveness of a GPCR to an agonist with time, is a physiological feedback mechanism important to protect against receptor overstimulation [72].

In comparison to the relatively fast receptor desensitization, internalization triggered by arrestin-recruitment occurs on the timescale of minutes upon GPCR stimulation [65]. β-Arrestins act as adaptors that link the receptors to clathrin-coated pits. β-Arrestins interact with clathrin itself and the β2-adaptin subunit of the AP-2 complex [73]. Soon afterwards, the receptor alone or together with β-arrestin internalizes to endosomes in a dynamin-dependent manner [74, 75]. From these intracellular compartments, receptors are either dephosphorylated and recycled back to the surface, initiate signaling or are degraded [76-78].

In addition to their role in receptor desensitization, β-arrestins have additional functions as adaptor proteins which facilitate the activation of the mitogen-activated protein (MAP) cascades, receptor de-/ubiquitination, NFκB signaling and targeting of effectors to certain subcellular locations [52, 79-82].

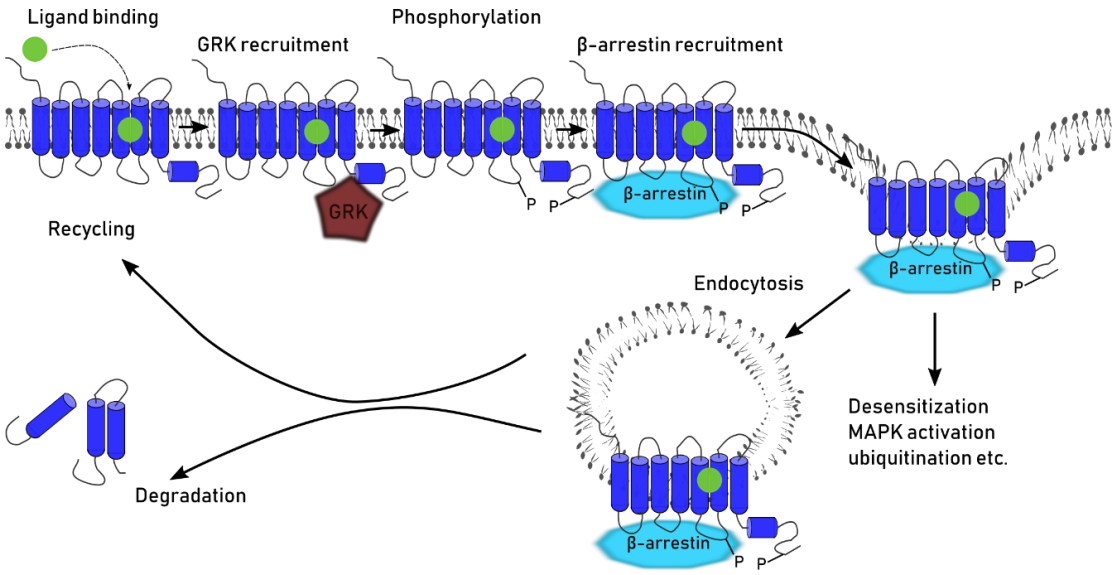

Figure 1.5 GPCR regulation by β-arrestins
After ligand binding, GRKs can phosphorylate specific receptor residues leading to β-arrestin recruitment. The GPCR-β-arrestin complex is internalized via clathrin-coated pits into intracellular compartments from where the receptor can signal, be degraded or get trafficked back to the membrane.

1.5.3 GPCR signaling from endosomal compartments

The paradigm that GPCR activation and signaling is restricted to the plasma membrane has been challenged by several groups in recent years. Several lines of evidence show that generation of second messengers and signaling cascades can persist when the receptor is internalized. It has been shown for different GPCRs such as the thyroid stimulating hormone (TSH) receptor [78], the parathyroid hormone (PTH) receptor [83] as well as the sphingosine-1-phosphate (S1P) receptor 1 [84]. These findings triggered deeper investigations questioning the classical model of receptor signaling [85, 86].
Taking it one step further, Thomsen *et* al. [87] set out to test the hypothesis of "megaplexes" by using a variety of cellular, biochemical and biophysical approaches. They were able to show that both G_S and β-arrestin can simultaneously interact with the receptor, providing the molecular basis for sustained G protein-signaling by GPCRs from endosomes.
Moreover, the biological relevance of endosomal GPCR signaling has been proven for two different receptors, which regulate hormone function and gene transcription. The internalized hGLP1R stimulates insulin secretion from pancreatic β-cells [88], and a second wave of cAMP production from internalized LH-receptors is responsible for mediating the biological effects of the luteinizing hormone [89].
Keeping this in mind, these observations suggest that there are many aspects of GPCRs yet to be unraveled, and traditional, well-accepted ideas should be thoroughly scrutinized.

1.5.4 Receptor desensitization

Proper signaling of GPCRs is essential for cells to function. However, continued signaling or overstimulation of receptors can be detrimental to the survival of cells or may lead to uncontrolled proliferation as in cancer. Therefore, healthy cells are able to blunt or desensitize GPCR signaling either transiently or over a longer period of time in order to maintain normal physiology [90]. The response of a GPCR to its ligand peaks within milliseconds to a few minutes, plateaus and then declines even if the agonist-receptor complex persists [91]. Furthermore, a decreased response is observed upon repeated stimulation of a GPCR in comparison to the initial response. This phenomenon of desensitization limits the repeated activation of GPCRs. A desensitized receptor can persist at the membrane surface, while it becomes refractory to repeated stimuli, or it is internalized and degraded. The response of GPCRs, exposed to their ligands over a period of many minutes, hours or days, is reduced due to the decreased receptor expression at the membrane. The downregulation of receptors is a longer term process (over tens of minutes to hours) associated with receptor internalization into vesicles and trafficking or degradation in lysosomes [92]. This regulation of GPCRs on the short term with transducer uncoupling or on the long term by receptor downregulation is a process which involves G proteins, GRKs, β-arrestins and downstream effectors [90].

There are two parallel mechanisms which drive receptor desensitization as reported in studies investigating the desensitization of the β_2-AR [93]. Homologous desensitization occurs following direct stimulation of the receptor with an agonist, by controlling the number of receptors on the plasma membrane or by regulating the efficacy of the receptors at the cell surface. The consequence is a loss of response to subsequent agonist stimulation. Heterologous desensitization in contrast, is a regulatory mechanism independent of receptor activation which can depend on effects further downstream [72]. The most rapid mechanism by which GPCRs are desensitized, is through phosphorylation by GRKs or second messenger kinases which leads to uncoupling from the G protein and β-arrestin recruitment [94]. But also the internalization to intramembranous compartments and trafficking or degradation play a considerable role [74].

1.6 GPCRs as drug targets

Since GPCRs regulate very diverse physiological processes, they have been of long-standing interest as pharmacological targets. The wide utility of GPCRs as drug targets is due to their interaction with a variety of chemical molecules as ligands and their expression at the plasma membrane making them well accessible for various pharmaceuticals. GPCRs regulate a wide array of intracellular signaling pathways, giving them a central role in the regulation of physiological processes. Mal-regulation and mal-function is prone to lead to various diseases, making GPCRs a useful target for intervention and restoration. By 2018, 134 GPCRs were identified as targets for approved drugs. Estimations based on data from different databases (ChEMBL, Guide to Pharmacology, Drugbank) state that approximately 700 approved drugs target GPCRs, constituting 35% of globally marketed drugs [95, 96]. With this, GPCRs are the family of protein most frequently targeted by approved drugs.

Hauser *et* al. report about 321 agents in clinical trials of which 60 (19%) target GPCRs for which no clinical treatment was available by 2017 [1].

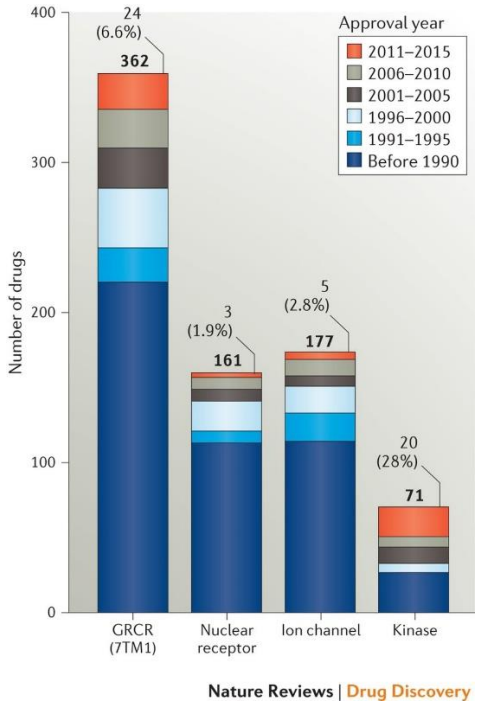

Figure 1.6 Drug approvals in four major target families
Most novel drugs approved between 2011 and 2015 target GPCRs (24 new chemical entities) stating the importance of GPCRs in drug discovery and development (extracted from [96] with permission from Springer Nature; license number 4578631425812).

1.7 Glucagon-like peptide 1 receptor (GLP1R)

The GLP1R belongs to class B of GPCRs. It mediates the action of the peptide hormone GLP1. The following section will deal with all important aspects of GLP1R-signaling [97].

1.7.1 Structural characteristics

The first cDNA for human GLP1R (hGLP1R) from pancreatic β-cells was cloned in 1993 [98] and showed a sequence of 463 residues. Its sequence resembled that of secretin, parathyroid hormone and calcitonin receptor and was therefore classified together with them within the class B GPCR family [99].

GLP1R is widely expressed in the pancreas, lung, brain, stomach, kidney and heart where it is described to confer cardio-protective effects, however it is not found in tissues involved in glucose metabolisms such as the liver, skeletal muscle and fat [100].

The GLP1R is a glycoprotein with an N-terminal signal peptide, containing various glycosylation sites, which are essential for the correct trafficking of the receptor [98, 101]. Similar to all other class B GPCRs, the GLP1R exhibits a long N-terminal domain of 143 residues, which was first separately crystallized and analyzed using X-ray diffraction. It has a critical role in ligand recognition and binding and contains two regions of antiparallel β-sheets, three disulfide bonds and an N-terminal α-helix [102]. The full-length rabbit GLP1R (sharing 92% identity with hGLP1R) has only recently been solved in an activated form in complex with the G_S protein using cryo-electron microscopy (EM) with a global resolution of 4.1 Å [48] (See Figure 1.7). The agonist GLP1 is stably anchored in its position by interacting with TM1, 2, 5, 7 ECL 1, 2 and the NTD. As mentioned above, the C-terminal domain of the peptidic agonist interacts with the receptor's long N-terminus. It is suggested that in the absence of ligand the receptor NTD is mobile to increase the probability of the initial recruiting interactions with the C terminus of GLP1. After the primary high-affinity binding of the C-terminus to the receptor NTD, the N-terminus of GLP1 penetrates into the receptor core, to a depth comparable to agonist BI-167107 in the structure of activated β_2-AR [8].

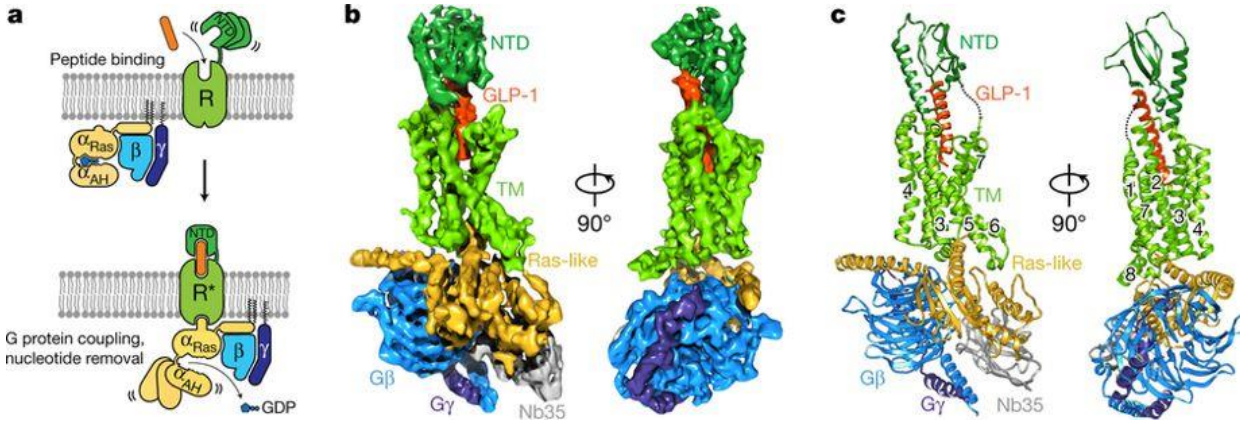

Figure 1.7 Cryo-EM structure of hGLP1-rabbit GLP1R-Gs complex
(a) Schematic of the two-domain binding mechanism typical for class B GPCRs. AH; α-helical domain. (b) Views of the GLP1R-Gs complex cryo-EM density map (transmembrane domains are light green, NTD in dark green, GLP1 in orange, $G\alpha_S$ Ras-like in gold, Gβ in light blue, Gγ in dark blue, Nb35 in grey). (c) Structure of the activated GLP1R-G_S complex in the same view and colour as in (b).
(extracted from [48] with permission from Springer Nature; license number: 4578780586672)

When the active GLP1R structure is compared to the inactive class B glucagon receptor (GCGR) (see Figure 1.8) as a reference to study the structural changes occurring during class B GPCR activation, the results show that in the extracellular half of the receptor, TM7 bends towards TM6. In the active GLP1R complex, TM6 moves outwards to allow interaction between the peptide N-terminus and the transmembrane domain binding pocket. The most profound change in the intracellular site is observed at TM6 which moves outwards by approximately 18 Å. This movement in association with the more limited shift of TM5 opens a cavity together with TM2, 3, 7 to which the Ras-like domain of $G\alpha_S$ can bind. In addition, Gβ interacts with ICL1 and α-helix 8 which is tilted towards the G-protein.

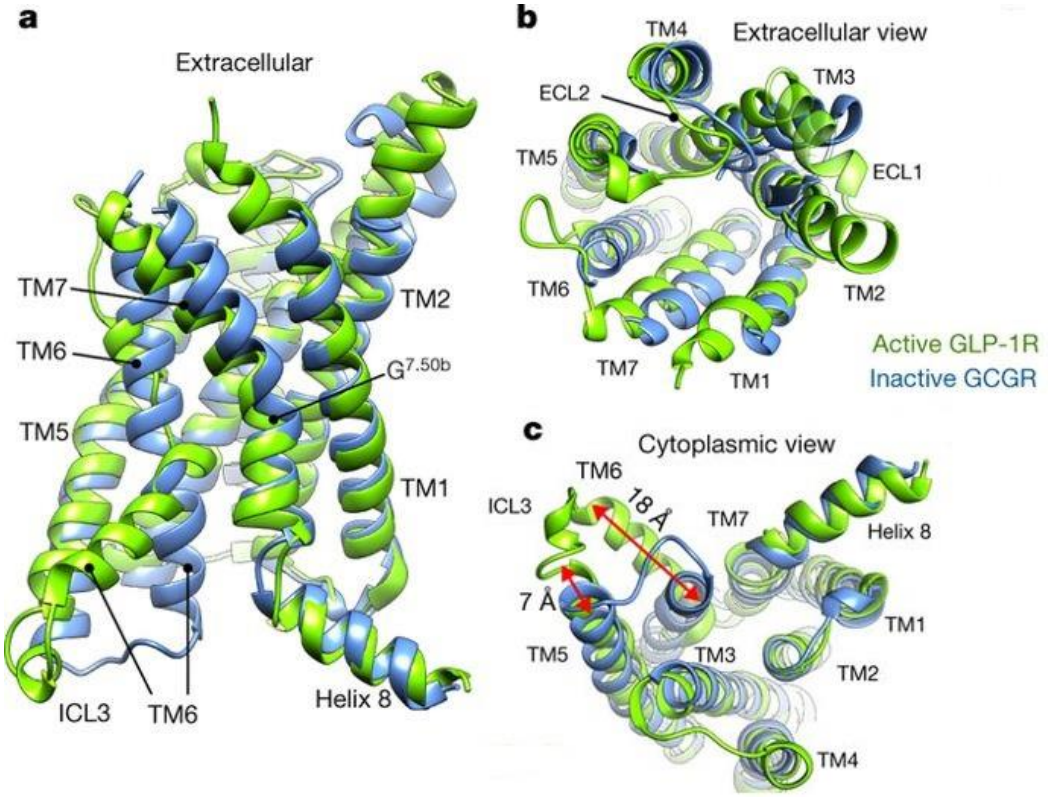

Figure 1.8 Comparison of active GLP1R with inactive GCGR
(a) Side, (b) extracellular and (c) cytoplasmatic views of the activated GLP1R (light green) superimposed to the inactive GCGR (blue) bound to an allosteric antagonist (not shown). Major conformational changes are observed within TM5 and TM6 on the cytoplasmatic site. On the extracellular site, TM2 of the GLP1R is extended by three helical turns, stabilized by the peptide ligand binding (extracted and modified from [48] with permission from Springer Nature; license number: 4601850358591)

The comparison of the active GLP1R structure with class A β_2-AR crystal structure (Figure 1.9) reveals that the G protein conformation is almost identical in both cases. Further, the global conformation of the 7TM helices is similar, with the difference of the longer α-helical extension of TM2 in GLP1R leading to the elevation of ECL1 that engages the bound peptide. Yet, even though the structural landscape is very comparable between active GLP1R and β_2-AR, the molecular details of the recognition pattern on the receptor are very diverse. The configurational flexibility of the α5-helix of G_S enables the formation of diverse interactions through the same C-terminal amino acids.

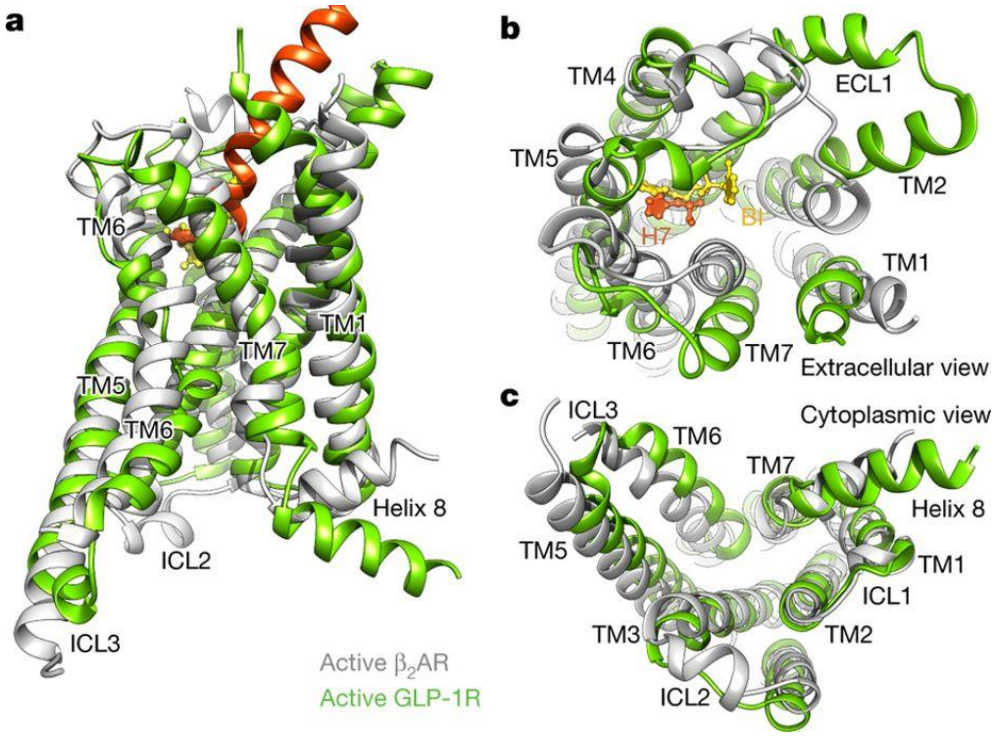

Figure 1.9 Comparison between active class A and B receptor crystal structures
(a) Side, (b) extracellular and (c) cytoplasmatic views of the activated GLP1R (light green, GLP1 in orange) superposed with the active β_2-AR (grey) bound to orthosteric agonist BI-167107 (extracted from [48] with permission from Springer Nature; license number: 4601850358591)

1.7.2 Physiological role

Glucose homeostasis is maintained by the insulinotropic activity of GLP1 which is strictly glucose-dependent and is mediated through the GLP1R expressed in pancreatic β-cells [103]. Glucose entering the β-cell through glucose transporter type 2 (GLUT-2) is converted (pyruvate as intermediate) to ATP. The increased ATP closes K_{ATP} channels, leading to depolarization of the membrane and increasing calcium influx. Thereupon calcium is released from intracellular stores through calcium-induced calcium release (CICR) [104], stimulating the exocytosis of the insulin secretory granules. GLP1R-signaling enhances glucose-dependent insulin secretion. Binding of GLP1 to its receptor leads to the recruitment of the G_S-protein, which in turns activates ACs to produce cAMP. The increased cAMP level leads to the activation of PKA and Epac2. PKA phosphorylates the sulfonylurea (SUR1) subunit of the K_{ATP} channels, which close and depolarize the membrane further. Epac2 additionally inhibits K_{ATP} by increasing their sensitivity to ATP [105]. Increased intracellular Ca^{2+} together with cAMP facilitates the exocytosis of insulin carrying vesicles [106, 107]. GLP1 additionally lowers blood glucose levels by suppressing the secretion of the hyperglycemic hormone glucagon from pancreatic α-cells [108]. Since the insulinotropic effect of GLP1 is highly glucose dependent, excessive GLP1 secretion or sensitivity will not lead to hypoglycemia [97].

Further physiological functions of GLP1 include the inhibition of gut motility and gastric emptying [109] together with the suppression of appetite and food intake. GLP1 is already marketed as an antidiabetic

drug, yet it is under investigation as it may additionally have therapeutic value for body weight reduction [110].

1.7.3 Endogenous agonist- glucagone-like peptide 1

GLP1 is a peptidic incretin hormone secreted from three tissues in humans: enteroendocrine L-cells in the intestine, pancreatic α-cells and the central nervous system (CNS) [111], exerting its function via the GLP1R. Incretin hormones are secreted upon oral glucose administration and potentiate insulin secretion in the presence of high plasma glucose levels. Endogenous GLP1, derived from preproglucagon by differential posttranslational processing, exists in two forms: GLP1-(7-36)-NH2 and non-amidated GLP1-(7-37) [112]. Both exhibit similar biological activities, although the amide form has a slightly improved stability [113]. GLP1 is rapidly inactivated in the circulation by the ubiquitous proteolytic enzyme dipeptidyl peptidase-4 (DPP-4), giving it a very short half-life of less than 2 minutes [114]

Pharmacological studies trying to solve the crystal structure of the ligand-bound ECD of hGLP1R, or the whole 7TM receptor proposed a two-domain binding mechanism of the peptide hormone ligand to secretin class B GPCRs [28, 115]. According to this mechanism, the α-helical C-terminus of the ligand forms an initial complex with the long N-terminal ECD of the receptor which then allows the peptide N-terminus to interact with the 7TM domain of the receptor to activate it. N-terminal truncation of the peptide leads to a decrease in affinity for the hGLP1R, suggesting that the interaction with both ECD and 7TM domains are important for GLP1 binding. The marketed GLP1 mimetic exendin-4 [116] and the antagonist exendin 9-39 derived from it have similar affinities for hGLP1R [115, 117].

1.7.4 GLP1 mimetics & other agonists

Due to the important role of GLP1 and GLP1R in maintaining glucose homeostasis, several peptidic- and small molecule agonists have been developed lately. All for the potential application in the treatment of diabetes, obesity and associated metabolic or cardiovascular diseases. The drawback of peptides as clinical drugs is their parenteral administration, due to the instability in the digestive track. Technological advancement has led to the development of subcutaneously (s.c.) administrable drugs, which improves the compliance of patients already [118]. However, small molecule agonists are always favoured in clinical therapy, due to their simple oral application. There are small nonpeptidic GLP1R-agonists available, although it is still challenging to make them adequately potent and bioavailable [119].

1.7.4.1 Peptidic GLP1-analogs

Several peptidic analogs are by now marketed drugs, exhibiting an improved half-life and/or protected from DPP-4 degradation. The first approved GLP1R agonist by the FDA was Exenatide (exendin-4) in 2005 [120]. Exendin-4 was isolated from the salivary glands of the gila monster (Heloderma suspectum). It is a 39-amino acid peptide, which shares 50% sequence identity with hGLP1 and was found to be highly active on hGLP1R. Other GLP1R agonists are listed in Table 1.4.

Analog	Description	Dosing regimen	Administration
Liraglutide	GLP1 analog linked to a fatty acid	Once daily	s.c.
Albiglutide	GLP1 analog fused to albumin	Once weekly	s.c.
Dulaglutide	GLP1 analog fused to Fc	Once weekly	s.c.
Semaglutide	GLP1 analog linked to a fatty acid	Once weekly	s.c.
Semaglutide NN9924 (not marketed yet)	GLP1 analog linked to a fatty di-acid	-	oral
Exenatide once weekly	Exendin-4	Once weekly	s.c.
Lixisenatide	Exendin-4 analog	Once daily	s.c.

Table 1.4 Peptidic GLP1R agonists that have been launched or are in late stage clinical trial (adapted from Graaf *et* al. [97])

1.7.4.2 Nonpeptidic modulators

There are only a few published nonpeptidyl-based GLP1R agonists, presumably because it is difficult to mimic the multiple peptide-receptor interaction interfaces with a small molecule. To date, there is only one nonpeptidic GLP1R agonist, TTP273, in clinical trials [121].
Boc5 is the only nonpeptidic GLP1R agonist to compete with the endogenous agonist in binding assays, suggesting that it acts like the natural peptide [122]. Other compounds such as Compound 1, 2, Compound B (BETP) were shown to potentiate glucose-dependent insulin secretion, but there are no in vivo studies to this day [123].
Further studies are examining the potential application of GLP1R agonists in neurological diseases. Since the GLP1R is expressed in the CNS and GLP1 was shown to improve learning in rats and exert neuroprotective effect, its therapeutic value for treatment of Alzheimer's disease or Parkinson is currently under investigation [124].

1.7.5 Signaling

The hGLP1R is pleiotropically coupled and can signal through G-protein dependent and independent pathways. The common pathway involves G_S-recruitment and cAMP elevation when overexpressed in recombinant cell lines [125, 126]. Although the mechanism is not yet uncovered, increased Ca^{2+} mobilization has been observed in CHO, HEK and COS cells. $G\alpha_q$ or PLC activation are considered to be responsible for this pathway [127]. The G protein independent pathways include recruitment of β-arrestin 1 or 2.

Diverse ligands can evoke different patterns of response while interacting with the GLP1R and thus lead to ligand-directed signal bias. This type of biased signaling presumably arises through the stabilization of distinct receptor conformations, which occur through the variable chemical contacts between the ligand and the receptor [128]. Signaling can be biased towards different pathways, however the best studied are cAMP accumulation, ERK phosphorylation, intracellular calcium mobilization (iCa^{2+}) and β-arrestin recruitment upon stimulation with different peptide agonists

(Oxyntomodulin, GLP1-(7-36)-NH2, GLP1-(1-36)-NH2 and the nonamidated forms) [126, 129]. The metabolites of the endogenous peptides exhibit biased signaling, different from the native peptide.

The few non-peptidic ligands which were developed for the hGLP1R, since an improved bioavailability is expected [130], also evoke biased signaling. The most extensively studied are BETP (4-(3-benzyloxyphenyl)-2-ethylsulfinyl-6-(trifluoromethyl)pyrimidine), Compound 2, Boc5 and TT15 [126]. While Boc5 and TT15 signal similarly at the hGLP1R through canonical pathways (cAMP, ERK, iCa^{2+}), BETP and compound 2 are described to preferably recruit β-arrestins [127, 131]. Since these compounds are chemically very diverse, it is not surprising they exhibit distinct profiles of signaling. The interaction patterns with the receptor are very different from peptidic ligands, in some cases involving topographically unique allosteric sites. Some of these small molecule ligands can bind simultaneously with peptidic ligands in a cooperative manner, altering the efficacy of peptide signaling. They are thus described as allosteric modulators [127, 130, 132, 133].

1.7.6 Regulation

1.7.6.1 Desensitization

Like all GPCRs, the activity of the hGLP1R is regulated by finely balancing receptor signaling, desensitization and resensitization. Acute GLP1 exposure of islet cells leads to rapid homologous desensitization of the receptor. Since sustained elevation of hGLP1R agonists is of clinical interest in regard of the therapeutic benefit for diabetes treatment, receptor desensitization has direct therapeutic relevance. There are only a few studies that addressed the relevance of GLP1R desensitization in vivo, one stating that chronic or intermittent GLP1 administration inhibited food intake and reduced weight gain in rats [134]. Since GLP1-mimetics exhibit a prolonged activity and stability compared to the native GLP1 [135], islet cells and extra-pancreatic GLP1-receptors will most likely be exposed for a greater period of time to these ligands. Exendin-4 is more potent than GLP1 in facilitating receptor desensitization, however the chronic exposure of transgenic mice to exendin-4 did not lead to a significant downregulation of GLP1R-dependent glucose homeostasis [136]. This was confirmed in patients treated twice daily with exendin-4 or once weekly with liraglutide [137]. Concluding, although hGLP1R clearly desensitizes in in-vitro experiments, there is little evidence that the degree of desensitization in-vivo is clinically meaningful in terms of glucose regulation.

1.7.6.2 Internalization

The hGLP1R rapidly internalizes in association with the bound ligand, when stimulated with GLP1, exendin-4, liraglutide and compound 2 [138, 139]. The mechanism for internalization may be tissue dependent, since internalization by both dynamin and clathrin-coated pits were described [138]. Although β-arrestin recruitment traditionally induces clathrin-mediated internalization, the literature indicates that they play only a partial role for the hGLP1R. It was shown that β-arrestin1 knockdown in INS-1 cells had no effect on internalization or desensitization [140]. On the other hand, enhancing β-arrestin2 action increases hGLP1R-endocytosis [141]. In any case, internalization seems to be crucial for full functionality of the hGLP1R, since the inhibition of its internalization reduced receptor signaling [139].

Although internalization contributes to desensitization of receptors, both events (internalization and desensitization) are two distinct phenomena. Internalization might terminate some hGLP1R signaling events; however, it does not terminate all signaling components. This suggests that internalized hGLP1Rs continue to signal [142], and that internalization does not necessarily mean the

desensitization of the receptor. This mechanism to spatiotemporally control signaling through compartmentation by internalization may be vital to fine-tune responses from the active hGLP1R. Hence, it might have physiological and therapeutical implications for targeting this receptor in disease management [97].

1.7.6.3 Trafficking

There is evidence suggesting the hGLP1R re-sensitizes after internalization, since it co-localizes with a marker for recycling endosomes [143]. Yet, the data about re-sensitization is scarce and requires further investigation.

Fundamental mechanisms controlling the signaling capacity of GPCRs is endocytosis and postendocytotic trafficking between recycling and endosomal degradation [144]. A very recent study, investigates the effect of internalization and trafficking on the physiological role of hGLP1R in insulin release [145]. Jones *et* al. find that different clinically marketed drugs and various ligands induce differential endosomal hGLP1R-sorting and trafficking, and with this influence surface expression. They additionally confirm the formerly doubted involvement of β-arrestins in receptor internalization and trafficking, and relate the effect of receptor internalization to physiological pathways as insulin secretion and blood glucose levels of treated mice. Ligands seem to play a big role in bias between β-arrestin and G protein signaling, showing that there must be further intracellular pathways linked to GLP1R-mediated insulin release.

1.8 Second messengers

The signals which reach the GPCRs at the cell surface are relayed throughout the cell by small molecules referred to as second messengers. Second messengers either diffuse rapidly, or simply transduce their message to protein targets within the cell, altering their activities as a response to the new information received by the receptor. A single second messenger molecule can activate multiple target proteins or enzymes and by this amplify the signal.

Chemically, second messengers can be divided into four different classes: cyclic nucleotides such as cAMP which signal within the cytosol. Lipid messengers which signal within cell membranes. Ions as Ca^{2+} that are responsible for signal transmission within or between cellular compartments and gases or free radicals which signal throughout the cell and even to neighboring cells [146].

Depending on the G protein recruited by the GPCR, the production of a specific second messenger is triggered and with it, a certain pathway starts. The three classical pathways are depicted in Figure 1.10:

I. Recruitment of G_S leads to the activation of ACs to catalyze the cyclization of ATP to 3’-5’-cyclic adenosine monophosphate (cAMP) [147].
II. The G_q protein activates PLC to generate IP_3 and DAG out of PIP_2. IP_3 subsequently leads to the release of calcium ions from intracellular stores and DAG activates protein kinase C (PKC) [148].
III. Stimulation of growth factor receptors activates phosphoinositide 3-kinase (PI3K) to generate the lipid second messenger phosphatidylinositol 3,4,5-triphosphate (PIP_3)

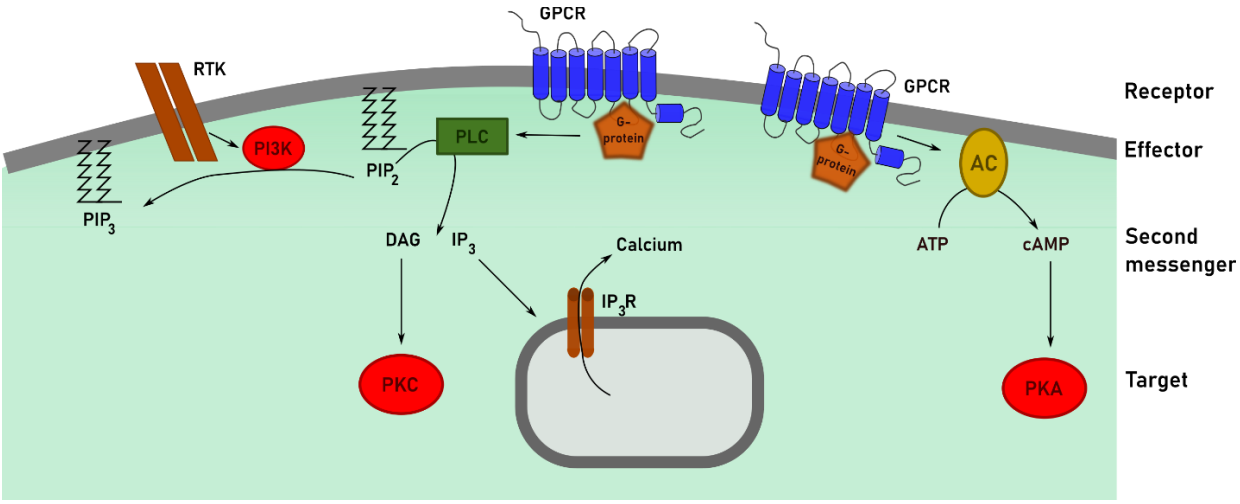

Figure 1.10 Three main pathways of second messenger generation
GPCRs (receptor) can either stimulate ACs (the effector) to produce cAMP (the second messenger) which activates PKA (the target), or stimulate PLC (the effector) to generate two second messengers DAG and IP_3. DAG activates PKC (the target), while IP_3 leads to the release of calcium from intracellular stores. On the left, binding of growth factors to a receptor tyrosine kinase (RTK), leads to the activation of PI3K, which generates PIP_3 (adapted from [146]).

Ions as second messengers control cellular activity by spreading electrical signals as action potentials in the heart and neurons for instance. They can additionally interact with specific protein targets and by this regulate cellular responses. Ions as second messengers are advantageous due to their fast response. The cells maintain a gradient of ions across their membranes, where they pass by activated channels or transporters to generate a rapid intracellular signal. They can additionally be mobilized from cellular stores (especially Ca^{2+}) as a response to a shift in the electrochemical potential of the cell [149]. Cells are able to generate spatiotemporal ionic patterns such as waves or oscillations, which dictate cellular signaling. Ca^{2+} as a second messenger is very versatile and controls a wide range of physiological processes. The effects of calcium occur either through direct binding of the ion to a target proteins, or the stimulation of calcium sensors which detect a change in its concentration and thus regulate different downstream effectors [150]. Calcium is especially important for muscle contraction by binding to proteins such as calmodulin and troponin C [151] and the fast release of neurotransmitters at nerve terminals [146, 152].

The levels of second messengers are exquisitely controlled by various homeostatic mechanisms to ensure precise cellular signaling, since a dysregulation in the output of second messengers can results in cellular dysfunction or disease. For example, continuous exposure of the heart tissue to cAMP, results in an uncontrolled und asynchronous growth of cardiomyocytes, leading to a pathological hypertrophy. The key advantage of second messengers being small molecules over proteins as effectors is that their levels are controlled with rapid kinetics. Unlike proteins, their levels change within microseconds, making them very efficient in signal transmission. The following section will deal with the properties the most prominent second messenger cAMP.

1.9 cAMP signaling

cAMP is a ubiquitous second messenger which mediates the extracellular signals of both G_S- and G_i-coupling receptors into an intracellular signal. It is produced upon binding of hormones, neurotransmitters or odorants to their cognate receptor and in turn it activates various intracellular effector proteins as will be discussed later in this section. cAMP regulates an array of cellular functions including important homeostatic mechanisms and enzymes, ion channel activity, smooth- and cardiac-muscle contractility, neuronal plasticity, immune response, cellular proliferation and apoptosis [153-155]. It is difficult to reconcile how this variety of extracellular receptors, all acting through one unique second messenger, are able to relay a specific message inside the cell and produce a distinct and appropriate cellular response. In recent years, the notion that cAMP may be compartmentalized into restricted domains to control signaling specificity is continuously being recognized.

The following sections will deal with various aspects of cAMP signaling covering its production, degradation, diffusion and compartmentalization.

1.9.1 cAMP generation

Adenylyl cyclases are the class of enzymes responsible for cAMP generation. They catalyze the conversion of a Mg^{2+}-ATP-complex to cAMP, by creating a cyclic phosphodiester bond. All eukaryotic ACs belong to class III of nucleotidyl cyclases, which are defined by a common sequence homology of their catalytic domains.

There are 10 distinct isoforms of ACs which can all be directly regulated by G proteins following the stimulation of GPCRs, whereby 9 are expressed transmembranously (AC 1-9) while AC 10 is soluble and is localized in the cytosol [156]. This section will focus on membranous AC.

The nine membrane-inserted isoforms of ACs are around 60% conserved in their catalytic domains, yet the divergent parts account for the significant differences in catalytic activity.

ACs have a molecular weight of 124 kDa [157] and exhibit a double six transmembrane-spanning architecture (Figure 1.11). A short cytoplasmatic amino terminus is followed by six transmembrane α-helices termed M1 and a large cytoplasmatic domain C1. This motif is repeated: a second set of six transmembrane spans M2 is followed by a second cytoplasmatic domain C2. The catalytic activity of ACs is conferred by the two well-conserved C1 and C2 domains [147, 158, 159]. The catalytic domains C1 and C2 form a “head-to-tail”, wreath like dimer stating the ventral surface giving space for ATP binding together with two Mg^{2+} ions. The interfacial contacts are relatively weak which results in high conformational flexibility facilitating the nucleotide binding, catalysis, regulation and cAMP dissociation. $G\alpha_S$ interacts mainly with the C2 domain, however both $G\alpha_S$- and ATP-binding are necessary to transfer the inactive open, into the active closed state [159, 160]. Earlier studies have demonstrated that the interaction between the two transmembrane domains is absolutely required for proper trafficking and functional assembly of the two parts of the catalytic domain at the plasma membrane, since the sole expression of either C1 or C2 does not lead to significant enzymatic activity. The same is true for expression of M1C1 or M2C2 (halves of the molecule) [161].

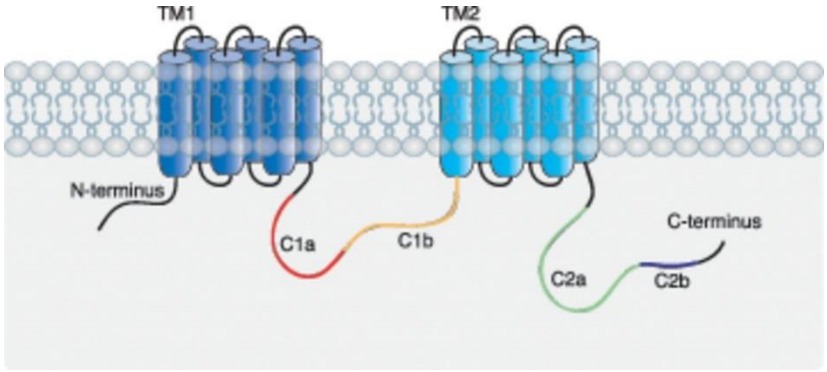

Figure 1.11 Structural domains of membrane-bound ACs
mACs comprise two transmembrane clusters (TM1, TM2) each consisting of six membrane-spanning domains. TM1 and TM2 are connected by an intracellular loop, which contains the C1a and C1b region. TM2 is followed by an intracellular tail composed of C2a and C2b before the carboxy-terminus (this figure was originally published by Cooper & Tabbasum in 2017 [162] http://www.biochemj.org/content/462/2/199.long)

ACs are differentially distributed in the plasma membrane. Since the lipid components forming the plasma membrane are highly diverse with different solubilities and mobilities, the plasma membrane is a very dynamic, heterogeneous entity. Lipid rafts within the membranes are viewed to be concentrations of cholesterol, phospholipids with unsaturated side chains and gangliosides. They include caveolae and are very distinct in lipid and protein composition from non-raft domains [163]. Earlier studies criticized the static biochemical procedures used to isolate rafts for studying and controverted the existence of rafts [164]. However, modern super resolution methods applied to observe the diverse protein and lipid composition of the membrane and their mobility put beyond doubt that the plasma membrane is dynamic and heterogeneous [165]. ACs are not equally distributed between non- raft and raft domains. ACs 1, 5, 6 and 8 occur in rafts, whereas the others do not [166, 167]. Yet, not only the distribution of ACs in different portions of the membrane plays a role in how they fulfill their task. The common output of all ACs is the production of cAMP, however as experimental observations show, not all AC isoforms regulate the identical cellular function. To explain this conundrum, the concept of cAMP signaling compartmentation was evoked [162, 168]. Indeed, it has been shown that some AC isoforms associate with GPCRs and form distinct complexes with downstream effectors in a certain cellular compartment [169]. This greater level of organization is achieved by AKAPs, which scaffold PKA with its substrate and bring together a diverse array of proteins involved in various signaling pathways. Several AKAPs interact with ACs in an isoform-specific manner and with this regulate cAMP signaling [170] (for further details see section about cAMP compartmentalization).

All AC isoforms are activated by both forskolin (except for AC9) and the GTP-bound α-subunit of the stimulatory G protein G_S. All are inhibited by certain adenosine analogs termed P-site inhibitors. ACs can also be indirectly regulated by distinct signaling pathways, for instance through calcium binding to calmodulin (CaM) which can stimulate AC1 and AC8, as well as inhibit AC5 and AC6 [171]. PKA and PKC are also known to regulate ACs in their activity [162]. Additionally, the phosphorylation state of proteins within the activation cascade of ACs modulates their activity. Particularly GPCRs which are desensitized and down-regulated following phosphorylation by cAMP dependent kinases influence the activity rate of ACs. Another putative mechanism is direct feedback inhibition of AC activity in response to their phosphorylation by cAMP dependent kinases, however evidence for this mechanism remains sparse to

this day [172]. Kawabe *et* al. have demonstrated that the G_q- and PKC-mediated phosphorylation of AC5 leads to a marked increase in enzymatic activity [173].

Since most cells and tissues express multiple AC isoforms, it is difficult to tease apart the physiological role for a given AC isoform. Therefore, the knowledge about the effect of specific AC isoforms in human pathophysiology is very limited and calls for more detailed studies regarding the expression and function of ACs in human disease [174].

Taken together, the cooperation between ACs and PDEs which degrade cAMP (discussed in the upcoming section) is essential to control the speed and expansion of the cAMP signal, and by this critical for the activation of downstream cellular responses [156].

1.9.2 cAMP degradation

The superfamily of phosphodiesterases (PDEs), responsible for cyclic nucleotide degradation, comprises eleven members transcribed from 21 genes, which generate nearly one hundred different isoforms based on amino acid sequence, regulatory properties and catalytic characteristics. Multiple promotors for one gene and alternative splicing variants of the mRNA contribute to the molecular diversity [175]. PDEs are responsible for hydrolyzing cAMP or cGMP and by this finely regulate the function of these second messengers in cell signaling. Each PDE has a different affinity for the two cyclic nucleotides and thus the catalytic activity is diverse. PDEs 1, 2, 3, 10, 11 hydrolyze both whereas PDE 4, 7, 8 are cAMP specific and PDE 5A, 6 and 9A are cGMP specific. (Table 7.6 in the annex shows PDEs with their characteristic features).

Each PDE contains a regulatory (R) and a catalytic (C) region. The C-region within the COOH-terminal portion of the protein is conserved within the PDE family, while the regulatory N-terminus is very variable and provides functional and localization differences. Additionally, there are numerous types of protein domains appended to the PDE C-region, which provide regulatory control. For instance, PDE1 family exhibits calcium/calmodulin-binding domains [176], PDEs 2, 5, 6, 10 and 11 have GAF domains [177], and there are UCR (upstream conserved) or autoinhibitory domains in other families [178]. GAF domains (named for cGMP-binding PDEs, *Anabaena* adenylyl cyclase and *E.coli* FhlA) can control cyclic nucleotide binding, protein-protein interactions within dimerizing PDEs as well as heterologous protein-protein interactions [179]. Posttranslational modifications (such as phosphorylation) can affect the PDE activity as well, and influence complexing with other proteins in signalosomes [180]. Mammalian PDEs are homodimers with the exception of PDE1 and 6 which form heterotetramers with other proteins. The dimerization contacts of PDEs involve the NH_2-terminal region (PDEs 2, 4, 5, 6, 10) or contacts in the C-domains (PDEs 2, 3, 4, 8, 11). Dimerization provides regulatory mechanisms such as ligand binding and autoinhibition [181, 182].

Exploiting both biochemical technologies and direct structural analysis of isolated R- and C-domains of PDEs, gave insight into the interaction of the cyclic nucleotides with the enzymes. It has been determined that isolated C-domains are catalytically active [183, 184]. They contain 17 invariant amino acids mostly located in the catalytic pocket and exhibit a globular, highly conserved topology. C-domains are comprised of 15-17 α-helices. The catalytic pocket has a depth of approximately 10 Å and contains two regions: a histidine-rich region that forms a binuclear metal-ion binding site where the catalysis occurs and the regions which interacts with the cyclic nucleotide purine termed as the “hydrophobic clamp” [181]. It is by now widely accepted that zinc within the metal-ion binding site is crucial for the catalytic function [185]. Magnesium seems to be the second important metal ion required for PDE-activity, since it has been shown that PKA phosphorylation of PDE4 increases the affinity for magnesium

[186]. This mechanism of variable affinities for an ion, together with the changing levels of divalent ions in the cells is likely to affect differentially compartmentalized PDEs and their activities.

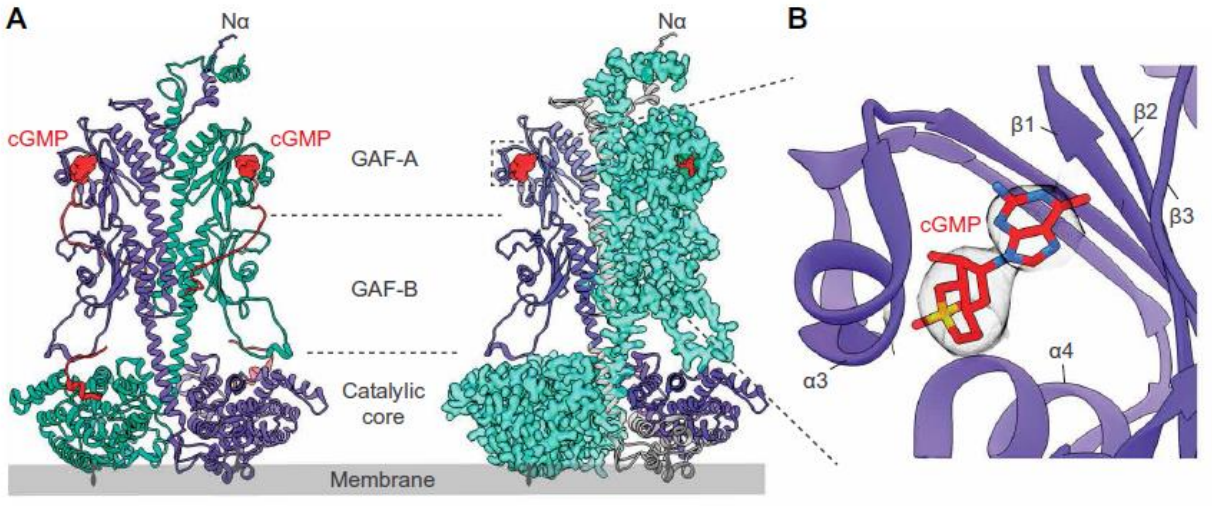

Figure 1.12 Structure of the PDE6αβ2γ complex
(A) Structure of the PDE6αβ homodimer (α in purple, β in green cyan). One cGMP molecule (red sphere) is bound to each of the GAF-A domains. (B) GAF-A cGMP binding pocket in a zoomed-in view depicting the orientation of the cGMP molecule within the secondary structures (figure taken from Gulati *et* al. [187] with permission according to the creative commons license 10.1126/sciadv.aav4322)

cAMP specific PDE activity is modulated in coordination with ACs and PKA, through different feedback pathways. It has been shown for instance, that PKA-mediated phosphorylation of PDE4 activates the enzyme and thus leads to lower cAMP levels and an arrest of the signal. By this, the cell maintains cAMP levels within optimum ranges for responsiveness to signals [188]. Together with ACs, PKA and putatively other effector proteins, PDEs generate nanodomain signalosomes by means of subtype- and isoform-specific localization. This way the influence of a cAMP signal can be limited to specific targeted proteins in the neighborhood [180].

PDE activities are modulated in response to a panoply of signals including hormones, neurotransmitters, cytokines or light. Their dysfunction has been associated with diseases such as asthma, erectile dysfunction, chronic obstructive pulmonary disease, hypertension, heart failure, schizophrenia, stroke and depression, which is why they state potential targets for new drugs to cure these diseases [179].

The coordinated action of PDEs together with AC establishes balanced cAMP levels within microdomains and with this, the second messenger can bind and affect effector molecules and exert its function in cellular signaling [189].

1.9.3 Effector proteins of cAMP

After the generation of cAMP by ACs it exerts its function as a second messenger by activating a subset of effector proteins. Edwin Krebs and Edmund Fischer were awarded with the Nobel Prize for their work on this second messenger, since they were the first to describe its action. They found that the principle task of cAMP is to stimulate the phosphorylation of proteins [190], which is achieved through

the activation of PKA [191, 192]. In addition to PKA, cAMP can activate two isoforms of the protein Epac [193], several cyclic nucleotide-gated ion channels (CNGCs) [194] and the more recently described Popeye domain-containing (POPDC) proteins [195]. A sperm-specific novel cyclic nucleotide receptor (CRIS) has also been described to be modulated by cAMP [196]. Each of these effectors controls a different specific task, adding to the array of cAMP dependent functions. The following paragraphs will focus on the two main effectors of cAMP namely PKA and EPAC.

1.9.3.1 Protein kinase A (PKA)

The cAMP-PKA pathway coordinates a multitude of cellular functions and by this physiological processes ranging from the regulation of cell cycle, microtubule dynamics, intracellular transport mechanism over the influence on the cardiovascular system through β-adrenergic signaling. Various metabolic pathways in adipocytes and immune responses are modulated together with several other effects mediated by hormones, neurotransmitters and ions.

The PKA holoenzyme is a hetero-tetramer, which consists of two catalytic subunits (C) that bind a dimer of two regulatory subunits (R). While the cAMP sensing R units are bound to the C units, the enzyme stays in its inactive state. Three genes for C subunits (Cα, Cβ and Cγ) and four R genes have been identified. R subunits are subdivided into two classes: RI (RIα, RIβ) and RII (RIIα, RIIβ) [197]. The C subunits have a bi-lobal subdomain, which consists of an N-terminal small lobe and a C-terminal large lobe (Figure 1.13). The active site of the enzyme together with the binding site for ATP is located in the cleft between the two lobes [198, 199]. As mentioned above, the R subunits which share 75% sequence identity, are responsible for cAMP sensing, with which they contribute to PKA specificity. They simultaneously associate with C subunits and AKAPs and therefore restrict the phosphotransferase-activity to a certain cellular location. RIα and RIIα are ubiquitously expressed in cells, whereas RIβ and RIIβ isoforms have a more tissue specific expression pattern [200]. The most significant difference between RI and RII isoforms is the potential for auto-phosphorylation at the inhibitor site (IS) of RII subunits. This is relevant for the interaction of RII with the C subunit and signal amplification as a consequence. A second big difference between PKA type I and II complexes is the absolute requirement for 2 Mg^{2+} ions and ATP to form the PKA type I holoenzyme, while type II PKA can form a high affinity complex without ATP [201]. PKA R subunit domains are relatively conserved in their structure. The dimerization- and docking- (D/D) domain is located at the N-terminus and is essential for R subunit dimer assembly as well as AKAP binding at a hydrophobic interface [202, 203]. Adjacent is a flexible linker which comprises the inhibitor site found in RIIα and RIIβ while missing in RIα and RIβ [204-206]. There are two cyclic nucleotide binding domains A and B (CNBA, CNBB) located at the C terminus behind the flexible linker which consist of an eight β-stranded sandwich that forms a basket like structure to which cAMP can dock. The conformational changes which occur upon cAMP binding, are the reason for PKA holoenzyme disassembly [204].

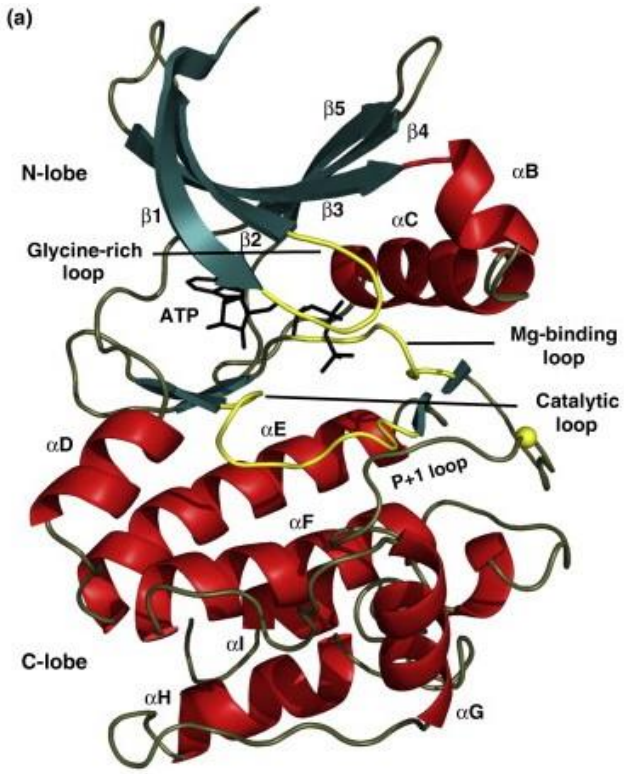

Figure 1.13 Structure of the conserved PKA core
Visible is the characteristic bi-lobal fold of PKA. The N-terminal lobe is coloured in teal and contains 5 β-strands with a universally conserved αC-helix. The C-lobe, coloured red, is mostly helical. ATP is bound inside of the cleft between the two lobes. Highlighted in yellow are catalytically important loops (this figure was originally published by Taylor *et* al. [198] used with permission from Copyright Clearance Center; license number 4580681004698)

PKA is targeted to specific intracellular domains, together with signal initiators, effectors and terminators, through its interaction with AKAPs (See Figure 1.14). The compartmentalization through AKAPs ensures the transmission of information between supramolecular signaling complexes. PKA substrates are phosphorylated as a consequence of cAMP mediated activation of PKA C subunits [207]. In addition, cAMP-independent activation mechanisms for PKA exist, which can involve NF-κB [208], transforming growth factor β (TGF-β) together with the SMAD family member 3 and 4 [209] or the ubiquitin proteasome system (UPS) [210].

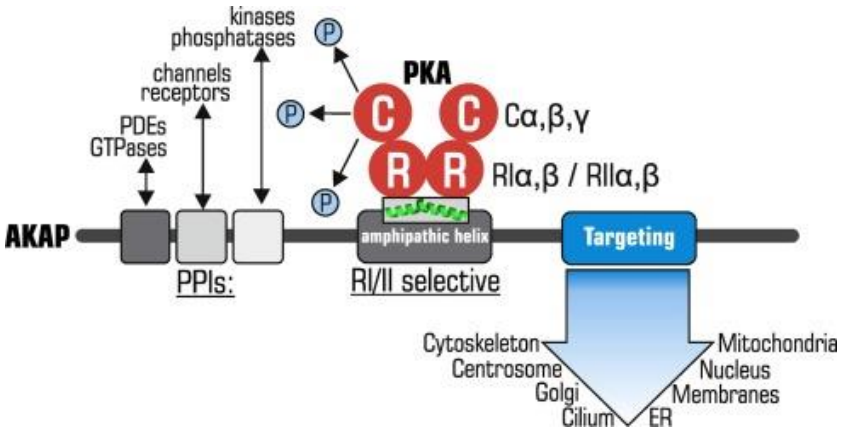

Figure 1.14 Domain organization and interaction of PKA with AKAPs
cAMP sensing R subunits mediate the PKA specificity by simultaneously associating with AKAPs and the PKA C subunits. This links the phosphotransferase activity of PKA to space restricted substrates in close proximity, facilitating specific downstream effects on various organelles (this figure was originally published by Torres-Quesada *et* al. [189] https://www.sciencedirect.com/science/article/pii/S0898656817301420?via%3Dihub#f0005)

The inactivation of PKA activity relies on different mechanisms. On one hand the receptor-AC-cAMP-PKA signaling axis is regulated by a negative feedback mechanism, on the other hand cAMP-PKA activities can be directly inhibited. GPCR desensitization or internalization, Gα protein hydrolysis or cAMP degradation by PDEs all lead to signal termination of the active PKA [211]. These feedback mechanisms involve the concerted action of kinases, phosphatases, PDEs and the ubiquitin proteasome system (UPS) on upstream located signaling nodes of the cAMP-PKA pathway and occur in time frames of seconds and minutes. As a consequence, cAMP levels are reduced, and the basal kinase state is reformed to a tetrameric PKA holoenzyme. The PKA inhibitor peptide (PKI) is a competitive inhibitor peptide, which can directly bind and inhibit the free PKA C subunit, leading to the export of the catalytic subunit out of the nucleus into the cytoplasm. By this, it inhibits nuclear PKA functions such as synaptic activity or cell-cycle regulation [212]. Other second messengers such as calcium can also indirectly affect PKA. Interaction between Ca^{2+} and cAMP signaling occurs at multiple levels to tune the activity of each other [213, 214]. One last mechanism to mention in this context is the phosphorylation of PKA itself. Phosphorylation of C and R subunits affects the stability and function of the PKA holoenzyme. The various enzymes involved in activation and termination of the signal cluster side by side and with this specify how the signal propagates [198].

The notion of PKA being organized in supramolecular signaling complexes is by now acknowledged, yet further studies regarding the composition of these signaling complexes are required to understand the modes of accurate signal transduction.

1.9.3.2 Exchange protein directly activated by cAMP (Epac)

Epac, an important effector protein of cAMP, exhibits unique signaling properties defined by its multi-domain architecture. It provides the structural basis in the temporal-dynamic control of autoinhibition and activation of this effector protein. Epac is also known as cAMP-guanine exchange factor (cAMP-GEF), and was identified during the search to unravel the mechanism of cAMP-dependent activation of the small GTPase Rap1 which is independent of PKA [215]. Rap functions as a molecular switch, which can alternate between an inactive GDP-bound and an active GTP-bound state. GEFs modulate the GDP/GTP activity of Rap and activate the switch in contrast to GTPase-activating proteins (GAPs) which inhibit Rap activity by accelerating its intrinsic GTPase activity [216, 217]. Two isoforms have been identified: Epac1 and Epac2, both being cAMP-regulated GEFs. They control cellular responses, which are initiated upon Rap activation by cAMP. They additionally serve as a link to other downstream effectors of the Ras superfamily of small GTPases (to which Rap1 belongs) [218-220]. Epac1 and Epac2 are expressed in different tissues depending on the developmental stage and the pathophysiological micro-environmental circumstances. Epac1 is mostly present in the heart, kidney, blood vessels and central nervous system (CNS), whereas Epac2 is most abundant in the adrenal gland, CNS and pancreas [215]. Both isoforms induce the activation of a plethora of effectors including the phospholipase C and D, extracellular signal regulated kinases (ERK1/2), the suppressor of cytokine signaling-3 (SOCS-3) and NF-κB [221]. This multiplicity in its signaling properties enables Epac to regulate the contraction of cardiomyocytes by modulating cellular calcium- and actin-microtubule cytoskeleton dynamics. In addition, it regulates cell fate, proliferation, differentiation and apoptosis by altered gene transcription and kinase activity. Dysfunction of the signaling properties of Epac is connected to diseases including cardiac hypertrophy, heart failure, Alzheimer's disease and Diabetes among many more [193].

Epac1 and 2 exhibit a multi-domain structure (Figure 1.15) with a catalytic site at the C terminus and an autoinhibitory N-terminal regulatory region [222, 223]. The exchange activity is located at the C-terminus within the catalytic domain responsible for GDP/GTP-exchange. The N-terminal regulatory region comprises a high-affinity cAMP binding domain (cAMP-B) and a membrane-anchoring DEP (disheveled-Egl-10pleckstrin) domain required for the distribution to the plasma membrane of Epac1 [224]. Epac2 has an additional low-affinity cAMP-binding domain (cAMP-A), which determines its intracellular location. The isolated fragments, which contain the cAMP-B domain, inhibit the regulatory region. This auto-inhibitory function is relieved when cAMP binds and a conformational change is induced that opens the catalytic domain to permit GTP-loading of Rap [222, 225]. It has been described that the activators of Epac act by modulating the protein dynamics, which proved to be the key allosteric modulator for Epac activation. The highly dynamic equilibrium between autoinhibition and activation in vitro can be studied by X-ray crystallography and NMR spectroscopy, while Epac based Förster resonance energy transfer cAMP sensors or GFP/Flag-tagged Epac proteins are applied to monitor the temporal dynamics of Epac activation in vivo [226, 227].

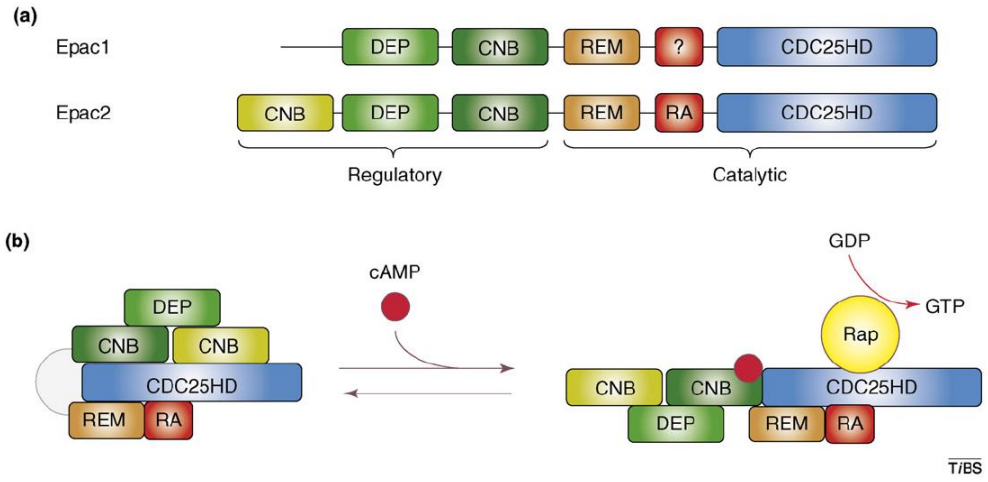

Figure 1.15 The multi-domain structure of Epac
(a) The multi-domain structure of Epac consists of a regulatory region with the CNBD (cyclic nucleotide binding domain) and the DEP-domain involved in membrane localization, and a catalytic region comprising the REM (Ras exchange motif), the RA motif (Ras-association) and the CDC25-homology domain. The question mark in Epac1 is a region homologous to the RA domain in Epac2 with unknown function.
(b) cAMP binding to Epac results in opening of the protein to enable interaction with Rap.
(This figure was originally published by Bos *et* al. [225] with permission from Copyright Clearance Center; license number 4578710801270)

Epac proteins are able to exert their biological functions either alone or together with PKA [221]. AKAPs might account for the formation of cAMP-sensitive multi-protein complexes, which are of key importance in such processes. Two distinct multi-protein complexes encompassing Epac1 and Epac2 have been identified in the heart and the brain [193]. On the level of metabolic regulation, several recent studies have shown that Epac2 takes part in the secretion of glucose, glucagon and insulin upon incretin stimulation from pancreatic β-cells. This occurs through multiple mechanisms including the inhibition of ATP-sensitive K^+-channels, activation of the ryanodine-sensitive Ca^{2+}-channel and subsequent Ca^{2+}-induced Ca^{2+}-release, recruitment of insulin granules to the plasma membrane and Rap1-regulated activation of PLC [193, 228, 229].

Further studying and understanding the cellular functions, expression patterns, modulating factors of the Epac proteins and the Epac signalosome will hopefully facilitate the development of improved pharmacotherapy in order to address various diseases connected to Epac signaling.

1.9.3.3 Cyclic nucleotide gated channels (CNGCs)

CNG channels are part of a heterogeneous superfamily of ion channels, which share a common transmembrane topology and pore structure. The binding domain for nucleoside-3',5'-cyclic monophosphates (cNMPs) lies within their COOH-terminal region. All CNG channels can be activated by both cAMP and cGMP to a different extent. They are non-selective cation channels, which only poorly discriminate between alkali ions and additionally allow the passage of divalent cations, especially Ca^{2+}. Their main function has been described in rod and cone photoreceptors, in extra-retinal photoreceptors and in sensory neurons of the olfactory epithelium, however their physiological function in other cells is

ill defined [194]. Hyperpolarization-activated cyclic nucleotide-gated channels (HCN), a sub class of CNGCs, are crucial for cardiac function in their role as pacemakers. All four isoforms HCN 1-4 are expressed in ventricular myocytes where they control cardiac excitability and thus the heart frequency [230].

1.9.3.4 Popeye domain containing (POPDC) proteins

3 different Popdc genes have been identified to this date, which are highly conserved in their amino acid sequence (Popdc1, 2, 3) [231]. All are expressed in cardiac and skeletal muscle, Popdc1 being additionally present in smooth muscle cells of multiple organs [232].
Popdc proteins exhibit a three transmembranous structure with an extracellular amino-terminus. They form homodimers stabilized by disulfide bonds, with their C-terminus located in the cytoplasm containing the Popeye domain. Adjacent to that lies the cyclic nucleotide binding domain, which has a very high affinity for cAMP and 40x less affinity for cGMP [233]. Determined by a radioligand binding assay, the cAMP affinity of Popdc proteins is about 10x higher than that of Epac1 and similar to that of PKA [233].

Popdc1 regulates epithelial function by being involved in cell-cell contact formation through tight junctions [234]. It further plays a role in vesicular transport and cell motility [235]. In general, Popdc proteins are associated with various types of cancer [236], they are known to interact with ion channels [233] and modulate the number and size of caveolae [237]. Since they are most abundantly expressed in striated muscle tissue as the heart, loss of function leads to severe arrhythmia or atrioventricular block [238]. Although a huge progress has been made in studying Popdc protein function during the last 19 years since their discovery, further studies are needed to understand the role of cAMP binding for Popdc protein function and its impact on the structural and functional level. Their regulation (alternative splicing, phosphorylation, glycosylation) is also not entirely uncovered, which would help in understanding the various physiological and pathophysiological processes they are associated with.

1.9.4 cAMP Compartmentalization

It is necessary for all afore mentioned players within the cAMP signaling cascade to be spatially and temporally coordinated in order to ensure proper signal transmission. The restriction of cAMP diffusion and its spatial confinement are factors, which could contribute to compartmentalized signaling. They would further support the notion of signaling happening in defined macromolecular, multi-protein complexes.

Buxton & Brunton provided the first evidence for compartmentalized cAMP in the early 1980ies. They treated a perfused rabbit heart with agonists of different GPCRs, either prostaglandin E1 (PGE_1) or isoproterenol, and compared cAMP-mediated PKA activation. They homogenized the heart after treatment, separated the soluble from the particulate fraction and measured the activity of PKA in each. The results showed that PGE_1 increased the activity primarily of soluble PKA, whereas isoproterenol increased PKA in the particulate fraction. In addition, they could link the increase in particulate, but not soluble, PKA activity with positive cardiac inotropy [239]. These were the first studies to suggest that cAMP delivers its message in a compartmentalized way, leading to different biological effects when signals are spatially segregated within a cell. Evidence for this hypothesis was provided shortly afterwards in an elegant set of experiments by Jurevicius & Fischmeister. The authors recorded cAMP-activated Ca^{2+} currents from two physically separated sites on a single cardiomyocyte upon stimulation

of β-ARs by patching the cell. The hypothesis was, that if cAMP elevation was homogenous throughout the cell, then locally applied adrenergic stimulation would activate calcium currents at both sites. Interestingly what they found was that the local stimulation with isoproterenol resulted in a restricted activation of calcium currents (indication for compartmentalization), while local application of forskolin activated the calcium currents throughout the whole cell [240].

The activation of PKA (or every other cAMP effector protein) requires the binding of cAMP to the CNBD. For this cAMP levels need to rise above the K_d of the respective protein (2.9 μM for PKA, 2.8 Epac1 [241]), with cAMP distribution in a non-compartmentalized way, effector activation could theoretically occur throughout the cell by any stimulus which elicits cAMP levels (intracellular cAMP values reported from 1-10μM [227, 242]). Again, this notion suggests that signaling has to occur in a compartmentalized way [243].

There are three basic requirements to define cAMP signaling compartments [244]:

I. localized signal generation: provided by differential distribution of ACs
II. restricted diffusion
III. localized signal response elements

One mechanism by which cAMP signals can be spatially and temporally restricted is in forming multi-molecular signaling complexes by A-kinase anchoring proteins (AKAPs) [245].
The AKAP family is very diverse, with over 50 known members. Their common feature as scaffolding proteins is to bind PKA and target it to different subcellular areas [246]. AKAPs additionally contain targeting sequences for multiple enzymes with which they can consolidate upstream activators with downstream targets and form multi-protein complexes in a compartmentalized manner. This way, cAMP sensing signalosomes can precisely integrate and communicate incoming signals [189].

The hallmark of all AKAPs is a unique sequence, which forms the binding site for the PKA R subunit. This 24-residue chain (termed Ht31) forms an amphipathic helix, which interacts with the RII dimer of PKA, binding it with nanomolar affinity [247, 248]. Cellular delivery of the Ht31 peptide, synthetic variants or stearated forms of it has become a standard technique to disrupt PKA-RII anchoring and with this, study the role of AKAPs in the coordination of cAMP mediated PKA activation [246]. Ht-31 is a PKA-II selective variant, which was used to demonstrate PKA uncoupling from AMPA-type glutamate receptors when perfused into cultured hippocampal neurons [249].

Most evidence for the physiological role of AKAPs has been collected in studying cardiac functions. PKA is responsible for the phosphorylation of various substrates which influence contractility, including L-Type Ca^{2+} channels, the ryanodine receptor or troponin I [250]. AKAPs are pivotal for phosphorylation of numerous PKA dependent substrates that regulate the cardiac function. Various PKA II targeting members such as muscle AKAP (mAKAP) [251], yotaio [252], AKAP18 [253] but also AKAP2 [254] which binds both type I and II PKA, are all associated with physiological functions in the heart. The nuclear envelope associated mAKAP serves as a scaffold for PKA, PDE4D3, Epac1 and controls cardiomyocyte hypertrophy through the regulation of ERK5. This way a highly structured cAMP-sensing multi-protein complex is assembled, in which signals can be regulated and focused to nearby substrates [251].

Another important role for AKAPs was described in the regulation of GLP1-mediated insulin secretion. This was identified using the disruptor peptide Ht-31. Lester *et* al. [255] showed that the insulinotropic effect of GLP1 was blocked in cells treated with Ht31, whereas the cAMP production and thus PKA activity was unaffected. The results suggest that the disruption of PKA targeting by AKAPs attenuates GLP1 dependent insulin secretion. In a second study, they demonstrate that AKAP79-

targeted PKA phosphorylates β-cell proteins and regulates insulin secretion together with protein phosphatase 2B (PP2B, calcineurin) [256].

The classical view states that intracellular signal transduction is driven by abundantly available molecules freely diffusing within the cell, catalyzing various processes, which in turn lead to the signal transduction. Studying scaffold proteins such as AKAPs however, has updated the paradigm. It has become clear that by scaffolding and organizing interacting proteins and molecules, intracellular signaling could occur in defined compartments in which relevant molecules are brought in close proximity in order to deliver a specific message. Concluding, enzyme specificity is conferred equally by co-localization and by the intrinsic selectivity of the active site [257].
There is not yet a consent about the size of the putative signaling compartments. Various groups which have tried to visualize the size of the signaling domains, mainly study PKA-activity domains [258, 259] and only a very few focus on actual cAMP compartments [260, 261].

1.9.5 cAMP diffusion

As cAMP activates numerous effector proteins and exerts pleiotropic effects within the cell, the pressing question is how cAMP reaches its effectors from the site of synthesis. Determining how fast cAMP diffuses inside of the cell is essential to understand its means of signaling specificity.
Older studies determining the diffusion speed of cAMP stated that this small, highly hydrophilic second messenger shows a very fast distribution in the cytosol with diffusion constants in the range of 270-780 $\mu m^2/s$ [262, 263]. This would make it as fast as in an electrolyte solution [264], giving it unrestricted access to all cellular areas where it could activate its effector proteins non-selectively. Based on these observations, cAMP has traditionally been regarded as a long-range second messenger, capable of travelling very fast to relay its information to far distanced sites [265]. However, the concept of freely diffusing cAMP contrasts with the model of localized, compartmentalized cAMP signalling as means of achieving cellular signalling specificity. Indeed, more recent studies show that cAMP diffusion is restricted, setting the molecular basis for spatially confined signaling compartments. Agarwal *et* al. have suggested a diffusion coefficient of 9.7 $\mu m^2/s$ in cardiomyocytes and 5 $\mu m^2/s$ in HEK-293 cells [266] which is in better agreement with this concept. The concept of a slow diffusion rate is not yet established and whether there are physical barriers restricting cAMP from flowing and contributing to a or PDEs stating an enzymatic barrier by degrading local cAMP before it diffuses away from the compartment is currently still a matter of speculation.

1.10 Resonance energy transfer-based techniques

1.10.1 Principle of fluorescence resonance energy transfer

Theodor Förster was the first to describe the principle of fluorescence resonance energy transfer (FRET) in 1946, therefore often referred to as *Förster* resonance energy transfer [267]. The principle relies on the non-radiative energy transfer from an excited molecular fluorophore (donor, D) to a second fluorophore (acceptor, A) by means of intermelocular long-range dipole-dipole coupling. Fluorescence is a phenomenon in which an electron in the ground singlet state (S_0) of the highest occupied molecular orbital (HOMO) absorbs energy and transitions to an excited state (S_1) of the lowest unoccupied molecular orbital (LUMO), while maintaining its single nature (singlet-singlet transition). This electron can transfer from the higher energy state S_1 due to internal relaxation and fall back into the ground state. The excessive energy is emitted as light of a characteristic wavelength. In FRET the S_1 electron of a donor molecule, transfers the energy to an adjacent ground state acceptor fluorophore via

dipole-dipole interactions (Figure 1.16). The excited acceptor electron can relax as well, and emit photons of a specific longer wavelength. As a conclusion, the resonance energy transfer (RET) results in quenching of the donor fluorescence intensity and excitation of an acceptor fluorophore, which emits photons of a characteristic wavelength.

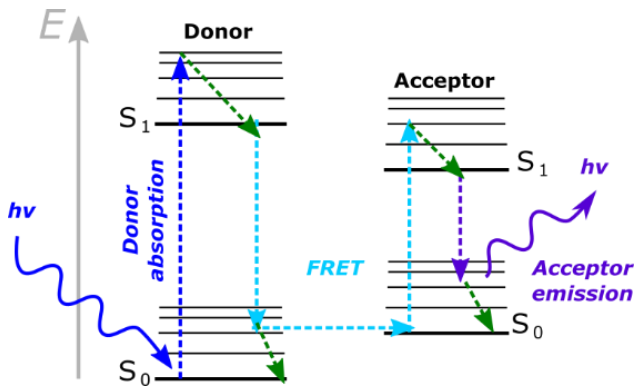

Figure 1.16 The basic principle of FRET
Jablonski diagram depicting the mechanism of FRET. Absorption of a photon by the donor fluorophore raises an electron to an excited energy state. The electron drops to the ground level of the excited state. Instability of the excited state leads to a relaxation back to the ground state within a few nanoseconds. The energy released from donor relaxation is absorbed by an acceptor fluorophore in close proximity which in turn leads to the emission of a photon from the acceptor fluorophore rather than the donor (adapted from [268]).

There are a few requirements essential to be fulfilled for FRET to occur. First is that the emission spectrum of D and the absorbance spectrum of A must overlap adequately (see Figure 1.17). This highly affects the FRET efficiency of a donor-acceptor pair and is represented by the overlap integral J(λ). FRET is highly distance dependent and requires the two interacting fluorophores to be in close proximity of 10 to 100 Å [269]. Furthermore, the quantum yield of the donor (Q_D- a measure for the efficiency of a fluorophore to convert absorbed to emitted photons) and the absorption coefficient of the acceptor (εA quantification of the ability to absorb energy) need to be sufficiently high [270].

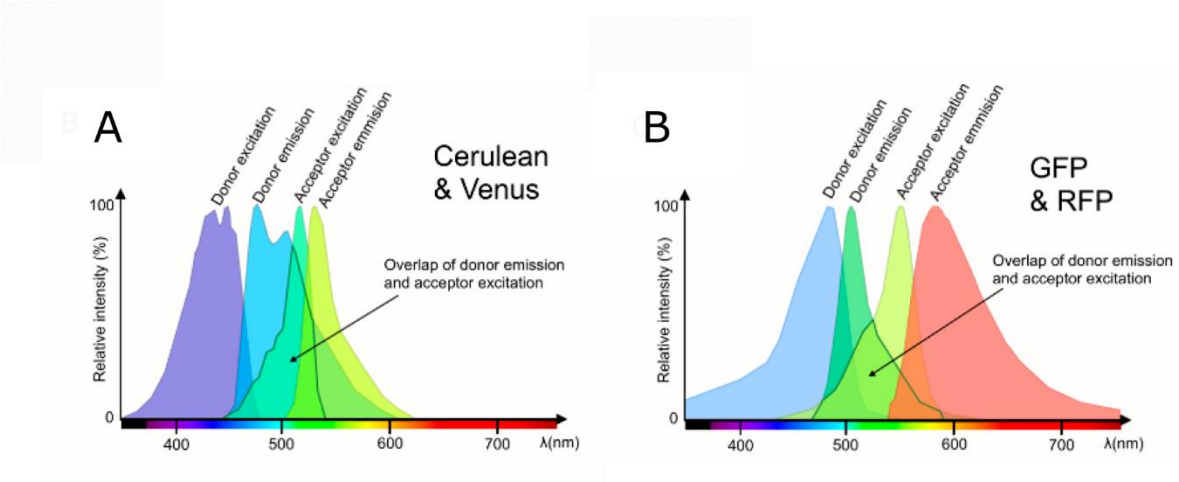

Figure 1.17 Spectra of fluorescent protein FRET-pairs
(A) The combination of a cyan emitting donor (cerulean) with a yellow emitting acceptor (venus) results in a large overlap of donor emission and acceptor excitation. **(B)** the combination of GFP as donor and RFP as acceptor shows a smaller spectral overlap (extracted and adapted from [268] according to Creative Commons Attribution License https://www.mdpi.com/1424-8220/15/10/26281).

The Förster radius (R_0) can be calculated from the physical properties of the fluorophores according to EQUATION 1. R_0 describes the distance between D and A at which 50% of the donor energy is transferred non-radiatively to the acceptor, giving half-maximal energy transfer efficiency.

$$R_0 = 9.78 \times 10^3 \times \sqrt[6]{\kappa^2 n^{-4} Q_D J(\lambda)} \text{ (in Å)}$$

EQUATION 1

κ^2 describes the relative dipole-dipole orientation of the FRET partners, at its best when they are approximately parallel, and n is the refractive index of the medium ascribed a value of 1.4 for biomolecules in aqueous solution [271].

Given the Förser Radius, the FRET efficiency (E) for a donor-acceptor pair can be calculated. It refers to the percentage of energy transfer from the donor to the acceptor and is quantitatively described in the following equation, where R is the distance between the fluorophore's dipoles:

$$E = \frac{1}{1 + (R/R_0)^6}$$

EQUATION **2**

From EQUATION 2 we can conclude that the FRET efficiency is proportional to the inverse sixth power of the distance between the fluorophores (Figure 1.18). Due to the sigmoidal relationship between the FRET efficiency and the distance R between the two fluorophores, a FRET-pair where R_0 approximates R gives a FRET-sensor with a maximized dynamic range. A fact important for the design of FRET-based biosensors for scientific research [272].

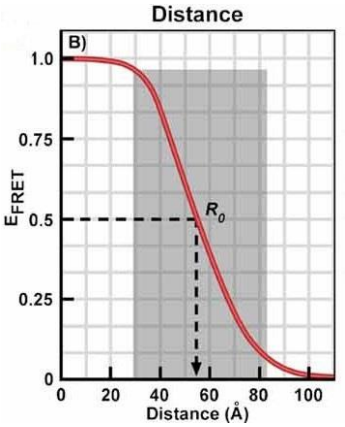

Figure 1.18 Distance-dependence of FRET efficiency
The Förster equation (EQUATION 2) used to determine the change in FRET efficiency as a function of the distance between the two fluorophores. The shaded area shows the range of 0.5 R_0 to 1.5 R_0 over which FRET can be accurately measured (this figure was originally published by Day *et* al. [273] with permission from Copyright Clearance Center; license number 4580780655594).

1.10.2 Techniques to measure FRET

There are several techniques, each requiring special instrumentation, to record FRET-signals. Three different strategies are used to detect FRET changes [272]:

1.10.2.1 Indirect FRET measurements

They include measuring FRET efficiency through spectral imaging (siFRET), acceptor photobleaching FRET (apFRET) and fluorescence lifetime imaging (FLIM-FRET).

In siFRET the FRET efficiency is calculated by fitting the collected emission spectrum of a FRET biosensor to the theoretical emission spectrum of the indicated FRET pair, calculated from the Förster formulas mentioned above. A drawback of this method is that it requires an exact donor-acceptor ratio and can thus only be used for intramolecular biosensors (described under1.11) [274, 275].

apFRET depends on the fact that the donor emission is quenched due to the energy transfer. When the acceptor is photobleached, the donor is de-quenched. With the following EQUATION 3 one can calculate FRET efficiency by indicating what proportion of energy the donor transfers to the acceptor.

$$E = 1 - (I_{pre} / I_{post})$$

EQUATION **3**

I_{pre} and I_{post} are the fluorescent intensities of the donor before and after photobleaching. This method offers a straightforward way to measure FRET efficiency for live cell experiments, but it is an irreversible endpoint assay since photobleaching destroys the biosensor. In addition, it does not allow observing time-dependent changes in FRET efficiency [276, 277].

Fluorescence lifetime is the average time a molecule spends in the excited state before dropping to the ground state. This nanosecond-scale decay pattern of emission is recorded in FLIM-FRET. FRET interaction leads to quenching of the donor emission and decreases the lifetime. The determination of FRET efficiency is possible by comparing the fluorescence lifetimes of the donor in presence and absence of the acceptor by following equation:

$$E = 1 - (\tau DA/\tau D)$$

EQUATION **4**

τDA and τD are the lifetimes of the donor in the FRET biosensor in presence and absence of the acceptor, respectively. FLIM-FRET is a very robust method and offers many advantages over intensity-based methods. It is independent of donor and acceptor concentrations and insensitive to spectral crosstalk. However, the expensive and highly specialized equipment needed, prevent its wide use in most laboratories [273, 278].

1.10.2.2 Direct FRET measurements

In contrast to indirect measurements, direct quantification of FRET relates changes in fluorescence emission intensity (sensitized emission seFRET) or fluorescence polarization (prFRET) to changes in FRET efficiency. The direct measurements are simple and have high temporal resolution, which makes them suitable for tracking fast molecular events and high-throughput drug screening. The most common type of seFRET is ratiometric FRET. In this method the doubly labeled sample is illuminated with the donor excitation wavelength and the signals are collected in both donor and

acceptor channel. A FRET index is then defined as the ratio of fluorescence intensities in the donor and acceptor channel, due to the fact that the ratio is very consistent [279]. It is possible to observe the change in FRET efficiency clearly by recording the antiparallel signals of donor and acceptor channel (Figure 1.19). For this method, several correction factors related to the fluorophore crosstalk need to be determined in independent control experiments:

I. Bleed through of the donor emission into the acceptor channel
II. Acceptor emission which is due to false excitation by the donor excitation wavelength

This method allows the investigation of FRET changes over a long time scale (if photostable fluorophores are used), which makes it a very well applicable method [280].

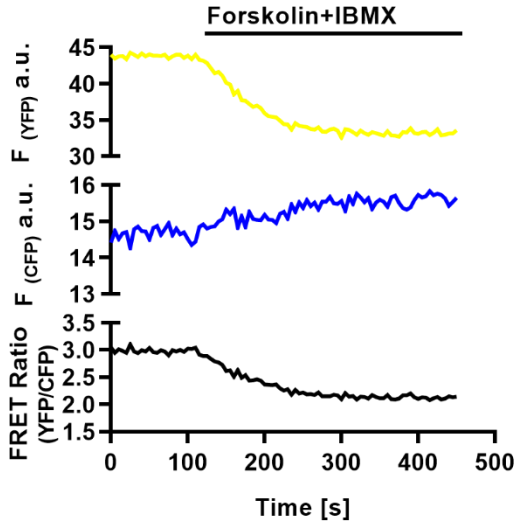

Figure 1.19 FRET traces in ratiometric measurements
In ratiometric FRET experiments the intensity of donor (CFP, blue) and acceptor (YFP, yellow) emissions are recorded to enable the calculation of the FRET ratio (black). The addition of forskolin+IBMX leads to an increase in cAMP detected by Epac1-camps. FRET efficiency of the biosensor is decreased, visible as antiparallel donor and acceptor emission intensities and a decrease of the calculated FRET ratio.

In prFRET use is being made of the fact that only fluorophores with a parallel dipole orientation to the polarized excitation light can be excited. Fluorescent proteins have the advantage of exhibiting highly polarized fluorescence. When energy transfer occurs, the fluorescence of the acceptor depolarizes partially because of the different dipole orientation to the donor [273]. The unique advantage of prFRET over all other FRET approaches is that it is the only technique with which homo-FRET can be detected: energy transfer between spectrally identical fluorophores. The dynamic range of this method is higher, and the detection is faster compared to FLIM-FRET. However, in hetero-FRET (spectrally divergent fluorophores), polarization can be increased, therefore correction factors analogous to seFRET need to be determined [272, 281, 282] .

1.10.2.3 Time resolved FRET measurements

The intrinsic fluorescence of proteins and other substances found in biological samples, which are studied using FRET as a technique states a serious limitation on sensitivity, since the high background can outweigh the signal from the fluorophores of the sensors. Considering that the background noise is rather short-lived, the use of long-lived fluorophores in time-resolved techniques should reduce the fluorescence interference. Lanthanides are attractive donors for their extremely long emission lifetimes (microsecond to millisecond range) and single exponential decay, which is easy to measure. Usually cryptates of europium Eu^{3+} or terbium Tb^{3+} are used as energy donors. The interesting feature of trFRET

is that the donor emission commences with a significant time delay after the excitation. This way, the lanthanide emission is recorded after a certain delay, during which the auto-fluorescence of the sample occurs and decays, to not interfere with the sample measurement anymore. The signal-to-noise ratio is improved as a result [283]. Another major advantage of using lanthanides as donors is that the measurable distance range is > 100 Å, giving the possibility to measure interaction between partners with bigger distance. Technically, lanthanide emission is not fluorescence (not singlet-to-singlet transition), therefore trFRET is also regarded to as lanthanide-based or luminescence resonance energy transfer (LRET) [284]. Nevertheless, the same rules as for regular FRET apply, with less dependence on the orientation of the fluorophores, making it a viable technique to measure FRET [285].

1.11 Relevance of FRET for life sciences

Since the FRET efficiency is related to the distance between donor and acceptor fluorophore, FRET has found many biological applications in the last decades, mainly to study interaction or co-localization of two probes which are bound to fluorophores. The discovery of green fluorescent protein (GFP) in 1962 [286], elucidation of its DNA sequence to allow linking it genetically to any protein of interest [287, 288], and its modification to create differently coloured fluorescent proteins (FPs) boosted the application of FRET in scientific research [289]. Genetically engineered FRET biosensors, based on fluorescent proteins, which respond to a change in the environment translating it into a change of distance detected by FRET, are valuable tools. Using this approach, diverse biological processes are made qualitatively visible and quantitatively measurable [268]. Biophysical methods including conventional microscopy are limited to a spatial resolution of ≈ 250 nm due to the diffraction of light [290]. Therefore, FRET biosensors, which can detect distance changes in the range of 1-10 nm complement these methods to study various biological processes. Super-resolution microscopy techniques such as PALM (photo-activated localization microscopy), STED (stimulated emission depletion microscopy), STORM (stochastic optical reconstruction microscopy) and SIM (structured illumination microscopy) have pushed the resolution limits to <100 nm. However, these techniques require long scanning times, which prevents studying fast, highly dynamic events in the cell [291]. FRET has the advantage of a high temporal and spatial resolution.

As described in the late nineties by Roger Tsien [292] FRET biosensors can be engineered to study int*er*- or int*ra*molecular interactions. In int*er*molecular FRET probes, two separate proteins in close proximity are fluorescently tagged, which enables studying their interaction. Protein-protein interaction, as well as trafficking of biomolecules can be monitored by this means. Bünemann *et* al. were among the first to record the real-time interaction of GPCRs with G proteins [293], and GPCR sorting from endosomes was visualized [294].

In contrast, int*ra*molecular FRET sensors carry the donor and acceptor on the same protein. By this means, conformational changes during protein activation are observed as for β-arrestins for instance [65]. As described by Zaccolo *et* al. already in 2000, fluctuations of second messenger such as cAMP can be measured by flanking the cAMP-binding domain of an effector protein with two fluorescent probes. The conformational change upon second messenger binding leads to a detectable FRET change, enabling the measurement of changes in cAMP levels intracellularly [295].

FRET sensors are widely applicable in various research fields. Studying intracellular ion concentrations [296] or pH [297], monitoring real-time drug release from nanomaterials in living cells [298] or in vivo [299] and visualizing cellular compartmentation of enzymes like PKA [259] are only a few examples of the various possible applications.

1.12 GPCR studies with FRET biosensors

FRET is by now a standard technique used to study GPCR-related questions. In theory, every event within the GPCR signaling cascade can be monitored using a FRET-based system, either in single cell experiments or in a microtiter format. For example, it is possible to monitor the binding process of fluorescently labeled GPCR ligands to their receptors by FRET [300, 301]. The development of FRET based assays enabled a rapid progress in receptor research, since they provide both spatial and temporal information on the binding properties of GPCR ligands, impossible to monitor with traditional binding assays.

The conformational changes within receptors, facilitated upon ligand binding allow the triggering of the GPCR signaling cascade. An increasing number of biochemical and structural data show that small shifts of the transmembrane helices around the binding pocket translate into larger movements at the intracellular site, thereby opening a pocket into which the G protein can dock. FRET sensors have been developed, based on the movement of the transmembrane helices. These sensors respond to the activation of the receptors with a change in FRET [18, 277, 285].

Additional FRET based assays have been developed, which enable capturing various GPCR-mediated signaling events along the cascade. In the early 2000s, the first generation of FRET-based biosensors to monitor G_S- and G_i-protein activation have been created [293, 302], and were later optimized for better performance and practicability [303, 304]. Sensors for G_q-activation and less common G protein subtypes were developed only several years later [305-307]. Of note are innovative G protein sensors which are subtype-independent since the FRET partners are introduced into the Gβγ subunits [308]. They are used as universal tools to study receptor activation of GPCRs, which couple to different G proteins.

It is possible to monitor the subsequent step to G protein activation along the signaling cascade by FRET-based biosensors. AC-activation sensors are available [309], as well as sensors monitoring fluctuations of intracellular second messengers like cAMP [310, 311], IP_1 [312] and calcium [313, 314]. Additionally, there are FRET sensors available for further downstream effectors such as ERK [315, 316].

Furthermore, several FRET sensors are at hand to monitor G protein independent receptor events as receptor oligomerization [317] and trafficking or internalization [143]. By selecting suitable donor-acceptor labelling sites, int*er*- and int*ra*molecular sensors for β-arrestin recruitment [318] and activation [65, 319] were developed.

FRET biosensors play an essential role in studying GPCR signaling compartments. As recent literature is showing, GPCRs may regulate various effector proteins and second messengers, within these signaling domains in a spatially and temporally confined manner, setting the basis for the regulation of many different physiological processes [260, 320, 321].

To sum up, FRET biosensors are useful tools to study a plethora of GPCR related events. Combining all these different assays may help in investigating the physiological role of GPCRs, understanding structure-activity relationships of ligands and putatively identifying novel drug candidates in order to modulate their action.

1.13 Means to study cAMP in cells

cAMP detection in cells has evolved from bulk biochemical analysis to targeted real time imaging in living cells [322, 323]. The following passage will cover most prominent techniques, used over the past 5 decades.

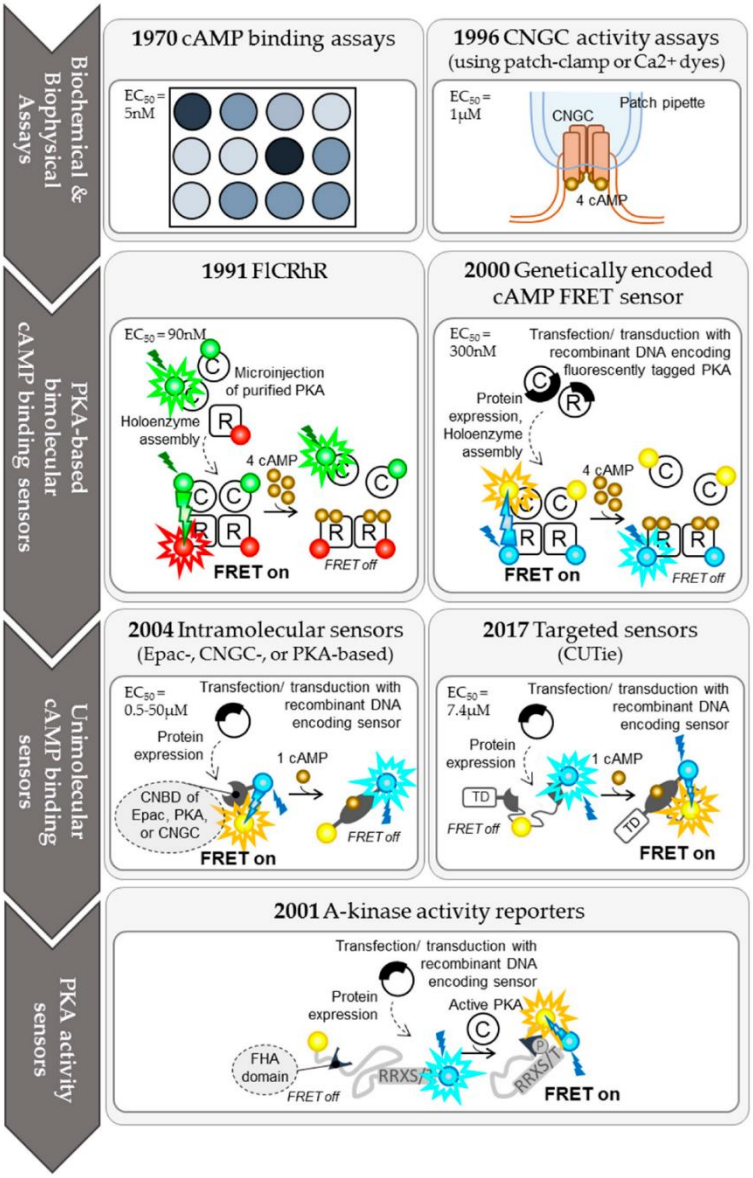

Figure 1.20 cAMP detection tools
Evolution of cAMP detection tools over time, from bulk biochemical analysis to targeted real-time imaging reporters in living cells. cAMP molecules are represented by golden spheres. EC_{50} value for cAMP is indicated for the different detection systems as reported in the literature (extracted from [323] according to Creative Commons Attribution License https://www.mdpi.com/2308-3425/5/1/17).

1.13.1 Biochemical methods

Traditionally, accumulation based assays were used for cAMP detection. In the early 1970ies Al Gilman was the first who proposed a very sensitive assay for the quantification of cAMP based on the competition for protein binding [324]. The general principle of accumulation assays relies on the competition between cAMP in the sample and a labeled form of cAMP for binding to an anti-cAMP antibody [325]. In the 1970ies, classical radioimmunoassays (RIAs) were the method of choice to quantify total cAMP in various cells and tissues [326]. RIAs use immobilized anti-cAMP antibodies and ^{125}I-labelled cAMP as a tracer molecule. The antibodies bind ^{125}I-labelled cAMP and a radioactive signal is detected. cAMP from added cell- or tissue lysates competes with the labelled probe and the radioactive signal decreases inversely proportional to the cAMP amount in the sample. The amount of cAMP in the sample can be inferred by creating a calibration curve [326].

Non-radioactive approaches to measure cAMP in vitro include enzyme-linked immunoassays. cAMP from the sample binds to a specific primary antibody and competes with a cAMP conjugated to alkaline-phosphatase or acetylcholine-esterase. The mixture is then incubated in a multiwell plate coated with a secondary antibody, and the enzyme activity can be quantified by adding the substrate for the conjugated enzyme, which is converted into a colored product [327].
cAMP amount can also be assessed in an indirect way using Western blot analysis. cAMP activates PKA which phosphorylates several substrates. These phosphorylated proteins can be detected by phospho-specific antibodies and the intracellular cAMP levels can be deduced.

All biochemical methods have the advantage of being quite sensitive and specific, however they require a high number of cells or tissue that need to be disrupted. Real-time monitoring of cAMP in various subcellular microdomains is impossible. Therefore additional approaches have been developed, allowing the visualization of cAMP in single living cells with high temporal and spatial resolution [322].

1.13.2 Cyclic nucleotide gated channels (CNGCs)

CNGCs are non-selective cation channels with four subunits, each having an intracellular binding site for cAMP. cAMP-binding activates the channel, allowing for cations to flow intracellularly and patch-clamp enables to record this cation current [328]. Alternatively, if the monitored current consists of Ca^{2+} ions, the influx can be visualized by using calcium sensitive dyes. Both approaches, however, are only an indirect measure of sub-sarcolemmal cAMP concentrations [329].

1.13.3 FRET-based sensors

Above mentioned techniques are suitable to measure cAMP concentrations in cell lysates or to monitor real-time dynamics at the plasma membrane. However, these approaches are too restricted to a specific cellular location. FRET-based sensors have been generated, which allow studying cAMP dynamics with higher spatial resolution (see Annex Table 7.2).

1.13.3.1 PKA based cAMP sensors

The first FRET-based cAMP sensors were based on PKA. In FlCRhR (pronounced “flicker”), the catalytic and regulatory PKA subunit are chemically labelled with fluorescein (donor) and rhodamine (acceptor) respectively. Energy transfer occurs in the intact PKA holoenzyme, while cAMP binding leads to C-R dissociation upon which the FRET signal decreases [330].

A genetically encoded cAMP FRET sensor was first developed by Zaccolo *et* al*.* by fusing different GFP mutants to the PKA subunits [295]. Since the initially used fluorescent proteins (FPs) were prone to

photobleaching, the sensor was improved by exchanging the FPs to CFP (fused to RII subunit) and YFP (fused to C subunit). cAMP measurements in microdomains of cardiomyocytes were made possible with this FRET probe, in addition to studying the effect of specific PDE isoforms on cAMP compartmentation [261, 331].

Despite their vast contribution to cAMP visualization in living cells, PKA based FRET sensors have several disadvantages. Both sensor subunits need to be expressed equally to form a functional heterotetrameric sensor. The fluorescently labelled sensor subunit might interact with endogenous R- and C-subunits, and the cooperative binding of cAMP to PKA leads to slow sensor kinetics [205]. Therefore simpler sensors, based on a single cAMP binding domain of the PKA subunit or on other effector proteins, were developed [311].

The most advanced, recently generated cAMP sensor CUTie (cAMP universal tag for imaging experiments) is based on the CNBD of PKA RIIβ subunit. In this probe, the FRET donor is fused to the C-terminus of the CNBD and the FRET acceptor is inserted in an intra-domain loop of the CNBD, leaving the N-terminus free to enable sensor targeting. The unique feature of this sensor is that it enables fusion of a targeting domain distal to the fluorescent proteins. This way, the targeting domain and FRET module are separated from each other, minimizing the steric hindrance on the conformational change required for energy transfer. This concept ensures that targeting of the CUTie to different domains does not perturb the dynamic range of the sensor [258]. This is not necessarily the case for the targeting of different sensors, since cAMP binding and the spectral properties of the FRET sensors can be influenced by the targeting domain. Accurate calibration of targeted sensors is required for the comparison of cAMP response at different sites.

1.13.3.2 Epac-based cAMP sensors

Several single-chain FRET sensors based on Epac were developed and published in 2004 [311] [332, 333]. Human Epac1 or murine Epac2 as cAMP binding domains, are sandwiched between CFP and YFP in different positions to generate Epac1-camp and Epac2-camp sensors (Figure 1.21). cAMP binding induces a conformational shift within the sensor which results in a decrease of the FRET signal. Epac1-camps seems to have a slightly lower cAMP affinity than Epac2-camps (2µM vs. 1µM), and it shows larger change in FRET ratio, therefore it is used preferably [311].

At the same time, Ponsioen *et* al. created a cAMP sensor based on the full length, or partially truncated Epac1 protein fused between CFP and YFP. It has an extended dynamic range compared to the PKA probes and shows, as Epac1,2-camps, a uniform distribution in the cytosol [333].
The third set of Epac-based cAMP sensors are termed ICUE (indicator of cAMP using Epac), which use the full length Epac1 or truncated versions of Epac2 placed between CFP and citrine [332]. ICUE1 shows the biggest change in FRET ratio and was used in further experiments, targeted to the membrane, nucleus or mitochondria to measure local cAMP levels. ICUE2 is an improved version of ICUE1, showing larger FRET signals while minimizing the affection of cellular functions [334].
All these single-chain Epac-based FRET sensors are superior to the tetrameric PKA sensors, since the technical limitations as unequal subunit expression are eliminated [322].

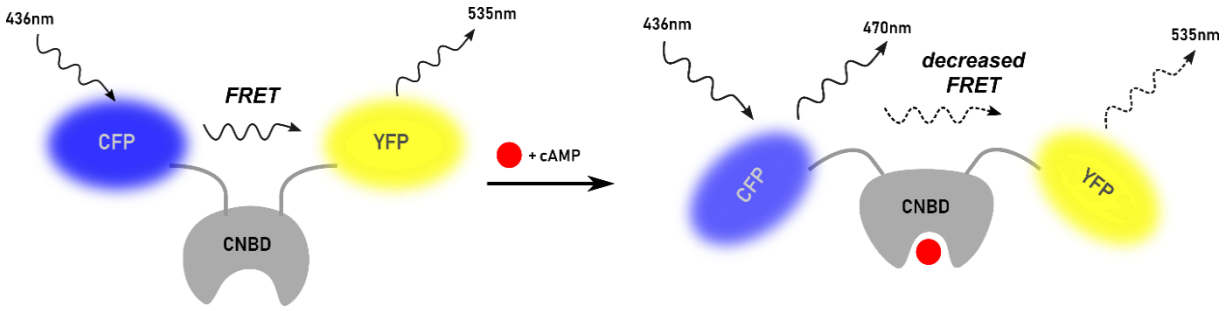

Figure 1.21 Principle of Epac-based cAMP sensor
In the cyclic nucleotide free state the two fluorophores CFP and YFP are in close proximity which enables efficient resonance energy transfer from CFP to YFP upon excitation of CFP. Binding of cAMP to the CNBD of Epac induces a conformational change within the sensor, detectable as a loss in FRET.

1.13.3.3 CNGC based cAMP sensors

The cAMP binding domain of CNGCs lies within the C-terminus and is involved in channel gating [335]. Using this domain from the murine hyperpolarization activated cyclic nucleotide-gated potassium channel 2 (HCN2) sandwiched between CFP and YFP led to the creation of HCN2-camps [336]. It has a high dynamic range and is more suitable for cells with higher basal cAMP activity since its sensitivity lies around EC_{50}= 6µM.

1.13.3.4 Single-wavelength fluorescent sensors for cAMP

In order to enable the monitoring of multiple signaling pathways simultaneously, single-wavelength fluorescent sensors have been proved useful. In Flamindo and Flamindo2, two halves of the EYFP variant citrine encompass the cAMP binding domain Epac1. Binding of cAMP decreases the fluorescence intensity of citrine [337].

In the second available single-wavelength fluorescent cAMP sensor, termed cAMPr, circularly permuted GFP (cpGFP) is bound by the full-length C subunit of PKA on one side, and an R subunit lacking the dimerization/docking domain on the other side. cAMP binding separates the PKA subunits which leads to an increase in GFP fluorescence [338].

cADDis (cAMP Difference Detector in situ) is an additional sensor using a similar approach as cAMPr. Here, cpGFP is positioned within the hinge region of Epac1 separating the catalytic and regulatory subunit. cAMP binding to the regulatory subunit leads to a large conformational shift, the positions of the catalytic and regulatory subunits are rearranged leading to a change in fluorescence intensity of cpGFP [339].

All above mentioned sensors were used in combination with calcium-sensing dyes in order to simultaneously record both pathways [338].

1.13.3.5 Monitoring cAMP signaling dynamics

An indirect way of measuring cAMP activity is to investigate the dynamics of cAMP signaling looking at the catalytic activity of PKA. With A kinase activity reporters (AKARs) it is possible to monitor PKA activity dynamics with high temporal and spatial resolution by FRET. These sensors constitute of a PKA substrate sequence and a phosphate-binding acceptor domain sandwiched between eCFP and

YFP/Venus [340, 341]. Phosphorylation of the substrate leads to the interaction with the phosphate-binding domain, facilitating the conformational change and with this a change in FRET efficiency. The most recently published and improved AKAR4 sensor uses cerulean instead of CFP and was targeted to the plasma membrane to measure compartmentalized PKA activity in this subcellular domain [342]. A unique feature of the sensor is that it allows dephosphorylation, providing the possibility to monitor PKA activity which increases FRET and phosphatase activity, which decreases FRET [343].

1.13.4 Targeting of FRET sensors

Genetically encoded FRET sensors are in general useful tools to study interactions of molecules and have been particularly instrumental in the elucidation of cAMP compartmentalization. Fusing a targeting domain to these sensors, allows directing them to a certain subcellular site where they can accurately monitor signaling events. In addition, proteins of interest can be tagged with these sensors to investigate their role in the signaling cascade [344].
The mechanism of targeting has been applied successfully to study compartmentalization of cAMP [258, 332, 345] or PKA phosphorylation [346, 347]. AKAPs have been proved useful as fusion targets to study compartmentalized signaling [258, 348, 349] especially AKAP79 [350, 351].

Targeting sequences are available for very distinct organelles such as the nucleus [332], mitochondria [352], cilia [353] or flagella [354]. Enzymes can be tagged like specific PDEs [355, 356] or distinct proteins within cardiomyocytes like AKAP18δ/SERCA/PLB complex localized at the sarcoplasmatic reticulum, TPNI complex localized at the myofilament or AKAP79 at the plasmalemma [258]. In principle, all cellular locations or proteins can be addressed by choosing the suitable targeting sequence. This opens up new ways to study localized signaling events, particularly cAMP dynamics, to broaden our understanding of compartmentalization.

1.14 Objective of the study

GPCRs are key players in virtually all cellular functions. They act via their second messengers and effector proteins to operate and regulate many physiological processes. Therefore, these membrane-embedded targets have been subject of major interest since understanding their molecular signaling mechanism might open up new ways to modulate their action and use them as therapeutical targets.

For G_S-coupled receptors, the second messenger cAMP mediates the signal coming from the plasma membrane by operating various effector proteins. Despite thorough studies by the scientific community trying to understand the receptor-second messenger-effector axis, it is still not entirely clear how such a plethora of events are being individually operated by one second messenger.

The paradigm of signaling compartmentation where cAMP stays local and the signaling partners are brought in close proximity as means to achieve signaling specificity is the currently most widely accepted hypothesis in the field. Hence, proving the existence, studying the putative size and the molecular details of such compartments and how they are maintained remains to be accomplished.

At present, the most valuable real-time approaches to study cAMP dynamics in living cells are biophysical techniques employing FRET-cAMP-reporters. The high spatial resolution of these sensors allows overcoming optical limitations and enables the detection of cAMP with a sub-microscopic resolution.

The goal of this project is to address the topic of signaling specificity and visualize high-concentration cAMP compartments, study them with regards to their location, size, dynamics and physiological impact. We set out to achieve this goal through four main research objectives:

1. Employ a FRET based cAMP sensor and molecular cloning techniques to target it to different cellular locations, monitor real time cAMP dynamics in different cellular compartments and find a high-concentration cAMP domain.
2. Characterize the cAMP domain by assessing its dynamics in response to stimuli from different GPCRs.
3. Investigate the spatial and temporal dynamics and the role of different proteins in establishing the high-concentration cAMP compartment.
4. Evaluate whether the compartmentalized cAMP signal translates into a physiological response, downstream of a certain GPCR.

2 Material and Methods

2.1 Materials

2.1.1 Cell lines

- Human embryonic kidney (HEK)-293 cells (ATCC)
- HEK-TsA cells (ATCC)
- Chinese hamster ovary CHO-K1 (ATCC)
- Clonal line stably expressing hGLP1R-camps generated from HEK-293 cells (this work)
- Clonal line stably expressing Epac1-camps-CAAX generated from HEK-293 (this work)
- Clonal line stably expressing Epac1-camps generated from HEK-293 (this work)

2.1.2 Cell culture media and supplements

- Dulbecco's modified Eagle medium (DMEM) 4.5g/L Glucose, w/o: L-glutamine, w: Sodium pyruvate, w: 3.7 g/L NaHCO3 (P04-03600 PAN Biotech GmbH)
- Opti-MEM I Reduced Serum Medium, no phenol red (11058021 Life Technologies GmbH)
- Ham's F12 Medium, without L-glutamine, with 1,176 g/l NaHCO3 (P04-14550 PAN Biotech GmbH)
- DMEM/F12, no phenol red (21041033 Life Technologies GmbH)
- Dulbecco's phosphate buffered saline (DPBS), calcium, magnesium (14040091 Life Technologies GmbH)
- Penicillin/Streptomycin 10.000 E/10.000 µg/ml (A 2213 Biochrom GmbH)
- L-Glutamine 200mM (P04-80050 PAN Biotech GmbH)
- Trypsin 0,05 %/EDTA 0,02 % in PBS, without Ca2+ and Mg2+ (P10-023100 PAN Biotech GmbH)
- Fetal bovine serum (F7524-500ML Sigma Aldrich Chemie GmbH)
- 2-Mercaptoethanol 55 mM (21985023 Life Technologies GmbH)
- Dimethylsulfoxide (DMSO) cell culture (A994.1 Carl Roth GmbH & Co. KG)
- Poly-D-Lysine hydrobromide (P0899-100mg Sigma Aldrich Chemie GmbH)
- G418 disulfate salt (G5013-250MG Sigma Aldrich Chemie GmbH)

2.1.3 Plasmids

Plasmid	Source
Epac1-camps in pcDNA3	Institute of Pharmacology and Toxicology
Epac1-R279E-camps in pcDNA3	Institute of Pharmacology and Toxicology
Epac2-camps-CAAX in pcDNA3	Institute of Pharmacology and Toxicology
Epac1-cAMPs-CAAX in pcDNA3	This work; Anton, Selma
Wildtype hGLP1R in pcDNA3	Kind gift from Christoph Klenk (University of Zürich, Switzerland)
hGLP1R-YFP in pcDNA3	This work; Zabel, Ulrike
hGLP1R-YFP +BmtI/BspEI sites in pcDNA3	This work; Zabel, Ulrike
hGLP1R-camps in pcDNA3	This work; Anton, Selma
hGLP1R-R279E-camps in pcDNA3	This work; Anton, Selma
hGLP1R-SAH30-camps in pcDNA3	This work; Anton, Selma

hGLP1R-SAH60-camps in pcDNA3	This work; Anton, Selma
SAH30 (ER/K) linker 30nm in pcDNA3	Institute of Pharmacology and Toxicology
SAH60 (ER/K) linker 60nm in pcDNA3	Synthesis by Eurofins Genomics. Institute of Pharmacology and Toxicology.
Epac1-CAAX +BmtI/BspEI sites in pcDNA3	This work; Zabel, Ulrike
Epac1-CAAX-SAH30 in pcDNA3	This work; Anton, Selma
Epac1-SAH60-CAAX in pcDNA3	This work; Anton, Selma
EPAC-1-ext1-CAAX in pcDNA3	This work; Anton, Selma
EPAC-1-ext2-CAAX in pcDNA3	This work; Anton, Selma
AKAR-4 in pcDNA3.1	Jin Zhang (UCSD San Diego, USA)
hGLP1R-AKAR4 in pcDNA3.1	This work; Anton, Selma
hGLP1R-IRES-AKAR4 in pcDNA3	This work; Anton, Selma
Lyn-Halo-SAH60-Halo-CAAX in pcDNA 3.1	Synthesis by Genescript

Table 2.1 Plasmids used in the course of this study

2.1.4 Primers

All Primers used for generation and amplification of cDNA were synthesized by Eurofins Genomics of BioTeZ GmbH. The sequence of all constructs was validated by sequencing of indicated plasmids through Eurofins Genomics or LGC Genomics.

Primer	Cloning of construct
Primer Insert forward: 5’ AAAA AAG CTT ATG GCC GGC GCC CCC GGC CCG 3’	WT-hGLP1R-stop
Primer insert reverse: 5’ TGC CAG GCC TCC TGC AGC TAA CTC GAG TTTT 3’	WT-hGLP1R-stop
Primer Insert forward: 5’ AAAA AAG CTT ATG GCC GGC GCC CCC GGC CCG 3’	WT-hGLP1R
Primer insert reverse: 5’ TGC CAG GCC TCC TGC AGC CTC GAG TTTT 3’	WT-hGLP1R
Primer insert forward: 5’ AAAA AAG CTT ATG GCC GGC GCC CCC GGC CCG 3’	hGLP1R-YFP
Primer insert reverse: 5’ TGC CAG GCC TCC TGC AGC TCT AGA TTTT 3’	hGLP1R-YFP
Primer insert forward 5’ AAA TCT AGA GCT AGC GGG TCC GGA GTG AGC AAG GGC GAG GAG 3’	hGLP1R-YFP +BmtI/BspEI sites
Primer insert reverse 5’ AAA AGC GGC CGC AAA GAA TTC CTT GTA CAG CTC GTC CAT 3’	hGLP1R-YFP +BmtI/BspEI sites
Primer insert forward: 5’ TTT CAG GGC GCT AGC GGA GAA 3’	hGLP1R-SAH30-camps
Primer insert reverse: 5’ AGA GCC TCC GGA GCC TCT TT 5’	hGLP1R-SAH30-camps
Primer vector forward: 5’ CTG TAC AAG GCT AGC GGG TCC GGA GGT GGA ACC GGT GGA AGT AAG AAA AAG TCT AAG ACT AAA TGT 3’	Epac1-ext1-CAAX

Primer vector reverse: 5’ ACA TTT AGT CTT AGA CTT TTT CTT ACT TCC ACC GGT TCC ACC TCC GGA CCC GCT AGC CTT GTA CAG 3’	Epac1-ext1-CAAX
Banana split forward: 5’ ATT CTA GTT GTG GTT TGT CCA AAC TCA TCA A 3’	Epac1-ext1-CAAX
Banana split reverse: 5’ TTG ATG AGT TTG GAC AAA CCA CAA CTA GAA T 3’	Epac1-ext1-CAAX
Primer vector forward: 5’ CTG TAC AAG GCT AGC GGG TCC GGA GGT GGA ACC GGT GGA AGT GGT GGA ACC GGT GGA AGT AAG AAA AAG TCT AAG ACT AAA TGT 3’	Epac1-ext2-CAAX
Primer vector reverse: 5’ ACA TTT AGT CTT AGA CTT TTT CTT ACT TCC ACC GGT TCC ACC ACT TCC ACC GGT TCC ACC TCC GGA CCC GCT AGC CTT GTA CAG 3’	Epac1-ext2-CAAX
Primer vector forward: 5’ TCT AGA GCT AGC GGG TCC GGA GAT AAG GAT CCC ATG GTG AGC 3’	hGLP1R-AKAR4
Primer vector reverse: 5’ CGG GCC GGG GGC GCC GGC CAT GGT GGC GGC CGC AAG CTT 3’	hGLP1R-AKAR4
Primer insert forward: 5’ CCC AAG CTT GCG GCC GCC ACC ATG GCC GGC GCC CCC GGC 3’	hGLP1R-AKAR4
Primer insert reverse: 5’ GCT CAC CAT GGG ATC CTT ATC TCC GGA CCC GCT AGC TCT AGA 3’	hGLP1R-AKAR4
Primer vector forward: 5’ GAT GAT AAT ATG GCC ACA ATG GTG AGC AAG GGC GAG 3’	hGLP1R-IRES-AKAR4
Primer vector reverse: 5’ GGG AGG GAG AGG GGC TTA TCC GGA CCC GCT AGC TCT 3’	hGLP1R-IRES-AKAR4
Insert primer forward: 5’ AGA GCT AGC GGG TCC GGA TAA GCC CCT CTC CCT CCC 3’	hGLP1R-IRES-AKAR4
Insert primer reverse: 5’ CTC GCC CTT GCT CAC CAT TGT GGC CAT ATT ATC ATC 3’	hGLP1R-IRES-AKAR4

Table 2.2 Primers used for cloning of all constructs in the course of this study

2.1.5 Cloning enzymes

All restriction enzymes, Polymerases, Ligases, Nucleotides and respective buffers were bought from New England Biolabs GmbH

- Hind III
- Xho I
- Xba I
- Not I
- Bmt I
- BspEI
- EcoRI
- T4 DNA Ligase
- Q5® High-Fidelity DNA Polymerase
- Phusion® High-Fidelity DNA Polymerase

2.1.6 Chemical compounds

- GLP1-(7-36)-NH2 (2082)- Tocris
- Forskolin (F3917), IBMX (3-Isobutyl-1-methylxanthine I5879), MDL (MDL-12,330A hydrochloride, M182), cAMP (Adenosine-3',5'-cyclic monophosphate sodium salt monohydrate, A9501), (-)-Isoproterenol x HCl (I6504), D-(+)-Glucose x monohydrate (49161) were purchased from Sigma-Aldrich
- St-Ht31 (V8211), St-Ht31-P (V8221) (InCELLect™) were purchased from Promega.
- 8-Br-O'-Me-cAMP-AM (B 028-01)- Biolog Life Science Institute
- Saponin was a kind gift from Prof. Manuela Zaccolo (Saponin from Quillaja bark S4521 Sigma-Aldrich 20-35% Sapogenin content)
- JF-646 Halo dye was a generous gift from Luke Lavis (Janelia)

2.1.7 Devices

- Brightfield fluorescence microscope: Axiovert 200 inverted microscope (Zeiss, Jena, Germany) with an oil immersion objective (plan-NEOFLUAR 63x/1.25). 505 dcxr beam splitter (Visitron Systems, Puchheim, Germany), high speed polychromator system (Visitron Systems), iXon Ultra EMCCD camera (Andor, Belfast, UK), Metafluor 7 software (Molecular Devices, Sunnyvale, CA, USA).
- Brightfield fluorescence microscope: Leica DMi8 inverted microscope (Leica Microsystems, Wetzlar, Germany) with an oil immersion objective (HC PL APO 63x/1.40-0.60 oil). Dichroic beamsplitter T505lpxr (Visitron Systems, Puchheim, Germany), Emission filter 470/24 nm and YFP emission filter 535/30 nm (Chroma technology corp.), Visichrome high-speed polychromator (Visitron Systems), Xe-Lamp 75W, 5.7 A (Hamamatsu Photonics), Photometrics Prime 95B CMOS camera (Visitron systems) with Optosplit II dual emission image splitter (Cairn). Visiview 4.0 imaging software (Visitron Systems).
- Confocal setup: Leica TCS SP5 or TCS SP8 with an oil immersion objective (HC PL APO 63x/1,40-0,60 oil)
- Plate reader: Synergy Neo2 plate reader (BioTek Instruments) equipped with a monochromator. Additionally various filter sets were used.

2.1.8 Commercially available kits

- Effectene Transfection Reagent (4 x 1 ml) (301427 Qiagen GmbH)
- Lipofectamine 2000 Transfection Reagent-0.3 mL (11668030 Life Technologies GmbH)
- FuGENE® HD Transfection Reagent (E2311 Promega)
- Gibson Assembly Master Mix (E2611L New England Biolabs GmbH)
- QIAGEN Plasmid Plus Midi Kit (12945 Qiagen GmbH)
- Monarch™ Plasmid Miniprep Kit (T1010L New England Biolabs GmbH)
- Monarch™ DNA Gel Extraction Kit (T1020L New England Biolabs GmbH)
- cAMP EIA Kit (*581001* Cayman chemical company)

2.1.9 Other consumables

- TC-Platte 6 Well, Standard F (833,920,005 SARSTEDT)
- TC-Schale 100, Standard (833,902 SARSTEDT)
- TC-Platte 96 Well, Standard F (833,924,005 SARSTEDT)

- TC-Schale 60, Standard (833,901 SARSTEDT)
- 96-well plates, black walled, black bottomed (BR781968-50EA Brand GmbH)
- Coverslips 24 mm Ø (0111640 Paul Marienfeld GmbH)

2.2 Methods

2.2.1 Molecular biology

2.2.1.1 Preparation of competent Escherichia coli (E. coli) for KCM-transformation

NEB DH5α-competent E. coli are spread on an lysogeny broth (LB)-plate without antibiotics and incubated over night at 37°C. The following day one single colony is picked to inoculate 50 ml LB-medium and grown over night at 37°C in a circulatory shaker (180 RPM, 5% CO_2). The next day, 4.5 ml of the pre-culture are used to inoculate 250 ml LB medium and incubated at 37°C in a circulatory shaker until the optical density of the suspension measured at 595 nm reaches 0.5 – 0.6. Collection of the bacteria by centrifugation for 10 minutes, 3500 RPM, 4°C. Resuspension of the pellet in 25 ml transformation storage buffer (TSB). Preparation of 100 µl aliquots, incubation on ice for 90 minutes, freezing in liquid nitrogen and storage at -80°C.

LB-medium (autoclaved):	1% (w/v) Trypton 0.5% (w/v) yeast extract 1% (w/v) NaCl H_2O
LB agar plates:	1% (w/v) agar in LB-medium Optional: selection antibiotic Ampicillin 100µg/ml, Kanamycin 50µg/ml
TSB (sterile filtered 0.2µm):	10% PEG3000 5% DMSO 20 mM $MgCl_2$ in LB-medium

2.2.1.2 Transformation of competent E. coli (KCM method)

Competent E. coli are transformed to take up a certain plasmid with the aim of amplifying the DNA. Competent cells of the strain DH5α are used for transformation. For this, 100 µl of the bacterial suspension are slowly defrosted on ice, mixed with 100 µl KCM-buffer and either 1 µl of plasmid DNA (1 µg/µl) or up to 20 µl ligation product. Incubation of the mixture for 20 minutes on ice and 10 minutes at room temperature. Addition of 1 ml LB-medium (no antibiotic), rotational shaking for 90 minutes (37 °C, 450 RPM) for regeneration. To isolate the transformed bacteria, either the whole sample (ligation product) or an aliquot of 50 µl is centrifuged (5 minutes, 5000 RPM); the pellet is re-suspended in fresh LB-medium and plated on agar plates containing the suitable selection antibiotic. Culture overnight at 37°C.

KCM buffer (sterile filtered 0.2µm):	100 mM KCL 30 mM $CaCl_2$ 50 mM $MgCl_2$

H_2O

2.2.1.3 Mini plasmid preparation

To isolate a small amount of DNA from competent E. coli transformed with a ligation product a mini plasmid preparation is done, or isolation using the kit. For the manual mini plasmid preparation, 4.5 ml LB-medium are inoculated with a single colony of transformed E. coli and the culture is grown for one night at 37°C in a circulatory shaker (180 RPM, 5% CO_2). Centrifugation of 1.5 ml of the culture (5 minutes, 5000 RPM), resuspension of the pellet in 300 µl P1 buffer. Addition of 300 µl lysis buffer P2, incubation for 2 minutes at room temperature. Bacterial RNA is degraded during lysis due to the supplemented ribonuclease (RNase A). Neutralization with 300 µl buffer P3. Centrifugation for 15 minutes, 14000 RPM, 4°C. Transfer of the supernatant to new tubes and additional centrifugation 5 minutes, 14000 RPM, 4°C. 700 µl of the supernatant is transferred to a new tube, mixed with 500 µl Isopropanol and centrifuged again for 15 minutes, 14000 RPM, 4°C. After discarding the supernatant, the DNA precipitate is washed with 600 µl 70% ethanol (centrifugation 5 minutes, 14000 RPM). After removal of the ethanol, the pellet is dried at room temperature and diluted in 30 µl bi-distilled water. Analysis of resulting DNA is done either through sequencing, or a restriction digest with unique restriction enzymes.

P1 buffer:	50 mM Tris 10 mM EDTA 100 µg/ml RNase A H_2O, pH=8.0
P2 buffer:	200mM NaOH 1% SDS
P3 buffer:	3 M potassium acetate, pH=5.0

2.2.1.4 Midi DNA preparation & adjustment of DNA concentration

To amplify plasmid DNA, a colony grown on an agar plate is picked and 100 ml LB-medium containing the suitable selection antibiotic are inoculated and let grow over night at 37°C in a circulatory shaker. The DNA was isolated and purified using the Plasmid midi kit from Qiagen according to the manufacturer's instructions. The bacterial cells are lysed with an alkaline buffer, and purification of DNA is achieved through chromatographical anion exchange.

After the purification, the concentration of resulting DNA solution is assessed photomerrically at 260 nm using either Nanodrop 2000 or Denovix DS-11 as a microvolume UV/Vis-spectrophotometer and set to 1 µg/µl. The purity of the sample can be evaluated via absorption measurement at 280 nm. Only sampled with an absorption ratio at 260 nm/280 nm ≥ 1.8 are subsequently used to exclude any contamination by proteins.

2.2.1.5 Polymerase-Chain-Reaction (PCR)

DNA fragments from a template plasmid required for cloning are amplified through PCR. Specially designed primers are used to set the starting (forward primer) and endpoint (reverse primer) of the desired fragment, while the DNA polymerase elongates the primers at the 3' end with suitable deoxyribonucleotides (dNTPs) according to the complementary DNA strand.

Standard PCR is performed in a thermal cycler (Biometra Trio- analytic jena), starting with the denaturation of the template DNA for 3 minutes at 94°C. 30 cycles of denaturation (30 seconds, 94°C), primer annealing (1 minute, 55°C), elongation (2.5 minutes, 72°C) follow before the final step of elongation (5 minutes 72°C). Duration and thermal conditions of each step are optimized for each DNA fragment.

Assay conditions:	100 ng plasmid DNA
	20 nmol of each dNTP (dATP, dTTP, dGTP, dCTP)
	50 pmol of each forward & reverse primer
	1 µl DNA Polymerase (3 units/ul)
	10 µl polymerase buffer (10x)
	H_2O ad 100 µl

2.2.1.6 Purification and Isolation of PCR products and DNA fragments on agarose gels

The negatively charged DNA fragments migrate with size dependent speed through an agarose gel in an electric field and thus can be separated and subsequently isolated. Ethidiumbromide is utilized to stain the DNA in the agarose gel, due to its ability to intercalate between the DNA bases, which leads to a fluorescence upon excitation with UV light. 1% agarose gels are prepared by dissolving agarose in tris-acetate buffer (TAE), boiling the solution and adding ethidiumbromide (0.06%). The liquid mixture is poured into a chamber, appropriate combs are mounted and let solidify at room temperature. The gel is then transferred to an electrophoresis chamber and covered with TAE buffer. The DNA samples are mixed with 10x DNA loading buffer and loaded onto the gel alongside 1 kilobase standard DNA ladder. Electrophoresis was performed at 110 V for 30-50 minutes.
The separated DNA bands are identified and excised above a UV lamp. DNA is extracted from the gel using Monarch's gel extraction kit according to the manufacturer's instructions.

TAE buffer (50x):	10 mM EDTA
	50 mM sodium acetate
	400 mM Tris-HCl
	H_2O, adjust pH=8.0
DNA loading buffer (10x)	0.25% (m/v) bromophenol blue
	50% glycerol
	100mM EDTA
	H_2O

2.2.1.7 Restriction enzyme cloning

Combination of DNA fragments and insertion into a vector is essential in order to create new DNA plasmids which in turn encode the proteins of interest. The vector pcDNA3 and pcDNA3.1 was used for all cloned constructs due to its good expression in mammalian cell lines. The plasmids encoding WT hGLP1R, Epac1-camps [311], AKAR4 [342] were used as starting points for all cloned constructs. The general protocol was followed: the desired DNA fragment was amplified through PCR from a suitable template. By designing unique primers, sequences for restriction enzymes are introduced to the desired DNA fragment. Both the PCR product and the vector are digested with the same restriction enzymes to

get complementary ends. After gel separation and purification of both fragments, DNA amount is estimated using a microvolume UV/Vis-spectrophotometer in order to combine vector and insert in an optimal ratio (1:3 or 1:6)

$$\text{Amount insert [ng]} = \frac{\text{amount vector [ng]} \times \text{size insert [kb]}}{\text{size vector [kb]}} \quad x3/6$$

(typical amounts were 12ng insert, 18ng vector)

EQUATION 5

The complementary restriction sites find each other and ligation of both fragments is done overnight at 16°C with the T4 DNA ligase, which catalyzes the formation of a phosphodiesterase bond between the 3'-hydroxy group of one strand and the 5' phosphate-residue of the adjoining strand. The resulting cyclized plasmid is transformed into competent E. coli. 5-10 clones per construct are picked, DNA is amplified and isolated according to the mini DNA preparation protocol. The DNA from each clone is tested by a control digestion, and the results from positive clones are further verified by DNA sequencing to assure the insert and vector were combined without a frame shift or other mutations.

Restriction digest:	4 µg DNA 1.5 µl of each restriction enzyme 5 µl digestion buffer (10x) optional: 5µl BSA (1 µg/µl) H_2O ad 50 µl
Ligation:	DNA fragments of insert & vector 1 µl T4 DNA ligase 2 µl ligase buffer (10x) H_2O ad 20 µl

2.2.1.8 Gibson cloning

By designing suitable primers for the insert and the vector, a complementary overhang sequence is introduced into each fragment. All fragments are PCR amplified and the DNA is separated and isolated from an agarose gel. DNA concentration is measured using a microvolume UV/Vis-spectrophotometer in order to combine the fragments in a suitable ratio (typically 0.03 pmol of each fragment / 3 fold excess of small fragments).

$$\text{Amount fragment [ng]} = \frac{0.03 \text{ pmol} \times \text{size [bp]} \times 650 \text{ daltons}}{1000}$$

Equation 6

Incubation of the mix for 15 minutes at 50°C. Transformation of 2 µl into competent E. coli and subsequent characterization as described in the section of restriction cloning.

Gibson assembly mix:	Total amount of fragments (0.02-0.05pmol) 10 µl Gibson assembly mix (2x) H_2O ad 20 µl

2.2.2 Cell biology

2.2.2.1 Cultivation and storage of cell lines

HEK-293, HEK-TSA and CHO cells were grown in cell culture medium at 37°C and 5% CO_2. Cells were passaged every 2-3 days when a confluence of 90-100% was reached. For this, old medium was aspirated and cells were washed once with DPBS. 1 ml of trypsin/EDTA solution was added (for a 10 cm dish, respective amount for other dish sizes), flown over the whole dish and immediately aspirated. After 2 minutes, cells were re-suspended in fresh culture medium and an aliquot was transferred to a new dish containing fresh medium. Cells were used between passage 5-30.
For long-term storage in liquid nitrogen, cells were harvested according to the above mentioned protocol, with the difference of resuspension in a DMSO and FBS-enriched freeze medium. Cells were aliquoted into cryo-vials and stored for one night in Nalgene® Mr. Frosty® Cryo 1°C Freezing Container at -80°C to ascertain a cooling rate of -1°C/minute. The next morning cells were transferred to a liquid nitrogen container.
To re-culture frozen cells, a cryo-vial was thawed quickly at 37°C, cells were washed once with fresh medium and centrifuged for 3 minutes at 800 RPM. Medium was aspirated to remove DMSO and cells were re-suspended in fresh culture medium and plated on cell culture dishes.

Cell culture medium HEK:	DMEM 4.5 g/l glucose 10% (v/v) FBS 100 U/ml penicillin, 100 µg/ml streptomycin 2mM L-glutamine
Freezing medium HEK:	80% (v/v) complete DMEM 10% (v/v) FBS 10% (v/v) DMSO
Culture medium CHO: (fluorescent measurements)	Ham's F12, without L-glutamine, with 1,176 g/l NaHCO3 10% (v/v) FBS 100 U/ml penicillin, 100 µg/ml streptomycin 2mM L-glutamine
Culture medium CHO: (STORM imaging)	DMEM/F12, no phenol red, without L-glutamine, with 1,176 g/l NaHCO3 10% (v/v) FBS 100 U/ml penicillin, 100 µg/ml streptomycin 2mM L-glutamine
Freezing medium CHO:	80% (v/v) complete Ham's F12 10% (v/v) FBS 10% (v/v) DMSO

2.2.2.2 Transient transfection of cells

For fluorescence measurements in HEK-TsA, cells were seeded on Poly-D-Lysine coated cover slips into 6-well plates (1.7 x 10^5 cells per well). 6-8 hours after seeding cells were transfected using Effectene transfection reagent according to the manufacturer's instructions. 400-600 ng of DNA were used per cover slip. In case two plasmids were co-transfected, the DNA of both was mixed at a ratio of 1:1 and 800-1200 ng of total DNA were transfected. Culture medium was renewed 24 hours post transfection. Fluorescence measurements were performed 48 or 64 hours after transfection.

For fluorescent measurements in CHO, cells were seeded on uncoated coverslips into 6-well plates and let adhere for 6-8 hours. Cells were transfected using FuGENE transfection reagent according to the manufacturer's protocol. 2 µg of DNA were transfected per cover slip. 24 hours after transfection culture medium was renewed and experiments were conducted another 24 hours later.

For dSTORM imaging, CHO cells were seeded the night before on uncoated coverslips into 6-well plates. 12-14 hours after seeding, cells were transfected using Effectene transfection reagent according to the manufacturer's protocol. 2 µg of DNA were used per cover slip. 4-5 hours after transfection cells were labelled and fixed. Experiments were conducted on the same day or 24 hours later.

2.2.2.3 Creation of stable cell lines

HEK-293 cells were used to generate a stable cell line. Cells were seeded onto 10 cm dishes and transfected with 10 µg DNA of desired constructs when they reached a density of 70% using Effectene transfection reagent according to the manufacturer's protocol. Transfected clones were selected with cell culture medium containing 800 µg/ml G-418 selection antibiotic. Single clones were picked and separated. From each clone the brightest cells were selected using fluorescence-assisted cell sorting (FACS). Stable cell lines were maintained in cell culture medium containing 200 µg/ml G-418 at 37°C with 5% CO_2.

2.2.2.4 Whole cell cAMP ELISA

HEK-TsA cells were seeded at a density of 2.5x10^5 into 6 well plates and let adhere overnight. On the next day, cells were transfected with either wild type GLP1R or hGLP1R-camps using calciumphosphate-transfection protocol (3 µl DNA, 3 µl empty pcDNA3, 135 µL H_2O, 15 µl 2,5M $CaCl_2$, 150 µl 2xBBS buffer, incubation for 20 minutes, adding to the cells). 24 hours after transfection culture medium was renewed. 48h after transfection ELISA was performed. Cells were washed once with FRET buffer and incubated for 25 minutes with the compounds. After incubation, buffer was aspirated and 260 µl of 0.1M HCl were added. Cells were incubated for 20 minutes at room temperature and then scraped off the surface. Mixture was centrifuged at 1000xg for 10 minutes and the supernatants were diluted 1:10 before proceeding with the ELISA according to the manufacturer's protocol.

2x BBS buffer (sterile filtered 0.2 µm):	50 mM BES (*N,N*-bis[2-hydroxyethyl]-2-aminoethanesulfonic acid) 280 mM NaCl 1.5 mM Na_2HPO_4 x 2 H_2O H_2O, pH=6.95 adjust at 20°C

2.2.3 Biophysical methods

2.2.3.1 FRET measurements on the microscope

FRET experiments were conducted 48 hours (hGLP1R-camps, WT-hGLP1R + Epac1-camps, WT-hGLP1R + Epac1-camps-CAAX, hGLP1R-AKAR4, WT-hGLP1R-IRES-AKAR4) or 64 hours (hGLP1R-SAH30-camps, hGLP1R-SAH60-camps) post transfection. Cells were washed once with FRET buffer and maintained in FRET buffer at room temperature throughout the experiment. 100ms excitation and image acquisition every 5 seconds.

FRET buffer:	10 mM HEPES
	140 mM NaCl
	5.4 mM KCl
	1 mM $MgCl_2$
	2 mM $CaCl_2$
	H_2O, pH=7.3

2.2.3.2 Confocal microscopy

Confocal images were obtained 48 hours after transfection. Cells were washed once with FRET buffer and maintained in FRET buffer at room temperature while imaging. CFP was excited with a diode laser at 458 nm laser line and fluorescence intensities were recorded from 470 to 550 nm. YFP was excited with a 514 nm laser line at 2-4% power. Fluorescence intensity was recorded from 525 to 600 nm. Settings for recording were kept constant at 1024 × 1024 pixel format, frame average 4, and 400 Hz. To avoid bleed through, parallel images of CFP and YFP were obtained in sequential scan mode using the settings described above.

2.2.3.3 Stochastic optical reconstruction microscopy (STORM)

STORM imaging was conducted 4-5 hours after transfection. Cells were labeled with 1µM of the HaloTag® ligand JF-646 for 20 minutes at 37°C. For this, cells were washed three times with PBS before adding 1 ml of 1 µM fluorophore solution. After labelling, cells were washed three times with DMEM/F12 medium, each time followed by 5 minutes incubation at 37°C. Cells were fixed with ice-cold methanol by adding 2ml to each well and incubating for 20 minutes at -20°C. Three times washing with PBS and storage in PBS at 4°C in case imaging was planned at a later stage. During imaging, cells were kept in Glox buffer at room temperature. STORM images were acquired at a TIRF illuminated Nikon Eclipse Ti2 microscope (Nikon) equipped with a 100x objective with a 1.49 NA automated correction collar. 405, 488, 561, 647 nm laser diodes coupled through an automated N-storm module and four iXON Ultra897 EMCCD Cameras (Andor). For STORM imaging, the automated objective collar and the hardware auto-focus were activated. The 647 nm laser was set to a power of 100% and images were acquired for at least 15000 frames or until blinking events were negligible. STORM movies were processed and analyzed in ImageJ using the Thunderstorm plugin [357].

Glox buffer:	0.56 mg/ml glucose oxidase
	34 µg/ml catalase
	10% glucose
	0.1 M mercaptoethylamine
	50 mM Tris

10 mM NaCl
H_2O, pH=8.0

2.2.3.4 Sensor Calibration

Epac1-camps targeted to the hGLP1R (hGLP1R-camps), to the plasma membrane (Epac1-camps-CAAX) or expressed in the cytosol was calibrated using two different approaches to evaluate its in vivo affinity for cAMP.

2.2.3.4.1 MDL Calibration

Calibration was assessed by single cell FRET measurements on an inverted fluorescence microscope 48 hours after transfection. During the calibration, HEK-TsA cells were maintained in FRET buffer at room temperature. All compounds were diluted using FRET buffer.
First, 100 µM MDL, which inhibits the adenylyl cyclases, was added to the cells. cAMP production is depleted and by this one can assess the minimum level of cAMP the sensor can detect.
After reaching a stable signal, various defined concentrations of 8-Br-O'-Me-cAMP-AM - a cell permeable analogue of cAMP- were added on top. At the end of each measurement 10 µM forskolin and 100 µM IBMX were added to saturate the sensor and normalize the signal to maximum stimulation. A concentration-response-curve was created and the resulting EC_{50} values can be used to compare the affinities of the differently targeted sensors for cAMP [227].

2.2.3.4.2 Saponin Calibration

Calibration was assessed by single cell FRET microscopy on an inverted fluorescence microscope 48 hours after transfection. The first step was to assess the right combination of a KCl- and K-glutamate-based intracellular buffer, since the different combination of buffers, leads to a shift of the concentration-response-curve resulting from the calibration of the sensor with cAMP (See Figure 2.1). This was done in CHO cells as their basal intracellular cAMP value is known to be 1 µM [358]. Since the x-crossing of the concentration-response-curve indicates this value, the curve using the right buffer combination should cross the axis at this value. The experiments resulted in a ratio of 45% KCl, 55% glutamate based buffer.
In the second step, the intracellular pH of HEK-TsA cells was determined as described before [358]. Since YFP is sensitive to changes in pH, it is crucial that the pH value of the intracellular buffer used in the calibration experiments later matches the real intracellular pH of the cells to assure that changes in fluorescence of the sensor stem from actual changes in cAMP and not changes of the pH value. All intracellular buffers were adjusted to the resulting pH value of 7.5.
The actual calibration of the sensors was conducted in HEK-TsA cells 48 hours after transfection. During the calibration experiments, cells were maintained in intracellular buffer at room temperature. 10-12 µg/ml saponin was added to permeabilize the cells, together with a defined concentration of cAMP (range 0-1 mM, one concentration per coverslip). From the resulting concentration-response-curves, one can see the dynamic ranges of the sensors, and compare their in vivo affinity to cAMP [358, 359].

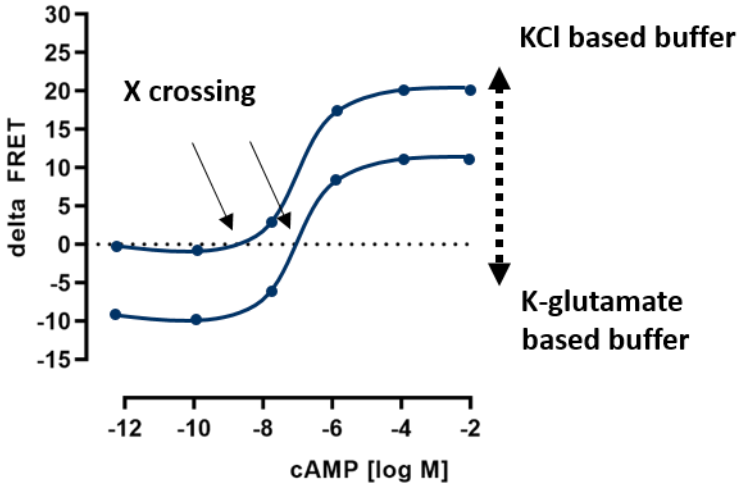

Figure 2.1 Schematic representation of concentration-response-curves using different buffer combinations
Simulated concentrations-response-curves from calibration experiments. Curve position can vary depending on the combination of KCl-/K-glutamate buffer used during calibration experiments.

Intracellular buffer KCl:	135 mM KCl 10 mM NaCl 6.49 mM $MgCl_2$ x $6H_2O$ 0.00073 mM $CaCl_2$ x $2H_2O$ 0.5 mM EGTA (ethylene glycol-bis(β-aminoethyl ether)-´N,N,N',N'-tetraacetic acid) 10 mM HEPES
Intracellular buffer K-glutamate:	135 mM K-glutamate x H_2O 10 mM NaCl 6.49 mM $MgCl_2$ x $6H_2O$ 0.00073 mM $CaCl_2$ x $2H_2O$ 0.5 mM EGTA 10 mM HEPES

2.2.4 Data analysis and statistics

In single cell fluorescence microscopy, FRET was calculated as the ratio between CFP emission at 480 nm and YFP emission at 535 nm with correction for spillover of CFP signal into the YFP channel (0.57 Zeiss Axiovert, 1.31 Leica DMi8) and for direct excitation of YFP (0.07 Zeiss Axiovert, 0.046 Leica DMi8). FRET traces were normalized to the maximum signal elicited by 10 µM forskolin + 100 µM IBMX at the end of each experiment. Data was analyzed using Origin Pro 2016G and Graphpad Prism 7.0 and plotted as mean ± standard error mean (SEM). Data from concentration response curve was fitted with a mono-exponential equation with a four-parameter fit. Kinetics were calculated with a one-phase decay fit or with a plateau followed by one-phase decay fit. Traces shown in Figure 3.10,Figure 3.11,Figure

3.12,Figure 3.13 were smoothed using adjacent average with 2nd order polynomial smoothing function. All data sets were tested for Gaussian distribution using D'Agostino & Pearson's normality test. Statistical differences were calculated with a Student's t-test or a 1-way ANOVA followed by Bonferroni's or Tukey's multiple comparison test. Differences were considered significant for $p < 0.05$. Confocal images were analyzed using Fiji/ImageJ. Each image was corrected by subtracting the average background fluorescence. Contrast was enhanced while keeping the saturated pixels at 0.1%.

3 Results

3.1 Designing a receptor sensor conjugate suitable for measuring cAMP close to a GPCR

Since the stimulus for cAMP elevation in cells originates at a GPCR, which couples to a G_S protein and leads to the activation of AC, we aimed to measure cAMP close to a G_S-coupled receptor [22]. We chose to use a FRET based approach in order to study cAMP dynamics in real-time in living cells. By cloning the Epac1-camp sensor (Epac1-camps) [311] to the C-terminus of the full length, wild type hGLP1R we created hGLP1R-camps. When expressed in HEK-TsA cells, the receptor-sensor conjugate shows a distribution at the plasma membrane (See Figure 3.1).

In order to be able to measure cAMP in gradual distances from the receptor, to assess the spatial dynamics of a putative cAMP compartment, we modified the hGLP1R-camp sensor. For this, we used rigid linkers with a defined length, which we placed between the receptor and the sensor. These linkers consist of an ER/K α-helix from a Kelch motif family protein found in *Trichonomis vaginalis* G3. A persistent length (Lp, length scale over which the structure is rigid) of 30 ± 10nm has been estimated for this linker [360]. We generated hGLP1R-SAH30-camps with one linker between receptor and sensor (30 nm distance), and hGLP1R-SAH60-camps where we doubled the sequence of the linker on the DNA level and with this obtain a linker length of approximately 60 nm. Figure 3.1 shows that all three constructs are expressed at the plasma membrane.

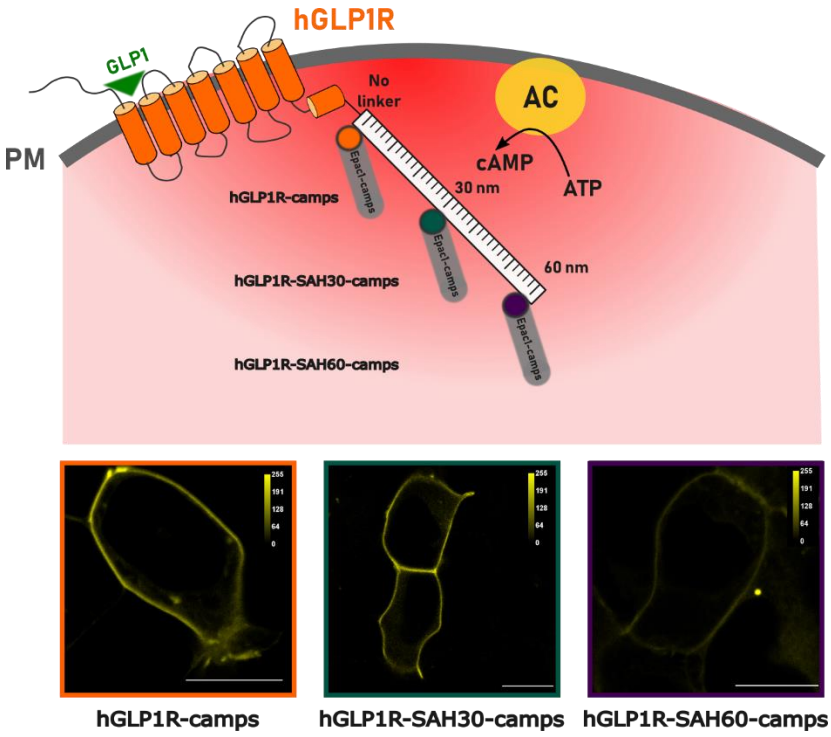

Figure 3.1 hGLP1R-camps detects cAMP at the receptor
Schematic representation of the FRET sensor Epac1-camps attached to the C-terminus of the hGLP1R, with no linker (orange), 30nm linker (petrol), 60nm linker (purple). Confocal images of a HEK-TsA cell individually expressing the indicated constructs at the plasma membrane. YFP channel. Scale bar = 10 µm.

In order to validate the length of the doubled 30 nm linker, we expressed a membrane targeted version of the linker in CHO cells and recorded STORM movies. This construct is targeted to the plasma membrane via the Lyn- and CAAX sequence [342] while it can be labeled with Halo dyes suitable for STORM imaging. Figure 3.3 shows a CHO cell transfected with above-mentioned construct, labeled with JF-646 dye. The average linker length is 68.8 ± 1.42 nm. Considering imaging was conducted five hours post transfection to assure low expression levels, protein folding might not be fully complete, thus the average length lies slightly above the expected 60 nm.

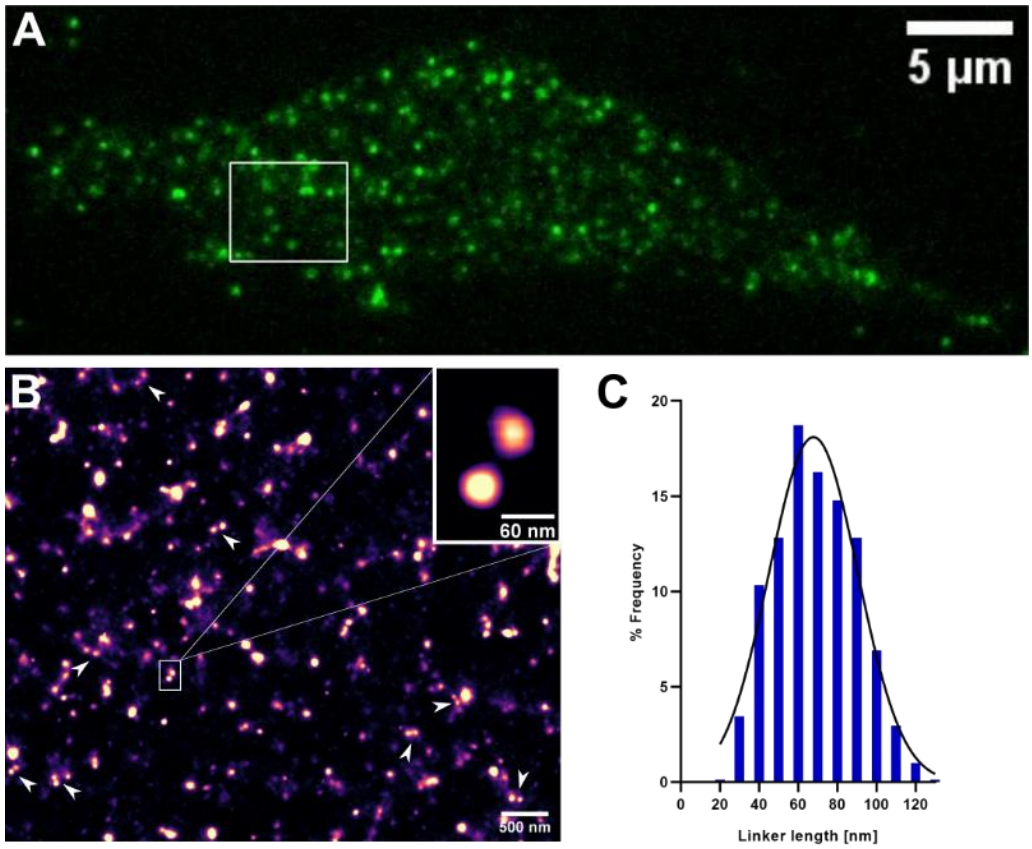

Figure 3.2 Assessment of SAH60 linker length
(A) Representative image from the localization microscopy stacks of a CHO cell expressing Lyn-Halo-SAH60-Halo-CAAX labeled with Halo JF-646, from which the reconstructed super-resolution image was generated.
(B) Reconstructed super-resolution close up view of the area indicated in (A). Inset: zoomed-in view of a double-labeled linker with 60 nm distance between both foci. Additional linkers indicated with white arrows.
(C) Histogram depicting the frequency distribution of linker length. The average length is 68.8 ± 1.42 nm (Mean±SEM n=203 linkers from 10 cells).

3.2 Targeting of the Epac1-camps sensor to subcellular locations

In order to compare cAMP levels measured at the hGLP1R using hGLP1R-camps with other subcellular cAMP levels, we chose to target Epac1-camps additionally to the plasma membrane and to express it in the cytosol. By cloning the CAAX-box from the small GTPase Rho [361] to the C-terminus of Epac1-camps, we directed the sensor to the non-lipid rafts of the plasma membrane, thereby creating Epac1-camps-CAAX. For the cytosolic compartment we left the sensor unchanged (Figure 3.3). When overexpressed in HEK-TsA cells, Epac1-camps shows a uniform distribution in the cytosol, whereas Epac1-camps-CAAX is expressed at the membrane.

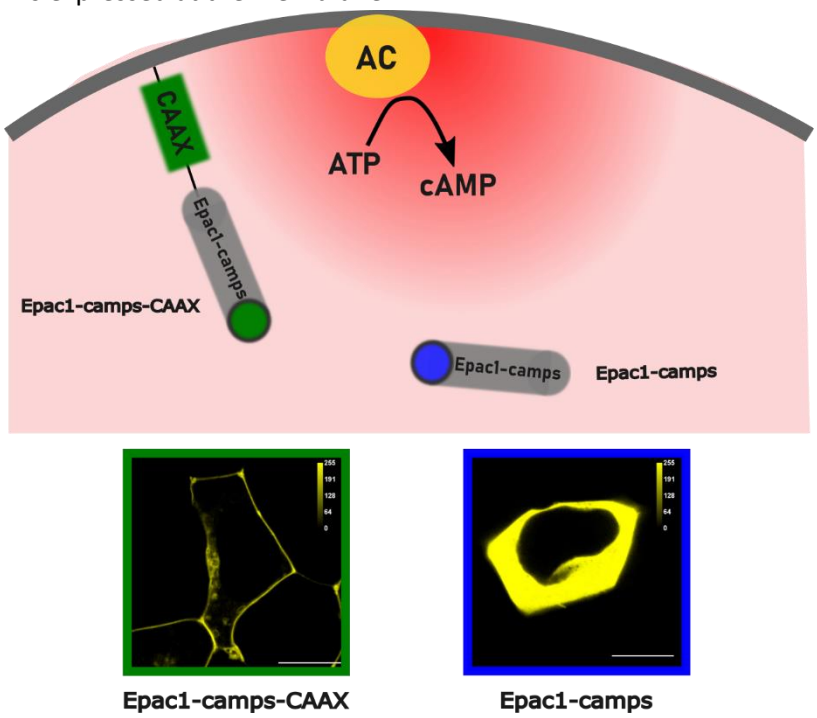

Figure 3.3 Epac1-camps targeted to different subcellular locations
Schematic representation of the FRET sensor Epac1-camps targeted by the CAAX-sequence to the plasma membrane, or untargeted and expressed in the cytosol. Confocal images of a HEK-TsA cells individually expressing Epac1-camps-CAAX or at the plasma membrane or Epac1-camps in the cytosol. YFP channel. Scale bar = 10 µm.

3.3 Characterization of hGLP1R-camps

Since FRET is highly dependent on the steric orientation and distance of both fluorophores, fusion of the Epac1-camp sensor to an attachment point might attenuate its ability to detect cAMP reliably. To confirm that the affinity of the differently targeted Epac1-camp sensor for cAMP is not perturbed we calibrated the differentially targeted sensors in vivo with two different methods.

3.3.1 MDL / 8-Br-O'-Me-cAMP-AM calibration

With the calibration method described by Börner *et* al. [227], it is possible to calibrate the Epac1-camps in intact cells and to assess its entire dynamic range. Cells transfected with the respective construct are first subject to application of 100 µM MDL-12,330A (MDL), a compound which inhibits ACs. When the basal cAMP is degraded by the PDEs, the sensor detects the minimum level of cAMP (R_{MIN}). In the second step 8-Br-O'-Me-cAMP-AM, a cell permeable analogue of cAMP, is added in

increasing concentrations (1 nM-20 µM). This compound presumably behaves like cAMP and binds to the sensor leading to a concentration dependent FRET change. A saturating concentration of 20 µM 8-Br-O'-Me-cAMP-AM with subsequent addition of 10 µM forskolin and 100 µM IBMX at the end of each experiment to assure complete saturation results in the R_{MAX} value - maximum cAMP level the sensor can detect. The resulting FRET traces were normalized to minimum and maximum cAMP level.
Visible in Figure 3.4 A, receptor-sensor and cytosolic unattached Epac1-camp sensor show a superposed curve. The membrane bound sensor has a slightly leftward shifted curve. By comparing the pEC_{50} values, Epac1-camps-CAAX shows a significantly different affinity for 8-Br-O'-Me-cAMP-AM compared to hGLP1R-camps and Epac1-camps (hGLP1R-camps 6.2±0.05; Epac1-camps 6.22±0.03; Epac1-camps-CAAX 6.75±0.07 n=6 for all). This apparently higher affinity would imply that Epac1-camps-CAAX could detect even lower levels of cAMP, giving it a higher sensitivity.

In comparison to the actual pEC_{50} values for cAMP, measured in vitro (5.6±0.091 [227]), these values are lower because 8-Br-O'-Me-cAMP-AM accumulates in cells and leads to a leftward shift of the curve. Therefore, EC_{50} values obtained from these experiments do not reflect the actual affinities but rather the apparent ones for cAMP and should be used to compare different constructs treated under the same conditions.

Since 8-Br-O'-Me-cAMP-AM is a lipophilic compound which is known to accumulate in the cell, and could putatively also stick to the plasma membrane (through its acetoxy-methylated residue), it is very likely this affects the results of the calibration for the membrane targeted sensor. Epac1-camps-CAAX is directly attached to the plasma membrane a geranylgeranyl group [361], whereas in the case of the receptor-targeted sensor, the receptor C-terminus separates the sensor from the plasma membrane. The 8-Br-O'-Me-cAMP-AM enriched membrane would bear a higher concentration of the cAMP-analogue compared to the area surrounding the receptor and the cytosol, which could affect the binding behavior of Epac1-camps-CAAX, leading to an artificial leftward shift. 8-Br-O'-Me-cAMP-AM can be useful to determine the maximum FRET amplitude of the sensor, when using only a saturating concentration of the compound. However, working with additive concentrations of the compound throughout the calibration might not necessarily ensure the delivery of these precise concentrations to the plasma membrane-targeted sensor, leading to the apparently higher affinity. Therefore, we doubt the accuracy of the results from these calibration experiments and disregard them, choosing a second, less artificial method to assess the affinities of the sensors.

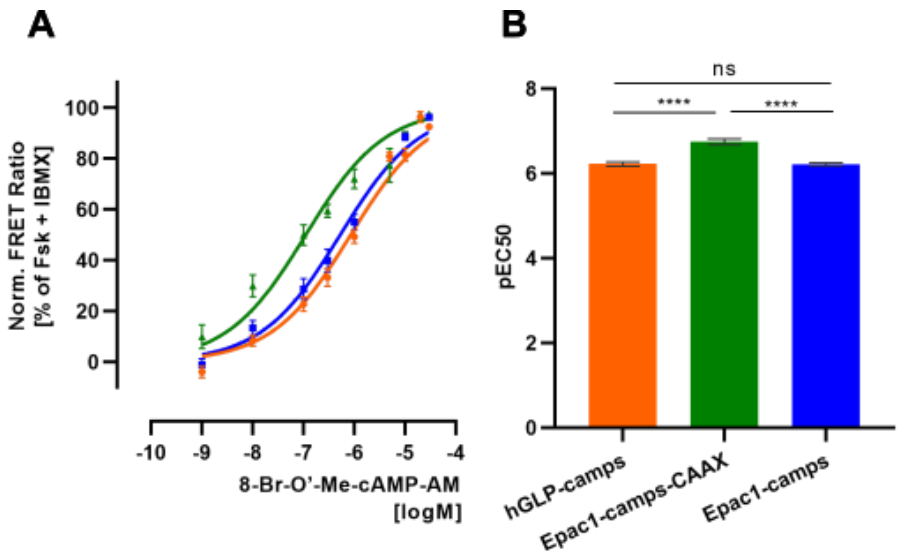

Figure 3.4 MDL calibration of differentially targeted Epac1-camps
(A) Concentration-response-curves from MDL calibration experiments. Normalized delta FRET ratio for Epac1-camps targeted to the hGLP1R (orange), plasma membrane (green) and cytosol (blue). Data shown as mean±SEM normalized to R_{MIN} and R_{MAX}, averaged from 6 independent experiments.
(B) pEC50 values from calibration experiments as described in **(A).** hGLP1R-camps= 6.2±0.05, Epac1-camps-CAAX= 6.75±0.07, Epac1-camps= 6.22±0.03 (mean±SEM n=6 independent experimental days for each of the three constructs). **** p<0.0001, p>0.05 ns no significant difference according to one-way ANOVA with Tukey's post hoc test.

3.3.2 Saponin calibration

This method relies on the permeabilization of cells with saponin from quillaja bark [359]. Due to its amphipatic nature, it can interact with the plasma membrane and create holes with the size of 40-50 Å [362], which enables the intracellular delivery of cAMP in defined concentrations from the extracellular space. Cells were transfected with the respective construct, maintained in intracellular buffer and a defined concentration of cAMP was added together with 10-12 µg/ml saponin. An increase or decrease in FRET was recorded until a stable signal was obtained (Figure 3.5 A-C). To assure complete equilibration between intra- and extracellular space, additional 2 µg of saponin were added at the end, and the experiment was run until all cells deceased.
Figure 3.5 D shows the concentration-response-curves resulting from the calibration experiments. The differently targeted sensors feature an equal affinity for cAMP since the comparison of the pEC50 values (Figure 3.5 E) shows no significant difference (hGLP1R-camps 5.31±0.04; Epac1-camps 5.3±0.04; Epac1-camps-CAAX 5.4±0.07 n=6 experimental days for each construct). The dynamic range for the targeted sensors however, is altered compared to the untargeted sensor (calculated from the min to the max of the calibration curve; hGLP1R-camps 15.12±0.4% n=29, Epac1-camps-CAAX 6.67±0.27% n=30, Epac1-camps 34.93±0.93% n=49 delta FRET).

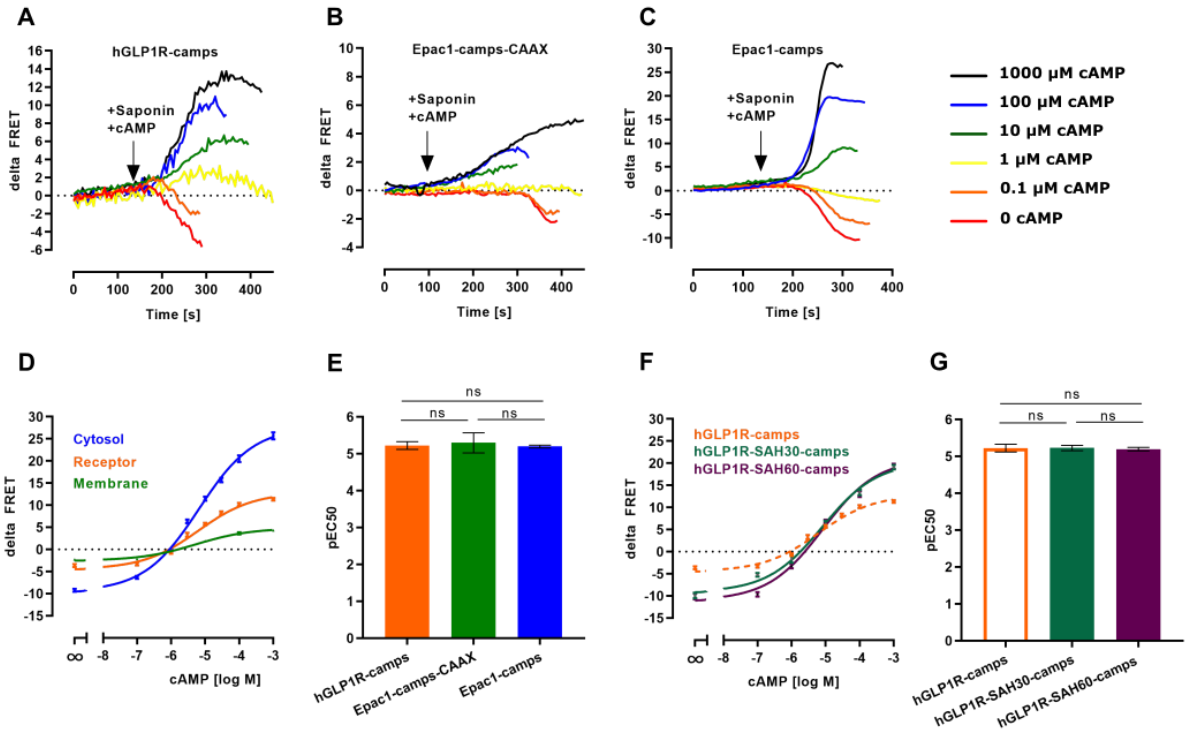

Figure 3.5 Saponin calibration of differently targeted Epac1-camp sensor
(A) (B) (C) Time courses of representative delta FRET traces recorded with hGLP1R-camps **(A),** Epac1-camps-CAAX **(B)** or Epac1-camps **(C)** during the calibration experiments upon stimulation with indicated cAMP concentrations.
(D) Concentration-response-curves from calibration experiments as shown in **(A), (B), (C).** Delta FRET ratio of cytosolic hGLP1R-camps (orange), membranous Epac1-camps-CAAX (green) and Epac1-camps (blue) upon treatment with increasing cAMP concentrations. Data shown as mean±SEM.
(E) pEC50 values from calibration experiments as described in **(D).** hGLP1R-camps= 5.31±0.04, Epac1-camps-CAAX= 5.4±0.07, Epac1-camps= 5.3±0.04 (mean±SEM n=6 independent experimental days for each of the three constructs). P>0.05 ns no significant difference according to one-way ANOVA with Tukey's post hoc test.
(F) Concentration-response-curves from calibration experiments for hGLP1R-camps, 30 & 60 nm linker construct. Delta FRET ratio of hGLP1R-camps (orange, shown in panel D), hGLP1R-SAH30-camps (petrol), hGLP1R-SAH60-camps (purple) upon treatment with increasing cAMP concentrations. Data shown as mean±SEM.
(G) pEC50 values from calibration experiments as described in **(D).** hGLP1R-camps as shown in panel E = 5.31±0.04, hGLP1R-SAH30-camps= 5.23±0.07, hGLP1R-SAH60-camps= 5.19±0.05. Mean±SEM n=6 independent experimental days for each of the three constructs. P>0.05 ns no significant difference according to one-way ANOVA with Tukey's post hoc test.

Figure 3.5 F, G shows the results for the calibration of the hGLP1R-SAH30/SAH60-camps constructs. The linker constructs show the same affinity for cAMP in living cells as above mentioned sensors (hGLP1R-SAH30-camps 5.23±0.07; hGLP1R-SAH60-camps 5.19±0.05 n=6 experimental days for each construct) and they exhibit a similar dynamic range to the untargeted sensor (hGLP1R-SAH30-camps 28.6±0.74% n=28; hGLP1R-SAH60-camps 30±0.76% n=28).
With this, we could show that targeted Epac1-camps can reliably be used as a tool to compare cAMP in different cellular locations. Having used two different calibration methods, we realized both methods have certain advantages and disadvantages to which we will deeper refer in the discussion.

3.3.2.1 Assessment of the dynamic range for hGLP1R-camps and Epac1-camps-CAAX

With saponin perturbing the architecture of the plasma membrane, the unexpectedly small dynamic range of the receptor- and membrane targeted Epac1-camp sensor could be attributed to this fact. Therefore, we conducted a second set of experiments where we assessed the dynamic range for the hGLP1R-camps and Epac1-camps-CAAX sensors independent of saponin. HEK-TsA cells were transiently transfected with the indicated constructs and MDL was added in the first step to inhibit ACs (detection of the minimum). In the second step a saturating concentration of 20 µM 8-Br-O'-Me-cAMP-AM together with 10 µM fsk + 100 µM IBMX was added (to detect the maximum). The resulting dynamic range is 25.3±1.8% n=5 for hGLP1R-camps and 16.64±0.82% n=8 for Epac1-camps-CAAX (Figure 3.6). These results are in better agreement with the dynamic range of the untargeted sensor. Even though targeting the sensor to a subcellular area, seems to decrease the dynamic range, the calibration experiments show that the affinity of the sensors to cAMP is equal.

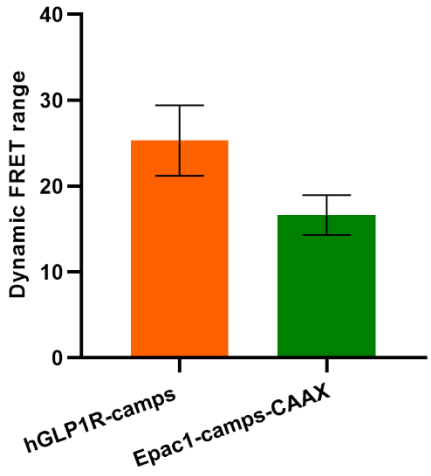

Figure 3.6 Dynamic range of differently targeted Epac1-camp sensor
Max delta FRET change of hGLP1R-camps or Epac1-camps-CAAX expressing cells (hGLP1R-camps 25.31±1.83% n=5; Epac1-camps-CAAX 16.64±0.82% n=8). Data shown as mean±SEM.

3.3.3 cAMP ELISA

To assess the functionality of the receptor-sensor in comparison to the WT-receptor in terms of cAMP production, a whole cell cAMP ELISA was performed. Both WT-GLP1R and hGLP1R-camps expressing cells were stimulated with different concentrations of their endogenous agonist GLP1-(7-36)-NH_2 [363] (herein referred to as GLP1) together with 100 µM IBMX. 10 µM fsk + 100 µM IBMX were used as a positive control for normalization, and cAMP amount was determined after cell lysis. As depicted in Figure 3.7, both WT-R and receptor sensor show a superimposed concentration-response-curve resulting from the assay. pEC_{50} values are not significantly different (hGLP1R-camps= 9.06±0.112, WT-hGLP1R= 9.056±0.115 n=3 experimental days for each construct).

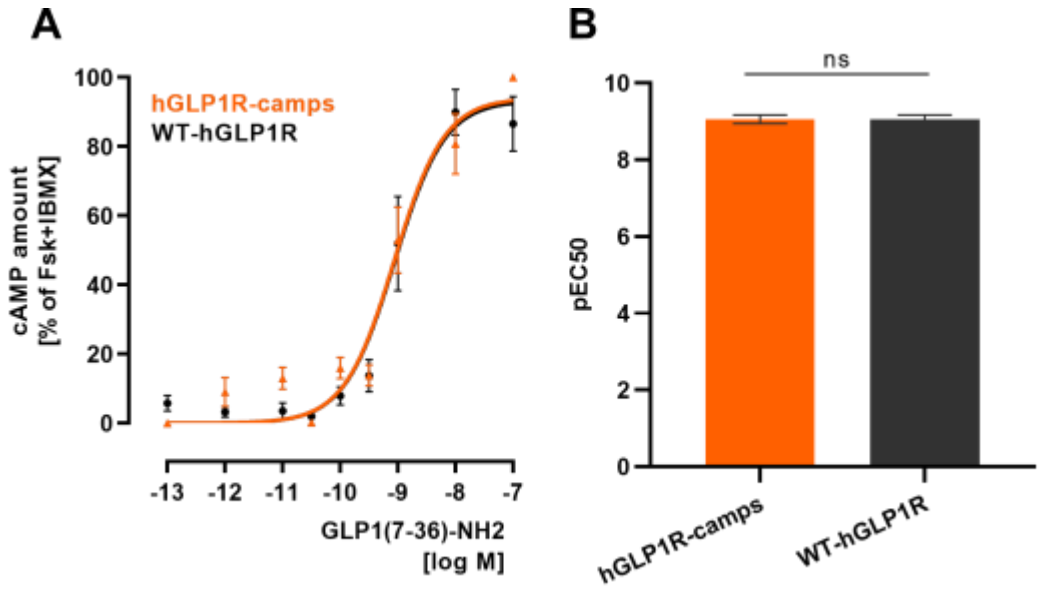

Figure 3.7 hGLP1R-camps is functional in generating cAMP
(A) Concentration-response-curves resulting from stimulation of the cells with different concentrations of GLP1-(7-36)-NH_2. cAMP amount normalized to maximum stimulation by fsk + IBMX. Data plotted as mean±SEM.
(B) pEC50 values from whole cell cAMP ELISA. hGLP1R-camps= 9.06±0.112, WT-hGLP1R= 9.056±0.115. Data shown as mean±SEM n=3 for each construct. P>0.05 ns no significant difference according to an unpaired t-test.

3.3.4 Characterization of hGLP1R-camps for single cell FRET measurements

Since hGLP1R-camps was generated for single cell FRET experiments to measure cAMP at the receptor under different conditions, it is crucial to ensure that the attached Epac1-camp sensor is still capable of detecting cAMP and giving antiparallel traces of the two fluorophores. For this, HEK-TsA cells were transfected with hGLP1R-camps (Figure 3.8 A) and stimulated with 10 nM of the endogenously active agonist GLP1. After the activation of hGLP1R, which in turn activates the $G\alpha_S$ and subsequently the ACs, cAMP is produced. We see antiparallel traces in the CFP- and YFP-channel, and an increase in the FRET Ratio (CFP/YFP). This leads to the conclusion that Epac1-camps is capable of reporting changes in cAMP levels.
Mutation of Epac1-camps at position 279 from arginine to glutamic acid is known to abolish cAMP binding. We cloned hGLP1R-camps-R279E, a cAMP binding-deficient version of the receptor-sensor,

which we used to control for unspecific effects that can occur during FRET experiments. As can be seen in Figure 3.8 B, stimulation of hGLP1R-camps-R279E expressing cells with various ligands which elicit cAMP levels, does not lead to any change in fluorescence of either CFP and YFP. In Figure 3.8 C we also controlled for unspecific effects of the compounds used throughout the MDL calibration (MDL, 8-Br-O'-Me-cAMP-AM). Again, no change in fluorescence intensities and ratio can be seen.

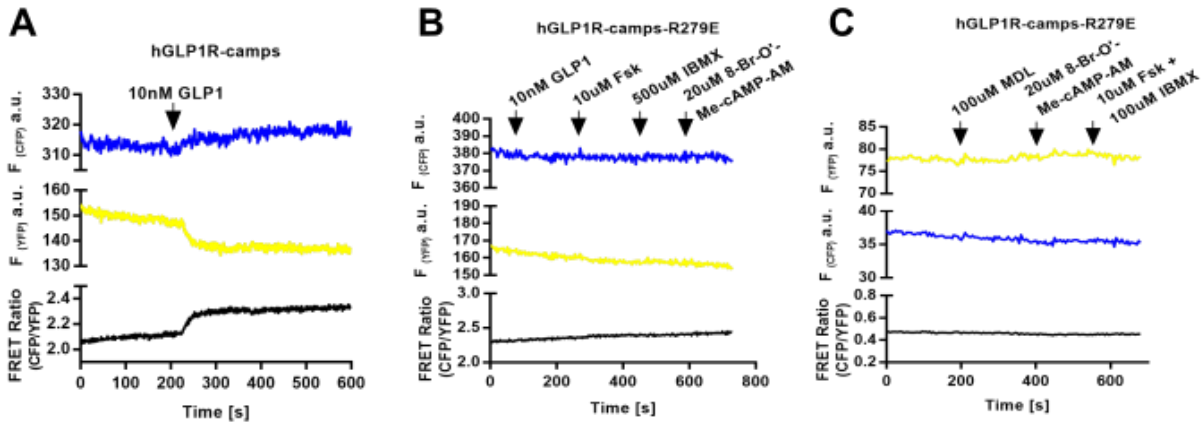

Figure 3.8 hGLP1R-camps & hGLP1R-camps-R279E subject to stimulation by different compounds
(A) Fluorescence intensity traces and FRET ratio (CFP/YFP) recorded in hGLP1R-camps expressing HEK-TsA cells. Antiparallel traces are detected in the CFP- and YFP-channel upon stimulation with 10nM GLP1.
(B), (C) Fluorescence intensity traces of CFP, YFP and FRET-ratio (CFP/YFP) of a cAMP binding-deficient mutant of Epac1-camps targeted to the hGLP1R. No changes are observed in the fluorophore intensities or FRET-ratio upon stimulation with various compounds that lead to cAMP production.

3.4 Utilizing targeted FRET sensors to detect basal cAMP levels in different cellular compartments

With the Epac1-camp sensor targeted to the hGLP1R, the plasma membrane or the cytosol, we aimed to compare basal cAMP levels of unstimulated cells in the different compartments. We first recorded a stable FRET ratio in the resting state, to then inhibit the ACs by adding 100 µM MDL. As soon as the PDEs start degrading the cAMP to AMP, we detect a decrease in the FRET ratio, since the cAMP level sinks. To saturate the sensor, we subsequently added 20 µM 8-Br-O'-Me-cAMP-AM which leads again to an increase of the FRET ratio. For saturation and normalization, we add 100 µM IBMX at the end of each experiment. Figure 3.9 A shows the principle of basal cAMP assessment in simulated traces. The initial ratio (R_{BASAL}) of the trace can vary and is dependent on the amount of cAMP present within the compartment. The higher the initial cAMP amount, the bigger the FRET change observed upon addition of MDL, which results in the minimum detectable cAMP level (R_{MIN}). After addition of a saturating concentration of 8-Br-O'-Me-cAMP-AM and IBMX, the sensor is maximally stimulated and gives the R_{MAX} value, corresponding to maximum detectable cAMP level. According to EQUATION 7, R_{BASAL} can be expressed as a function of R_{MIN} (set to 0) and R_{MAX} (set to 100). It serves as a surrogate parameter for the basal level of cAMP within the compartment.

$$\text{Basal cAMP} = \frac{R_{BASAL}-R_{MIN}}{R_{MAX}-R_{MIN}}$$

EQUATION 7

As can be observed in Figure 3.9 B and concluded from Figure 3.9 C, the receptor and the membrane compartments each enclose a similarly high level of cAMP, which is 4-fold higher than the cytosolic cAMP level (receptor 47.3±2.5% n=24, plasma membrane 49.2±2.3% n=31, cytosol 10.6±1% n=27).

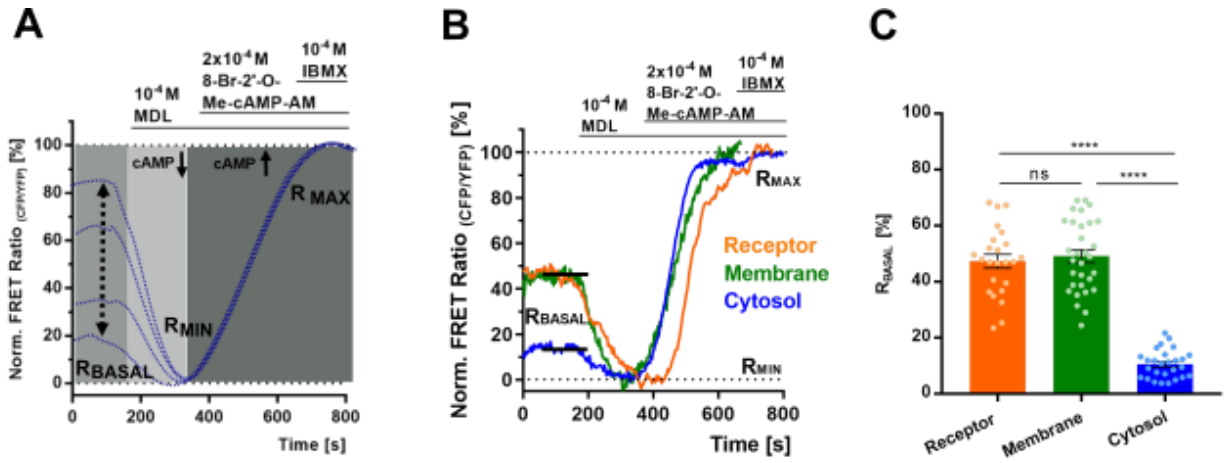

Figure 3.9 Targeted cAMP sensors reveal cAMP levels are diverse within different compartments
(A) Simulated traces for delta FRET ratios to illustrate the concept of basal cAMP-level assessment. The initial FRET ratio (R_{BASAL}) can vary depending on the basal cAMP level. Inhibition of AC with MDL leads to minimum FRET ratio (R_{MIN}). Saturation with a cell-permeable cAMP analogue- 8-Br-2'-O-Me-cAMP-AM and IBMX stimulation gives the maximum FRET ratio (R_{MAX}).
(B) Time course of agonist induced FRET changes recorded in HEK-TsA cells expressing Epac1-camps at the receptor, membrane and cytosol. MDL, 8-Br-2'-O-Me-cAMP-AM, IBMX were added as indicated in the panel. Shown are representative traces normalized to R_{MIN} (set to 0) and R_{MAX} (set to 100).
(C) Comparison of basal cAMP signals in the three different compartments. Values are calculated from experiments as shown in panel **(A), (B).** Receptor 47.3±2.5% n=24, plasma membrane 49.2±2.3% n=31, cytosol 10.6±1% n=27. Data shown as mean±SEM. Difference was analyzed by one-way ANOVA followed by Tukey's post hoc test. ****p<0.0001, ns no significant difference.

Opposed to the calibration experiments, in this experimental setting we only use one, namely the saturating 8-Br-O'-Me-cAMP-AM concentration and not a gradual increase. Therefore, we trust all sensors respond equally to the stimulus.

3.5 GLP1 stimulation creates a receptor-specific cAMP domain in a concentration-dependent manner

After determining the basal cAMP levels surrounding the receptor, at the plasma membrane and in the cytosol, we sought to discover how the cAMP signal propagates through the cell upon stimulation of the hGLP1R.

Figure 3.10 A shows the predicted localization of the differentially targeted Epac1-camp sensor individually transfected in HEK-TsA cells. In single cell FRET experiments, we challenged the receptor with four different concentrations of GLP1 and recorded the resulting FRET ratios at the receptor, at the plasma membrane and in the cytosol. For normalization, the cells were stimulated with the direct AC-activator forsklin (10 µM) together with the unspecific PDE-inhibitor IBMX (100 µM) at the end of each experiment (normalization to fsk + IBMX treatment).

Already 10 fM of the agonist (Figure 3.10 B, C) elicit a cAMP signal at the hGLP1R (23.4±1.43% n=21), which is 3-fold as high as at the plasma membrane (5.9±0.9% n=10), while in the cytosol the signal is negligible (2.1±0.4 n=18).

For a sub-EC_{50} concentration of 1pM GLP1 [127] (Figure 3.10 D, E) the highest cAMP amplitude was recorded at the hGLP1R (43.7±3% n=32), cAMP signal evoked at the membrane (18.2±2% n=12) is less than 50% compared to the receptor, and the cytosol (6.2±0.6% n=26) shows only 12% of the signal. There is a steep gradient between cAMP level of the receptor compartment to the membrane and cytosolic one.

1 nM of the agonist (Figure 3.10 F, G) again induces a higher and faster cAMP amplitude at the receptor (75.6±1.9% n=11) compared to the membrane (29.5±4.4% n=11) and the cytosol (33.1±4.9% n=20), however with this concentration of the agonist, cAMP signal evoked at the membrane and cytosol is equal in terms of amplitude.

At the very high concentration of 100 nM GLP1 (Figure 3.10 H, I), the receptor compartment is almost saturated with cAMP (89.3±1.5% n=24). The amplitude of the cAMP signal at the membrane (79.8±4.3% n=15) and in the cytosol (81.1±1.5% n=22) rises to 90% of the signal evoked in the receptor compartment, yet membrane- and cytosolic compartment are not fully saturated with cAMP even at this high GLP1 concentration.

Stimulation with the endogenous agonist induces domains with unequal cAMP levels, which leads to the conclusion the are spatially separated. 10 fM and 1 pM agonist lead to a receptor specific elevation in cAMP with a steep gradient towards the membranous and cytosolic compartment. 1 nM of the agonist induces a 2.5-fold larger signal in the receptor compartment compared to the latter two, nevertheless membranous and cytosolic compartment equilibrate in their cAMP amplitude. Even at a saturating concentration of 100 nM GLP1, the receptor compartment stays distinct from the membrane and cytosolic compartment in terms of cAMP signal amplitude, yet the gradient is not as steep.

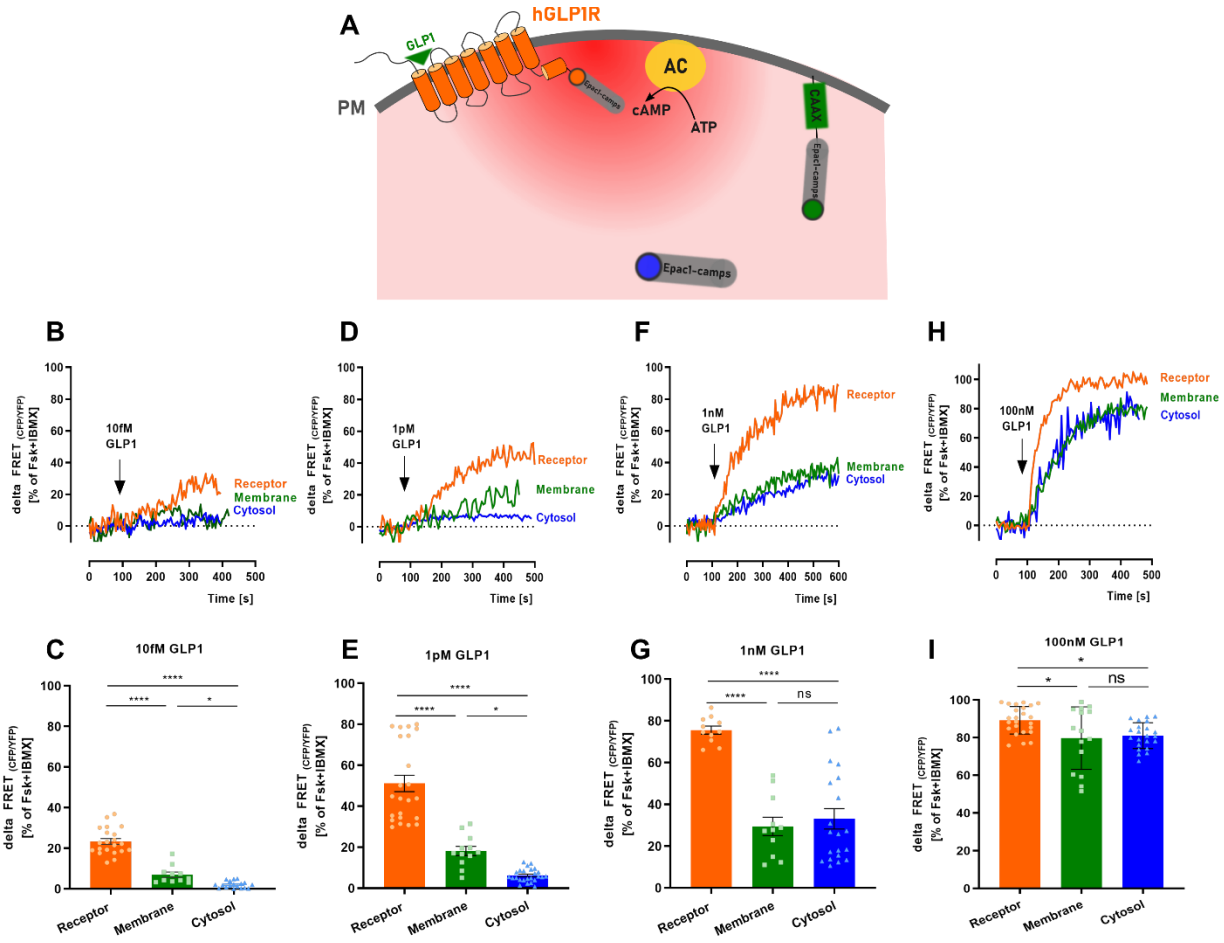

Figure 3.10 Stimulation with GLP1 produces spatially segregated pools of cAMP
(A) Scheme of the experimental setup. Stimulation of hGLP1R with its endogenous agonist GLP1 leads to cAMP production. cAMP elevation can be monitored by the targeted Epac1-cAMP-sensor, either directly at the hGLP1R (orange), at the membrane (green) or in the cytosol (blue).
(B), (D), (F), (H) Time course of agonist induced FRET changes recorded in HEK-TsA cells expressing differentially targeted Epac1-camps: at the receptor, membrane and cytosol for 10 fM **(B)**, 1 pM **(D),** 1 nM **(F)** or 100 nM **(H)** GLP1. Shown are representative traces normalized to fsk + IBMX treatment.
(C), (E), (G), (I) Comparison of cAMP levels generated in the different compartments upon stimulation with 10 fM **(C),** 1 pM **(E),** 1 nM **(G)** or 100 nM **(I)** GLP1. 10 fM and 1pM of the agonist induce a massive cAMP signal in the receptor compartment while at the membrane and in the cytosol the signal is minor. Stimulation with 1 nM increases cAMP signal in all compartment, yet the receptor compartment stays distinct from the latter two. 100 nM agonist stimulation gives the highest detectable cAMP signal. However, the membrane and the cytosolic compartments are never fully saturated with cAMP coming from the receptor. Data shown as mean delta FRET-ratios ± SEM. ****p<0.0001, *p<0.05, ns no significant difference according to a one-way ANOVA followed by Tukey's post hoc test.

In addition to the evaluation of the cAMP level within each compartment, we calculated the time constants of the FRET changes obtained in the experiments described in 3.5. The resulting T values are shown in Figure 7.2 in the appendix.

3.6 hGLP1-receptor compartment is specific to stimulation by GLP1 but not isoproterenol

After discovering a receptor-specific cAMP domain surrounding the hGLP1R, we set out to study the crosstalk between different G_S-coupled receptors. Using isoproterenol to stimulate endogenous β-ARs, we recorded cAMP levels at the hGLP1-receptor, the membrane and the cytosol. Figure 3.11 A shows that Epac1-camps is targeted to the same compartments as in Figure 3.10, yet in the current experimental setup, β-ARs are the source for cAMP generation. We used various concentrations of isoproterenol to activate the adrenergic receptors and normalized the traces to fsk + IBMX signal.

10 pM isoproterenol stimulation (Figure 3.11 B,C) leads to an increase in cAMP exclusively at the plasma membrane (21.7±2.2% n=10), while there is no increase over baseline for the hGLP1-receptor compartment (2.8±1.1% n=13) and the cytosol (2.6±0.6% n=11).

An increase of cAMP at the hGLP1R (23.9±1.9% n=13) and cytosol (8±1.7% n=12) can be detected by stimulation with 100 pM isoproterenol (Figure 3.11 D, E), yet still to a lower extent than at the plasma membrane (42.7±4.6% n=9).

At a stimulation with 1 nM agonist (Figure 3.11 F, G), the cAMP signal detected at the hGLP1-receptor (30.3 ± 3.3% n=19) and the cytosol (25.2 ± 2.1% n=19) is not significantly different from each other, however still smaller by 40% than the signal detected at the membrane (44.8 ± 2.8% n=8).

Figure 3.11 H, I shows all three compartments equilibrate in their cAMP amplitude by stimulation with 10 nM isoproterenol (hGLP1R compartment 52.7±4% n=21, membrane 52.5±5% n=16, cytosol 59.1±4.3% n=25). Further increase of the agonist concentration to 100 nM (Figure 3.11 J, K) raises the cAMP level in all compartments, without creating significant differences (hGLP1R compartment 59.2 ± 4.8% n=15, membrane 70.8 ± 3.2% n=17, cytosol 64.3 ± 4.1% n=25).

Interestingly, at a stimulation with 1 µM isoproterenol, the membrane (79.2 ± 2.8% n=17) repeatedly shows a bigger cAMP amplitude compared to the hGLP1-receptor (65.3 ± 3% n=23) and the cytosol (63.7 ± 4.4% n=24). This difference is abolished once more at a stimulation with 10 µM isoproterenol (hGLP1-receptor 75.8 ± 2.6% n=22, membrane 76.8 ± 1.8% n=19, cytosol 82.9 ± 2.8% n=14).

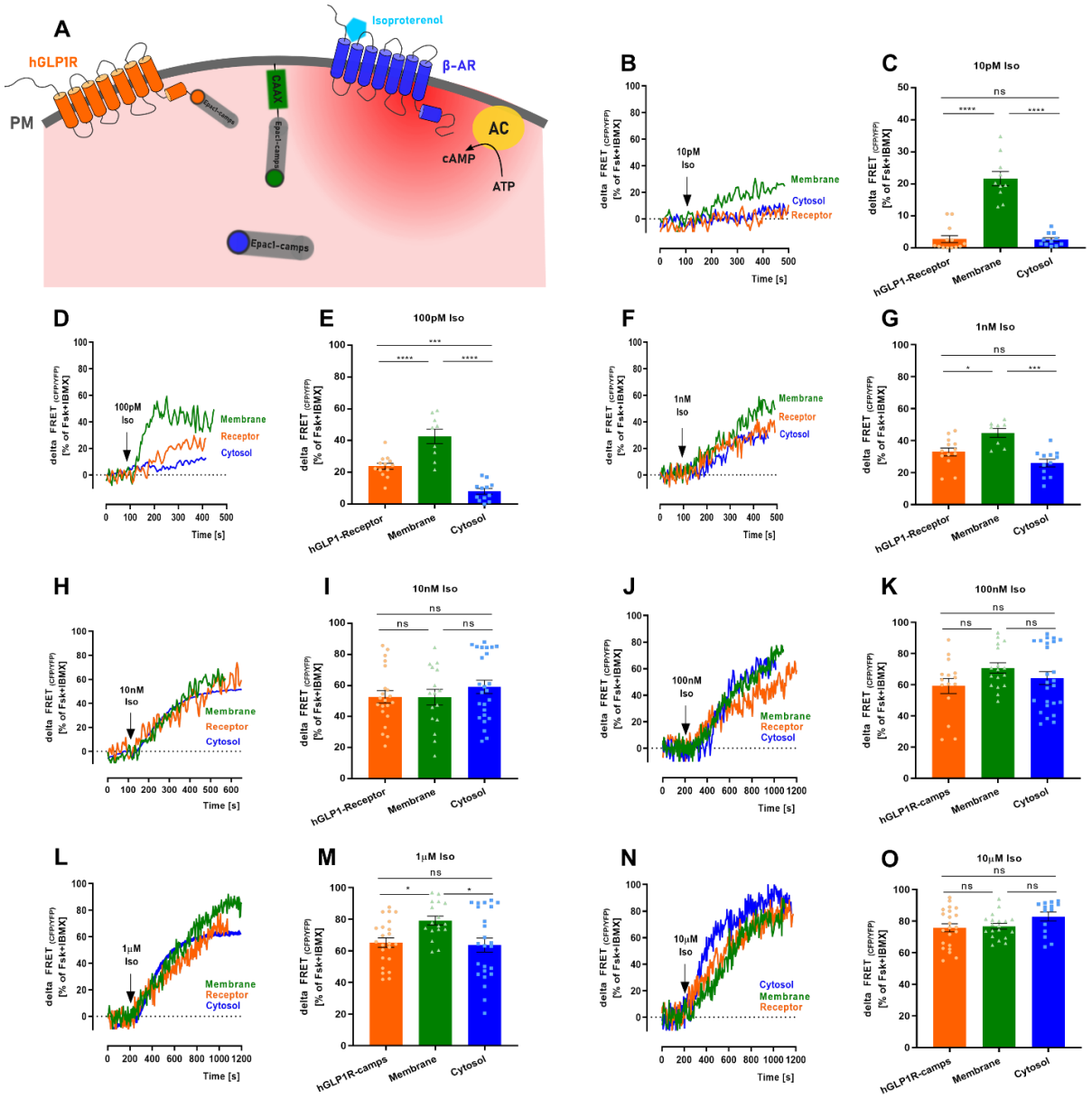

Figure 3.11 Propagation of cAMP generated at β-ARs into the hGLP1R-compartment, membrane and cytosolic compartment

(A) Schematic representation of the experimental setup. β-ARs are stimulated by their agonist isoproterenol. cAMP is produced surrounding the β-ARs and diffuses to reach the membrane-bound Epac1-camp sensor as well as the hGLP1R-bound and cytosolic one.

(B), (D), (F), (H), (J), (L), (N) Time course of agonist induced FRET changes recorded in HEK-TsA cells expressing differentially targeted Epac1-camps: to the hGLP1R, membrane and cytosol for 10 pM **(B)**, 100 pM **(D)** 1nM **(F)**, 10 nM **(H)**, 100 nM **(J),** 1 µM **(L)** or 10 µM **(N)** isoproterenol. Shown are representative traces normalized to fsk + IBMX stimulation.

(C), (E), (G), (I), (K), (M), (O) Comparison of cAMP signals generated in the different compartments upon stimulation with 10 pM **(C)**, 100pM **(E)** or 1 nM **(G)**, 10 nM **(I),** 100 nM **(K),** 1 µM **(M)** or 10 µM **(O)** isoproterenol. Data shown as mean delta FRET-ratios ± SEM ****p<0.0001, ***p<0.001, ns no significant difference. All according to a 1-way ANOVA followed by Tukey's post hoc test.

3.7 Size and dynamics of the hGLP1R-cAMP compartment

To closer characterize the cAMP-compartment surrounding the hGLP1R, we set out to assess its size. To this goal, we used above mentioned hGLP1R-camps constructs with inserted nanolinkers of 30nm and 60nm length and measured cAMP in gradual distances from the receptor (Figure 3.12 A).

We transfected HEK-TsA cells with either hGLP1R-camps or the constructs with 30nm- and 60nm-linker and stimulated with 10 fM, 1 pM, 1 nM or 100 nM of GLP1. Traces were normalized to fsk + IBMX treatment.

As depicted in Figure 3.12 B, C the stimulation with 10 fM GLP1 evokes a high cAMP signal directly at the receptor (no linker 23.4 ± 1.4% n=21) which continuously decreases with increasing distance from the receptor. The signal in 30nm distance from the receptor (30nm linker 14.5 ± 1.1% n=17) exhibits 60% of the size in direct vicinity of the receptor, while in 60nm distance (60nm linker 9.2 ± 0.9% n=50) the signal is reduced to 40% of the original size. Cytosolic cAMP is at a negligible level of 2.1 ± 0.4% n=18 (Figure 3.10). cAMP forms a clear gradient around the hGLP1R, spanning a size of up to 60 nm and staying very distinct from the cytosolic compartment.

1 pM agonist stimulation (Figure 3.12 D, E) similarly leads to the formation of a clear cAMP gradient, where the amplitude of the cAMP signal decreases stepwise with increasing distance from the source. We record the highest cAMP signal in close proximity of the receptor (no linker 43.7±3% n=32), at 30nm distance we detect 50% of the receptor signal (30nm linker 22.4±0.9% n=36) and only 30% at 60nm distance (60nm linker 13.3±0.7% n=44). The cytosolic cAMP signal (6.2±0.6% n=25), indicated by the dotted line, constitutes only 15% of the signal directly at the receptor.

1nM of the agonist (Figure 3.12 F, G) leads to an elevation in cAMP levels at which the detected signals match each other in all distances from the receptor, while the gradient along the linkers is abolished (no linker 76.7±2.4% n=24; 30nm linker 80.5±1.3% n=24; 60nm linker 76.7±2.1% n=35). The cytosolic cAMP signal makes up only 40% of the signal at the receptor (33.1±4.9% n=20).

With an agonist concentration of 100 nM GLP1 (Figure 3.12 H, I), the whole compartment surrounding the receptor in a distance up to 60nm is filled up with cAMP. We detect equal cAMP amplitudes in all distances from the receptor (no linker 89.3±1.5% n=24; 30nm linker 87.2±2.9% n=15; 60nm linker 81.3±3.9% n=14). Using this high agonist concentration, even cytosolic cAMP signals match the ones recorded in 30nm- and 60nm-distance from the receptor and show no significant difference (cytosol 81.1±1.5% n=22).

These data suggest that the size of the receptor-enclosing cAMP sphere lies in the range of tens of nanometers when a sub-saturation concentration of 10 fM or 1 pM agonist induces the signal. However, the size of the compartment is dynamic and is modulated by the force of the stimulus, as 1nM and 100 nM agonist broaden up the compartment to a size bigger than 60nm and increase the amount of detectable cAMP. Calculated time constants of the FRET changes from the hGLP1R-camps-linker constructs are shown in Figure 7.3 in the appendix.

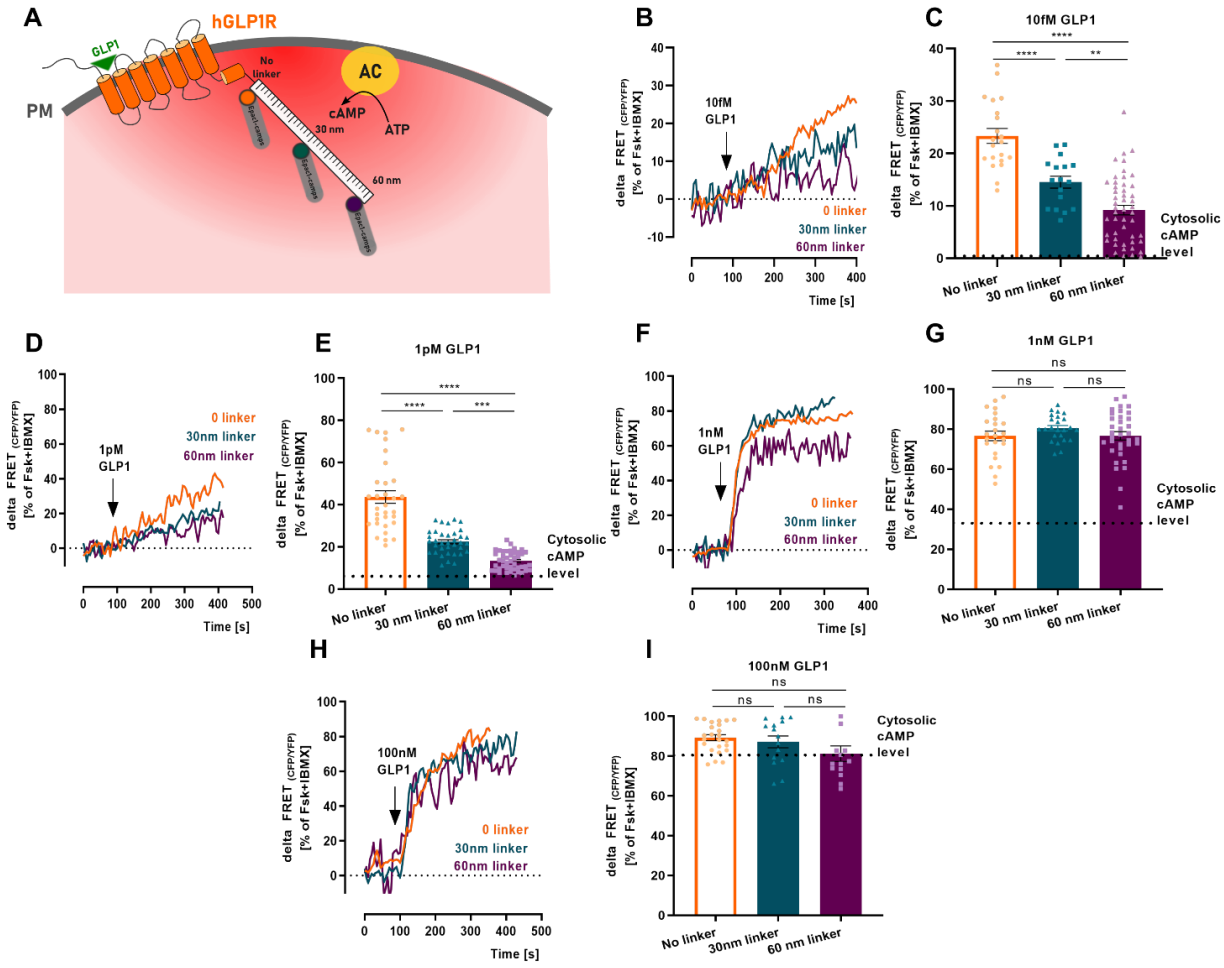

Figure 3.12 Assessing the spatial dynamics of the cAMP domain surrounding the hGLP1R
(A) Schematic representation of the experimental setup. The cAMP sensor is attached to the receptor in gradual distances of 0nm, 30nm and 60nm, thereby enabling the assessment of cAMP surrounding the receptor.
(B), (D), (F), (H) Time course of agonist induced FRET changes recorded in HEK-TsA cells expressing hGLP1R-camps with different linkers (0, 30nm, 60nm) for 10 fM **(B),** 1 pM **(D),** 1 nM **(F)** or 100 nM **(H)** GLP1. Shown are representative traces normalized to fsk + IBMX treatment.
(C), (E), (G) Comparison of cAMP signals generated in different distances from the receptor (0, 30nm, 60nm) upon stimulation with 10 fM **(C),** 1 pM **(E),** 1nM **(G)** or 100nM **(I)** GLP1. The dotted line indicates cytosolic cAMP level upon stimulation with the same agonist concentration. Mean delta FRET-ratios ± SEM ****p<0.0001, ***p<0.001, **p<0.01, ns no significant difference according to a one-way ANOVA followed by Tukey's post hoc test (No linker, and cytosolic data as plotted in Figure 3.10, repeated for better comparability)

3.8 PDEs are key factors in establishing the cAMP gradient

PDEs are the only enzymes known to degrade cAMP and by this decrease its cellular concentration [179]. Different PDE subtypes are expressed in various subcellular locations, and their coordinated action together with ACs in establishing balanced cAMP levels aids in finely regulating cAMP signaling. Some studies speculate that they form an enzymatic barrier by which they hinder cAMP diffusion from the site of synthesis to the bulk cytosol [364, 365]. To test the hypothesis of whether and how PDEs contribute to establishing the GLP1-induced receptor cAMP-compartment, we conducted a set of experiments where we first inhibited the PDEs using 100µM IBMX and subsequently challenged the cells with different concentrations of GLP1. cAMP signals were recorded in direct vicinity or in 30nm and 60nm distance from the receptor and normalized to fsk + IBMX treatment.

In contrast to the data with intact PDEs, 10 fM GLP1 stimulation upon PDE inhibition (Figure 3.13 A, B) evokes an equally high cAMP signal in direct vicinity of the hGLP1R (no linker 33.5 ± 2.2% n=29) and in 30nm distance (36.5 ± 2% n=20). Only 60% of the signal amplitude is evoked in 60nm distance (22.5 ± 1.9% n=36). The cAMP level measured in the cytosol (15.3 ± 1% n=22) makes up less than 50% of the signal directly at the receptor.

Similar as stimulation by 10 fM GLP1, 1 pM (Figure 3.13 C, D) evokes an equal cAMP signal directly at the receptor and in 30nm distance (no linker 60.7±4.8% n=29; 30nm linker 59.9±2.3% n=36). The signal at 60nm distance shows 50% of the amplitude recorded at the receptor and in 30nm distance (60nm linker 31.3±1.3% n=45). The gradient visible with intact PDEs (Figure 3.12 B, C, D, E) is abolished when we pre-stimulate the cells with IBMX. The cytosolic cAMP signal (16.3 ± 1.2% n=26) indicated with a dotted line is higher than without IBMX pre-stimulation, however it makes up only 30% of the cAMP signal in direct vicinity of the receptor.

As depicted in Figure 3.13 E, F 1 nM of the agonist leads to an equilibration of cAMP signals in all distances from the hGLP1R (no linker 82.8±1.4% n=30; 30nm linker 84.6±0.9% n=17; 60nm linker 81.4±1.6% n=36). The cAMP gradient is abrogated, even between 30nm and 60nm distance from the receptor. Yet, not all of the generated cAMP at the receptor reaches the cytosol (68.7±2.9% n=51), since the detected cAMP signal does not exceed 85% of the signal recorded within the hGLP1-receptor compartment.

Equilibration between receptor- and cytosolic cAMP levels is achieved by stimulation with 100 nM GLP1. cAMP signals in all distances from the receptor (no linker 88.7±1.9% n=22; 30nm linker 87.3±1.7% n=26; 60nm linker 85.2±2.3% n=17) match the cytosolic amplitude (90.3±1.6% n=25).

In general, we can state that the pre-stimulation of the cells with 100µM IBMX leads to higher cAMP signals within the receptor compartment and the cytosol compared to the state with intact PDEs (Figure 3.12). These enzymes are potentially involved in the formation of a cAMP gradient within the receptor compartment at a light stimulus with 10 fM or 1pM GLP1 and may constitute one of the diffusion-limiting factors for cAMP. Again, these data illustrate that the receptor compartment is dynamic in its size, depending on the force of the stimulus, GLP1 concentration increase and PDE inhibition enlarges the compartments. Nevertheless, the cAMP nanodomain surrounding the receptor formed due to the stimulation with 10 fM and 1 pM agonist stays intact and up to stimulation with 1 nM agonist separated from the cytosol, even upon deactivation of PDEs.

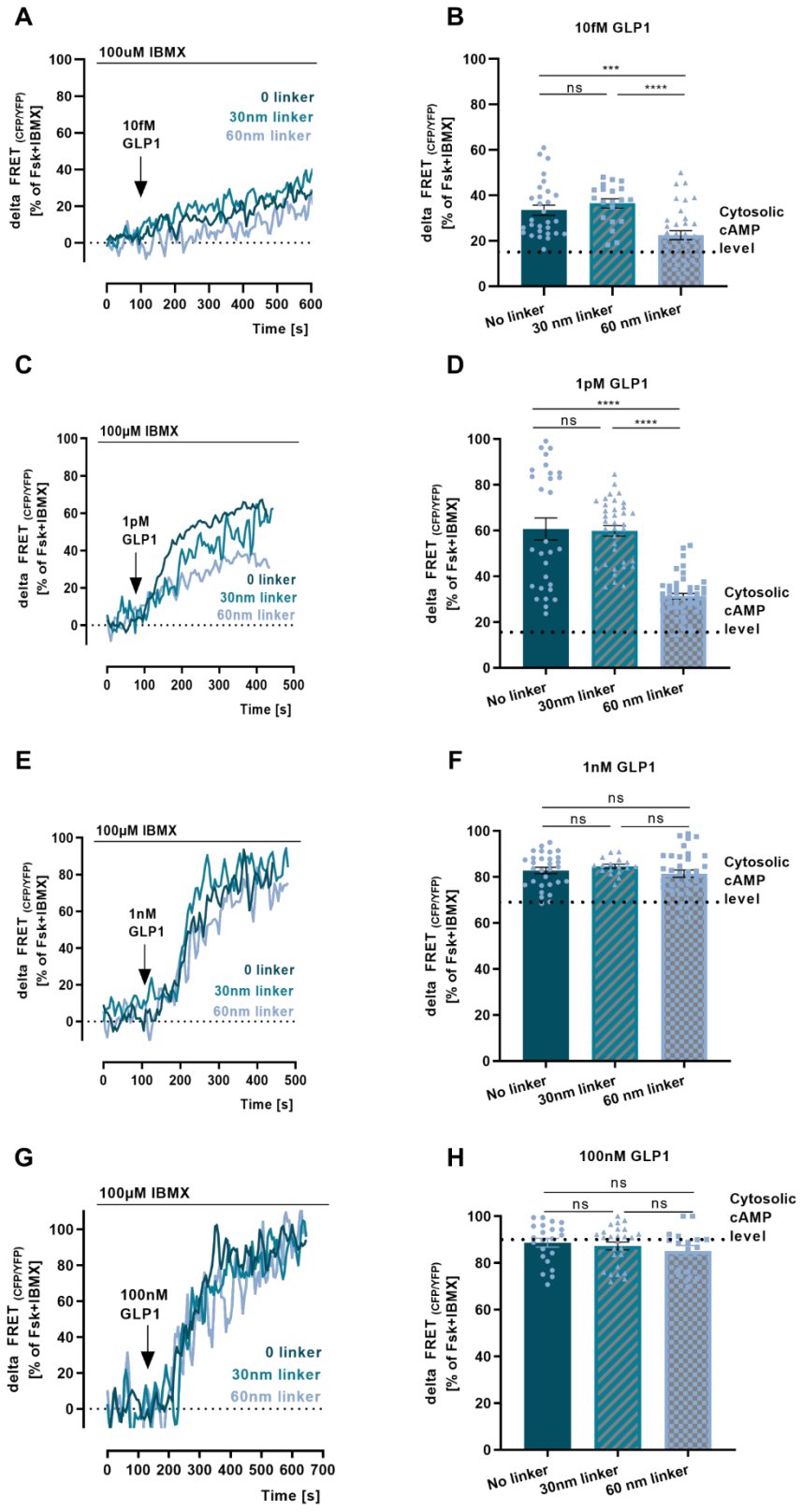

Figure 3.13 Assessing the role of PDEs in forming the cAMP gradient surrounding the hGLP1R
(A), (B), (C), (D) Time course of agonist induced FRET changes recorded in HEK-TsA cells expressing hGLP1R-camps with different linkers (0, 30nm, 60nm) for 10fM **(A),** 1pM **(C),** 1nM **(E)** or 100nM **(G)** GLP1. Shown are representative traces normalized to fsk + IBMX treatment.
(B), (D), (F), (H) Comparison of cAMP signals generated in different distances from the receptor (0, 30nm, 60nm) upon stimulation with 10 fM **(B)** 1 pM **(D),** 1 nM **(F)** or 100 nM **(H)** GLP1. The dotted line indicates cytosolic cAMP level upon stimulation with the same agonist concentration. Mean delta FRET-ratios ± SEM ****p<0.0001, ***p<0.001, ns no significant difference according to a one-way ANOVA followed by Tukey's post hoc test.

3.9 Generation of a receptor-sensor to detect PKA phosphorylation

The subsequent step to cAMP production along the signaling cascade of the hGLP1R is PKA activation and phosphorylation of its effector proteins [366]. To investigate whether the locally produced cAMP within the receptor compartment is capable of activating the PKA, we fused AKAR4 [342] to the C-terminus of the hGLP1R (Figure 3.14). With this, we created hGLP1R-AKAR4, a sensor that detects real-time PKA activity dynamics inside of the nanocompartment. To compare with global PKA activation in the cytosol, we generated WT-hGLP1R-IRES-AKAR4, an IRES (internal ribosomal entry site) construct [367] carrying the WT-hGLP1R with cytosolic AKAR4. This method is advantageous since one vector can carry several genes with IRES sequences in between, while they need only one promotor and terminator. Hence, stoichiometric expression of both proteins is ensured.

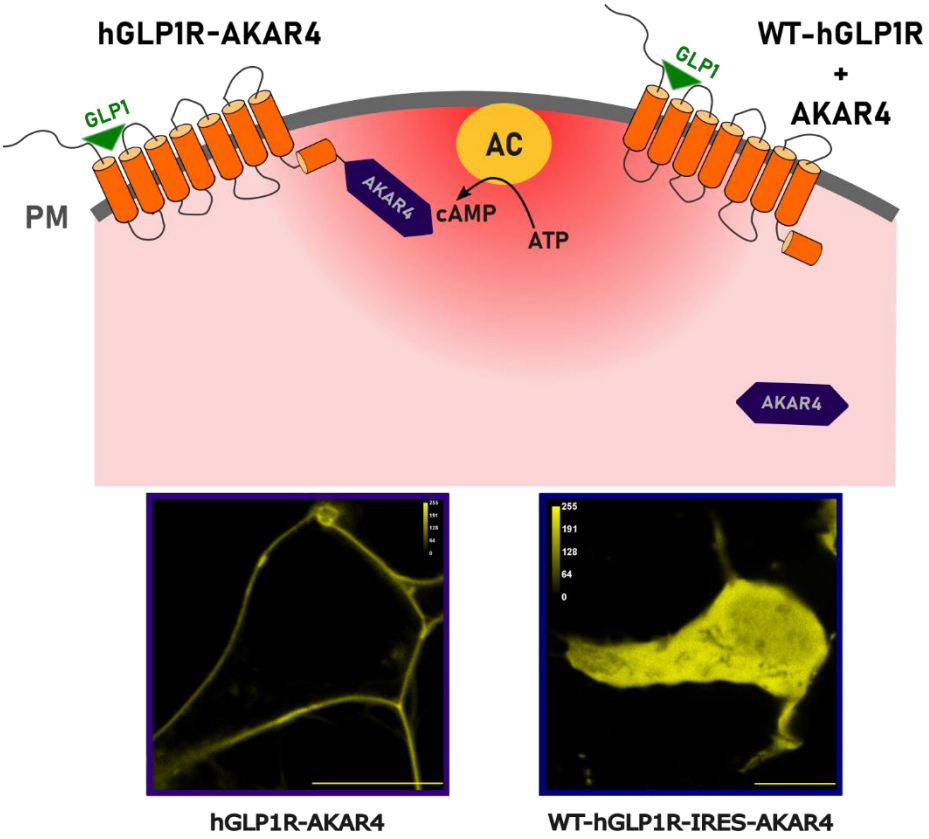

Figure 3.14 Receptor sensor for PKA-phosphorylation assessment
Schematic representation of the PKA-phosphorylation sensor AKAR4 attached to the C-terminus of the hGLP1R (hGLP1R-AKAR4) or expressed separately as cytosolic AKAR4 along with membranous WT-hGLP1R in cells carrying an IRES construct (WT-hGLP1R-IRES-AKAR4). Confocal images of a HEK-TsA cell expressing the indicated constructs. YFP channel. Scale bar = 10 µm.

3.10 Comparison of PKA phosphorylation within the hGLP1R-compartment and the cytosol

In single cell FRET experiments, HEK-TsA cells were individually transfected with hGLP1R-AKAR4 or WT-hGLP1R-IRES-AKAR4 and stimulated with 1 pM or 1nM GLP1 to measure PKA phosphorylation. FRET traces were normalized to fsk + IBMX signal.

From the results presented in Figure 3.15 A, B, it is visible that cAMP produced by 1 pM GLP1 leads to a high phosphorylation rate of the PKA inside of the hGLP1-receptor compartment (79.3±3.6% n=19). Cytosolic PKA is also active, (13.4±1.1% n=22) albeit only to a fifth of the degree detected at the hGLP1R.

The application of 1 nM GLP1 (Figure 3.15 C, D) leads to a saturated PKA activity in both compartments (hGLP1R-compartment 96.1±0.7% n=25, cytosol 98.2±0.3% n=29).

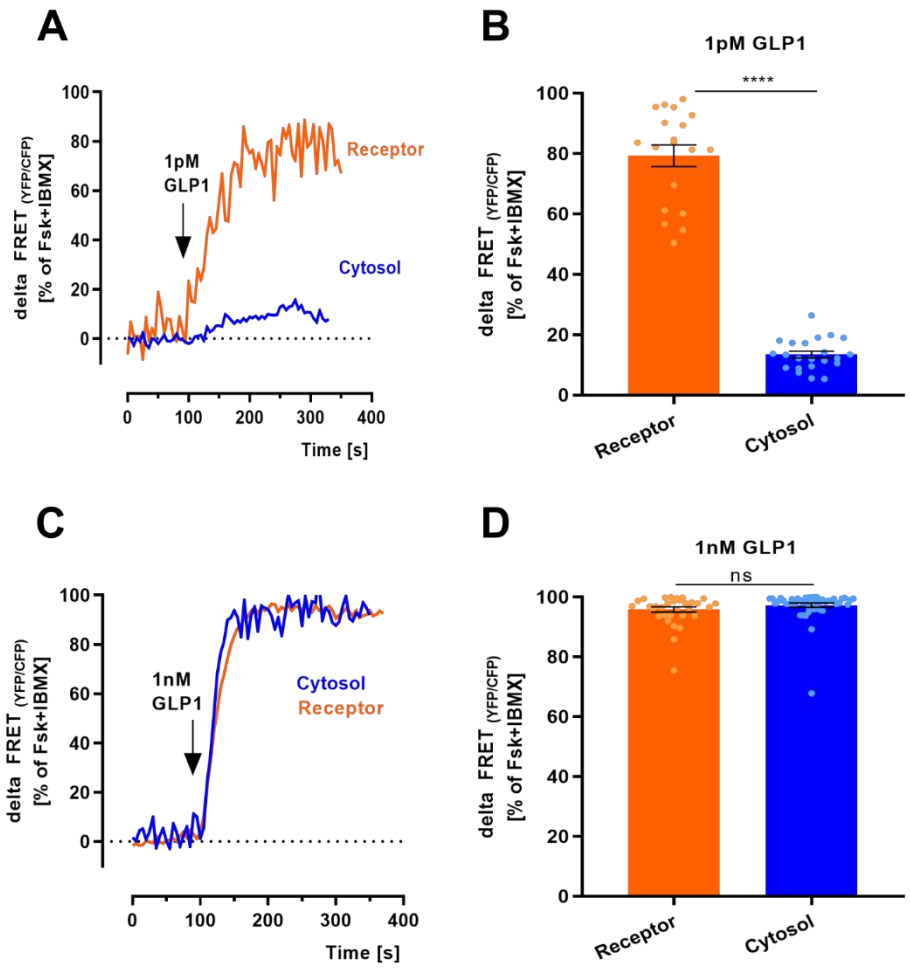

Figure 3.15 PKA is highly active inside the hGLP1R-domain
(A), (C) Time course of agonist induced FRET changes recorded in HEK-TsA cells expressing AKAR4 either at the hGLP1-receptor or in the cytosol upon stimulation with 1pM **(A)** or 1nM **(C)** GLP1. Shown are representative traces normalized to fsk + IBMX treatment.
(B), (D) Comparison of PKA phosphorylation at the receptor and in the cytosol upon stimulation with 1pM **(B)** or 1nM **(D)** GLP1. ****p<0.0001, p>0.05 ns no statistical difference according to an unpaired t-test.

3.11 Effect of AKAP disruption on PKA phosphorylation

AKAPs are proteins known to target PKA to specific subcellular locations [257] and with this orchestrate cAMP signaling in defined compartments. To investigate whether AKAPs are relevant for PKA activation within the receptor cAMP-compartment we transfected HEK-TsA cells with hGLP1R-AKAR4 and pre-incubated with 100 µM St-Ht31 for 30 minutes, a cell permeable peptide known to disrupt PKA subunit-binding to AKAPs [248]. 10 µM St-Ht31 were present throughout the experiment, to maintain its effect on the cells. As presented in Figure 3.16 A, stimulation with either 1 pM or 1 nM GLP1 does not lead to any increase in FRET-signal (YFP/CFP) over baseline, meaning no PKA phosphorylation can be detected in the compartment. Therefore, values could not be normalized but are shown as absolute FRET ratio. On the other hand, 1 nM GLP1 stimulation of WT-hGLP1R-IRES-AKAR4 expressing HEK-TsA cells pretreated with St-Ht31 gave a saturating PKA-phosphorylation signal (Figure 3.16 B 94.7±1.9% n=14), analogous as without pretreatment (Figure 3.15 C).

PKA phosphorylation within the hGLP1 receptor-compartment was unchanged when cells were pretreated with the control peptide St-Ht31-P [347] (Figure 3.16 C, D 1 pM: 75.9±4.1% n=16, 1 nM: 96.4±0.6 n=27). These values do not significantly differ from PKA phosphorylation signals of untreated cells (Figure 3.15).

Taken together, these results imply that AKAPs are present and crucial for PKA activity inside the cAMP nanocompartment surrounding the hGLP1R. In contrast, cytosolic PKA-phosphorylation activity is unaffected when PKA-AKAP binding is disrupted.

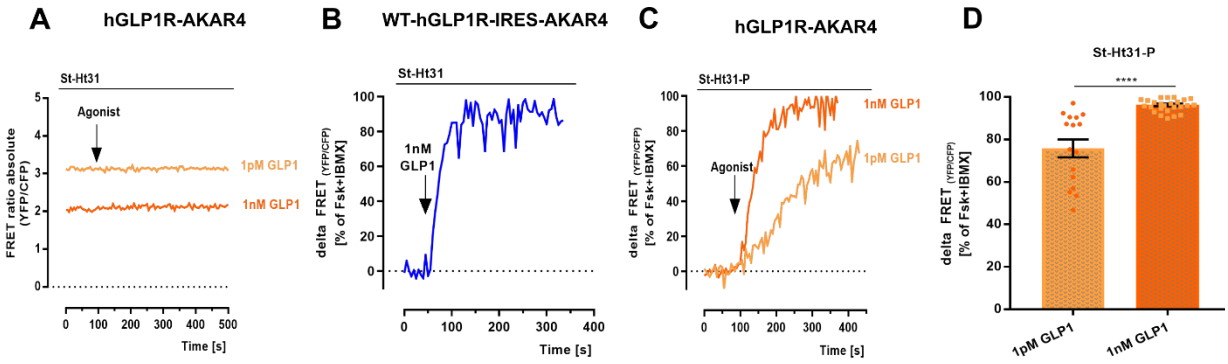

Figure 3.16 AKAP disruption in hGLP1R domain leads to perturbed PKA phosphorylation
(A) Time course of FRET ratios recorded in HEK-TsA cells expressing AKAR4 at the hGLP1-receptor (hGLP1R-AKAR4) upon stimulation with 1 pM or 1 nM GLP1. Cells were pre-incubated with 100µM St-Ht31 for 30 minutes. Shown are absolute FRET ratios, since the addition of ligand and fsk + IBMX did not lead to a FRET change, precluding normalization.
(B) Time course of agonist induced FRET changes recorded in HEK-TsA cells expressing AKAR4 in the cytosol, upon stimulation with 1 nM GLP1. Cells were pre-incubated with 100 µM St-Ht31 for 30 minutes. Representative trace normalized to fsk + IBMX treatment.
(C) Time course of agonist induced FRET changes recorded in HEK-TsA cells expressing AKAR4 at the hGLP1-receptor (hGLP1R-AKAR4) upon stimulation with 1 pM or 1 nM GLP1. Cells were pre-incubated with 100 µM St-Ht31-P for 30 minutes. Shown are representative traces normalized to fsk + IBMX treatment.
(D) Comparison of PKA phosphorylation-rate within the hGLP1-receptor compartment induced by 1 pM or 1 nM GLP1 upon pre-incubation with 100 µM St-Ht31-P. ****p<0.0001 according to an unpaired t-test.

4 Discussion

4.1 hGLP1R-camps constitutes a novel tool to measure cAMP in the direct vicinity of a GPCR

In this work, we have created to our knowledge the first tool, which enables the measurement of cAMP levels in the direct vicinity of the hGLP1R in real time in living cells. The receptor sensor conjugate hGLP1R-camps is as potent in cAMP generation as its wildtype counterpart (Figure 3.7), it is not impaired by attaching Epac1-camps to the C-terminus and the G_S protein can be recruited unrestrictedly. By functionally characterizing the effect of cAMP modulating compounds, we ascertained that the FRET-sensor is capable of reliably reporting changes in cAMP levels (Figure 3.8). The antiparallel fluorophore traces in the functional hGLP1R-camps sensor, compared to the binding-deficient mutant hGLP1R-camps-R279E indicate that the FRET changes are due to changes in cAMP levels, not artifacts caused by compounds or conformational changes within the receptor C-terminus.

Other groups have targeted cAMP sensors to GPCRs, however not with the aim of monitoring receptor exclusive cAMP levels. In 2013 Richter *et* al. measured cAMP in the vicinity of the β_1-AR by attaching Epac2-camps, albeit in an indirect way. They showed that stimulation of the receptor with antagonists leads to the dissociation of associated PDE4 thereby increasing surrounding cAMP levels.

Moore *et* al. employed the single colour cAMP sensor cADDis [339] attached to the 5-Hydroxytryptamine receptor 6 with the aim of targeting the receptor to the cilia of mouse embryonic fibroblasts (MEFs). They compared ciliary cAMP levels with bulk cytosolic ones to find that cAMP levels in cilia are about 5-fold higher. They report that ACs 5/6 are responsible for tonic ciliary cAMP production, yet in a GPCR independent manner. Knock down of $G\alpha_S$ by siRNA does not affect basal ciliary cAMP levels, which suggests a G protein independent regulation of AC5/6 for cAMP production. PIP_3 seems to be the molecule required for cAMP production in cilia. Both groups targeted class A GPCRs, whereas in our study we were interested in a class B subtype.

Insertion of the rigid ER/K-linkers of different lengths within the receptor-sensor conjugate to create nanorulers, extends its application to measure cAMP in defined distances from the receptor. With these tools in hand, we are able to study the size of the hGLP1R-cAMP compartment.

4.2 Targeting of Epac1- camps to different subcellular locations

With our goal of finding and describing high-concentration cAMP compartments in living cells it is necessary to be able to measure cAMP in discrete domains. Knowing that G_SPCRs initiate the signal for cAMP generation we hypothesized the vicinity of aforementioned GPCR constitutes such a domain. It is an established mechanism by now to tag proteins of interest with FRET sensors or to target the reporters to different subcellular compartments in order to study local changes in second messenger levels [258, 332, 345].

By attaching the Epac1-camp sensor either to the C-terminus of the hGLP1R, or by linking it via the CAAX sequence to the non-lipid rafts of the plasma membrane, we created localized sensors which detect cAMP in two distinct subcellular compartments. Untargeted Epac1-camps additionally detects cytosolic cAMP. With these tools, properly calibrated and characterized, we were able to compare basal and stimulated cAMP levels in the discrete compartments. For further studies, to examine cAMP compartmentalization in different cellular areas, one would employ a targeting sequence for a certain organelle like the nucleus, mitochondria, cilia or flagella [332, 352-354].

4.3 Comparison of the different calibration methods used to functionally characterize hGLP1R-camps

Two different methods were used to calibrate the hGLP1R-camp sensor, comparing its affinity for cAMP to the untargeted Epac1-camps sensor and to the plasma membrane targeted Epac1-camps-CAAX. The first approach using MDL and the cell permeable cAMP analogue 8-Br-O'-Me-cAMP-AM has been described in the literature to be a method for in vivo calibration of second messenger sensors, equally reliable as more commonly performed in vitro calibrations [227]. Yet it has some drawbacks in our eyes, making it only the second method of choice for calibration.

Foremost, it does not use actual cAMP but an analogue, which most likely exhibits a different affinity for the cAMP sensor. Thus, the EC_{50} values obtained cannot be compared to actual EC_{50} values for cAMP but should rather be regarded as relative values to compare different cAMP sensors. Furthermore, the diffusion of 8-Br-O'-Me-cAMP-AM into the cells is very slow, especially at low concentrations. The equilibration between intra- and extracellular concentration is very much time dependent, causing a high variability in the assay results. In the experimental procedure we used, we added the different 8-Br-O'-Me-cAMP-AM concentrations cumulatively which is not the most accurate approach, since the concentrations add up. Furthermore, it has been shown than MDL can be slightly toxic for some cell lines, altering the physiological behavior which could affect the calibration procedure. For short experiments (such as basal cAMP assessment described in 3.4) this should not pose a problem, yet for longer experiments such as the calibration, this could affect the results.

The results obtained from this first method do state that hGLP1R-camps and untargeted Epac1-camps exhibit a similar affinity for cAMP and can therefore be used to compare cAMP levels in different compartments (Figure 3.9). The Epac1-camps-CAAX sensor however, shows a putatively higher affinity for cAMP, which is counter-intuitive. This could be due to the fact that cAMP at the membrane is higher, MDL incompletely inhibiting the ACs, which is why the sensor is already partially saturated. The resulting concentration response curve would artificially be leftward shifted (See Figure 4.1).

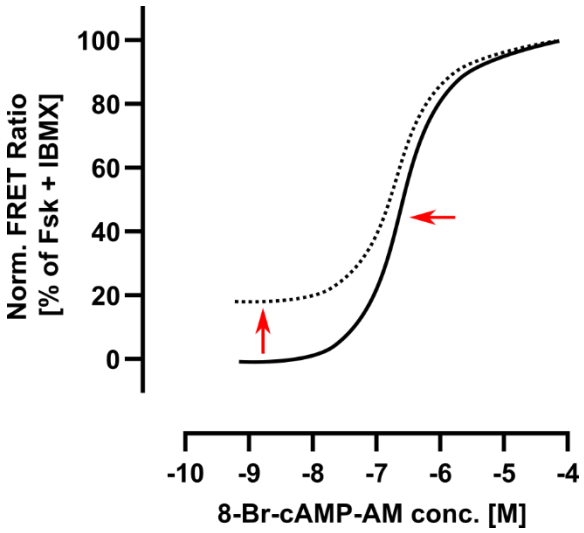

Figure 4.1 Simulated traces for MDL calibration
Higher basal cAMP concentrations would lead to higher basal FRET ratios, artificially leading to a leftward shift of the curve and the resulting EC50 value.

In addition, the physical properties of 8-Br-O'-Me-cAMP-AM to accumulate in cells and most likely also in the membrane, as discussed earlier in the results, make it an unreliable compound for the actual in-cell calibration.

With these disadvantages in mind, we decided to employ a second calibration procedure to examine the affinity of the differentially targeted sensors. The second method based on cell permeabilization with saponin is straight forward since it uses actual cAMP. Hence, the resulting EC_{50} values from the calibration curves state the true affinity for cAMP in vivo. All three sensors exhibit a similar pEC_{50} value which correspond to an EC_{50} of 4.9 µM for hGLP1R-camps, 5.2 µM for Epac1-camps and 4 µM for Epac1-camps-CAAX. Compared to the EC_{50} value of Epac1-camps (2.5±0.6 µM) determined by in vitro calibration of cytosolic HEK-293 cell-preparations with cAMP [227], our results indicate a slightly lower affinity. The divergence between in cell and in vitro measured value can be due to several reasons. In vivo, a portion of the infused cAMP might be buffered by effector proteins and thus not be available for binding to the sensor, while in vitro the suspension contains a defined amount of cAMP. A second reason could be that the cellular pits created by saponin are too small to allow fast equilibration between intra- and extracellular medium, thus the intracellular cAMP concentration is lower than intended. This case, however, is very unlikely since additional 2 µg of saponin are added at the end of each experiment to assure complete equilibration.
Nevertheless, since the affinity for cAMP of all three constructs is significantly similar, they can reliably be used to compare detected cAMP levels.

This method seems to be superior to the MDL-calibration, therefore we chose to calibrate the hGLP1R-linker constructs according to the same protocol. Both hGLP1R-SAH30-camps and hGLP1R-SAH60-camps possess a similar EC_{50} to above mentioned constructs (hGLP1R-SAH30-camps EC50=5.9 µM, hGLP1R-SAH60-camps EC_{50}=6.4 µM), with no statistical significant difference. Hence, they are equally reliable for cAMP detection.

Regarding the dynamic range of the targeted Epac1-camp sensors there are substantial deviations between the different constructs. Epac1-camps, hGLP1R-SAH30-camps, hGLP1R-SAH60-camps exhibit the same big dynamic range (Epac1-camps 34.9% delta FRET, hGLP1R-SAH30-camps 28.6%, hGLP1R-SAH60-camps 30%). hGLP1R-camps and membrane targeted Epac1-camps-CAAX on the other hand, show a reduced dynamic range (hGLP1R-camps 15.12%, Epac1-camps-CAAX 6.68).
Since the delta FRET value for hGLP1R-camps and Epac1-camps-CAAX, both expressed at the membrane, seemed very small, we hypothesized that the applied saponin might change the architecture of the plasma membrane during the calibration experiments. As it creates holes up to 40-50 Å [362], it might perturb the orientation of the membrane bound Epac1-camps-CAAX sensor and its fluorophores, which results in the small dynamic range. Therefore, we assessed the dynamic range again with the MDL/8-Br-O'-Me-cAMP-AM method. This method allows the reliable measurement of both the minimum and maximum cAMP detection level of the sensor (using MDL for the minimum, and the highest 8-Br-O'-Me-cAMP-AM concentration for the maximum). The repeated measurement resulted in a value of 25.3% for hGLP1R-camps and 16.6% for Epac1-camps-CAAX, meaning it is likely our hypothesis was true, and the sensors are impaired only in the saponin calibration experiments. Not however in the regular experiments throughout this work and they can be used to accurately detect cAMP at the receptor and the plasma membrane. hGLP1R-SAH30-camps and hGLP1R-SAH60-camps are also expressed at the plasma membrane, yet their dynamic ranges are not impaired. The added linker between the receptor and the sensor might restore the flexibility of the fluorophores within the sensor to its origin so that the dynamic range does not get impaired.

Since targeting of cAMP sensors can lead to an impaired dynamic range, efforts were made to develop sensors which are not affected by targeting [258]. Traditionally, targeting is achieved by attaching the targeting sequence to the sensor N-terminus, which comprises a fluorescent protein. A novel approach whereby YFP is inserted into the CNBD of the regulatory subunit IIβ of PKA resulted in a new cAMP sensor termed CUTie. Moving YFP away from the amino terminus circumvents the interference of the N-terminal targeting domain with the fluorophores. This sensor retains its dynamic range even if targeted to different subcellular locations and can thus be universally applied to tag proteins of interest without affecting the properties of the sensor.
For further studies exploring cAMP dynamics in cellular compartments one would employ such a sensor, since it does not need to be calibrated within each compartment and thus saves a lot of effort in the course of the study. However, depending on the aim of the study, it is important to choose the correct cAMP sensor in terms of affinity, as the various available sensors all exhibit disparate values. Typically FRET sensors work in a concentration window of ≈100 nM to ≈10 µM [227]. Depending on the cell type or the subcellular location where cAMP is supposed to be detected, basal levels can vary from <100 nM up to the µM range [353]. Therefore, the appropriate sensor must be selected to cover the range of cAMP concentrations relevant for each cell type or subcellular compartment. Table 7.2 in the annex shows all available cAMP sensors with their reported affinity.

Although protocols are described to translate changes in FRET into actual cAMP values [227, 368], we deliberately chose not to allocate the changes in FRET we observe with our differentially targeted sensors into actual cAMP concentrations. The first reason is that we measure cAMP in very small compartments. While the law of mass action implies that all pharmacological effects are concentration related, there is evidence that the mass-action law is violated in confined systems with a small number of molecules [369]. In a nanocompartment with a small number of cAMP molecules deterministic assumptions are no longer valid, and the calculation of a concentration would result in artificially high and unrealistic values.
Above-mentioned calculations to express cAMP concentrations are based on EC_{50} values, hill coefficients of concentration-response curves and maximum delta FRET values for the applied sensors. The values used in the mathematical formulas are derived partially from in cell and in vitro experiments, determined through different experimental approaches and are thus unreliable to calculate actual cAMP concentrations in nanodomains. Therefore, we chose to compare FRET amplitudes as a parameter for cAMP levels between the different compartments without allocating actual concentrations to them.

4.4 Divergent basal cAMP levels in different cellular compartments

With the Epac1-camp sensor targeted to three different cellular locations, we detected basal cAMP levels at the hGLP1R, in the non-lipid rafts of the plasma membrane and in the cytosol. Various groups were already able to show that the plasma membrane bears higher cAMP levels compared with the bulk cytosol. We were able to extend the knowledge to a third compartment, the surrounding of the hGLP1R to show it contains equal cAMP levels as the general plasma membrane. In the unstimulated cell, the plasma membrane, with the various incorporated receptors and channels can thus be regarded as a cellular area with a uniform cAMP level.

In detail, targeted sensors revealed basal cAMP levels in different compartments of interest. One of the first groups to measure basal cAMP levels targeted Epac2-camps to the plasma membrane, to AC8 and to the cytosol [345]. They reported higher levels at the plasma membrane and close to AC8

compared to the bulk cytosol and argue that the high cAMP level in these areas reflects the close proximity of the sensor to the source (ACs), without PDEs in close proximity of ACs.

By inhibition of basal AC activity Agarwal *et* al. [370] have shown that non-lipid raft areas of the plasma membrane express a higher cyclase activity and thus a higher cAMP level compared to the lipid rafts and the cytoplasm. A study conducted by the same group, 4 years later [371] reveals contradicting data. Using the same approach but this time translating the delta FRET values into actual cAMP amounts, they state that the cytosol and the non-lipid raft domains bear equally high amounts of cAMP, though less than the lipid raft domains.

Both groups used the Epac2-camp sensor which exhibits a higher affinity for cAMP compared to Epac1-camps as in our study (Epac2-camps 0.9 µM vs. Epac1-camps 2.5 µM [372]). As mentioned above, intracellular cAMP concentration can vary between 100 nM in resting conditions up to tens of µM under stimulated conditions, with 1µM cytosolic cAMP being the value most often mentioned in the literature [227, 345, 368, 373]. Therefore, we believe Epac1-camps is more suitable than Epac2-camps for detection of cAMP, since we planned to detect both basal and stimulated cAMP levels in cells. To assure the sensor is not saturated by cAMP, it is advisable to choose a sensor with an EC_{50} value in the mid-range of detected cAMP.

The fact that cAMP is higher at the membrane and does not equilibrate with cytosolic cAMP level suggests that it cannot freely diffuse from its site of synthesis but is restricted by certain mechanisms to the plasma membrane.

4.5 Receptor stimulation leads to unequal rise of cAMP in different compartments

Since FRET tools became available for measuring cAMP levels in living cells, they have extensively been used to study changes in cAMP upon stimulation of different GPCRs. The differential effect of PGE_1 on cytosolic vs. membranous cAMP has been explored [371, 374], as well as the stimulation of β-ARs by isoproterenol and its effect on cytosolic, membranous, mitochondrial and nuclear cAMP [332]. Nikolaev *et* al. studied the spatial and temporal cAMP dynamics in the cytosol after stimulation of β_1- and β_2-ARs [336].

In this study we investigated the cAMP dynamics upon stimulation of the hGLP1R with its endogenous agonist GLP1, to find that cAMP rises unevenly in the three compartments of the hGLP1R, the plasma membrane and the cytosol although stimulation occurred by the same specific agonist concentration.

4.5.1 High-concentration cAMP compartment surrounding hGLP1R

Starting from concentrations as low as 10fM GLP1 (Figure 3.10) cAMP rises exclusively at the hGLP1R and stays below the limit of detection at the general plasma membrane and the cytosol. The trend is similar for higher concentrations of 1 pM or 1 nM GLP1. cAMP appears first at the receptor and exhibits a smaller amplitude at the membrane and the cytosol. Even at a saturating concentration of 100nM GLP1, the receptor compartment stays distinct from the latter two. With an EC_{50} value of the hGLP1R for GLP1 in whole cell cAMP assays described to be in the picomolar range (4.16 pM [115] 85 pM [127]), 10 fM of the agonist lie outside the range of the concentration-response-curve. We are one of the first groups to describe a cAMP signal for such a low agonist concentration.

A recently published paper [375] reports the activation of several GPCRs by femtomolar concentrations of their ligands. Among them the adenosine A_{2B} receptor, β_1-& β_2-ARs, α-adrenergic receptor, PGE_1R and dopamine D_2&D_4 receptors all endogenously expressed in HEK-293 cells. Stimulation with 1fM of their

respective endogenous ligand, led to cAMP accumulation. They additionally tested whether the hGLP1R responds to femtomolar GLP1 concentrations, however they could not detect any cAMP signal. They further report a rise in membranous cAMP upon stimulation of the cells with 1fM isoproterenol, detected by plasma membrane targeted Epac2-camps. They hypothesize that the response to femtomolar concentrations of the ligand depends on a preassembled signaling complex, and were able to show that the cAMP response at the plasma membrane to femtomolar isoproterenol is dependent on AKAP250 and β-arrestins. Mathematical modeling suggests that the responses to sub-nanomolar concentrations of the ligand were triggered in a cell by one or two binding events with signal amplification being required. The preassembled signaling complexes could play an important role in the amplification of the response.

Our data are partially in line with these findings while they contradict some other parts. The experimental approach we use allows us to detect cAMP in direct vicinity of the hGLP1R, in comparison to the cAMP accumulation assay used throughout the afore mentioned study. We report cAMP elevation as a response to femtomolar ligand stimulation, whereby the cAMP level surrounding the receptor rises with increasing ligand concentrations. In contrast, higher concentrations of agonists, which led to a cAMP signal at femtomolar concentrations in afore mentioned study, do not increase the cAMP level further, until very high micromolar concentrations are used. Our approach states a more precise and direct way of measuring cAMP inside of a distinct compartment.

cAMP being and staying higher within the detection range of hGLP1R-camps argues for the existence of a receptor specific compartment, which forms upon stimulation by the ligand and is segregated from the general plasma membrane opposed to the unstimulated state, where receptor and membrane exhibit equal cAMP amplitudes. Even at higher agonist concentrations above EC_{50}, the receptor cAMP level stays distinct from the membrane and the cytosolic one. This suggests there are mechanisms, which keep cAMP local, contributing to the establishment of a receptor specific cAMP domain. As discussed in the following section, restricted cAMP diffusion could play a role.

4.5.2 cAMP diffusion

The hypothetical mechanisms which could contribute to restricted cAMP diffusion are diverse and until this day not fully understood. It is speculated that elements of the endoplasmatic reticulum which are localized beneath the plasma membrane might limit cAMP diffusion to the cytosol [364]. Major efforts have been put in studying the effect of PDEs, since they are thought to contribute to the generation of cytosolic cAMP gradients. They presumably act as a functional barrier, which limits diffusion and leads to lower cAMP levels distal to the production site or as a sink that depletes cAMP in localized areas [365, 376, 377]. As shown by Zaccolo and Pozzan, the cAMP microdomains shaped in cardiomyocytes upon stimulation of β-ARs were completely abolished in the presence of PDE inhibitors, and led to a generalized PKA activation throughout the cell [261]. The many isoforms of PDEs within the superfamily differ in their regulatory and kinetic features, which might affect their contribution to the gradient formation. Of notice is that the kinetics of cAMP degradation by some PDEs appears to be faster than the speed of cAMP synthesis [331, 378]. Additionally, the targeting of PDEs to subcellular compartments or recruitment into multi-protein signalling-complexes provides means to terminate the cAMP signal in a spatially restricted manner [379]. These features strongly support the role of PDEs as enzymatic barriers to cAMP diffusion.

Computational modelling is a useful tool to investigate the relative contribution of PDEs to cAMP diffusion speed and compartmentalization. All modeling studies show that PDE activity is

necessary, however some suggest that it is not alone sufficient to explain the compartmentalized behaviour of cAMP signaling [376]. Also the mathematical analysis based on PDE activity and cAMP diffusion rate together with FRET-based measurements of cAMP concentration shows that PDE activity alone is insufficient to explain cAMP compartmentation on a nanometer scale [356].

The concept of diffusion barriers, whether physical or enzymatic, does not fully satisfy the requirements for specific activation of compartmentalized effector proteins. A sub-membranous barrier would establish a gradient of cAMP from the site of synthesis to the cytosol, showing a high level at the plasma membrane and progressively decreasing away from the membrane. As a result, PKA, Epac or other effector proteins localized at the plasma membrane would be preferentially activated compared to cytosolic pools of effectors. In such a scenario, it is difficult to explain how selective activation of effector proteins in the cytosol might occur without concurrent activation at the plasma membrane. An alternative hypothesis, which would better explain specified activation of effector proteins, irrespective of their distance from the site of synthesis, pictures freely diffusing cAMP throughout the cell, with local PDEs degrading cAMP effectively in restricted domains to prevent generalized activation of effector proteins. In this model PDEs would not form diffusion barriers, but rather quench cAMP in defined compartments to protect its targets from inappropriate activation [380].

Another putative factor contributing to the restricted diffusion of cAMP is its buffering by regulatory PKA subunits [381]. Estimations state that a mammalian cardiomyocyte contains 0.5-1µM PKA, which would correspond to a cAMP buffering capacity of up to 2µM [381, 382]. Under these circumstances, the number of binding sites exceeds the cAMP concentration, and a large portion of cellular cAMP would be bound to RII subunits of PKA [383]. A study combining mathematical modelling and live-cell imaging showed that cAMP levels are stabilized near a region of maximal PKA sensitivity, due to the low diffusivity of PKA regulatory subunits [384].

In order to fully understand cAMP signaling, the molecular and structural mechanisms influencing cAMP diffusion need to further be studied with regards to its compartmentation in cells.

4.6 Spatial dimension of the hGLP1R-compartment

4.6.1 Putative size of signaling compartments

Since the notion of compartmentalized signaling arose as a paradigm to explain signaling specificity, various groups have tried to investigate the size these domains. Elucidating the spatial dimension of these signaling compartments might aid in understanding the means by which a cell achieves this precision in signaling. Depending on the size of these compartments, assumptions about the nature and amount of involved proteins, effectors, enzymes or involved cytoskeletal framework can be made. There is not yet a consent about the exact dimension of these compartments; various groups have tried to visualize either cAMP or PKA-activity domains and they are estimated at the micrometer range of size.

Maiellaro *et* al., who have studied cAMP compartmentalization in Drosophila motor neurons upon stimulation of GPCRs, found that cAMP signals are limited to single synaptic boutons. They describe three distinct cAMP signaling compartments within a motor neuron: boutons, axons and cell body with a distinct mechanism in each responsible for cAMP segregation. Depending on the dimension of these anatomical structures, compartments are described to be in the micrometer range of size (1-10 µm) [260]. A second study dealing with cAMP compartmentalization describes the range of action of this second messenger to be on the order of tens to hundreds of micrometers [261].

A more recent study [258] in which the cAMP sensor CUTie was targeted to different myocardial structures to monitor local cAMP signals comes to the conclusion that the domains are about 300 nm in size. For the first time these domains are attributed a nanometer size.

Taking it to the next step within the signaling cascade, Mo *et* al. [259] applied super-resolution microscopy in order to visualized PKA activity microdomains on the plasma membrane of living cells. They developed a fluorescence fluctuation increase by contact (FLINC)-based biosensor to monitor PKA phosphorylation rate, targeted it to the plasma membrane and generated super resolution activity maps of PKA with pcSOFI (photochromic stochastic optical fluctuation imaging). The active puncta revealed by this technique exhibit a mean diameter of 250 nm on the basal membrane of HeLa cells.

These findings show that cellular compartments are smaller than initially believed. However, further research is needed since afore mentioned studies only hint that these cAMP- or PKA-domains are in the nanometer range of size, but never fully visualize cAMP compartments themselves.

4.6.2 Size and shape of the hGLP1R compartment

In this work, we studied the spatial dimension of the receptor specific cAMP domain to report about the existence of a nanocompartment with a size that lies in the rage of tens of nanometers (Figure 3.12). We additionally found that the cAMP amount decreases stepwise with increasing distance from the receptor. At a light stimulus of either 10 fM or 1 pM GLP1, cAMP forms a clear gradient surrounding the receptor, with the lowest amount detected in 60nm distance. The spatially limiting factors for the compartment at 60nm distance keep the cytosolic cAMP levels considerably lower, leading to both receptor- and cytosolic-compartments still being distinct.
At concentrations of 1 nM GLP1 and above the compartment loses its graded shape to exhibit an equally high cAMP level in all distances from the receptor. At 1 nM GLP1 it is still distinguishable from the cytosol in its cAMP amplitude, while at 100 nM all cellular compartments even out in their cAMP level.

It seems logical to assume that the cAMP generating AC(s) must be in close proximity of the hGLP1R, where direct cross talk can occur, as has been reported for some receptor- and cyclase subtypes [169].

One could hypothesize that low concentrations of the ligand facilitate signal transmission of cAMP between two or three key proteins to occur in a very specific manner while the receptor compartment is as small as approximately 60nm. This way the signal coming from the GPCR could be delivered in a very precise manner. Broadening of the compartment upon stimulation with higher ligand concentrations may open up the possibility to reach effectors located in further distance to the receptor. Since we do not possess a receptor-sensor conjugate with a longer linker, we could not measure the size of this high-stimulus compartments. Nevertheless, we can hypothesize about a mechanism for cells to maintain signaling specificity. With low agonist concentrations the compartment is small, and the signals reach only very local effectors (<60nm), while a strong stimulus is far reaching (>60nm).

Assuming this nanodomain constitutes a signaling compartment where receptor, cAMP and effectors are brought in close proximity, we try to estimate the size of a putative signaling complex comprised of involved signaling partners. Each of the involved proteins exhibits a different molecular size, ranging from smaller ones such as the hGLP1R with 53 kDa [385] and PKA with 38 kDa for the catalytic subunit [386] to bigger ones as Epac with 103 kDa [387], over ACs with 124 kDa [157] to AKAPs which are described to be very diverse in their molecular weight [246, 388]. Unifying them along with other putative signaling partners, they could form multi-protein signaling complexes. It has been

described that such complexes can be up to 2 MDa in size [389]. One approach which tries to visualize the physical dimension of proteins or complexes, defines an R_{min} value- the minimum radius of a sphere which could contain the given mass of a protein [390]. Afore mentioned cAMP effectors would be in the range of 2-3 nm, the hGLP1R would take in a space of about 2.4 nm and ACs or AKAPs are the biggest proteins with a radius up to 4 nm. Protein complexes as big as 2 MDa would exhibit a radius of 8 nm. Concluding, a receptor compartment of a spherical shape with a radius of up to 60nm would give plenty of space to comprise one or even more multi-protein signaling complexes.

Although we obtain some evidence now, which states that the receptor compartment is nanometer sized, further studies are needed to describe the precise size and shape.

4.7 hGLP1R cAMP-domain is specific for stimulation with its cognate ligand

During our study, we did not only detect and characterize the dynamics of the high-level cAMP compartment surrounding the hGLP1R, which arises as a consequence of cognate GPCR activation. We additionally sought to study crosstalk between different receptors, by stimulating endogenous β-ARs and detecting cAMP dynamics inside the hGLP1R compartment. Stimulation of receptors other than the hGLP1R first leads to a generalized cAMP signal at the plasma membrane before the hGLP1R-compartment is reached. This indicates that the receptor-compartment is protected from exterior signals to maintain a secluded area.

More in detail, the stimulation of cells with a sub-saturating concentration of 10 pM isoproterenol that lies beneath the reported affinity of β-ARs (β1 pKi 6.6-7, β2 pKi 6.4 [391]) does lead to cAMP generation, however the signal appears solely at the plasma membrane and not within the hGLP1R-compartment and the cytosol. If we believe each GPCR is surrounded by an exclusive cAMP nanodomain upon stimulation with its ligand, cAMP will first be restricted to this compartment and stay local. A stronger stimulus might lead cAMP to surpass into the adjacent compartment of the general plasma membrane. However, it seems there are mechanisms, which restrain it from appearing inside a foreign compartment, the hGLP1R-compartment in this case. By these means, the cell could protect the effector proteins belonging to each receptor, from being activated by cAMP from a different source.
The trend stays the same for higher concentrations of agonist as 100 pM or 1nM isoproterenol. cAMP is highest at the membrane, and less is detected in the cytosol and the hGLP1R-compartment. An equilibrium between all compartments occurs at agonist concentrations (10 nM) around the reported EC_{50} value for β-ARs [392] (14.5 nM for β_2-AR in a whole cell cAMP assay).
We can only speculate about the processes taking place surrounding the β-ARs upon their stimulation, but we believe a similar scenario occurs as for the hGLP1R. A receptor specific cAMP nanocompartment forms, with gradual decrease of cAMP levels, but staying distinct from the cytosol and the neighbouring receptor compartments.

Depending on their size and type, cells exhibit a very variable amount of GPCRs on their cell surface, among other proteins or channels. Single-molecule and super resolution microscopic techniques are continuously shedding light on receptor dynamics and spatial organization between receptors [393]. β-AR dynamics have extensively been studied using various high-resolution techniques. Super-resolved images of receptor positions were constructed via PALM microscopy, and the mechanistic role of the cytoskeleton in clustering and confinement of receptor-motion was studied with single-molecule tracking methods [394]. Super resolution techniques additionally allow to assess the dimerization or oligomerization state of receptors.

It has been reported that the plasma membrane is compartmentalized in small domains of 300-600 nm in diameter (0.04-0.24 μm^2), where immobile receptors assemble on a time scale of 3-30 s [395]. A more recent study using STORM super resolution imaging reports that CB1 cannabinoid receptor are distributed on the nanometer scale on the surface of membranes, while the diameter of a GPCR 7TM bundle approximately occupies 3 nm. With regards to the receptor cAMP-compartments which putatively surround different receptors, the lateral distribution of receptors would leave enough space for such compartments to arise without reciprocally affecting each other.
GPCRs reportedly dimerize or even oligomerize into higher order receptor clusters, which will certainly have implications on their movement on the plasma membrane, their trafficking and signaling [396-398]. How this in turn will affect the formation of cAMP nanodomains and the cross correlation between different receptor domains is yet to be studied, however it will without doubt contribute to the pharmacological diversity of GPCR signaling

4.8 The role of PDEs in maintaining the high-level cAMP compartment

In the course of this study, we investigated the role of PDEs in establishing the cAMP gradient of the receptor compartment. From our results, we can hypothesize about the location of PDEs within the nanocompartment. In detail, what we observe (Figure 3.13) is at the stimulation with low agonist concentrations of 10 fM or 1 pM GLP1 in the case of inhibited PDEs, cAMP levels and the speed by which they rise are evened out in direct vicinity of the receptor and at 30nm distance. This is contradicting to what we observe with intact PDEs, where we detect a clear gradient surrounding the receptor. This could be by the reason that in general more cAMP is present within the compartment, and that existent PDEs do not constitute a barrier anymore. These data are in line with former studies showing that PDEs contribute to the formation of cAMP gradients in cells [374, 376]. From these findings, we speculate that the PDEs may sit within a radius of 30 nm from the receptor. When they are intact, they can shape a gradient, with high levels of cAMP observed close to the receptor within the PDE collar and lower cAMP levels outside since some of it is degraded. In contrast, the inhibition of PDEs leads to equal amounts of cAMP within and outside of the PDE collar.

In a distance of 60nm we still detect a significantly lower amount of cAMP, with the gradient staying intact. Presumably, not PDEs but other mechanisms are responsible for its formation such as elements from the endoplasmatic reticulum or the cytoskeleton. There is evidence, which suggests that the endoplasmatic reticulum can come into close contact with the plasma membrane, thus defining a physical barrier [399, 400].

At a stimulation with higher agonist concentrations as 1 nM and 100 nM GLP1 upon PDE inhibition, we observe the same results as with intact ones. cAMP amplitudes are equal in all distances from the receptor. Yet even with inhibited PDEs the receptor compartment stays distinct from the cytosol at agonist concentrations up to 1 nM, while the cAMP levels equilibrate only at a very strong stimulus from 100 nM GLP1. This suggests that up to a certain amount, not all the cAMP produced at the receptor site reaches the cytosol. Either, there are still unaffected PDEs which degrade cAMP, or it binds to effector proteins within the compartment and is thus buffered away. Since the cytosol represents a rather big compartment, presumably a very high amount of cAMP is needed to saturate it. These data support the concept described in the previous section where signal transmission possibly occurs in a very specific manner at low agonist concentrations and very locally at the receptor, while higher agonist concentrations broaden up the compartment and lead to further reaching signals.

As we have used a general PDE inhibitor for this set of experiments, all subtypes of PDEs should be inhibited. Since it has been described that different isoforms of PDEs localize in different cellular areas and exhibit varying affinities for cAMP [180, 401], it would be of interest to further elucidate the role of specific PDE subtypes in the establishment of the cAMP compartments. For this, inhibitors for certain PDE isoforms are available, which could be used to investigate the effect of each PDE on the cAMP dynamics (Annex Table 7.6).

4.9 hGLP1R compartment specific PKA activation

In the course of the study, we demonstrated that the locally generated cAMP signal at the hGLP1 receptor compartment translates into PKA phosphorylation within the compartment, but also in the cytosol.

The stimulation with 1 pM GLP1 leads to the generation of cAMP within the receptor compartment (Figure 3.15), yet no cAMP signal is detected in the cytosol. On the other hand, we can detect PKA phosphorylation in both compartments albeit to a different extent. Since we detect a cAMP signal solely at the hGLP1R, it seems logical to assume that PKA phosphorylation within the receptor compartment stems from locally available PKA, which is activated by local cAMP. As it has been described that activated PKA catalytic subunits dissociate from the regulatory ones [197], we hypothesize that they might be able to travel and lead to cytosolic phosphorylation of substrates, which we detect with the cytoplasmatic sensor. Since signal amplification occurs due to active PKA C-subunits phosphorylating multiple targets, we detect a higher rate of PKA phosphorylation compared to the cAMP signal (Compare Figure 3.10 with Figure 3.15).

At a stimulation with 1 nM agonist cAMP is available both in the receptor compartment and in the cytosol, where it can lead to PKA activation. Thus, the PKA phosphorylation in the cytosol might emanate from two sources: active PKA C-subunits traveling out of the receptor compartment into the cytosol or local cytosolic PKA being activated by cAMP. The signal is amplified to a degree that PKA phosphorylation is saturated in both compartments.

It would be of great value if we could find a way to dissect where the intercompartment-phosphorylation signal comes from. Studying the kinetics of the PKA phosphorylation signal in the different compartments might already give a hint, although it might not be accurate enough to discriminate whether the locally generated cAMP travels to activate PKA or the activated catalytic PKA subunits diffuse.

4.10 PKA phosphorylation inside the hGLP1R-compartment but not in the cytosol is dependent on AKAPs

In the set of experiments where we disrupted PKA anchoring by AKAPs, we were able to show that PKA phosphorylation within the receptor specific domain is abolished if we pretreat the cells with the disruptor peptide (Figure 3.16), but not with the control peptide. These results are in line with the literature, which states that AKAPs target PKA to subcellular locations [246], and confirms our hypothesis that PKA phosphorylation inside the receptor compartment derives from locally available kinases. Cytosolic PKA phosphorylation in contrast, is independent of AKAP targeting, since the disruption of PKA-AKAP anchoring does not influence the phosphorylation rate. This would speak for the existence of a cytosolic set of PKA untargeted by AKAPs and thus its signaling is unaffected by the disruption.

It has already been shown that AKAP79 and AKAP250 scaffolds bind to the β_2-AR [402] and regulate its function. For the hGLP1R no direct interaction between certain AKAPs and the receptor were proved, but it was determined that the dissociation between AKAPs and RII subunit of PKA blocks GLP1-mediated insulin secretion [255]. AKAP150 seems to be responsible for PKA anchoring in pancreatic β cells, since selective ablation reduces the influx by L-type Ca^{2+}-channels, suppresses glucose-mediated insulin secretion and diminishes glucose tolerance in mice [403].
Taken together, these data provide indications for the formation of a macromolecular signaling complex surrounding the hGLP1R. We demonstrated that ACs must be in close vicinity to the hGLP1R since cAMP is generated in a very localized manner. PDEs are responsible for the sustenance of the cAMP gradient within the compartment, and PKA is locally activated if anchored by AKAPs. The presence of AKAPs would provide means for all afore mentioned players to be brought in close proximity with the purpose of creating a densely packed signalosome to assure specific signal transmission.

4.11 Conclusion

This work represents one of the first studies dealing with the compartmentalization of the second messenger cAMP on a nanometer scale. It describes the localization, spatial and temporal dynamics of cAMP compartments in association with the hGLP1R and provides further insight into the mechanisms behind this spatial arrangement. The examination of different cellular areas regarding their cAMP dynamics provides insight into the intracellular relay mechanism of membranous signals. This study further demonstrates that compartmentalization plays a role in the spatially restricted activation of effector proteins. Ultimately, we have designed and characterized special tools to study site-specific cAMP compartmentalization. These tools can be utilized to monitor the effect of different extracellular stimuli on the cAMP nanocompartments in real-time in living cells.

4.12 Outlook

The key finding of this work is the utilization of established FRET based cAMP reporters to study the compartmentalization of this second messenger at a GPCR. The key development in comparison with former studies is targeting of the sensor to distinct cellular locations and upgrading it to enable monitoring the size of afore mentioned compartments. Studying spatial and temporal dynamics of second messenger molecules in real-time, provides insight into the communicational processes of living cells whereby GPCR play a substantial role. Understanding the molecular details behind the relay of information in living cells will grant us the ability to modulate these signals or eventually restore malfunctioning signaling in diseased cells to the physiological healthy state.

Implementing this technique could be of benefit in the field of drug discovery and pharmacovigilance. Studying the effect of different ligands on the cAMP compartmentation upon stimulation of a certain GPCR could provide insight into the differential pharmacological effect of already marketed drugs or aid in identifying new drug candidates, based on known therapeutics. Furthermore, the comparison of the compartmentalization behavior of different classes of GPCRs is of interest. Since these receptors are very diverse in their expression pattern, function and ligand types, studying whether this diversity is also true for the molecular signaling mechanism will enable deeper characterization of the different receptor families.
Our tools further enable studying the kinetics for the generation, lifetime and degradation of cAMP nanocompartments. From this temporal information, we will be able to deduce differential ligand-GPCR interaction effects and further characterize GPCR therapeutics.

One major aim is to simultaneously study different cellular processes. Monitoring cAMP compartmentation together with downstream PKA activation or even insulin release in the case of the hGLP1R would provide a clear picture of the order of these events. These findings would deepen our understanding of signaling pathways in temporal and spatial regards. The insertion of spectrally separated fluorophore-pairs into specific sensors used to monitor different signaling events (cAMP compartmentalization, PKA activation, channel activation, insulin release etc.), together with a 4-channel FRET setup would fulfill the technical requirements to accomplish this task.
Ultimately, thoroughly studying GPCRs, the compartmentalization of their second messengers and their signaling partners in turn could open up the avenue to fathom the fundamental physiology and eventually influence the function.

5 Summary

GPCRs constitute a large and very diverse family of membrane proteins whose primary function is to relay extracellular stimuli into intracellular signals. Due to their ubiquitous expression throughout the human body, they are responsible for the control of essentially all cellular functions, thereby regulating an array of physiological processes such as sensory perception, cell communication and neurotransmission. GPCRs are linked to different diseases including heart failure, cancer, neurological disorders and metabolic diseases and have therefore been of long-standing interest as pharmacological targets. The vast expression of GPCRs at the plasma membrane makes them easily accessible, and their chemically diverse set of specific ligands additionally favours their druggability. Hence, already 30% of worldwide approved drugs target GPCRs.

GPCRs exert their function mainly by binding to G proteins, which in turn trigger the production of various second messengers, cAMP being the main signaling molecule for receptors coupling to the stimulatory G_S protein. cAMP relays hundreds of incoming signals in a highly specific manner through binding to various effector proteins in different cellular locations. By this means, it operates a plethora of cellular signaling cascades, ranging from the regulation of ion channel activity, smooth- and cardiac muscle contractility to gene expression, cell proliferation and apoptosis. Due to the pleiotropic effects regulated by cAMP, the pressing question arises of how G_SPCRs achieve signaling specificity while acting through one single second messenger.

Traditionally cAMP was assumed to be homogenously distributed throughout the cell due to unrestricted diffusion. However, this notion contradicts signaling specificity since cAMP could unselectively activate all its effector proteins in the entire cell. Therefore, the hypothesis of cAMP compartmentation arose, where a cell would comprise locally confined areas with high or low levels of cAMP. Yet, evidence was lacking for the existence and the molecular composition of putative domains. Therefore, we set out to localize high-concentration cAMP compartments in the cell, to describe their spatial dimension and elucidate their role in achieving cellular signaling specificity. In this work, we employed a FRET-based cAMP reporter, targeted to the hGLP1R as a prototype of G_S-coupling receptors to measure cAMP values at the origin of the signal. We report the existence of a confined cAMP domain surrounding the stimulated receptor, where cAMP levels are elevated upon stimulation with a GLP1 concentration as low as 10 fM (Figure 3.10), while staying local and segregated from the plasma membrane and the cytosol. We show the hGLP1R-compartment is protected from signals originating at other G_S-coupled receptor (Figure 3.11). To measure the spatial dimension of this compartment, we utilized nanorulers of 30nm and 60nm length as spacers between the receptor and the cAMP sensor

(Figure 3.12) describing the nanodomain to extend up to 60nm, while exhibiting a clear gradient. We further demonstrate that PDEs are key factors in forming the gradient of cAMP surrounding the hGLP1R by constraining its diffusion to the cytosol (Figure 3.13). Moreover, we show that receptor specific cAMP signals actuate PKA phosphorylation within the receptor compartment (Figure 3.15) and determine that AKAPs are fundamental for nanodomain PKA activity, whereas cytosolic PKA phosphorylation is independent of AKAP targeting of PKA (Figure 3.16).

Taken together, our results report the existence of a high-concentration cAMP nanodomain surrounding a G_S-coupled receptor. Simultaneous studies of our group show cAMP is largely immobile and diffusion limited in the cell, which provides the proof for restricted diffusion as a molecular requirement for the formation of signaling compartments. We anticipate our results to be a starting point for the elucidation of receptors as a source for signaling compartments, yet further studies are necessary to determine the molecular composition and involved proteins within this signaling domain. Understanding signaling cascades on a molecular level might at some point enable us to manipulate cellular responses in order to restore malfunctioning signaling in diseased cells. Since hGLP1R is crucial for maintaining balanced glucose levels, perceiving the molecular details of its compartmentalized signaling would enable fine-tuning of its signals, using it as a specific target in antidiabetic treatment.

6 Zusammenfassung

G Protein gekoppelte Rezeptoren (GPCRs) stellen eine große und sehr vielfältige Familie an Membranproteinen dar, deren primäre Funktion die Signalübertragung von extrazellulären Stimuli in intrazelluläre Signale ist. Dank ihrer breiten Expression im gesamten menschlichen Körper regulieren sie unterschiedliche zelluläre Prozesse und damit deren physiologische Funktion, unter anderem die Sinnesempfindung, zelluläre Kommunikation und Neurotransmission. GPCRs stehen im Zusammenhang mit unterschiedlichen Erkrankungen wie Herzinsuffizienz, Krebs, neurologischen Funktionsstörungen und diverser metabolischer Krankheiten, weswegen sie als Ziele („Targets“) zur Behandlung verschiedener Erkrankungen erforscht und genutzt werden. Aufgrund ihrer Expression auf der Zelloberfläche sind sie leicht zugänglich, und die Diversität ihrer Liganden begünstigt zusätzlich ihre Nutzung als pharmakologische Targets. Heutzutage vermitteln bereits 30% aller weltweit zugelassenen Arzneistoffe ihre Wirkung an GPCRs.

GPCRs üben ihre Funktion aus, indem sie hauptsächlich an G Proteine binden, welche wiederum die Produktion sogenannter second messenger in Gang setzen. cAMP ist das Hauptsignalmolekül der Rezeptoren, welche an das stimulatorische G_S Protein koppeln. cAMP überträgt hunderte ankommende Signale in einer hochspezifischen Weise, indem es an unterschiedliche Effektorproteine bindet, welche sich in bestimmten zellulären Regionen befinden. Dadurch koordiniert dieses Signalmolekül eine Vielzahl zellulärer Prozesse, angefangen bei der Regulierung von Ionenkanalaktivität über die Kontraktilität glatter- und quergestreifter Muskulatur bis hin zur Genexpression, Zellproliferation und Apoptose. Durch die pleiotropen Effekte, welche durch cAMP reguliert werden, stellt sich die Frage, wie G_S-gekoppelte Rezeptoren Signalspezifität erreichen, obwohl sie ihre Funktion durch dieses eine Signalmolekül ausführen.

Ursprünglich ging man von einer uneingeschränkten Diffusion und dadurch homogenen Verteilung von cAMP in der Zelle aus. Diese Vorstellung ist jedoch nicht mit der Signalisierungsspezifität von GPCRs vereinbar, da unter diesen Umständen cAMP unselektiv all seine Effektorproteine in der gesamten Zelle aktivieren könnte. Daher entstand die Hypothese der cAMP-Kompartimentierung, wobei die Zelle lokal begrenzte Bereiche mit hohen oder niedrigen cAMP Konzentrationen umfassen würde.

Jedoch gab es bisher keinerlei Beweise für die Existenz und die molekulare Zusammensetzung mutmaßlicher Domänen. Folglich setzten wir uns als Ziel, hochkonzentrierte cAMP-Kompartimente in der Zelle zu lokalisieren, ihre räumliche Dimension aufzuklären und ihre Rolle zur Realisierung zellulärer Signalisierungsspezifität zu ermitteln. Im Rahmen der vorliegenden Studie setzten wir einen Förster resonance energy transfer (FRET)-basierten cAMP Sensor ein, fusionierten ihn mit dem humanen glucagone-like peptide 1 Rezeptor (hGLP1R) als Prototyp eines G_S-koppelnden Rezeptors, um cAMP am Ursprung des Signals zu messen. Mittels dieser Sensoren weisen wir eine Rezeptor-umgebende begrenzte cAMP Domäne nach, welche eine erhöhte cAMP Konzenztration aufweist (Figure 3.10). Bei Stimulation des Rezeptors mit GLP1 Konzenztrationen beginnend bei 10 fM entsteht eine Rezeptordomäne mit lokal erhöhten cAMP Konzentrationen, welche getrennt von Plasmamembran und Cytosol ist. Wir zeigen, dass das hGLP1R-Kompartiment geschützt ist vor cAMP Signalen, welche an weiteren, unabhängigen G_S-gekoppelten Rezeptoren ihren Ursprung haben (Figure 3.11). Um die räumliche Dimension dieser Domäne zu untersuchen, verwendeten wir Nanolinker der Länge 30- und 60 nm als Abstandhalter zwischen Rezeptor und Sensor (Figure 3.12) und zeigen dabei, dass sich die Domäne über eine Länge von 60 Nanometern erstreckt, wobei ein abnehmender cAMP-Gradient erkennbar ist. Weiterhin beweisen wir, dass Phosphodiesterasen (PDEs) Schlüsselfaktoren für die Bildung des cAMP-Gradienten um den Rezeptor herum sind, indem sie die Diffusion ins Cytosol beschränken (Figure 3.13). Darüber hinaus zeigen wir (Figure 3.15), dass Rezeptor-spezifische cAMP Signale PKA-Phosphorylierung in der Rezeptordomäne auslösen und, dass AKAPs elementar für nanodomänen PKA-Aktivität sind, wohingegen die cytosolische PKA-Phosphorylierung unabhängig von AKAP-Targeting der PKA ist (Figure 3.16).

Zusammenfassend beweisen unsere Ergebnisse die Existenz einer Rezeptor-umgebenden Nanodomäne mit erhöhten cAMP Spiegeln eines G_S-gekoppelten Rezeptors. Zeitgleiche Studien in unserer Gruppe zeigen, dass cAMP in der Zelle weitgehend gebunden vorliegt und diffusionslimitiert ist. Dies stellt den Nachweis für eine eingeschränkte Diffusion als molekulare Voraussetzung für die Bildung von Signalkompartimenten dar. Wir gehen davon aus, dass unsere Ergebnisse ein Ausgangspunkt für die Aufklärung von Rezeptoren als Quelle für Signalkompartimente darstellen, jedoch bedarf es weiterer Studien, um die präzise molekulare Zusammensetzung und die beteiligten Proteine dieser Signaldomäne zu untersuchen. Das Grundverständnis der Signalisierungskaskaden auf molekularer Ebene könnte es uns ermöglichen, die zellulären Reaktionen zu manipulieren, um eine Fehlfunktion der Signalisierung in erkrankten Zellen wiederherzustellen. Da der hGLP1R entscheidend für Aufrechterhaltung ausgeglichener Blutglucosespiegel ist, würde die Erfassung der molekularen Details der kompartimentalisierten Signalübertragung die Feinabstimmung der Rezeptorsignale ermöglichen, um ihn als spezifisches Target zur Behandlung von Diabetes Mellitus einzusetzen.

7 Annex

Table 7.1 Resolved cystal structures of GPCRs
(As of 6th of June 2019) Taken from http://gpcrdb.org (Pandy-Szekeres *et* al. [6])

GPCR family	Receptor	Number of unique structures	PDB code
A	Serotonin 5-HT2A	2	6A93, 6A94
	5HT1B	4	6G79, 5V54, 4IAQ, 4IAR
	5HT2B	8	6DRZ, 6DSO, 6DRY, 6DRX, 6TUD, 6TVN, 4NC3, 4IB4
	5HT2C	2	6BQH, 6BQG
	Muscarinic Acetylcholin M1 receptor	1	5ZKC
	Muscarinic Acetylcholin M2 receptor	7	5YC8, 5ZKB, 5ZK8, 5ZK3, 4MQT, 4MQS, 3UON
	Muscarinic Acetylcholin M3 receptor	4	4U14, 4U15, 4U16, 4DAJ
	Muscarinic Acetylcholin M4 receptor	1	5DSG
	Adenosine A1	3	5N2S, 5UEN, 6GDG
	Adenosine A_{2A}	44	5WF5, 5WF6, 5OLV, 5OM1, 5OLH, 5OLZ, 5OM4, 5OLG, 5OLO, 6AQF, 5VRA, 5NM2, 5NM4, 5NLX, 5N2R, 5MZJ, 5MZP, 5JTB, 5UVI, 5UIG, 5K2B, 5K2A, 5K2C, 5K2D, 5G53, 5IU4, 5IU7, 5IUB, 5IUA, 5IU8, 4UG2, 4UHR, 4EIY, 3UZC, 3UZA, 3VGA, 3VG9, 3RFM, 3REY, 3PWH, 2YDV, 2YDO, 3QAK, 3EML
	Adrenergic β_1 receptor	24	6H7J, 6H7O, 6H7N, 6H7L, 6H7M, 5F8U, 5A8E, 4BVN, 3ZPR, 3ZPQ, 4GPO, 4AMI, 4AMJ, 2YCY, 2YCX, 2YCZ, 2YCW, 2Y01, 2Y02, 2Y00, 2Y03, 2Y04, 2VT4, 6MXT
	Adrenergic β_2 receptor	21	5X7D, 5D6L, 5JQH, 5D5A, 5D5B, 4QKX, 4LDL, 4LDE, 4LDO, 4GBR, 3SN6, 3P0G, 3PDS, 3NY8, 3NY9, 3NYA, 3KJ6, 3D4S, 2R4S, 2R4R, 2RH1
	Angiotensin AT_1	3	6DOI, 4ZUD, 4YAY
	Angiotensin AT_2	4	5XJM, 5UNG, 5UNH, 5UNF
	Apelin	1	5VBL
	Cannabinoin CB_1	5	6N4B, 5XR8, 5XRA, 5U09, 5TGZ
	Cannabinoin CB_2	1	5ZTY
	Chemokine CCR2	3	6GPX, 6GPS, 5T1A
	Chemokine CCR5	5	6MET, 6MEO, 6AKY, 6AKX, 5UIW

	Chemokine CCR9	1	4MBS
	Chemokine CXCR4	6	4RWS, 3ODU, 3OE9, 3OE8, 3OE6, 3OE0
	Complement peptide $C5_{a1}$	3	6C1R, 6C1Q, 5O9H
	Dopamine D_2	1	6CM4
	Dopamine D_3	1	3PBL
	Dopamine D_4	2	5WIV, 5WIU
	Endothelin ET_B	6	6IGK, 6IGL, 5XPR, 5X93, 5GLH, 5GLI
	Free fatty acid FFA1	4	5KW2, 5TZY, 5TZR, 4PHU
	Histamin H_1	1	5RZE
	Leukotriene BLT_1	1	5X33
	Lysophospholipid LPA_1	3	4Z34, 4Z36, 4Z35
	Lysophospholipid LPA_6	1	5XSZ
	Lysophospholipid $S1P_1$	2	3V2Y, 3V2W
	Neuropeptide Y_1	2	5ZBQ, 5ZBH
	Neurotensin NTS_1	8	5T04, 4XEE, 4XES, 4BWB, 4BUO, 3ZEV, 4BV0, 4GRV
	δ-Opioid receptor	4	4RWA, 4RWD, 4N6H, 4EJ4
	κ-Opioid receptor	2	6B73, 4DJH
	μ-Opioid receptor	4	6DDF, 6DDE, 5C1M, 4DKL
	NOP receptor	3	5DHH, 5DHG, 4EA3
	Rhodopsin	49	6FUF, 6CMO, 6FKB, 6FK9, 6FKD, 6FK7, 6FKC, 6FK8, 6FKA, 6FK6, 5WKT, 5W0P, 5TE5, 5TE3, 5EN0, 5DYS, 5DGY, 4X1H, 4ZWJ, 4WW, 4PXF, 4J4Q, 4BEY, 4BEZ, 4A4M, 3AYM, 3AYN, 2X72, 3PXO, 3PQR, 3OAX, 3DQB, 3C9M, 3C9L, 3CAP, 2Z73, 2ZIY, 2PED, 2J4Y, 2I35, 2I37, 2I36, 2G87, 2HPY, 1U19, 1GZM, 1L9H, 1HZX, 1F88
	Orexin OX_1	2	5WS3, 5WQC
	Orexin OX_2	3	4ZJC, 4ZJ8, 4S0V
	$P2Y_1$	2	4XNW, 4XNV
	$P2Y_{12}$	3	4PXZ, 4PY0, 4NTJ
	Platelet-activating factor PAF	2	5ZKQ, 5ZKP
	Prostanoid TP	2	6IIV, 6IIU
	Prostanoid EP_3	2	6M9T, 6AK3
	Prostanoid EP_4	2	5YWY, 5YHL
	Prostanoid DP_2	2	6D26, 6D27
	Proteinase activated PAR1	1	3VW7
	Proteinase activated PAR2	3	5NDZ, 5NDD, 5NJ6
	Tachykinin NK_1	6	6J21, 6J20, 6HLO, 6HLP, 6HLL, 6E59
	US28	4	5WB2, 5WB1, 4XT3, 4XT1

B	Calcitonin CT	2	6NIY, 5UZ7
	Calcitonin like	1	6E3Y
	Corticotropin-releasing factor CRF_1	2	4Z9G, 4K5Y
	Glucagon GLP1	5	5VAI, 6B3J, 5NX2, 5VEW, 5VEX
	Glucagon receptor	5	5YQZ, 5XF1, 5XEZ, 5EE7, 4L6R
	Parathyroid homrone PTH1	1	6FJ3
C	Glutamate $mGlu_1$	1	4OR2
	Glutamate $mGlu_5$	7	6N52, 6N51, 6FFI, 6FFH, 5CGD, 5CGC, 4OO9
F	Frizzled FZD_4	1	6BD4
	Frizzled SMO	11	6D32, 6D35, 5V57, 5V56, 5L7D, 5L7I, 4QIM, 4QIN, 4O9R, 4N4W, 4JKV

Table 7.2 Currently available genetically encoded cAMP reporters
(~) indicates that dynamic range was estimated from the figures of cited papers.
*co-transfection of two or ** three separate constructs required;
(extracted from [372] with permission from Copy Clearance Center; license number: 4578630454182)

cAMP sensor	Design	Dynamic Range	cAMP Affinity
FlCRhR	cPKA-fluorescein + rPKA-rhodamine	50%	88 nM
RII-EBFP/C-S65T	rII-PKA-EBFP + cPKA-S65T*	NA	NA
R-CFP/C-YFP	rPKA-CFP + cPKA-YFP (CFP-R2C2-YFP)*	~17%	0.3 µM
RR230K-CFP/C-YFP	rPKA(R230K)-CFP + cPKA-YFP (CFP-R2C2-YFP)*	~15%	31.3 µM
Epac1-camps	YFP-^{E157}Epac1^{E316}CFP	~24%	2.4 µM
Epac2-camps	YFP-^{E285}Epac2^{E443}-CFP	~17%	0.9 µM
PKA-camps	YFP-^{M264}rIIβB-PKA^{A403}-CFP	~15%	1.9 µM
CFP-Epac-YFP	CFP-^{M1}Epac1^{P881}-YFP	~30%	50 µM
CFP-Epac(δDEP-CD)-YFP	CFP-^{P149}Epac1(T781A/F782A)^{P881}-YFP	~45%	14 µM
ICUE1	ECFP-^{V2}Epac1^{P881}-citrine	20%	NA
HCN-camps	YFP-^{A467}HCN2^{K638}-CFP	~20%	6 µM
ΔRIIβ-CFP/Cα-YFP	81rIIβ-PKA416-CFP + CPKAα-YFP*	82%	NA
G^{nd}Δ-Epac-mRFP (H81)	GFP(A206K)-^{P149}Epac1(T781A/F782A)^{P881}-mRFP	29%	NA
C^{nd}-Epac-V^{d} (H84)	CFP(A206K)-^{P149}Epac1(T781A/F782A)^{P881}-Venus	31%	NA
C^{nd}-Epac-cp173V^{d} (H90)	CFP(A206K)-^{P149}Epac1(T781A/F782A)^{P881}-cp173Venus	36%	NA
G^{nd}-Epac-mCherry (H94)	GFP(A206K)-^{P149}Epac1(T781A/F782A)^{P881}-mCherry	23%	NA
C^{d}Δ-Epac-cp173V/V^{d} (H96)	^{1}CFP^{225}-^{P149}Epac1(T781A/F782A)^{P881}-cp173Venus-Venus	36%	NA
ICUE2	ECFP-^{E148}Epac1^{P881}-citrine	60%	12.5 µM

ICUE3	ECFP-^{E148}Epac1^{P881}-cpVenus(L194)	102%	NA
Epac2-camps300	YFP-^{E285}Epac2(K405E) ^{E443}-CFP	80%	0.3 µM
Epac2-camps300-Cit	YFP-^{E285}Epac2(K405E) ^{E443}-citrine	92%	NA
TEpac^{VV} (H74)	mTurquoiseΔ-^{P149}Epac1(T781A/F782A)^{P881}-^{cp173}Venus-Venus	82%/84%	NA
Nano-lantern (cAMP0.4)	^{1}VenusΔC10^{228}-^{4}N-RLuc8ΔN3^{228}-^{M245}PKARIαB^{V381}-Linker-^{229}C-RLuc8(S257G)^{311}	NA	0.4 µM
Nano-lantern (cAMP3.3)	^{1}VenusΔC10^{228}-^{4}N-RLuc8ΔN3^{228}-^{G170}Epac1(Q270E)^{A327}-Linker-^{229}C-RLuc8(S257G)^{311}	NA	3.3 µM
Nano-lantern (cAMP1.6)	^{1}VenusΔC10^{228}-^{4}N-RLuc8ΔN3^{228}-^{G170}Epac1(Q270E)^{A327}-^{229}C-RLuc8(S257G)^{311}	130%	1.6 µM
cit-mCNBD-cer	citrine-^{202}mCRIS^{353}-cerulean	NA	NA
Flamindo	^{1}N-citrine(Q69M)^{144}-^{157}mEpac1^{316}-^{146}C-citrine^{238}	100%	2.1 µM
Flamindo2	^{1}N-citrine(Q69M)^{144}-ALKK-^{157}mEpac1^{316}-^{146}C-citrine^{238}	300%	3.2 µM
Epac-S^{H187}	mTurquoise2Δ-^{P149}Epac1(Q270E/T781A/F782A)^{P881}-td^{cp173}Venus-Venus	163.90%	NA
Epac-S^{H134}	mTurquoise2Δ- ^{P149}Epac1(Q270E/T781A/F782A)^{P881}-^{cp173}Venus-Venus	86%	4 µM
Epac-S^{H126}	mTurquoise2Δ-^{P149}Epac1(T781A/F782A)^{P881}-^{cp173}Venus-Venus	80.40%	9.5 µM
pPHT-PKA	RA-cPKA + B-rPKA + Free GA**	NA	NA
RIα #7	cp173Venus-^{245}rIα-PKA^{381}-ECFP	38%	37.2 nM
mlCNBD-FRET	Citrine-^{F223}mlotiK1^{R349}-cerulean-His$_{10}$	47%	66 nM

7.1 Kinetics of cAMP amplitudes

Kinetic FRET studies are ideally conducted in a single-cell assay where a syringe, which delivers the ligand, is positioned in close proximity (<100 µm) of the cells of interest. This setup enables rapid exchange of the superfusion solutions (<10 ms) to monitor exclusively the dynamics of the process of interest.

The setup in which we conducted the experiments had some technical limitations. The ligand was added by bath application, not superfusion, where it needs to diffuse within the chamber to reach the cells (Figure 7.1). The concentration of the cell-covering solution must equilibrate before cAMP generation starts and kinetics are monitored. This lag time should in theory be constant, however it is part of the τ values we report. Therefore, the values we report show a large scatter. We can use the values to compare the different compartments or ligand concentration effect, but they should not be regarded as absolute values, which state cAMP generation constants.

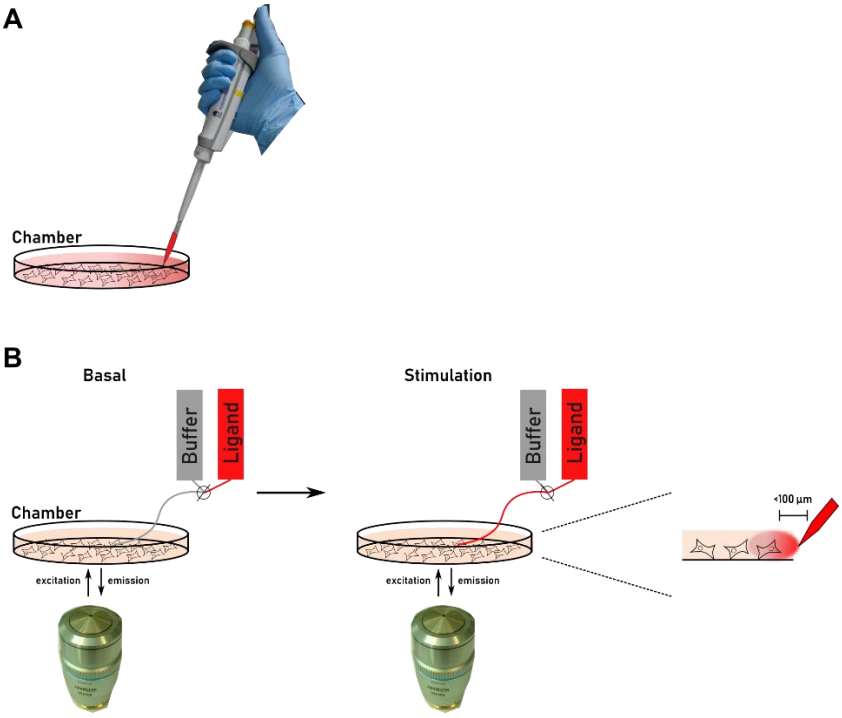

Figure 7.1 Common techniques used for ligand application
(A) Bath application of the ligand to the chamber during imaging. The time limiting step is the diffusion and homogenization of the added solution with the cell covering buffer within the whole chamber. (B) A highly specialized perfusion system allows precise and continuous superfusion of the cells with different solutions while rapid solution exchange is possible.

7.1.1 cAMP kinetics in different cellular compartments

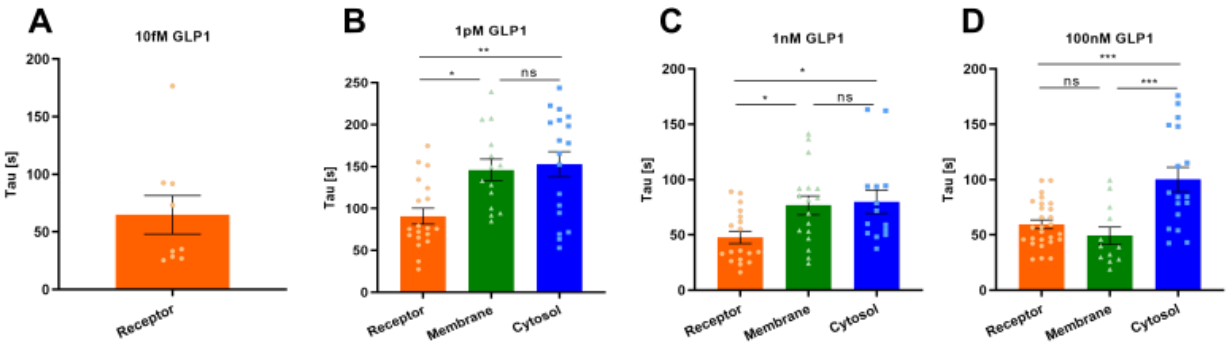

Figure 7.2 Kinetics of cAMP-rise in different cellular compartments
(A), (B), (C), (D) Time constant (T) of FRET changes induced by stimulation with 10 fM **(A),** 1pM **(B),** 1nM **(C)** or 100nM **(D)** GLP1 for the three compartments receptor, membrane and cytosol. Mean ± SEM ***p<0.001, **p<0.01, *p<0.05, ns no significant difference according to a 1-way ANOVA followed by Tukey's post hoc test.

Table 7.3 Summary of kinetic values for cAMP generation in different cellular compartments

		GLP1 concentration			
		10fM	1pM	1nM	100nM
T [s]	Receptor	64.9 ± 16.8 n=9	90.8 ± 9.4 n=19	47.9 ± 5.6 n=18	59.6 ± 4 n=27
	Membrane	Not converged	146 ± 12.8 n=14	76.7 ± 8.5 n=17	49.4 ± 7.8 n=12
	Cytosol	Not converged	152.9 ± 14.9 n=18	80 ± 10.6 n=14	100.2 ± 10.8 n=17

7.1.2 Kinetics of cAMP amplitudes in different distances from the receptor

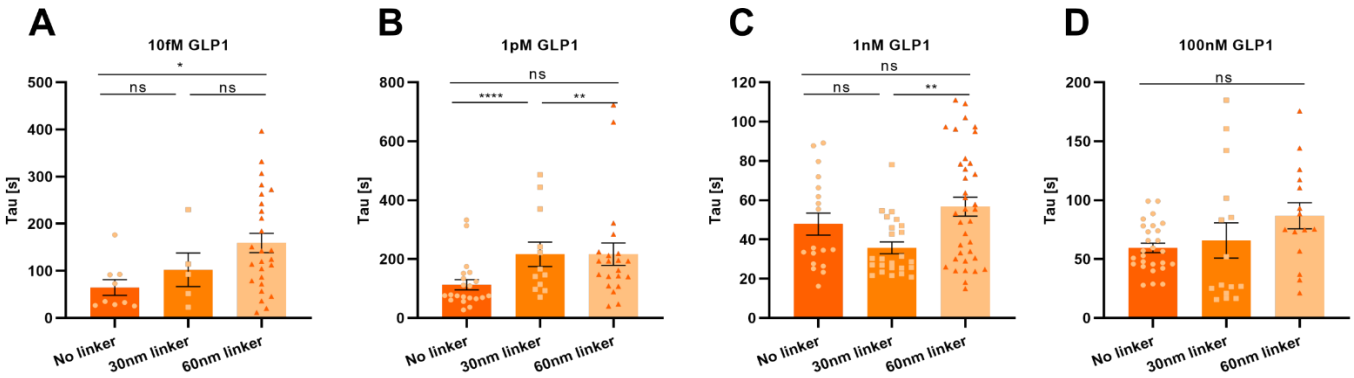

Figure 7.3 Kinetics of cAMP signal within the hGLP1R compartment
(A), (B), (C), (D) Time constant (T) of FRET changes induced by stimulation with 10 fM **(A)**, 1 pM **(B)**, 1 nM **(C)** or 100 nM **(D)** GLP1 measured in different distances from the hGLP1R. Mean ± SEM ****p<0.0001, **p<0.01, *p<0.05, ns no significant difference according to a 1-way ANOVA followed by Tukey's post hoc test.
The values for the construct with no linker are the same as depicted in Figure 7.2 repeated for better comparability.

Table 7.4 Summary of kinetic values for cAMP generation in different distances from the receptor

		GLP1 concentration			
		10fM	1pM	1nM	100nM
T [s]	No linker	64.9 ± 16.8 n=9	90.8 ± 9.4 n=19	47.9 ± 5.6 n=18	59.6 ± 4 n=27
	30nm linker	102.5 ± 35.6 n=5	216.3 ± 41.1 n=12	35.8 ± 3 n=24	65.8 ± 14.9 n=15
	60nm linker	159.4 ± 20.4 n=26	166.7 ± 16.6 n=19	56.8 ± 4.8 n=36	86.8 ± 11 n=15

7.1.3 Effect of PDE inhibition on compartment kinetics

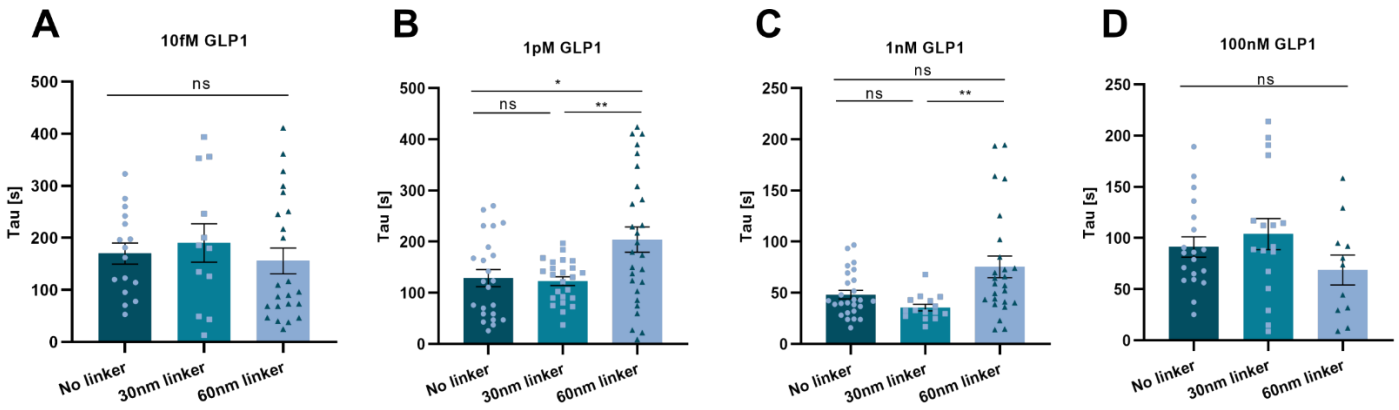

Figure 7.4 Kinetics of cAMP signal within the hGLP1R compartment upon PDE inhibition
(A), (B), (C), (D) Time constant (T) of FRET changes induced by stimulation with 10 fM **(A),** 1 pM **(B),** 1 nM **(C)** or 100 nM **(D)** GLP1 measured in different distances from the hGLP1R. Mean ± SEM **p<0.01, *p<0.05, ns no significant difference according to a 1-way ANOVA followed by Tukey's post hoc test (A, B, D), **p=0.005, ns no significant difference according to a Kruskal-Wallis-test (C).

Table 7.5 Summary of kinetic values for cAMP generation in different distances from the receptor upon PDE inhibition

		GLP1 concentration			
		10fM	1pM	1nM	100nM
T [s]	No linker	170 ± 20.2 n=16	128.9 ± 16.5 n=23	48.3 ± 4.3 n=26	91.3 ± 9.9 n=19
	30nm linker	190.3 ± 36.8 n=12	123 ± 8.5 n=24	35.6 ± 3.2 n=15	103.9 ± 15.2 n=17
	60nm linker	155.8 ± 24.8 n=23	204.1 ± 24.8 n=27	75.5 ± 10.5 n=25	68.8 ± 14.6s n=11

Table 7.6 PDE enzymes and their characteristic regulatory features, substrate selectivity and reported selective inhibitors

Compounds marked with an asterisk function with an IC_{50} < 10nM. Adapted from [180, 404, 405]

PDE	Subtypes	Selectivity	Inhibitors	Regulating features	Intracellular location
PDE1	1A, 1B, 1C	cAMP/cGMP	Vinpocetine, ITI214* (Intra-Cellular Therapies Inc.), PF4822163* (Pfizer Inc.)	Ca2+/CaM stimulated	Cytosolic
PDE2	2A	cAMP/cGMP	Bay-60-7550* (Bayer Pharmaceuticals), EHNA, PF05180999* (Pfizer Inc.)	cGMP stimulated	Membrane bound or cytosolic
PDE3	3A, 3B	cAMP/cGMP	Cilostamide*, Milrinone, Enoximone, Cilostazol OPC-33540*	cGMP inhibited	Membrane bound or cytosolic
PDE4	4A, 4B, 4C, 4D	cAMP	Rolipram, Cilomilast, Roflumilast* GSK256066* (Glaxo Smith Kline) CHF6001* (Chiesi Farmaceutici S.p.A), MK0952* (Merck Sharp and Dohme)	N-terminal region facilitates intracellular targeting, cGMP insensitive	Membrane bound or cytosolic
PDE5	5A	cGMP	Sildenafil*, Tadalafil*, Vardenafil*, Avanafil, Dipyridamol, Zaprinast	cGMP stimulated, PKA-PKG phosphorylated	Cytosolic
PDE6	6A, 6B, 6C	cGMP	Zaprinast, Dipyridamol, DMPPO, Sildenafil, Vardenafil	cGMP/ transducin stimulated	Cytosolic
PDE7	7A, 7B	cAMP	BRL50481 (Glaxo Smith Kline), IC242*, BMS586353*, Thiadiazoles (Pfizer)	Rolipram-insensitive	Cytosolic
PDE8	8A, 8B	cAMP	PF04957325* (Pfizer Inc.)	cAMP (IBMX-& Rolipram insensitive)	Membrane bound or cytosolic
PDE9	9A	cGMP	BAY-73-6691* (Bayer Pharmaceuticals), PF04447943*, PF4181366*, PF04449613* (Pfizer Inc.), WYQ-C28L* (University of North Carolina)	(IBMX insensitive)	Cytosolic or nuclear
PDE10	10A	cAMP, cGMP	Papaverine, TP-10, MP-10	cGMP sensitive	Cytosolic or particulate
PDE11	11A	cAMP, cGMP	None selective	cGMP sensitive	Cytosolic

8 Abbreviations

9 References

1. Hauser, A.S., et al., *Trends in GPCR drug discovery: new agents, targets and indications.* Nat Rev Drug Discov, 2017. **16**(12): p. 829-842.
2. Southan, C., et al., *The IUPHAR/BPS Guide to PHARMACOLOGY in 2016: towards curated quantitative interactions between 1300 protein targets and 6000 ligands.* Nucleic Acids Res, 2016. **44**(D1): p. D1054-68.
3. Liapakis, G., A. Cordomi, and L. Pardo, *The G-protein coupled receptor family: actors with many faces.* Curr Pharm Des, 2012. **18**(2): p. 175-85.
4. Manglik, A. and A.C. Kruse, *Structural Basis for G Protein-Coupled Receptor Activation.* Biochemistry, 2017. **56**(42): p. 5628-5634.
5. Zhou, X.E., K. Melcher, and H.E. Xu, *Structure and activation of rhodopsin.* Acta Pharmacol Sin, 2012. **33**(3): p. 291-9.
6. Pandy-Szekeres, G., et al., *GPCRdb in 2018: adding GPCR structure models and ligands.* Nucleic Acids Res, 2018. **46**(D1): p. D440-d446.
7. Carpenter, B., et al., *Structure of the adenosine A(2A) receptor bound to an engineered G protein.* Nature, 2016. **536**(7614): p. 104-7.
8. Rasmussen, S.G., et al., *Crystal structure of the beta2 adrenergic receptor-Gs protein complex.* Nature, 2011. **477**(7366): p. 549-55.
9. Huang, W., et al., *Structural insights into micro-opioid receptor activation.* Nature, 2015. **524**(7565): p. 315-21.
10. Carpenter, B. and C.G. Tate, *Active state structures of G protein-coupled receptors highlight the similarities and differences in the G protein and arrestin coupling interfaces.* Curr Opin Struct Biol, 2017. **45**: p. 124-132.
11. Ballesteros, J. and K. Palczewski, *G protein-coupled receptor drug discovery: implications from the crystal structure of rhodopsin.* Curr Opin Drug Discov Devel, 2001. **4**(5): p. 561-74.
12. Latorraca, N.R., A.J. Venkatakrishnan, and R.O. Dror, *GPCR Dynamics: Structures in Motion.* Chem Rev, 2017. **117**(1): p. 139-155.
13. Deupi, X. and B.K. Kobilka, *Energy landscapes as a tool to integrate GPCR structure, dynamics, and function.* Physiology (Bethesda), 2010. **25**(5): p. 293-303.
14. Manglik, A. and B. Kobilka, *The role of protein dynamics in GPCR function: insights from the beta2AR and rhodopsin.* Curr Opin Cell Biol, 2014. **27**: p. 136-43.
15. Knierim, B., et al., *Sequence of late molecular events in the activation of rhodopsin.* Proc Natl Acad Sci U S A, 2007. **104**(51): p. 20290-5.
16. Lohse, M.J., I. Maiellaro, and D. Calebiro, *Kinetics and mechanism of G protein-coupled receptor activation.* Curr Opin Cell Biol, 2014. **27**: p. 87-93.
17. Castro, M., et al., *Turn-on switch in parathyroid hormone receptor by a two-step parathyroid hormone binding mechanism.* Proc Natl Acad Sci U S A, 2005. **102**(44): p. 16084-9.
18. Vilardaga, J.P., et al., *Measurement of the millisecond activation switch of G protein-coupled receptors in living cells.* Nat Biotechnol, 2003. **21**(7): p. 807-12.
19. Attwood, T.K. and J.B. Findlay, *Fingerprinting G-protein-coupled receptors.* Protein Eng, 1994. **7**(2): p. 195-203.
20. Hu, G.M., T.L. Mai, and C.M. Chen, *Visualizing the GPCR Network: Classification and Evolution.* Sci Rep, 2017. **7**(1): p. 15495.
21. Fredriksson, R., et al., *The G-protein-coupled receptors in the human genome form five main families. Phylogenetic analysis, paralogon groups, and fingerprints.* Mol Pharmacol, 2003. **63**(6): p. 1256-72.

22. Pierce, K.L., R.T. Premont, and R.J. Lefkowitz, *Seven-transmembrane receptors.* Nat Rev Mol Cell Biol, 2002. **3**(9): p. 639-50.
23. Palczewski, K., et al., *Crystal structure of rhodopsin: A G protein-coupled receptor.* Science, 2000. **289**(5480): p. 739-45.
24. Rasmussen, S.G., et al., *Crystal structure of the human beta2 adrenergic G-protein-coupled receptor.* Nature, 2007. **450**(7168): p. 383-7.
25. Jaakola, V.P., et al., *The 2.6 angstrom crystal structure of a human A2A adenosine receptor bound to an antagonist.* Science, 2008. **322**(5905): p. 1211-7.
26. Harmar, A.J., *Family-B G-protein-coupled receptors.* Genome Biol, 2001. **2**(12): p. Reviews3013.
27. Kratochwil, N.A., et al., *G protein-coupled receptor transmembrane binding pockets and their applications in GPCR research and drug discovery: a survey.* Curr Top Med Chem, 2011. **11**(15): p. 1902-24.
28. Hollenstein, K., et al., *Insights into the structure of class B GPCRs.* Trends Pharmacol Sci, 2014. **35**(1): p. 12-22.
29. Rondard, P., et al., *The complexity of their activation mechanism opens new possibilities for the modulation of mGlu and GABAB class C G protein-coupled receptors.* Neuropharmacology, 2011. **60**(1): p. 82-92.
30. Dijksterhuis, J.P., J. Petersen, and G. Schulte, *WNT/Frizzled signalling: receptor-ligand selectivity with focus on FZD-G protein signalling and its physiological relevance: IUPHAR Review 3.* Br J Pharmacol, 2014. **171**(5): p. 1195-209.
31. Katanaev, V.L., *The Wnt/Frizzled GPCR signaling pathway.* Biochemistry (Mosc), 2010. **75**(12): p. 1428-34.
32. Monk, K.R., et al., *Adhesion G Protein-Coupled Receptors: From In Vitro Pharmacology to In Vivo Mechanisms.* Mol Pharmacol, 2015. **88**(3): p. 617-23.
33. Hamann, J., et al., *International Union of Basic and Clinical Pharmacology. XCIV. Adhesion G protein-coupled receptors.* Pharmacol Rev, 2015. **67**(2): p. 338-67.
34. Gilman, A.G., *G proteins: transducers of receptor-generated signals.* Annu Rev Biochem, 1987. **56**: p. 615-49.
35. Simon, M.I., M.P. Strathmann, and N. Gautam, *Diversity of G proteins in signal transduction.* Science, 1991. **252**(5007): p. 802-8.
36. Downes, G.B. and N. Gautam, *The G protein subunit gene families.* Genomics, 1999. **62**(3): p. 544-52.
37. Wettschureck, N. and S. Offermanns, *Mammalian G proteins and their cell type specific functions.* Physiol Rev, 2005. **85**(4): p. 1159-204.
38. Rhee, S.G. and Y.S. Bae, *Regulation of phosphoinositide-specific phospholipase C isozymes.* J Biol Chem, 1997. **272**(24): p. 15045-8.
39. Riobo, N.A. and D.R. Manning, *Receptors coupled to heterotrimeric G proteins of the G12 family.* Trends Pharmacol Sci, 2005. **26**(3): p. 146-54.
40. Khan, S.M., et al., *The expanding roles of Gbetagamma subunits in G protein-coupled receptor signaling and drug action.* Pharmacol Rev, 2013. **65**(2): p. 545-77.
41. Syrovatkina, V., et al., *Regulation, Signaling, and Physiological Functions of G-Proteins.* J Mol Biol, 2016. **428**(19): p. 3850-68.
42. Milligan, G. and E. Kostenis, *Heterotrimeric G-proteins: a short history.* Br J Pharmacol, 2006. **147 Suppl 1**: p. S46-55.
43. Kimple, A.J., et al., *Regulators of G-protein signaling and their Galpha substrates: promises and challenges in their use as drug discovery targets.* Pharmacol Rev, 2011. **63**(3): p. 728-49.
44. Hein, P., et al., *Dynamics of receptor/G protein coupling in living cells.* Embo j, 2005. **24**(23): p. 4106-14.

45. Tolkovsky, A.M. and A. Levitzki, *Mode of coupling between the beta-adrenergic receptor and adenylate cyclase in turkey erythrocytes.* Biochemistry, 1978. **17**(18): p. 3795.
46. Gales, C., et al., *Probing the activation-promoted structural rearrangements in preassembled receptor-G protein complexes.* Nat Struct Mol Biol, 2006. **13**(9): p. 778-86.
47. Sungkaworn, T., et al., *Single-molecule imaging reveals receptor-G protein interactions at cell surface hot spots.* Nature, 2017. **550**(7677): p. 543-547.
48. Zhang, Y., et al., *Cryo-EM structure of the activated GLP-1 receptor in complex with a G protein.* Nature, 2017. **546**(7657): p. 248-253.
49. Liang, Y.L., et al., *Cryo-EM structure of the active, Gs-protein complexed, human CGRP receptor.* Nature, 2018. **561**(7724): p. 492-497.
50. Hilger, D., M. Masureel, and B.K. Kobilka, *Structure and dynamics of GPCR signaling complexes.* Nat Struct Mol Biol, 2018. **25**(1): p. 4-12.
51. Flock, T., et al., *Selectivity determinants of GPCR-G-protein binding.* Nature, 2017. **545**(7654): p. 317-322.
52. Peterson, Y.K. and L.M. Luttrell, *The Diverse Roles of Arrestin Scaffolds in G Protein-Coupled Receptor Signaling.* Pharmacol Rev, 2017. **69**(3): p. 256-297.
53. Benovic, J.L., et al., *Functional desensitization of the isolated beta-adrenergic receptor by the beta-adrenergic receptor kinase: potential role of an analog of the retinal protein arrestin (48-kDa protein).* Proc Natl Acad Sci U S A, 1987. **84**(24): p. 8879-82.
54. Craft, C.M., D.H. Whitmore, and A.F. Wiechmann, *Cone arrestin identified by targeting expression of a functional family.* J Biol Chem, 1994. **269**(6): p. 4613-9.
55. Vishnivetskiy, S.A., et al., *Transition of arrestin into the active receptor-binding state requires an extended interdomain hinge.* J Biol Chem, 2002. **277**(46): p. 43961-7.
56. Aubry, L., D. Guetta, and G. Klein, *The arrestin fold: variations on a theme.* Curr Genomics, 2009. **10**(2): p. 133-42.
57. Scheerer, P. and M.E. Sommer, *Structural mechanism of arrestin activation.* Curr Opin Struct Biol, 2017. **45**: p. 160-169.
58. Hirsch, J.A., et al., *The 2.8 A crystal structure of visual arrestin: a model for arrestin's regulation.* Cell, 1999. **97**(2): p. 257-69.
59. Komolov, K.E. and J.L. Benovic, *G protein-coupled receptor kinases: Past, present and future.* Cell Signal, 2018. **41**: p. 17-24.
60. Butcher, A.J., A.B. Tobin, and K.C. Kong, *Examining site-specific GPCR phosphorylation.* Methods Mol Biol, 2011. **746**: p. 237-49.
61. Tobin, A.B., A.J. Butcher, and K.C. Kong, *Location, location, location...site-specific GPCR phosphorylation offers a mechanism for cell-type-specific signalling.* Trends Pharmacol Sci, 2008. **29**(8): p. 413-20.
62. De Lean, A., J.M. Stadel, and R.J. Lefkowitz, *A ternary complex model explains the agonist-specific binding properties of the adenylate cyclase-coupled beta-adrenergic receptor.* J Biol Chem, 1980. **255**(15): p. 7108-17.
63. Gurevich, V.V., et al., *Agonist-receptor-arrestin, an alternative ternary complex with high agonist affinity.* J Biol Chem, 1997. **272**(46): p. 28849-52.
64. Kim, Y.J., et al., *Crystal structure of pre-activated arrestin p44.* Nature, 2013. **497**(7447): p. 142-6.
65. Nuber, S., et al., *beta-Arrestin biosensors reveal a rapid, receptor-dependent activation/deactivation cycle.* Nature, 2016. **531**(7596): p. 661-4.
66. Schleicher, A., H. Kuhn, and K.P. Hofmann, *Kinetics, binding constant, and activation energy of the 48-kDa protein-rhodopsin complex by extra-metarhodopsin II.* Biochemistry, 1989. **28**(4): p. 1770-5.

67. Kirchberg, K., et al., *Conformational dynamics of helix 8 in the GPCR rhodopsin controls arrestin activation in the desensitization process.* Proc Natl Acad Sci U S A, 2011. **108**(46): p. 18690-5.
68. Cahill, T.J., 3rd, et al., *Distinct conformations of GPCR-beta-arrestin complexes mediate desensitization, signaling, and endocytosis.* Proc Natl Acad Sci U S A, 2017. **114**(10): p. 2562-2567.
69. Lohse, M.J., et al., *beta-Arrestin: a protein that regulates beta-adrenergic receptor function.* Science, 1990. **248**(4962): p. 1547-50.
70. Marion, S., et al., *A beta-arrestin binding determinant common to the second intracellular loops of rhodopsin family G protein-coupled receptors.* J Biol Chem, 2006. **281**(5): p. 2932-8.
71. Shukla, A.K., et al., *Visualization of arrestin recruitment by a G-protein-coupled receptor.* Nature, 2014. **512**(7513): p. 218-222.
72. Ferguson, S.S., *Evolving concepts in G protein-coupled receptor endocytosis: the role in receptor desensitization and signaling.* Pharmacol Rev, 2001. **53**(1): p. 1-24.
73. Pierce, K.L. and R.J. Lefkowitz, *Classical and new roles of beta-arrestins in the regulation of G-protein-coupled receptors.* Nat Rev Neurosci, 2001. **2**(10): p. 727-33.
74. Ferguson, S.S., et al., *Molecular mechanisms of G protein-coupled receptor desensitization and resensitization.* Life Sci, 1998. **62**(17-18): p. 1561-5.
75. Lohse, M.J., *Molecular mechanisms of membrane receptor desensitization.* Biochim Biophys Acta, 1993. **1179**(2): p. 171-88.
76. Goodman, O.B., Jr., et al., *Beta-arrestin acts as a clathrin adaptor in endocytosis of the beta2-adrenergic receptor.* Nature, 1996. **383**(6599): p. 447-50.
77. von Zastrow, M. and B.K. Kobilka, *Ligand-regulated internalization and recycling of human beta 2-adrenergic receptors between the plasma membrane and endosomes containing transferrin receptors.* J Biol Chem, 1992. **267**(5): p. 3530-8.
78. Calebiro, D., et al., *Persistent cAMP-signals triggered by internalized G-protein-coupled receptors.* PLoS Biol, 2009. **7**(8): p. e1000172.
79. Shenoy, S.K., et al., *Beta-arrestin-dependent signaling and trafficking of 7-transmembrane receptors is reciprocally regulated by the deubiquitinase USP33 and the E3 ligase Mdm2.* Proc Natl Acad Sci U S A, 2009. **106**(16): p. 6650-5.
80. Kovacs, J.J., et al., *Beta-arrestin-mediated localization of smoothened to the primary cilium.* Science, 2008. **320**(5884): p. 1777-81.
81. Luttrell, L.M., et al., *Beta-arrestin-dependent formation of beta2 adrenergic receptor-Src protein kinase complexes.* Science, 1999. **283**(5402): p. 655-61.
82. Kang, J., et al., *A nuclear function of beta-arrestin1 in GPCR signaling: regulation of histone acetylation and gene transcription.* Cell, 2005. **123**(5): p. 833-47.
83. Ferrandon, S., et al., *Sustained cyclic AMP production by parathyroid hormone receptor endocytosis.* Nat Chem Biol, 2009. **5**(10): p. 734-42.
84. Mullershausen, F., et al., *Persistent signaling induced by FTY720-phosphate is mediated by internalized S1P1 receptors.* Nat Chem Biol, 2009. **5**(6): p. 428-34.
85. Irannejad, R., et al., *Conformational biosensors reveal GPCR signalling from endosomes.* Nature, 2013. **495**(7442): p. 534-8.
86. Tsvetanova, N.G. and M. von Zastrow, *Spatial encoding of cyclic AMP signaling specificity by GPCR endocytosis.* Nat Chem Biol, 2014. **10**(12): p. 1061-5.
87. Thomsen, A.R., et al., *GPCR-G Protein-beta-Arrestin Super-Complex Mediates Sustained G Protein Signaling.* Cell, 2016. **166**(4): p. 907-19.
88. Thompson, A. and V. Kanamarlapudi, *Agonist-induced internalisation of the glucagon-like peptide-1 receptor is mediated by the Galphaq pathway.* Biochem Pharmacol, 2015. **93**(1): p. 72-84.

89. Lyga, S., et al., *Persistent cAMP Signaling by Internalized LH Receptors in Ovarian Follicles.* Endocrinology, 2016. **157**(4): p. 1613-21.
90. Rajagopal, S. and S.K. Shenoy, *GPCR desensitization: Acute and prolonged phases.* Cell Signal, 2018. **41**: p. 9-16.
91. Lefkowitz, R.J., *A brief history of G-protein coupled receptors (Nobel Lecture).* Angew Chem Int Ed Engl, 2013. **52**(25): p. 6366-78.
92. Tsao, P., T. Cao, and M. von Zastrow, *Role of endocytosis in mediating downregulation of G-protein-coupled receptors.* Trends Pharmacol Sci, 2001. **22**(2): p. 91-6.
93. Stadel, J.M., et al., *Desensitization of the beta-adrenergic receptor of frog erythrocytes. Recovery and characterization of the down-regulated receptors in sequestered vesicles.* J Biol Chem, 1983. **258**(5): p. 3032-8.
94. Jorgensen, R., et al., *Beta-arrestin2 as a competitor for GRK2 interaction with the GLP-1 receptor upon receptor activation.* Pharmacology, 2011. **88**(3-4): p. 174-81.
95. Sriram, K. and P.A. Insel, *GPCRs as targets for approved drugs: How many targets and how many drugs?* Molecular Pharmacology, 2018: p. mol.117.111062.
96. Santos, R., et al., *A comprehensive map of molecular drug targets.* Nat Rev Drug Discov, 2017. **16**(1): p. 19-34.
97. Graaf, C., et al., *Glucagon-Like Peptide-1 and Its Class B G Protein-Coupled Receptors: A Long March to Therapeutic Successes.* Pharmacol Rev, 2016. **68**(4): p. 954-1013.
98. Dillon, J.S., et al., *Cloning and functional expression of the human glucagon-like peptide-1 (GLP-1) receptor.* Endocrinology, 1993. **133**(4): p. 1907-10.
99. Segre, G.V. and S.R. Goldring, *Receptors for secretin, calcitonin, parathyroid hormone (PTH)/PTH-related peptide, vasoactive intestinal peptide, glucagonlike peptide 1, growth hormone-releasing hormone, and glucagon belong to a newly discovered G-protein-linked receptor family.* Trends Endocrinol Metab, 1993. **4**(10): p. 309-14.
100. Dunphy, J.L., R.G. Taylor, and P.J. Fuller, *Tissue distribution of rat glucagon receptor and GLP-1 receptor gene expression.* Mol Cell Endocrinol, 1998. **141**(1-2): p. 179-86.
101. Thorens, B., *Expression cloning of the pancreatic beta cell receptor for the gluco-incretin hormone glucagon-like peptide 1.* Proc Natl Acad Sci U S A, 1992. **89**(18): p. 8641-5.
102. Runge, S., et al., *Crystal structure of the ligand-bound glucagon-like peptide-1 receptor extracellular domain.* J Biol Chem, 2008. **283**(17): p. 11340-7.
103. Kreymann, B., et al., *Glucagon-like peptide-1 7-36: a physiological incretin in man.* Lancet, 1987. **2**(8571): p. 1300-4.
104. MacDonald, P.E., J.W. Joseph, and P. Rorsman, *Glucose-sensing mechanisms in pancreatic beta-cells.* Philos Trans R Soc Lond B Biol Sci, 2005. **360**(1464): p. 2211-25.
105. Kang, G., et al., *Role of the cAMP sensor Epac as a determinant of KATP channel ATP sensitivity in human pancreatic beta-cells and rat INS-1 cells.* J Physiol, 2008. **586**(5): p. 1307-19.
106. Prentki, M. and F.M. Matschinsky, *Ca2+, cAMP, and phospholipid-derived messengers in coupling mechanisms of insulin secretion.* Physiol Rev, 1987. **67**(4): p. 1185-248.
107. Renstrom, E., L. Eliasson, and P. Rorsman, *Protein kinase A-dependent and -independent stimulation of exocytosis by cAMP in mouse pancreatic B-cells.* J Physiol, 1997. **502 (Pt 1)**: p. 105-18.
108. Gromada, J. and P. Rorsman, *New insights into the regulation of glucagon secretion by glucagon-like peptide-1.* Horm Metab Res, 2004. **36**(11-12): p. 822-9.
109. Wettergren, A., et al., *Truncated GLP-1 (proglucagon 78-107-amide) inhibits gastric and pancreatic functions in man.* Dig Dis Sci, 1993. **38**(4): p. 665-73.

110. Tang-Christensen, M., N. Vrang, and P.J. Larsen, *Glucagon-like peptide 1(7-36) amide's central inhibition of feeding and peripheral inhibition of drinking are abolished by neonatal monosodium glutamate treatment.* Diabetes, 1998. **47**(4): p. 530-7.
111. Mojsov, S., et al., *Preproglucagon gene expression in pancreas and intestine diversifies at the level of post-translational processing.* J Biol Chem, 1986. **261**(25): p. 11880-9.
112. Holst, J.J., et al., *Truncated glucagon-like peptide I, an insulin-releasing hormone from the distal gut.* FEBS Lett, 1987. **211**(2): p. 169-74.
113. Wettergren, A., et al., *Amidated and non-amidated glucagon-like peptide-1 (GLP-1): non-pancreatic effects (cephalic phase acid secretion) and stability in plasma in humans.* Regul Pept, 1998. **77**(1-3): p. 83-7.
114. Deacon, C.F., et al., *Both subcutaneously and intravenously administered glucagon-like peptide I are rapidly degraded from the NH2-terminus in type II diabetic patients and in healthy subjects.* Diabetes, 1995. **44**(9): p. 1126-31.
115. Donnely, D., *The structure and function of the glucagon-like peptide-1 receptor and its ligands.* British Journal of Pharmacology, 2012. **166**(1).
116. Moretto, T.J., et al., *Efficacy and tolerability of exenatide monotherapy over 24 weeks in antidiabetic drug-naive patients with type 2 diabetes: a randomized, double-blind, placebo-controlled, parallel-group study.* Clin Ther, 2008. **30**(8): p. 1448-60.
117. Montrose-Rafizadeh, C., et al., *High potency antagonists of the pancreatic glucagon-like peptide-1 receptor.* J Biol Chem, 1997. **272**(34): p. 21201-6.
118. Nauck, M.A., et al., *A Phase 2, Randomized, Dose-Finding Study of the Novel Once-Weekly Human GLP-1 Analog, Semaglutide, Compared With Placebo and Open-Label Liraglutide in Patients With Type 2 Diabetes.* Diabetes Care, 2016. **39**(2): p. 231-41.
119. Yang, D.H., et al., *Landmark studies on the glucagon subfamily of GPCRs: from small molecule modulators to a crystal structure.* Acta Pharmacol Sin, 2015. **36**(9): p. 1033-42.
120. Cvetkovic, R.S. and G.L. Plosker, *Exenatide: a review of its use in patients with type 2 diabetes mellitus (as an adjunct to metformin and/or a sulfonylurea).* Drugs, 2007. **67**(6): p. 935-54.
121. Gustavson, S., et al., *TTP273, an Orally-Available Glucagon-like Peptide-1 (GLP-1) Agonist, Notably Reduces Glycemia in Subjects with Type 2 Diabetes Mellitus (T2DM)*. Vol. 63. 2014. A41-A41.
122. Chen, D., et al., *A nonpeptidic agonist of glucagon-like peptide 1 receptors with efficacy in diabetic db/db mice.* Proc Natl Acad Sci U S A, 2007. **104**(3): p. 943-8.
123. Sloop, K.W., et al., *Novel small molecule glucagon-like peptide-1 receptor agonist stimulates insulin secretion in rodents and from human islets.* Diabetes, 2010. **59**(12): p. 3099-107.
124. Oka, J., E. Suzuki, and Y. Kondo, *Endogenous GLP-1 is involved in beta-amyloid protein-induced memory impairment and hippocampal neuronal death in rats.* Brain Res, 2000. **878**(1-2): p. 194-8.
125. Wheeler, M.B., et al., *Functional expression of the rat glucagon-like peptide-I receptor, evidence for coupling to both adenylyl cyclase and phospholipase-C.* Endocrinology, 1993. **133**(1): p. 57-62.
126. Wootten, D., et al., *Differential activation and modulation of the glucagon-like peptide-1 receptor by small molecule ligands.* Mol Pharmacol, 2013. **83**(4): p. 822-34.
127. Coopman, K., et al., *Comparative effects of the endogenous agonist glucagon-like peptide-1 (GLP-1)-(7-36) amide and the small-molecule ago-allosteric agent "compound 2" at the GLP-1 receptor.* J Pharmacol Exp Ther, 2010. **334**(3): p. 795-808.
128. Shonberg, J., et al., *Biased agonism at G protein-coupled receptors: the promise and the challenges--a medicinal chemistry perspective.* Med Res Rev, 2014. **34**(6): p. 1286-330.

129. Koole, C., et al., *Allosteric ligands of the glucagon-like peptide 1 receptor (GLP-1R) differentially modulate endogenous and exogenous peptide responses in a pathway-selective manner: implications for drug screening.* Mol Pharmacol, 2010. **78**(3): p. 456-65.
130. Knudsen, L.B., et al., *Small-molecule agonists for the glucagon-like peptide 1 receptor.* Proc Natl Acad Sci U S A, 2007. **104**(3): p. 937-42.
131. Cheong, Y.H., et al., *Two small molecule agonists of glucagon-like peptide-1 receptor modulate the receptor activation response differently.* Biochem Biophys Res Commun, 2012. **417**(1): p. 558-63.
132. Nolte, W.M., et al., *A potentiator of orthosteric ligand activity at GLP-1R acts via covalent modification.* Nat Chem Biol, 2014. **10**(8): p. 629-31.
133. Leach, K., P.M. Sexton, and A. Christopoulos, *Allosteric GPCR modulators: taking advantage of permissive receptor pharmacology.* Trends Pharmacol Sci, 2007. **28**(8): p. 382-9.
134. Davis, H.R., Jr., et al., *Effect of chronic central administration of glucagon-like peptide-1 (7-36) amide on food consumption and body weight in normal and obese rats.* Obes Res, 1998. **6**(2): p. 147-56.
135. Young, A.A., et al., *Glucose-lowering and insulin-sensitizing actions of exendin-4: studies in obese diabetic (ob/ob, db/db) mice, diabetic fatty Zucker rats, and diabetic rhesus monkeys (Macaca mulatta).* Diabetes, 1999. **48**(5): p. 1026-34.
136. Baggio, L.L., J.G. Kim, and D.J. Drucker, *Chronic exposure to GLP-1R agonists promotes homologous GLP-1 receptor desensitization in vitro but does not attenuate GLP-1R-dependent glucose homeostasis in vivo.* Diabetes, 2004. **53 Suppl 3**: p. S205-14.
137. Buse, J.B., et al., *Effects of exenatide (exendin-4) on glycemic control over 30 weeks in sulfonylurea-treated patients with type 2 diabetes.* Diabetes Care, 2004. **27**(11): p. 2628-35.
138. Widmann, C., W. Dolci, and B. Thorens, *Agonist-induced internalization and recycling of the glucagon-like peptide-1 receptor in transfected fibroblasts and in insulinomas.* Biochem J, 1995. **310 (Pt 1)**: p. 203-14.
139. Roed, S.N., et al., *Functional consequences of glucagon-like peptide-1 receptor cross-talk and trafficking.* J Biol Chem, 2015. **290**(2): p. 1233-43.
140. Sonoda, N., et al., *Beta-Arrestin-1 mediates glucagon-like peptide-1 signaling to insulin secretion in cultured pancreatic beta cells.* Proc Natl Acad Sci U S A, 2008. **105**(18): p. 6614-9.
141. Jorgensen, R., et al., *Characterization of glucagon-like peptide-1 receptor beta-arrestin 2 interaction: a high-affinity receptor phenotype.* Mol Endocrinol, 2005. **19**(3): p. 812-23.
142. Kuna, R.S., et al., *Glucagon-like peptide-1 receptor-mediated endosomal cAMP generation promotes glucose-stimulated insulin secretion in pancreatic beta-cells.* Am J Physiol Endocrinol Metab, 2013. **305**(2): p. E161-70.
143. Roed, S.N., et al., *Real-time trafficking and signaling of the glucagon-like peptide-1 receptor.* Mol Cell Endocrinol, 2014. **382**(2): p. 938-49.
144. Syme, C.A., L. Zhang, and A. Bisello, *Caveolin-1 regulates cellular trafficking and function of the glucagon-like Peptide 1 receptor.* Mol Endocrinol, 2006. **20**(12): p. 3400-11.
145. Jones, B., et al., *Targeting GLP-1 receptor trafficking to improve agonist efficacy.* Nat Commun, 2018. **9**(1): p. 1602.
146. Newton, A.C., M.D. Bootman, and J.D. Scott, *Second Messengers.* Cold Spring Harb Perspect Biol, 2016. **8**(8).
147. Taussig, R. and A.G. Gilman, *Mammalian membrane-bound adenylyl cyclases.* J Biol Chem, 1995. **270**(1): p. 1-4.
148. Hubbard, K.B. and J.R. Hepler, *Cell signalling diversity of the Gqalpha family of heterotrimeric G proteins.* Cell Signal, 2006. **18**(2): p. 135-50.
149. Clapham, D.E., *Calcium signaling.* Cell, 2007. **131**(6): p. 1047-58.

150. Berridge, M., *Conformational coupling: a physiological calcium entry mechanism.* Sci STKE, 2004. **2004**(243): p. pe33.
151. Kuo, I.Y. and B.E. Ehrlich, *Signaling in muscle contraction.* Cold Spring Harb Perspect Biol, 2015. **7**(2): p. a006023.
152. Berridge, M.J., *Calcium microdomains: organization and function.* Cell Calcium, 2006. **40**(5-6): p. 405-12.
153. Matulef, K. and W.N. Zagotta, *Cyclic nucleotide-gated ion channels.* Annu Rev Cell Dev Biol, 2003. **19**: p. 23-44.
154. Beavo, J.A. and L.L. Brunton, *<Beavo_2002_cAMP.pdf>.* Nature Reviews, Cyclic nucleotide research — still expanding after half a century.
155. Nguyen, P.V. and N.H. Woo, *Regulation of hippocampal synaptic plasticity by cyclic AMP-dependent protein kinases.* Prog Neurobiol, 2003. **71**(6): p. 401-37.
156. Halls, M.L. and D.M.F. Cooper, *Adenylyl cyclase signalling complexes - Pharmacological challenges and opportunities.* Pharmacol Ther, 2017. **172**: p. 171-180.
157. Krupinski, J., et al., *Adenylyl cyclase amino acid sequence: possible channel- or transporter-like structure.* Science, 1989. **244**(4912): p. 1558-64.
158. Sunahara, R.K., C.W. Dessauer, and A.G. Gilman, *Complexity and diversity of mammalian adenylyl cyclases.* Annu Rev Pharmacol Toxicol, 1996. **36**: p. 461-80.
159. Zhang, G., et al., *Structure of the adenylyl cyclase catalytic core.* Nature, 1997. **386**(6622): p. 247-53.
160. Tesmer, J.J., et al., *Crystal structure of the catalytic domains of adenylyl cyclase in a complex with Gsalpha.GTPgammaS.* Science, 1997. **278**(5345): p. 1907-16.
161. Gu, C., A. Sorkin, and D.M. Cooper, *Persistent interactions between the two transmembrane clusters dictate the targeting and functional assembly of adenylyl cyclase.* Curr Biol, 2001. **11**(3): p. 185-90.
162. Cooper, D.M. and V.G. Tabbasum, *Adenylate cyclase-centred microdomains.* Biochem J, 2014. **462**(2): p. 199-213.
163. Pike, L.J., et al., *Lipid rafts are enriched in arachidonic acid and plasmenylethanolamine and their composition is independent of caveolin-1 expression: a quantitative electrospray ionization/mass spectrometric analysis.* Biochemistry, 2002. **41**(6): p. 2075-88.
164. Munro, S., *Lipid rafts: elusive or illusive?* Cell, 2003. **115**(4): p. 377-88.
165. Foster, L.J., C.L. De Hoog, and M. Mann, *Unbiased quantitative proteomics of lipid rafts reveals high specificity for signaling factors.* Proc Natl Acad Sci U S A, 2003. **100**(10): p. 5813-8.
166. Crossthwaite, A.J., et al., *The cytosolic domains of Ca2+-sensitive adenylyl cyclases dictate their targeting to plasma membrane lipid rafts.* J Biol Chem, 2005. **280**(8): p. 6380-91.
167. Thangavel, M., et al., *The C1 and C2 domains target human type 6 adenylyl cyclase to lipid rafts and caveolae.* Cell Signal, 2009. **21**(2): p. 301-8.
168. Ostrom, R.S., et al., *Choreographing the adenylyl cyclase signalosome: sorting out the partners and the steps.* Naunyn Schmiedebergs Arch Pharmacol, 2012. **385**(1): p. 5-12.
169. Ostrom, R.S. and P.A. Insel, *The evolving role of lipid rafts and caveolae in G protein-coupled receptor signaling: implications for molecular pharmacology.* Br J Pharmacol, 2004. **143**(2): p. 235-45.
170. Bauman, A.L., et al., *Dynamic regulation of cAMP synthesis through anchored PKA-adenylyl cyclase V/VI complexes.* Mol Cell, 2006. **23**(6): p. 925-31.
171. Gu, C. and D.M. Cooper, *Calmodulin-binding sites on adenylyl cyclase type VIII.* J Biol Chem, 1999. **274**(12): p. 8012-21.

172. Premont, R.T., O. Jacobowitz, and R. Iyengar, *Lowered responsiveness of the catalyst of adenylyl cyclase to stimulation by GS in heterologous desensitization: a role for adenosine 3',5'-monophosphate-dependent phosphorylation.* Endocrinology, 1992. **131**(6): p. 2774-84.
173. Kawabe, J., et al., *Differential activation of adenylyl cyclase by protein kinase C isoenzymes.* J Biol Chem, 1994. **269**(24): p. 16554-8.
174. Dessauer, C.W., et al., *International Union of Basic and Clinical Pharmacology. CI. Structures and Small Molecule Modulators of Mammalian Adenylyl Cyclases.* Pharmacol Rev, 2017. **69**(2): p. 93-139.
175. Bender, A.T. and J.A. Beavo, *Cyclic nucleotide phosphodiesterases: molecular regulation to clinical use.* Pharmacol Rev, 2006. **58**(3): p. 488-520.
176. Sonnenburg, W.K., et al., *Identification of inhibitory and calmodulin-binding domains of the PDE1A1 and PDE1A2 calmodulin-stimulated cyclic nucleotide phosphodiesterases.* J Biol Chem, 1995. **270**(52): p. 30989-1000.
177. Anantharaman, V., E.V. Koonin, and L. Aravind, *Regulatory potential, phyletic distribution and evolution of ancient, intracellular small-molecule-binding domains.* J Mol Biol, 2001. **307**(5): p. 1271-92.
178. Bolger, G., et al., *A family of human phosphodiesterases homologous to the dunce learning and memory gene product of Drosophila melanogaster are potential targets for antidepressant drugs.* Mol Cell Biol, 1993. **13**(10): p. 6558-71.
179. Francis, S.H., M.A. Blount, and J.D. Corbin, *Mammalian cyclic nucleotide phosphodiesterases: molecular mechanisms and physiological functions.* Physiol Rev, 2011. **91**(2): p. 651-90.
180. Kokkonen, K. and D.A. Kass, *Nanodomain Regulation of Cardiac Cyclic Nucleotide Signaling by Phosphodiesterases.* Annu Rev Pharmacol Toxicol, 2017. **57**: p. 455-479.
181. Ke, H. and H. Wang, *Crystal structures of phosphodiesterases and implications on substrate specificity and inhibitor selectivity.* Curr Top Med Chem, 2007. **7**(4): p. 391-403.
182. Baillie, G.S., et al., *Sub-family selective actions in the ability of Erk2 MAP kinase to phosphorylate and regulate the activity of PDE4 cyclic AMP-specific phosphodiesterases.* Br J Pharmacol, 2000. **131**(4): p. 811-9.
183. Fink, T.L., et al., *Expression of an active, monomeric catalytic domain of the cGMP-binding cGMP-specific phosphodiesterase (PDE5).* J Biol Chem, 1999. **274**(49): p. 34613-20.
184. Huai, Q., et al., *Crystal structures of phosphodiesterases 4 and 5 in complex with inhibitor 3-isobutyl-1-methylxanthine suggest a conformation determinant of inhibitor selectivity.* J Biol Chem, 2004. **279**(13): p. 13095-101.
185. Xu, R.X., et al., *Atomic structure of PDE4: insights into phosphodiesterase mechanism and specificity.* Science, 2000. **288**(5472): p. 1822-5.
186. Saldou, N., et al., *Comparison of recombinant human PDE4 isoforms: interaction with substrate and inhibitors.* Cell Signal, 1998. **10**(6): p. 427-40.
187. Gulati, S., et al., *Cryo-EM structure of phosphodiesterase 6 reveals insights into the allosteric regulation of type I phosphodiesterases.* Sci Adv, 2019. **5**(2): p. eaav4322.
188. Sette, C., S. Iona, and M. Conti, *The short-term activation of a rolipram-sensitive, cAMP-specific phosphodiesterase by thyroid-stimulating hormone in thyroid FRTL-5 cells is mediated by a cAMP-dependent phosphorylation.* J Biol Chem, 1994. **269**(12): p. 9245-52.
189. Torres-Quesada, O., J.E. Mayrhofer, and E. Stefan, *The many faces of compartmentalized PKA signalosomes.* Cell Signal, 2017. **37**: p. 1-11.
190. Fischer, E.H. and E.G. Krebs, *Conversion of phosphorylase b to phosphorylase a in muscle extracts.* J Biol Chem, 1955. **216**(1): p. 121-32.
191. Krebs, E.G., *Nobel Lecture. Protein phosphorylation and cellular regulation I.* Biosci Rep, 1993. **13**(3): p. 127-42.

192. Gilman, A.G., *Nobel Lecture. G proteins and regulation of adenylyl cyclase.* Biosci Rep, 1995. **15**(2): p. 65-97.
193. Schmidt, M., F.J. Dekker, and H. Maarsingh, *Exchange protein directly activated by cAMP (epac): a multidomain cAMP mediator in the regulation of diverse biological functions.* Pharmacol Rev, 2013. **65**(2): p. 670-709.
194. Kaupp, U.B. and R. Seifert, *Cyclic nucleotide-gated ion channels.* Physiol Rev, 2002. **82**(3): p. 769-824.
195. Schindler, R.F. and T. Brand, *The Popeye domain containing protein family--A novel class of cAMP effectors with important functions in multiple tissues.* Prog Biophys Mol Biol, 2016. **120**(1-3): p. 28-36.
196. Krahling, A.M., et al., *CRIS-a novel cAMP-binding protein controlling spermiogenesis and the development of flagellar bending.* PLoS Genet, 2013. **9**(12): p. e1003960.
197. Scott, J.D., et al., *Type II regulatory subunit dimerization determines the subcellular localization of the cAMP-dependent protein kinase.* J Biol Chem, 1990. **265**(35): p. 21561-6.
198. Taylor, S.S. and A.P. Kornev, *Protein kinases: evolution of dynamic regulatory proteins.* Trends Biochem Sci, 2011. **36**(2): p. 65-77.
199. Smith, C.M., et al., *The catalytic subunit of cAMP-dependent protein kinase: prototype for an extended network of communication.* Prog Biophys Mol Biol, 1999. **71**(3-4): p. 313-41.
200. Cadd, G. and G.S. McKnight, *Distinct patterns of cAMP-dependent protein kinase gene expression in mouse brain.* Neuron, 1989. **3**(1): p. 71-9.
201. Wu, J., et al., *PKA type IIalpha holoenzyme reveals a combinatorial strategy for isoform diversity.* Science, 2007. **318**(5848): p. 274-9.
202. Banky, P., L.J. Huang, and S.S. Taylor, *Dimerization/docking domain of the type Ialpha regulatory subunit of cAMP-dependent protein kinase. Requirements for dimerization and docking are distinct but overlapping.* J Biol Chem, 1998. **273**(52): p. 35048-55.
203. Gold, M.G., et al., *Molecular basis of AKAP specificity for PKA regulatory subunits.* Mol Cell, 2006. **24**(3): p. 383-95.
204. Taylor, S.S., et al., *Assembly of allosteric macromolecular switches: lessons from PKA.* Nat Rev Mol Cell Biol, 2012. **13**(10): p. 646-58.
205. Diller, T.C., et al., *Molecular basis for regulatory subunit diversity in cAMP-dependent protein kinase: crystal structure of the type II beta regulatory subunit.* Structure, 2001. **9**(1): p. 73-82.
206. Diskar, M., et al., *Molecular basis for isoform-specific autoregulation of protein kinase A.* Cell Signal, 2007. **19**(10): p. 2024-34.
207. Tasken, K. and E.M. Aandahl, *Localized effects of cAMP mediated by distinct routes of protein kinase A.* Physiol Rev, 2004. **84**(1): p. 137-67.
208. Zhong, H., et al., *The transcriptional activity of NF-kappaB is regulated by the IkappaB-associated PKAc subunit through a cyclic AMP-independent mechanism.* Cell, 1997. **89**(3): p. 413-24.
209. Zhang, L., et al., *A transforming growth factor beta-induced Smad3/Smad4 complex directly activates protein kinase A.* Mol Cell Biol, 2004. **24**(5): p. 2169-80.
210. Rinaldi, L., et al., *A dynamic interface between ubiquitylation and cAMP signaling.* Front Pharmacol, 2015. **6**: p. 177.
211. Scott, J.D., C.W. Dessauer, and K. Tasken, *Creating order from chaos: cellular regulation by kinase anchoring.* Annu Rev Pharmacol Toxicol, 2013. **53**: p. 187-210.
212. Dalton, G.D. and W.L. Dewey, *Protein kinase inhibitor peptide (PKI): a family of endogenous neuropeptides that modulate neuronal cAMP-dependent protein kinase function.* Neuropeptides, 2006. **40**(1): p. 23-34.
213. Borodinsky, L.N. and N.C. Spitzer, *Second messenger pas de deux: the coordinated dance between calcium and cAMP.* Sci STKE, 2006. **2006**(336): p. pe22.

214. Ahuja, M., et al., *cAMP and Ca(2)(+) signaling in secretory epithelia: crosstalk and synergism.* Cell Calcium, 2014. **55**(6): p. 385-93.
215. de Rooij, J., et al., *Epac is a Rap1 guanine-nucleotide-exchange factor directly activated by cyclic AMP.* Nature, 1998. **396**(6710): p. 474-7.
216. Quilliam, L.A., J.F. Rebhun, and A.F. Castro, *A growing family of guanine nucleotide exchange factors is responsible for activation of Ras-family GTPases.* Prog Nucleic Acid Res Mol Biol, 2002. **71**: p. 391-444.
217. Gloerich, M. and J.L. Bos, *Regulating Rap small G-proteins in time and space.* Trends Cell Biol, 2011. **21**(10): p. 615-23.
218. Krugmann, S., et al., *ARAP3 is a PI3K- and rap-regulated GAP for RhoA.* Curr Biol, 2004. **14**(15): p. 1380-4.
219. Maillet, M., et al., *Crosstalk between Rap1 and Rac regulates secretion of sAPPalpha.* Nat Cell Biol, 2003. **5**(7): p. 633-9.
220. Liu, C., et al., *The interaction of Epac1 and Ran promotes Rap1 activation at the nuclear envelope.* Mol Cell Biol, 2010. **30**(16): p. 3956-69.
221. Grandoch, M., S.S. Roscioni, and M. Schmidt, *The role of Epac proteins, novel cAMP mediators, in the regulation of immune, lung and neuronal function.* Br J Pharmacol, 2010. **159**(2): p. 265-84.
222. de Rooij, J., et al., *Mechanism of regulation of the Epac family of cAMP-dependent RapGEFs.* J Biol Chem, 2000. **275**(27): p. 20829-36.
223. Rehmann, H., et al., *Structure of the cyclic-AMP-responsive exchange factor Epac2 in its auto-inhibited state.* Nature, 2006. **439**(7076): p. 625-8.
224. Ponsioen, B., et al., *Direct spatial control of Epac1 by cyclic AMP.* Mol Cell Biol, 2009. **29**(10): p. 2521-31.
225. Bos, J.L., *Epac proteins: multi-purpose cAMP targets.* Trends Biochem Sci, 2006. **31**(12): p. 680-6.
226. Willoughby, D. and D.M. Cooper, *Live-cell imaging of cAMP dynamics.* Nat Methods, 2008. **5**(1): p. 29-36.
227. Borner, S., et al., *FRET measurements of intracellular cAMP concentrations and cAMP analog permeability in intact cells.* Nat Protoc, 2011. **6**(4): p. 427-38.
228. Ozaki, N., et al., *cAMP-GEFII is a direct target of cAMP in regulated exocytosis.* Nat Cell Biol, 2000. **2**(11): p. 805-11.
229. Kelley, G.G., et al., *Glucose-dependent potentiation of mouse islet insulin secretion by Epac activator 8-pCPT-2'-O-Me-cAMP-AM.* Islets, 2009. **1**(3): p. 260-5.
230. Herrmann, S., S. Schnorr, and A. Ludwig, *HCN channels--modulators of cardiac and neuronal excitability.* Int J Mol Sci, 2015. **16**(1): p. 1429-47.
231. Brand, T., *The Popeye domain-containing gene family.* Cell Biochem Biophys, 2005. **43**(1): p. 95-103.
232. Andree, B., et al., *Isolation and characterization of the novel popeye gene family expressed in skeletal muscle and heart.* Dev Biol, 2000. **223**(2): p. 371-82.
233. Froese, A., et al., *Popeye domain containing proteins are essential for stress-mediated modulation of cardiac pacemaking in mice.* J Clin Invest, 2012. **122**(3): p. 1119-30.
234. Russ, P.K., et al., *Bves modulates tight junction associated signaling.* PLoS One, 2011. **6**(1): p. e14563.
235. Luftman, K., et al., *Silencing of VAMP3 inhibits cell migration and integrin-mediated adhesion.* Biochem Biophys Res Commun, 2009. **380**(1): p. 65-70.
236. Micalizzi, D.S., S.M. Farabaugh, and H.L. Ford, *Epithelial-mesenchymal transition in cancer: parallels between normal development and tumor progression.* J Mammary Gland Biol Neoplasia, 2010. **15**(2): p. 117-34.

237. Alcalay, Y., et al., *Popeye domain containing 1 (Popdc1/Bves) is a caveolae-associated protein involved in ischemia tolerance.* PLoS One, 2013. **8**(9): p. e71100.
238. Kirchmaier, B.C., et al., *The Popeye domain containing 2 (popdc2) gene in zebrafish is required for heart and skeletal muscle development.* Dev Biol, 2012. **363**(2): p. 438-50.
239. Buxton, I.L.O. and L.L. Brunton, *Compartments of Cyclic AMP and Protein Kinase in Mammalian Cardiomyocytes.* The Journal of biological Chemistry, 1982.
240. Jurevicius, J. and R. Fischmeister, *cAMP compartmentation is responsible for a local activation of cardiac Ca2+ channels by beta-adrenergic agonists.* Proc Natl Acad Sci U S A, 1996. **93**(1): p. 295-9.
241. Dao, K.K., et al., *Epac1 and cAMP-dependent protein kinase holoenzyme have similar cAMP affinity, but their cAMP domains have distinct structural features and cyclic nucleotide recognition.* J Biol Chem, 2006. **281**(30): p. 21500-11.
242. Salonikidis, P.S., et al., *Quantitative measurement of cAMP concentration using an exchange protein directly activated by a cAMP-based FRET-sensor.* Biophys J, 2008. **95**(11): p. 5412-23.
243. Cheepala, S., et al., *Cyclic nucleotide compartmentalization: contributions of phosphodiesterases and ATP-binding cassette transporters.* Annu Rev Pharmacol Toxicol, 2013. **53**: p. 231-53.
244. Johnstone, T.B., et al., *cAMP Signaling Compartmentation: Adenylyl Cyclases as Anchors of Dynamic Signaling Complexes.* Mol Pharmacol, 2018. **93**(4): p. 270-276.
245. Jarnaess, E. and K. Tasken, *Spatiotemporal control of cAMP signalling processes by anchored signalling complexes.* Biochem Soc Trans, 2007. **35**(Pt 5): p. 931-7.
246. Carnegie, G.K., C.K. Means, and J.D. Scott, *A-kinase anchoring proteins: from protein complexes to physiology and disease.* IUBMB Life, 2009. **61**(4): p. 394-406.
247. Carr, D.W., et al., *Interaction of the regulatory subunit (RII) of cAMP-dependent protein kinase with RII-anchoring proteins occurs through an amphipathic helix binding motif.* J Biol Chem, 1991. **266**(22): p. 14188-92.
248. Carr, D.W., et al., *Association of the type II cAMP-dependent protein kinase with a human thyroid RII-anchoring protein. Cloning and characterization of the RII-binding domain.* J Biol Chem, 1992. **267**(19): p. 13376-82.
249. Rosenmund, C., et al., *Anchoring of protein kinase A is required for modulation of AMPA/kainate receptors on hippocampal neurons.* Nature, 1994. **368**(6474): p. 853-6.
250. Olson, E.N., *A decade of discoveries in cardiac biology.* Nat Med, 2004. **10**(5): p. 467-74.
251. Dodge-Kafka, K.L., et al., *The protein kinase A anchoring protein mAKAP coordinates two integrated cAMP effector pathways.* Nature, 2005. **437**(7058): p. 574-8.
252. Kurokawa, J., et al., *Regulatory actions of the A-kinase anchoring protein Yotiao on a heart potassium channel downstream of PKA phosphorylation.* Proc Natl Acad Sci U S A, 2004. **101**(46): p. 16374-8.
253. Lygren, B., et al., *AKAP complex regulates Ca2+ re-uptake into heart sarcoplasmic reticulum.* EMBO Rep, 2007. **8**(11): p. 1061-7.
254. Tingley, W.G., et al., *Gene-trapped mouse embryonic stem cell-derived cardiac myocytes and human genetics implicate AKAP10 in heart rhythm regulation.* Proc Natl Acad Sci U S A, 2007. **104**(20): p. 8461-6.
255. Lester, L.B., L.K. Langeberg, and J.D. Scott, *Anchoring of protein kinase A facilitates hormone-mediated insulin secretion.* Proc Natl Acad Sci U S A, 1997. **94**(26): p. 14942-7.
256. Lester, L.B., et al., *Targeted protein kinase A and PP-2B regulate insulin secretion through reversible phosphorylation.* Endocrinology, 2001. **142**(3): p. 1218-27.
257. Kritzer, M.D., et al., *AKAPs: the architectural underpinnings of local cAMP signaling.* J Mol Cell Cardiol, 2012. **52**(2): p. 351-8.

258. Surdo, N.C., et al., *FRET biosensor uncovers cAMP nano-domains at beta-adrenergic targets that dictate precise tuning of cardiac contractility.* Nat Commun, 2017. **8**: p. 15031.
259. Mo, G.C., et al., *Genetically encoded biosensors for visualizing live-cell biochemical activity at super-resolution.* Nat Methods, 2017.
260. Maiellaro, I., et al., *cAMP Signals in Drosophila Motor Neurons Are Confined to Single Synaptic Boutons.* Cell Rep, 2016. **17**(5): p. 1238-1246.
261. Zaccolo, M. and T. Pozzan, *Discrete microdomains with high concentration of cAMP in stimulated rat neonatal cardiac myocytes.* Science, 2002. **295**(5560): p. 1711-5.
262. Chen, C., T. Nakamura, and Y. Koutalos, *Cyclic AMP diffusion coefficient in frog olfactory cilia.* Biophys J, 1999. **76**(5): p. 2861-7.
263. Bacskai, B.J., et al., *Spatially resolved dynamics of cAMP and protein kinase A subunits in Aplysia sensory neurons.* Science, 1993. **260**(5105): p. 222-6.
264. Dworkin, M. and K.H. Keller, *Solubility and diffusion coefficient of adenosine 3':5'-monophosphate.* J Biol Chem, 1977. **252**(3): p. 864-5.
265. Kasai, H. and O.H. Petersen, *Spatial dynamics of second messengers: IP3 and cAMP as long-range and associative messengers.* Trends Neurosci, 1994. **17**(3): p. 95-101.
266. Agarwal, S.R., C.E. Clancy, and R.D. Harvey, *Mechanisms Restricting Diffusion of Intracellular cAMP.* Sci Rep, 2016. **6**: p. 19577.
267. Forster, T., *Energy migration and fluorescence. 1946.* J Biomed Opt, 2012. **17**(1): p. 011002.
268. Hochreiter, B., A.P. Garcia, and J.A. Schmid, *Fluorescent proteins as genetically encoded FRET biosensors in life sciences.* Sensors (Basel), 2015. **15**(10): p. 26281-314.
269. Wu, P. and L. Brand, *Resonance energy transfer: methods and applications.* Anal Biochem, 1994. **218**(1): p. 1-13.
270. Clegg, R.M., *Fluorescence resonance energy transfer.* Curr Opin Biotechnol, 1995. **6**(1): p. 103-10.
271. Sapsford, K.E., L. Berti, and I.L. Medintz, *Materials for fluorescence resonance energy transfer analysis: beyond traditional donor-acceptor combinations.* Angew Chem Int Ed Engl, 2006. **45**(28): p. 4562-89.
272. Bajar, B.T., et al., *A Guide to Fluorescent Protein FRET Pairs.* Sensors (Basel), 2016. **16**(9).
273. Day, R.N. and M.W. Davidson, *Fluorescent proteins for FRET microscopy: monitoring protein interactions in living cells.* Bioessays, 2012. **34**(5): p. 341-50.
274. Zimmermann, T., et al., *Spectral imaging and linear un-mixing enables improved FRET efficiency with a novel GFP2-YFP FRET pair.* FEBS Lett, 2002. **531**(2): p. 245-9.
275. Thaler, C., et al., *Quantitative multiphoton spectral imaging and its use for measuring resonance energy transfer.* Biophys J, 2005. **89**(4): p. 2736-49.
276. Broussard, J.A., et al., *Fluorescence resonance energy transfer microscopy as demonstrated by measuring the activation of the serine/threonine kinase Akt.* Nat Protoc, 2013. **8**(2): p. 265-81.
277. Hoffmann, C., et al., *A FlAsH-based FRET approach to determine G protein-coupled receptor activation in living cells.* Nat Methods, 2005. **2**(3): p. 171-6.
278. Pietraszewska-Bogiel, A. and T.W. Gadella, *FRET microscopy: from principle to routine technology in cell biology.* J Microsc, 2011. **241**(2): p. 111-8.
279. Muller, S.M., et al., *Quantification of Forster resonance energy transfer by monitoring sensitized emission in living plant cells.* Front Plant Sci, 2013. **4**: p. 413.
280. Shrestha, D., et al., *Understanding FRET as a research tool for cellular studies.* Int J Mol Sci, 2015. **16**(4): p. 6718-56.
281. Levitt, J.A., et al., *Fluorescence lifetime and polarization-resolved imaging in cell biology.* Curr Opin Biotechnol, 2009. **20**(1): p. 28-36.

282. Rizzo, M.A. and D.W. Piston, *High-contrast imaging of fluorescent protein FRET by fluorescence polarization microscopy.* Biophys J, 2005. **88**(2): p. L14-6.
283. Bazin, H., E. Trinquet, and G. Mathis, *Time resolved amplification of cryptate emission: a versatile technology to trace biomolecular interactions.* J Biotechnol, 2002. **82**(3): p. 233-50.
284. Selvin, P.R., *Principles and biophysical applications of lanthanide-based probes.* Annu Rev Biophys Biomol Struct, 2002. **31**: p. 275-302.
285. Lohse, M.J., S. Nuber, and C. Hoffmann, *Fluorescence/bioluminescence resonance energy transfer techniques to study G-protein-coupled receptor activation and signaling.* Pharmacol Rev, 2012. **64**(2): p. 299-336.
286. Shimomura, O., *Discovery of green fluorescent protein (GFP) (Nobel Lecture).* Angew Chem Int Ed Engl, 2009. **48**(31): p. 5590-602.
287. Prasher, D.C., et al., *Primary structure of the Aequorea victoria green-fluorescent protein.* Gene, 1992. **111**(2): p. 229-33.
288. Chalfie, M., et al., *Green fluorescent protein as a marker for gene expression.* Science, 1994. **263**(5148): p. 802-5.
289. Schmid, J.A. and H. Neumeier, *Evolutions in science triggered by green fluorescent protein (GFP).* Chembiochem, 2005. **6**(7): p. 1149-56.
290. Abbe, E., *Beitrage zur Theorie des Mikroskops und der mikroskopischen Wahrnehmung.* Springer, 1873.
291. Sydor, A.M., et al., *Super-Resolution Microscopy: From Single Molecules to Supramolecular Assemblies.* Trends Cell Biol, 2015. **25**(12): p. 730-748.
292. Tsien, R.Y., *The green fluorescent protein.* Annu Rev Biochem, 1998. **67**: p. 509-44.
293. Bunemann, M., M. Frank, and M.J. Lohse, *Gi protein activation in intact cells involves subunit rearrangement rather than dissociation.* Proc Natl Acad Sci U S A, 2003. **100**(26): p. 16077-82.
294. Sposini, S., et al., *Integration of GPCR Signaling and Sorting from Very Early Endosomes via Opposing APPL1 Mechanisms.* Cell Rep, 2017. **21**(10): p. 2855-2867.
295. Zaccolo, M., et al., *A genetically encoded, fluorescent indicator for cyclic AMP in living cells.* Nat Cell Biol, 2000. **2**(1): p. 25-9.
296. Aper, S.J., P. Dierickx, and M. Merkx, *Dual Readout BRET/FRET Sensors for Measuring Intracellular Zinc.* ACS Chem Biol, 2016. **11**(10): p. 2854-2864.
297. Chan, Y.H., et al., *Development of ultrabright semiconducting polymer dots for ratiometric pH sensing.* Anal Chem, 2011. **83**(4): p. 1448-55.
298. Chen, H., et al., *A graphene quantum dot-based FRET system for nuclear-targeted and real-time monitoring of drug delivery.* Nanoscale, 2015. **7**(37): p. 15477-86.
299. Cayre, F., et al., *In Vivo FRET Imaging to Predict the Risk Associated with Hepatic Accumulation of Squalene-Based Prodrug Nanoparticles.* Adv Healthc Mater, 2018. **7**(3).
300. Ilien, B., et al., *Fluorescence resonance energy transfer to probe human M1 muscarinic receptor structure and drug binding properties.* J Neurochem, 2003. **85**(3): p. 768-78.
301. Fernandez-Duenas, V., et al., *Molecular determinants of A2AR-D2R allosterism: role of the intracellular loop 3 of the D2R.* J Neurochem, 2012. **123**(3): p. 373-84.
302. Gales, C., et al., *Real-time monitoring of receptor and G-protein interactions in living cells.* Nat Methods, 2005. **2**(3): p. 177-84.
303. Semack, A., R.U. Malik, and S. Sivaramakrishnan, *G Protein-selective GPCR Conformations Measured Using FRET Sensors in a Live Cell Suspension Fluorometer Assay.* J Vis Exp, 2016(115).
304. van Unen, J., et al., *A New Generation of FRET Sensors for Robust Measurement of Galphai1, Galphai2 and Galphai3 Activation Kinetics in Single Cells.* PLoS One, 2016. **11**(1): p. e0146789.
305. Adjobo-Hermans, M.J., et al., *Real-time visualization of heterotrimeric G protein Gq activation in living cells.* BMC Biol, 2011. **9**: p. 32.

306. Mastop, M., et al., *A FRET-based biosensor for measuring Galpha13 activation in single cells.* PLoS One, 2018. **13**(3): p. e0193705.
307. Yano, H., et al., *Development of novel biosensors to study receptor-mediated activation of the G-protein alpha subunits Gs and Golf.* J Biol Chem, 2017. **292**(49): p. 19989-19998.
308. Candelario, J. and M. Chachisvilis, *Real-time detection of G protein activation using monomolecular Ggamma FRET sensors.* J Recept Signal Transduct Res, 2013. **33**(1): p. 63-72.
309. Ritt, M. and S. Sivaramakrishnan, *Correlation between Activity and Domain Complementation in Adenylyl Cyclase Demonstrated with a Novel Fluorescence Resonance Energy Transfer Sensor.* Mol Pharmacol, 2016. **89**(4): p. 407-12.
310. Klarenbeek, J., et al., *Fourth-generation epac-based FRET sensors for cAMP feature exceptional brightness, photostability and dynamic range: characterization of dedicated sensors for FLIM, for ratiometry and with high affinity.* PLoS One, 2015. **10**(4): p. e0122513.
311. Nikolaev, V.O., et al., *Novel single chain cAMP sensors for receptor-induced signal propagation.* J Biol Chem, 2004. **279**(36): p. 37215-8.
312. Trinquet, E., R. Bouhelal, and M. Dietz, *Monitoring Gq-coupled receptor response through inositol phosphate quantification with the IP-One assay.* Expert Opin Drug Discov, 2011. **6**(10): p. 981-94.
313. Evanko, D.S. and P.G. Haydon, *Elimination of environmental sensitivity in a cameleon FRET-based calcium sensor via replacement of the acceptor with Venus.* Cell Calcium, 2005. **37**(4): p. 341-8.
314. Mank, M., et al., *A FRET-based calcium biosensor with fast signal kinetics and high fluorescence change.* Biophys J, 2006. **90**(5): p. 1790-6.
315. Harvey, C.D., et al., *A genetically encoded fluorescent sensor of ERK activity.* Proc Natl Acad Sci U S A, 2008. **105**(49): p. 19264-9.
316. Vandame, P., et al., *Optimization of ERK activity biosensors for both ratiometric and lifetime FRET measurements.* Sensors (Basel), 2014. **14**(1): p. 1140-54.
317. Cottet, M., et al., *Time resolved FRET strategy with fluorescent ligands to analyze receptor interactions in native tissues: application to GPCR oligomerization.* Methods Mol Biol, 2011. **746**: p. 373-87.
318. Bertrand, L., et al., *The BRET2/arrestin assay in stable recombinant cells: a platform to screen for compounds that interact with G protein-coupled receptors (GPCRS).* J Recept Signal Transduct Res, 2002. **22**(1-4): p. 533-41.
319. Charest, P.G., S. Terrillon, and M. Bouvier, *Monitoring agonist-promoted conformational changes of beta-arrestin in living cells by intramolecular BRET.* EMBO Rep, 2005. **6**(4): p. 334-40.
320. Lefkimmiatis, K. and M. Zaccolo, *cAMP signaling in subcellular compartments.* Pharmacol Ther, 2014. **143**(3): p. 295-304.
321. Wright, P.T., S. Schobesberger, and J. Gorelik, *Studying GPCR/cAMP pharmacology from the perspective of cellular structure.* Front Pharmacol, 2015. **6**: p. 148.
322. Sprenger, J.U. and V.O. Nikolaev, *Biophysical techniques for detection of cAMP and cGMP in living cells.* Int J Mol Sci, 2013. **14**(4): p. 8025-46.
323. Schleicher, K. and M. Zaccolo, *Using cAMP Sensors to Study Cardiac Nanodomains.* J Cardiovasc Dev Dis, 2018. **5**(1).
324. Gilman, A.G., *A protein binding assay for adenosine 3':5'-cyclic monophosphate.* Proc Natl Acad Sci U S A, 1970. **67**(1): p. 305-12.
325. Berrera, M., et al., *A toolkit for real-time detection of cAMP: insights into compartmentalized signaling.* Handb Exp Pharmacol, 2008(186): p. 285-98.
326. Brooker, G., et al., *Radioimmunoassay of cyclic AMP and cyclic GMP.* Adv Cyclic Nucleotide Res, 1979. **10**: p. 1-33.

327. Williams, C., *cAMP detection methods in HTS: selecting the best from the rest.* Nat Rev Drug Discov, 2004. **3**(2): p. 125-35.
328. Frings, S., et al., *Profoundly different calcium permeation and blockage determine the specific function of distinct cyclic nucleotide-gated channels.* Neuron, 1995. **15**(1): p. 169-79.
329. Abi-Gerges, A., et al., *Decreased expression and activity of cAMP phosphodiesterases in cardiac hypertrophy and its impact on beta-adrenergic cAMP signals.* Circ Res, 2009. **105**(8): p. 784-92.
330. Adams, S.R., et al., *Fluorescence ratio imaging of cyclic AMP in single cells.* Nature, 1991. **349**(6311): p. 694-7.
331. Mongillo, M., et al., *Fluorescence resonance energy transfer-based analysis of cAMP dynamics in live neonatal rat cardiac myocytes reveals distinct functions of compartmentalized phosphodiesterases.* Circ Res, 2004. **95**(1): p. 67-75.
332. DiPilato, L.M., X. Cheng, and J. Zhang, *Fluorescent indicators of cAMP and Epac activation reveal differential dynamics of cAMP signaling within discrete subcellular compartments.* Proc Natl Acad Sci U S A, 2004. **101**(47): p. 16513-8.
333. Ponsioen, B., et al., *Detecting cAMP-induced Epac activation by fluorescence resonance energy transfer: Epac as a novel cAMP indicator.* EMBO Rep, 2004. **5**(12): p. 1176-80.
334. Violin, J.D., et al., *beta2-adrenergic receptor signaling and desensitization elucidated by quantitative modeling of real time cAMP dynamics.* J Biol Chem, 2008. **283**(5): p. 2949-61.
335. Zagotta, W.N., et al., *Structural basis for modulation and agonist specificity of HCN pacemaker channels.* Nature, 2003. **425**(6954): p. 200-5.
336. Nikolaev, V.O., et al., *Cyclic AMP imaging in adult cardiac myocytes reveals far-reaching beta1-adrenergic but locally confined beta2-adrenergic receptor-mediated signaling.* Circ Res, 2006. **99**(10): p. 1084-91.
337. Odaka, H., et al., *Genetically-encoded yellow fluorescent cAMP indicator with an expanded dynamic range for dual-color imaging.* PLoS One, 2014. **9**(6): p. e100252.
338. Hackley, C.R., E.O. Mazzoni, and J. Blau, *cAMPr: A single-wavelength fluorescent sensor for cyclic AMP.* Sci Signal, 2018. **11**(520).
339. Tewson, P.H., et al., *New DAG and cAMP Sensors Optimized for Live-Cell Assays in Automated Laboratories.* J Biomol Screen, 2016. **21**(3): p. 298-305.
340. Allen, M.D. and J. Zhang, *Subcellular dynamics of protein kinase A activity visualized by FRET-based reporters.* Biochem Biophys Res Commun, 2006. **348**(2): p. 716-21.
341. Zhang, J., et al., *Genetically encoded reporters of protein kinase A activity reveal impact of substrate tethering.* Proc Natl Acad Sci U S A, 2001. **98**(26): p. 14997-5002.
342. Depry, C., M.D. Allen, and J. Zhang, *Visualization of PKA activity in plasma membrane microdomains.* Mol Biosyst, 2011. **7**(1): p. 52-8.
343. Zhang, J., et al., *Insulin disrupts beta-adrenergic signalling to protein kinase A in adipocytes.* Nature, 2005. **437**(7058): p. 569-73.
344. Musheshe, N., et al., *Targeting FRET-Based Reporters for cAMP and PKA Activity Using AKAP79.* Sensors (Basel), 2018. **18**(7).
345. Wachten, S., et al., *Distinct pools of cAMP centre on different isoforms of adenylyl cyclase in pituitary-derived GH3B6 cells.* J Cell Sci, 2010. **123**(Pt 1): p. 95-106.
346. Lefkimmiatis, K., D. Leronni, and A.M. Hofer, *The inner and outer compartments of mitochondria are sites of distinct cAMP/PKA signaling dynamics.* J Cell Biol, 2013. **202**(3): p. 453-62.
347. Gorshkov, K., et al., *AKAP-mediated feedback control of cAMP gradients in developing hippocampal neurons.* Nat Chem Biol, 2017. **13**(4): p. 425-431.
348. Oliveria, S.F., L.L. Gomez, and M.L. Dell'Acqua, *Imaging kinase--AKAP79--phosphatase scaffold complexes at the plasma membrane in living cells using FRET microscopy.* J Cell Biol, 2003. **160**(1): p. 101-12.

349. Li, X., M.M. Nooh, and S.W. Bahouth, *Role of AKAP79/150 protein in beta1-adrenergic receptor trafficking and signaling in mammalian cells.* J Biol Chem, 2013. **288**(47): p. 33797-812.
350. Willoughby, D., et al., *A key phosphorylation site in AC8 mediates regulation of Ca(2+)-dependent cAMP dynamics by an AC8-AKAP79-PKA signalling complex.* J Cell Sci, 2012. **125**(Pt 23): p. 5850-9.
351. Shen, J.X. and D.M. Cooper, *AKAP79, PKC, PKA and PDE4 participate in a Gq-linked muscarinic receptor and adenylate cyclase 2 cAMP signalling complex.* Biochem J, 2013. **455**(1): p. 47-56.
352. Di Benedetto, G., et al., *Mitochondrial Ca(2)(+) uptake induces cyclic AMP generation in the matrix and modulates organelle ATP levels.* Cell Metab, 2013. **17**(6): p. 965-75.
353. Moore, B.S., et al., *Cilia have high cAMP levels that are inhibited by Sonic Hedgehog-regulated calcium dynamics.* Proc Natl Acad Sci U S A, 2016. **113**(46): p. 13069-13074.
354. Mukherjee, S., et al., *A novel biosensor to study cAMP dynamics in cilia and flagella.* Elife, 2016. **5**.
355. Herget, S., M.J. Lohse, and V.O. Nikolaev, *Real-time monitoring of phosphodiesterase inhibition in intact cells.* Cell Signal, 2008. **20**(8): p. 1423-31.
356. Lohse, C., et al., *Experimental and mathematical analysis of cAMP nanodomains.* PLoS One, 2017. **12**(4): p. e0174856.
357. Ovesný, M., et al., *ThunderSTORM: a comprehensive ImageJ plug-in for PALM and STORM data analysis and super-resolution imaging.* Bioinformatics, 2014. **30**(16): p. 2389-2390.
358. *cAMP Signaling*. Methods in Molecular Biology, ed. M. Zaccolo. 2015: Humana Press.
359. Nausch, L.W., et al., *Differential patterning of cGMP in vascular smooth muscle cells revealed by single GFP-linked biosensors.* Proc Natl Acad Sci U S A, 2008. **105**(1): p. 365-70.
360. Sivaramakrishnan, S., et al., *Dynamic charge interactions create surprising rigidity in the ER/K alpha-helical protein motif.* Proc Natl Acad Sci U S A, 2008. **105**(36): p. 13356-61.
361. Zacharias, D.A., et al., *Partitioning of lipid-modified monomeric GFPs into membrane microdomains of live cells.* Science, 2002. **296**(5569): p. 913-6.
362. Seeman, P., D. Cheng, and G.H. Iles, *Structure of membrane holes in osmotic and saponin hemolysis.* J Cell Biol, 1973. **56**(2): p. 519-27.
363. Orskov, C., et al., *Tissue and plasma concentrations of amidated and glycine-extended glucagon-like peptide I in humans.* Diabetes, 1994. **43**(4): p. 535-9.
364. Rich, T.C., et al., *Cyclic nucleotide-gated channels colocalize with adenylyl cyclase in regions of restricted cAMP diffusion.* J Gen Physiol, 2000. **116**(2): p. 147-61.
365. Barnes, A.P., et al., *Phosphodiesterase 4D forms a cAMP diffusion barrier at the apical membrane of the airway epithelium.* J Biol Chem, 2005. **280**(9): p. 7997-8003.
366. Doskeland, S.O., E. Maronde, and B.T. Gjertsen, *The genetic subtypes of cAMP-dependent protein kinase--functionally different or redundant?* Biochim Biophys Acta, 1993. **1178**(3): p. 249-58.
367. Pelletier, J. and N. Sonenberg, *Internal initiation of translation of eukaryotic mRNA directed by a sequence derived from poliovirus RNA.* Nature, 1988. **334**(6180): p. 320-5.
368. Iancu, R.V., et al., *Cytoplasmic cAMP concentrations in intact cardiac myocytes.* Am J Physiol Cell Physiol, 2008. **295**(2): p. C414-22.
369. Brogioli, D., *Violation of the mass-action law in dilute chemical systems.* J Chem Phys, 2013. **139**(18): p. 184102.
370. Agarwal, S.R., et al., *Role of membrane microdomains in compartmentation of cAMP signaling.* PLoS One, 2014. **9**(4): p. e95835.
371. Agarwal, S.R., et al., *Compartmentalized cAMP Signaling Associated With Lipid Raft and Non-raft Membrane Domains in Adult Ventricular Myocytes.* Front Pharmacol, 2018. **9**: p. 332.

372. Jiang, J.Y., et al., *Interrogating cyclic AMP signaling using optical approaches.* Cell Calcium, 2017. **64**: p. 47-56.
373. Koschinski, A. and M. Zaccolo, *Activation of PKA in cell requires higher concentration of cAMP than in vitro: implications for compartmentalization of cAMP signalling.* Sci Rep, 2017. **7**(1): p. 14090.
374. Terrin, A., et al., *PGE(1) stimulation of HEK293 cells generates multiple contiguous domains with different [cAMP]: role of compartmentalized phosphodiesterases.* J Cell Biol, 2006. **175**(3): p. 441-51.
375. Civciristov, S., et al., *Preassembled GPCR signaling complexes mediate distinct cellular responses to ultralow ligand concentrations.* Sci Signal, 2018. **11**(551).
376. Yang, P.C., et al., *A Computational Modeling and Simulation Approach to Investigate Mechanisms of Subcellular cAMP Compartmentation.* PLoS Comput Biol, 2016. **12**(7): p. e1005005.
377. Brunton, L.L., *PDE4: arrested at the border.* Sci STKE, 2003. **2003**(204): p. Pe44.
378. Nikolaev, V.O., et al., *Real-time monitoring of the PDE2 activity of live cells: hormone-stimulated cAMP hydrolysis is faster than hormone-stimulated cAMP synthesis.* J Biol Chem, 2005. **280**(3): p. 1716-9.
379. Baillie, G.S., J.D. Scott, and M.D. Houslay, *Compartmentalisation of phosphodiesterases and protein kinase A: opposites attract.* FEBS Lett, 2005. **579**(15): p. 3264-70.
380. Zaccolo, M., et al., *Restricted diffusion of a freely diffusible second messenger: mechanisms underlying compartmentalized cAMP signalling.* Biochem Soc Trans, 2006. **34**(Pt 4): p. 495-7.
381. Beavo, J.A., P.J. Bechtel, and E.G. Krebs, *Activation of protein kinase by physiological concentrations of cyclic AMP.* Proc Natl Acad Sci U S A, 1974. **71**(9): p. 3580-3.
382. Saucerman, J.J., E.C. Greenwald, and R. Polanowska-Grabowska, *Mechanisms of cyclic AMP compartmentation revealed by computational models.* J Gen Physiol, 2014. **143**(1): p. 39-48.
383. Corbin, J.D., et al., *Compartmentalization of adenosine 3':5'-monophosphate and adenosine 3':5'-monophosphate-dependent protein kinase in heart tissue.* J Biol Chem, 1977. **252**(11): p. 3854-61.
384. Saucerman, J.J., et al., *Systems analysis of PKA-mediated phosphorylation gradients in live cardiac myocytes.* Proc Natl Acad Sci U S A, 2006. **103**(34): p. 12923-8.
385. Thompson, A. and V. Kanamarlapudi, *Distinct regions in the C-Terminus required for GLP-1R cell surface expression, activity and internalisation.* Mol Cell Endocrinol, 2015. **413**: p. 66-77.
386. Limbutara, K., et al., *Phosphorylation Changes in Response to Kinase Inhibitor H89 in PKA-Null Cells.* Sci Rep, 2019. **9**(1): p. 2814.
387. http://www.signaling-gateway.org/molecule/query?afcsid=A000481
388. Faux, M.C., et al., *Mechanism of A-kinase-anchoring protein 79 (AKAP79) and protein kinase C interaction.* Biochem J, 1999. **343 Pt 2**: p. 443-52.
389. Lewis, B.A., *Understanding large multiprotein complexes: applying a multiple allosteric networks model to explain the function of the Mediator transcription complex.* Journal of Cell Science, 2010. **123**(2): p. 159-163.
390. Erickson, H.P., *Size and shape of protein molecules at the nanometer level determined by sedimentation, gel filtration, and electron microscopy.* Biological procedures online, 2009. **11**: p. 32-51.
391. Sato, Y., et al., *Molecular characterization of pharmacological properties of T-0509 for beta-adrenoceptors.* Eur J Pharmacol, 1996. **315**(3): p. 363-7.
392. Summerhill, S., et al., *A cell-based assay to assess the persistence of action of agonists acting at recombinant human beta(2) adrenoceptors.* J Pharmacol Toxicol Methods, 2008. **58**(3): p. 189-97.

393. Stone, M.B., S.A. Shelby, and S.L. Veatch, *Super-Resolution Microscopy: Shedding Light on the Cellular Plasma Membrane.* Chemical reviews, 2017. **117**(11): p. 7457-7477.
394. Valentine, C.D. and P.M. Haggie, *Confinement of β(1)- and β(2)-adrenergic receptors in the plasma membrane of cardiomyocyte-like H9c2 cells is mediated by selective interactions with PDZ domain and A-kinase anchoring proteins but not caveolae.* Molecular biology of the cell, 2011. **22**(16): p. 2970-2982.
395. Kusumi, A., Y. Sako, and M. Yamamoto, *Confined lateral diffusion of membrane receptors as studied by single particle tracking (nanovid microscopy). Effects of calcium-induced differentiation in cultured epithelial cells.* Biophysical journal, 1993. **65**(5): p. 2021-2040.
396. Calebiro, D. and T. Sungkaworn, *Single-Molecule Imaging of GPCR Interactions.* Trends Pharmacol Sci, 2018. **39**(2): p. 109-122.
397. Scarselli, M., et al., *Enlightening G-protein-coupled receptors on the plasma membrane using super-resolution photoactivated localization microscopy.* Biochem Soc Trans, 2013. **41**(1): p. 191-6.
398. Ciruela, F., et al., *G protein-coupled receptor oligomerization for what?* J Recept Signal Transduct Res, 2010. **30**(5): p. 322-30.
399. Patterson, R.L., D.B. van Rossum, and D.L. Gill, *Store-operated Ca2+ entry: evidence for a secretion-like coupling model.* Cell, 1999. **98**(4): p. 487-99.
400. Ma, H.T., et al., *Requirement of the inositol trisphosphate receptor for activation of store-operated Ca2+ channels.* Science, 2000. **287**(5458): p. 1647-51.
401. Conti, M., D. Mika, and W. Richter, *Cyclic AMP compartments and signaling specificity: role of cyclic nucleotide phosphodiesterases.* J Gen Physiol, 2014. **143**(1): p. 29-38.
402. Malbon, C.C., J. Tao, and H.Y. Wang, *AKAPs (A-kinase anchoring proteins) and molecules that compose their G-protein-coupled receptor signalling complexes.* Biochem J, 2004. **379**(Pt 1): p. 1-9.
403. Hinke, S.A., et al., *Anchored phosphatases modulate glucose homeostasis.* Embo j, 2012. **31**(20): p. 3991-4004.
404. Ahmad, F., et al., *Cyclic nucleotide phosphodiesterases: important signaling modulators and therapeutic targets.* Oral diseases, 2015. **21**(1): p. e25-e50.
405. Azevedo, M.F., et al., *Clinical and molecular genetics of the phosphodiesterases (PDEs).* Endocrine reviews, 2014. **35**(2): p. 195-233.

10 Acknowledgements

Primarily, I would like to express gratitude to my supervisor Prof. Dr. Martin J. Lohse, for granting me the opportunity to conduct research under his supervision and to complete my doctoral studies in this excellent research laboratory. The scientific discussions we had were always of great value for the progress of the project and his outstanding pharmacological experience, as well as his strategic advices were and are immensely valuable especially in the preparation of the manuscript. Additionally, I admire his will to always strive higher and never stand still, which lead to the transfer of our laboratory to Berlin. Although skeptical at the beginning, I quickly found myself in an excellent research community, which helped profoundly in the progress of the scientific project.

Secondly, a huge thank you is addressed to Dr. Andreas Bock and Dr. Isabella Maiellaro. Both have been indescribably valuable for the scientific and personal development. I have started under the guidance of Andreas and I am extremely thankful for always being available for any kind of support. He is responsible for the initial excitement I developed for the project and throughout my PhD studies, he was constantly available for scientific discussions and advice. Soon, I was also lucky to get Isabella as a supervisor, who was able to awaken the fascination for FRET in me. Her advice was always invaluable, especially when it came to the technical difficulties. From both Andreas and Isabella I learned how to plan and conduct experiments in a very efficient way, and to critically analyze and interpret the results. I admire Isabella for being a truly passionate and very accurate scientist who is able to coordinate both science and a family and to Andreas I am especially thankful for his vast knowledge in pharmacology which is essential to understand and interpret the processes we are studying. And for his constant optimism and support which I found very motivating.

A special thank you goes to Prof. Manuela Zaccolo for being my second supervisor and for hosting me in her lab. Under her supervision together with Dr. Andreas Koschinski I gained insight into new experimental techniques and had to chance to experience working in a foreign lab, revising and amending my own scientific benchwork. The discussions with her were always very inspiring, efficient and valuable for the success of some key experiments.

I want to thank also Prof. Peter Gmeiner and Prof. Katrin Heinze for being part of my thesis committee. Their remarks during the committee meeting were of great help to critically reassess the results and defend them with scientific reasoning.

Many thanks go to all the members of the AG Lohse, both in Würzburg and Berlin. The technique of cloning which I learned from Dr. Ulrike Zabel and Monika Frank was fundamental for my research. Ruth Pareja, Nicole Grunert and Marlies Grieben who lightened my workload, which allowed me to focus on the actual experiments. To Jan Möller, Hannes Schihada, Ali Isbilir, Eugene Grushevskyi with whom I started in the lab I'm thankful for the scientific support and the many funny hours we spent. Many thanks also to the more recent lab members Katarina Nemec, Philipp Gmach, Marc Bathe-Peter, Romy Thomas. Thanks especially to Katarina who made dealing with the sometimes testosterone-overloaded lab very much easier.

Zu guter Letzt möchte ich mich bei den Menschen bedanken ohne die ich heute nicht hier wäre, und ohne die ich diese Arbeit nicht durchgestanden hätte- meine Familie in Deutschland und Israel und

meinem Partner Matthias. Meinem Vater der mir die Liebe zur Pharmazie und Pharmakologie vererbt hat und mich in all meinen Vorhaben unterstützt auch wenn sie nicht immer seinen Vorstellungen entsprechen, und meiner Mutter mit der ich die ersten wissenschaftlichen Experimente durchgeführt habe- in der Grundschule. Meine beiden Brüder die mir immer wieder zeigen dass man sich selbst nicht zu ernst nehmen darf und mit mir über mich lachen, aber vor allem Matthias der alle Hochs- und Tiefs dieser Doktorarbeit am eigenen Leib erfahren musste und mich immer wieder aufgebaut hat. Ihr habt durch diese spannende und zeitweise sehr herausfordernde Lebensphase begleitet und ich hoff euch mit dem Ergebnis etwas stolz machen zu können.

اخيرا وليس اخرا اريد ان اشكر الاشخاص الذين ولو فضلهم علي لعجزت عن انجاز هذا الهدف.

شكرا خاص لعائلتي الشهمة في اسرائيل وكذلك في المانيا. لقد دعمتنني معنويا وكنتم لي سندا قويا طوال هذه المسيرة نحوى النمو المعرفي. انها كانت فترة مليئة بالعلم ةالتحديات والتشويق.

دمتم ودامت المحبة في ربوع هذه العائلة الوقورة.